

Space Time Processing for Third Generation CDMA Systems

Fakhrul Alam

Dissertation submitted to the faculty of the
Virginia Polytechnic Institute & State University
in partial fulfillment of the requirements for the degree of

Doctor of Philosophy
in
Electrical Engineering

Brian D. Woerner, Chair
Ira Jacobs
Jeffrey H. Reed
William H. Tranter
Stephen G. Wilson

November, 2002
Blacksburg, Virginia

Keywords: Smart Antenna, Adaptive Antenna, Beamforming, Array Algorithm, Space Time Processing, Beamformer-Rake, WCDMA, OFDM

Copyright 2002, Fakhrul Alam

Space Time Processing for Third Generation CDMA Systems

Fakhrul Alam

ABSTRACT

The capacity of a cellular system is limited by two different phenomena, namely multipath fading and multiple access interference (MAI). A Two Dimensional (2-D) receiver combats both of these by processing the signal both in the spatial and temporal domain. An ideal 2-D receiver would perform joint space-time processing, but at the price of high computational complexity. In this dissertation we investigate computationally simpler technique termed as a Beamformer-Rake. In a Beamformer-Rake, the output of a beamformer is fed into a succeeding temporal processor to take advantage of both the beamformer and Rake receiver. Wireless service providers throughout the world are working to introduce the third generation (3G) cellular service that will provide higher data rates and better spectral efficiency. Wideband CDMA (WCDMA) has been widely accepted as one of the air interfaces for 3G. A Beamformer-Rake receiver can be an effective solution to provide the receivers enhanced capabilities needed to achieve the required performance of a WCDMA system. This dissertation investigates different Beamformer-Rake receiver structures suitable for the WCDMA system and compares their performance under different operating conditions. This work develops Beamformer-Rake receivers for WCDMA uplink that employ Eigen-Beamforming techniques based on the Maximum Signal to Noise Ratio (MSNR) and Maximum Signal to Interference and Noise Ratio (MSINR) criteria. Both the structures employ Maximal Ratio Combining (MRC) to exploit temporal diversity.

MSNR based Eigen-Beamforming leads to a Simple Eigenvalue problem (SE). This work investigates several algorithms that can be employed to solve the SE and compare the algorithms in terms of their computational complexity and their performance. MSINR based Eigen-Beamforming results in a Generalized Eigenvalue problem (GE). The dissertation describes several techniques to form the GE and algorithms to solve it. We propose a new low-complexity algorithm, termed as the Adaptive Matrix Inversion (AMI), to solve the GE. We compare the performance of the AMI to other existing algorithms. Comparison between different techniques to form the GE is also compared. The MSINR based beamforming is demonstrated to be superior to the MSNR based beamforming in the presence of strong interference.

There are Pilot Symbol Assisted (PSA) beamforming techniques that exploit the Minimum Mean Squared Error (MMSE) criterion. We compare the MSINR based Beamformer-Rake with the same that utilizes Direct Matrix Inversion (DMI) to perform MMSE based beamforming in terms of Bit Error Rate (BER). In a wireless system where the number of co-channel interferers is larger than the number of elements of a practical antenna array, we can not perform explicit null-steering. As a result the advantage of beamforming is partially lost. In this scenario it is better to attain diversity gain at the cost of spatial aliasing. We demonstrate this with the aid of simulation.

Orthogonal Frequency Division Multiplexing (OFDM) is a multi-carrier technique that has recently received considerable attention for high speed wireless communication. OFDM has been accepted as the standard for Digital Audio Broadcast (DAB) and Digital Video Broadcast (DVB) in Europe. It has also been established as one of the modulation formats for the IEEE 802.11a wireless LAN standard. OFDM has emerged as one of the primary candidates for the Fourth Generation (4G) wireless communication systems and high speed ad hoc wireless networks. We propose a simple pilot symbol assisted frequency domain beamforming technique for OFDM receiver and demonstrate the concept of sub-band beamforming. Vector channel models measured with the MPRG Viper test-bed is also employed to investigate the performance of the beamforming scheme.

Acknowledgments

I would like to express my gratitude to Dr. Brian D. Woerner for his constant encouragement and belief in me. He has been everything that one could want in an advisor. I am deeply indebted to my committee members Dr. Jeffrey H. Reed, Dr. W. H. Tranter, Dr. Ira Jacobs and Dr. Stephen G. Wilson for providing valuable advice. I also want to thank LGIC and DARPA for sponsoring this research work. Special thanks to Raqibul Mostafa, William G. Newhall, James Hicks and Patrick Cheung for their comments and insights. I also want to thank Donghee Shim for sharing his expertise of adaptive beamforming. I thank the wonderful staff of MPRG for their assistance. Finally, most of all, I thank my wife and my parents for their unconditional love and support.

Contents

1 Introduction	1
1.1 Introduction	1
1.2 Literature Survey	3
2 Fundamental Concepts of Space Time Processing	9
2.1 Introduction	9
2.2 Antenna Array	10
2.2.1 Uniform Linear Array	10
2.3 Beamformer	14
2.3.1 Example of a Simple Beamforming Example with ULA	15
2.4 Array Ambiguity	17
2.5 Spatial Sampling Theorem	18
2.6 Spatial Diversity Gain	18
2.7 Temporal Processing: Rake Receiver for CDMA	19
2.8 Beamformer-Rake Receiver	20
3 Beamforming Criteria	23
3.1 Introduction	23
3.2 MSNR Beamforming	23
3.2.1 Maximizing the Signal to Noise Ratio	23
3.2.2 Alternate SE for MSNR Beamforming	26
3.2.3 Phase Ambiguity in Eigen-Beamforming	27
3.3 MSINR Beamforming	28
3.3.1 Maximizing the Signal to Interference and Noise Ratio	29
3.3.1 Maximizing the Received Signal to Interference and Noise Ratio	31
3.4 MMMSE Beamforming Criterion	31
3.5 Comparison of MSINR and MMSE Beamforming for a Simple Scenario	33
3.5.1 Simulation Environment	33
3.5.2 Estimation of Second Order Statistics for Beamforming	34
3.5.2 Simulation Results	35
4 WCDMA	38
4.1 Introduction	38

4.2	Cellular Standards: From 1G to 3G	38
4.2.1	First Generation (1G) Cellular Systems	38
4.2.2	Second Generation (2G) Cellular Systems	39
4.2.3	Transition towards 3G: 2.5G Cellular Systems	39
4.2.4	Third Generation (3G) Cellular Systems	40
4.3	WCDMA: Air Interface for 3G	42
4.3.1	WCDMA Key Features	42
4.3.2	WCDMA Key Technical Characteristics	43
4.4	WCDMA Physical Layer at the Uplink	43
4.4.1	Physical Channel Structure	44
4.4.1.1	Uplink Spreading and Modulation	44
4.4.1.2	Uplink Frame Structure	45
4.4.1.3	Uplink Channelization Codes	46
4.4.1.4	Uplink Scrambling Codes	48
4.4.1.4.1	Uplink Long Scrambling Codes	49
4.4.1.4.2	Uplink Short Scrambling Codes	50
4.4.1.5	Summary of WCDMA Uplink Modulation	52
4.4.2	Channel Coding	53
4.4.2.1	Error Detection	53
4.4.2.2	Error Correction	53
4.5	Development Status of 3G around the World	54
4.5.1	Status of 3G in the USA	54
4.5.2	Status of 3G in Europe	56
4.5.3	Status of 3G in the South America	56
4.5.4	Status of 3G in Asia	57
4.5.4.1	3G in Korea	57
4.5.4.2	3G in Japan	58
4.5.4.3	3G in China	58
4.5.4.4	3G in India	58
4.5.5	Status of 3G in Australia	58
5	Eigen-Beamforming based on MSNR Criterion	59
5.1	Introduction	59
5.2	Adaptive Algorithms to Solve the Simple eigenvalue Problem	59
5.2.1	Metric for Computational Complexity	59
5.2.2	Power Method	60

5.2.3	Lagrange Multiplier Method	62
5.2.4	Conjugate Gradient Method	65
5.2.5	Summary of Algorithms	69
5.3	Block Processing for Slow Varying Channel	69
5.4	MSNR Based Beamformer-Rake Receiver for WCDMA Uplink	69
5.5	Simulation Results	71
6	Eigen-Beamforming based on MSINR Criterion	80
6.1	Introduction	80
6.2	MSINR Beamforming for CDMA Systems	80
6.2.1	Code Filtering Approach	80
6.2.2	Modified CFA (M-CFA)	81
6.2.3	Code Gated Algorithm	82
6.3	Algorithms to Solve the GE	83
6.3.1	Generalized Power Method	83
6.3.2	Generalized Lagrange Multiplier Method	84
6.3.3	Adaptive Matrix Inversion Method (AMI)	86
6.4	MSINR Based Beamformer-Rake Receiver for WCDMA Uplink	91
6.5	Simulation Environment	93
6.6	Simulation Results for MSINR Beamforming for the Beamformer-Rake	93
6.7	Comparison of MSINR and MSNR Beamforming Techniques for Beamformer- Rake...	101
7	Beamformer-Rake based on MMSE Criterion	105
7.1	Introduction	105
7.2	MMSE Beamforming Criterion	105
7.2.1	Direct Matrix Inversion (DMI)	106
7.2.2	Method of Steepest Descent	107
7.2.3	Least Mean Square (LMS) Algorithm	109
7.3	Pilot Symbol Assisted DMI-based Beamformer-Rake Receiver for WCDMA	110
7.4	Performance Comparison with MSINR Beamforming	111
7.5	Diversity Gain vs. Spatial Aliasing	115
7.5.1	Simulation Results: Spatial Aliasing vs. Diversity Gain	115
8	Beamforming for OFDM Systems	119
8.1	Introduction	119

8.2	Fundamental Concepts of OFDM	119
8.3	Inter Symbol Interference in OFDM	120
8.4	Spectrum Shaping of OFDM	121
8.5	Frequency Domain Beamformer for OFDM Receiver	121
8.6	Simulation Study of the Proposed Beamforming Scheme	125
8.6.1	Description of the OFDM System	125
8.6.2	Recursive Least Square Algorithm	126
8.6.3	Simulation in Simple AWGN Environment	127
8.6.4	Simulation in Frequency Selective Multipath Channel	130
8.7	Performance in Vector Channel based on Measurement Data	133
9	Conclusions and Future Work	139
9.1	Conclusions	139
9.2	List of Publications	140
9.3	Future Work	141
9.3.1	Further Development of Efficient Algorithm for Eigen-Beamforming	141
9.3.1.1	Alternate Linear Lagrange Multiplier Method	142
9.3.1.2	Linear Power Method	146
9.3.1.3	Alternate Linear Generalized Lagrange Multiplier Method	147
9.3.2	Study the Effect of Quantization on Adaptive Algorithms	149
9.3.3	Investigation of the Applicability of Beamformer-Rake Structure at the Handset	149
9.3.2	Extension of the Beamforming Scheme for OFDM System	149
A	Beamforming in Multipath Environment	150
B	Alternate Beamformer-Rake for WCDMA Uplink	154
C	2-D Diversity Combiners	156
C.1	Combining Techniques for Improved SNR	156
C.1.1	Selection Diversity	156
C.1.2	Maximal Ratio Combining	157
C.1.2	Equal Gain Combining	157
C.1	Conventional 2-D Diversity Combiners for CDMA Systems	157
C.2.1	Analysis of Decision Statistics for the 2-D Diversity Combiners.....	158
	References	162
	Vita	174

List of Figures

2.1	Plane wave incident on a ULA with an AOA of θ	11
2.2a	Beamformer Principle	15
2.2b	Typical array gain pattern	15
2.3	Beam pattern for the elementary beamformer. The AOA of the desired user is 0^0 and the AOA of the interferer is 45^0	17
2.4	Rake receiver	20
2.5a	Beamformer-Rake structure	20
2.5b	Different weight vector accentuates different multipath component of the desired user ..	20
2.6	Performance comparison among various receivers under different user distribution	22
3.1	Examples of beam pattern. The desired user is at 30^0 . The interferers are at 60^0 and -60^0 (300^0) respectively. Both the interferers are being received at 20 dB higher power level than the desired user	36
3.2	Examples of beam pattern. The desired user is at 30^0 . The interferers are at 60^0 and -60^0 (300^0) respectively. Both the interferers are being received at 10 dB higher power level than the desired user	36
3.3	BER vs. E_b/N_0 . Both the interferers are being received at 20 dB higher power level than the desired signal	36
3.4	BER vs. E_b/N_0 . Both the interferers are being received at 10 dB higher power level than the desired signal	36
3.5	BER vs. E_b/N_0 . Both the interferers are being received at equal power level compared to the desired signal	36
3.6	BER vs. E_b/N_0 . Both interferers are being received at 10 dB lower power level than the desired signal	36
3.7	BER vs. E_b/N_0 for MSINR beamforming. Both the interferers are being received at 20 dB higher power level than the desired signal. Different number of samples are being used to compute the required statistics	37
3.8	BER vs. E_b/N_0 for MMSE beamforming. Both the interferers are being received at 20 dB higher power level than the desired signal. Different number of samples are being used to compute the required statistics	37
4.1	Evolution toward 3G	41
4.2	Uplink spreading and modulation	44
4.3	Frame structure for uplink DPDCH/DPCCH	45
4.4	Code-tree for generation of OVSF codes	47
4.5	Auto-correlation for two OVSF codes of SF=256	48
4.6	Generation of scrambling codes	49
4.7	Uplink long scrambling code generator	50

4.8	Uplink short scrambling code generator	51
4.9	Initial conditions at the shift registers	52
5.1	Flowchart of the Lagrange multiplier method	63
5.2	Flowchart of the simple linear Lagrange multiplier method	64
5.3	Flowchart of the modified conjugate gradient method	67
5.4	Flowchart of the linear modified conjugate gradient method	68
5.5	MSNR based Beamformer-Rake receiver for WCDMA uplink	70
5.6	BER vs. E_b/N_0 performance of the MSNR based Beamformer-Rake receiver. There are 5 interferers. The user distribution is <i>uniform</i> . Three different algorithms are applied to solve the Simple Eigenvalue Problem. Circular channel model describes the propagation condition	72
5.7	BER vs. E_b/N_0 performance of the MSNR based Beamformer-Rake receiver. There are 5 interferers. The user distribution is <i>non-uniform</i> . Three different algorithms are applied to solve the Simple Eigenvalue Problem. Circular channel model describes the propagation condition	72
5.8	BER vs. E_b/N_0 performance of the MSNR based Beamformer-Rake receiver. There are 10 interferers. The user distribution is <i>uniform</i> . Three different algorithms are applied to solve the Simple Eigenvalue Problem. Circular channel model describes the propagation condition	73
5.9	BER vs. E_b/N_0 performance of the MSNR based Beamformer-Rake receiver. There are 10 interferers. The user distribution is <i>non-uniform</i> . Three different algorithms are applied to solve the Simple Eigenvalue Problem. Circular channel model describes the propagation condition	73
5.10	BER vs. E_b/N_0 performance of the MSNR based Beamformer-Rake receiver. There are 5 interferers. The user distribution is <i>uniform</i> . Three different algorithms are applied to solve the Simple Eigenvalue Problem. Elliptical channel model describes the propagation condition	74
5.11	BER vs. E_b/N_0 performance of the MSNR based Beamformer-Rake receiver. There are 5 interferers. The user distribution is <i>non-uniform</i> . Three different algorithms are applied to solve the Simple Eigenvalue Problem. Elliptical channel model describes the propagation condition	74
5.12	BER vs. E_b/N_0 performance of the MSNR based Beamformer-Rake receiver. There are 10 interferers. The user distribution is <i>uniform</i> . Three different algorithms are applied to solve the Simple Eigenvalue Problem. Elliptical channel model describes the propagation condition	75
5.13	BER vs. E_b/N_0 performance of the MSNR based Beamformer-Rake receiver. There are 10 interferers. The user distribution is <i>non-uniform</i> . Three different algorithms are applied to solve the Simple Eigenvalue Problem. Elliptical channel model describes the propagation condition	75
5.14	BER vs. E_b/N_0 performance of the Power method for a MSNR based Beamformer-Rake receiver. There are 5 & 10 interferers. The solid and the dashed curves represent uniform and non-uniform user distributions respectively. Circular channel model describes the propagation condition	76
5.15	BER vs. E_b/N_0 performance of the Power method for a MSNR based Beamformer-Rake receiver. There are 5 & 10 interferers. The solid and the dashed curves represent uniform and non-uniform user distributions respectively. Elliptical channel model	76

describes the propagation condition	
5.16 BER vs. E_b/N_0 performance of the Lagrange multiplier method for a MSNR based Beamformer-Rake receiver. There are 5 & 10 interferers. The solid and the dashed curves represent uniform and non-uniform user distributions respectively. Circular channel model describes the propagation condition	77
5.17 BER vs. E_b/N_0 performance of the Lagrange multiplier method for a MSNR based Beamformer-Rake receiver. There are 5 & 10 interferers. The solid and the dashed curves represent uniform and non-uniform user distributions respectively. Elliptical channel model describes the propagation condition	77
5.18 BER vs. E_b/N_0 performance of the linear MCGM for a MSNR based Beamformer-Rake receiver. There are 5 & 10 interferers. The solid and the dashed curves represent uniform and non-uniform user distributions respectively. Circular channel model describes the propagation condition	78
5.19 BER vs. E_b/N_0 performance of the linear MCGM for a MSNR based Beamformer-Rake receiver. There are 5 & 10 interferers. The solid and the dashed curves represent uniform and non-uniform user distributions respectively. Elliptical channel model describes the propagation condition	78
6.1 CDMA despreading	80
6.2 The concept of CGA	83
6.3 Flowchart of the GLM	86
6.4 Flowchart of the AMI	88
6.5 Flowchart of the linear AMI	91
6.6 CGA based Beamformer-Rake receiver for WCDMA uplink	91
6.7 Modified CFA based Beamformer-Rake receiver for WCDMA uplink	92
6.8 BER vs. E_b/N_0 of MSINR based Beamformer-Rake when the user distribution is <i>uniform</i> . 5 interferers, CGA beamforming, Circular channel	94
6.9 BER vs. E_b/N_0 of MSINR based Beamformer-Rake when the user distribution is <i>non-uniform</i> . 5 interferers, CGA beamforming, Circular channel	94
6.10 BER vs. E_b/N_0 of MSINR based Beamformer-Rake when the user distribution is <i>uniform</i> . 10 interferers, CGA beamforming, Circular channel	94
6.11 BER vs. E_b/N_0 of MSINR based Beamformer-Rake when the user distribution is <i>uniform</i> . 10 interferers, CGA beamforming, Circular channel	94
6.12 BER vs. E_b/N_0 of MSINR based Beamformer-Rake when the user distribution is <i>uniform</i> . 5 interferers, CGA beamforming, Elliptical channel	95
6.13 BER vs. E_b/N_0 of MSINR based Beamformer-Rake when the user distribution is <i>non-uniform</i> . 5 interferers, CGA beamforming, Elliptical channel	95
6.14 BER vs. E_b/N_0 of MSINR based Beamformer-Rake when the user distribution is <i>uniform</i> . 10 interferers, CGA beamforming, Elliptical channel	95
6.15 BER vs. E_b/N_0 of MSINR based Beamformer-Rake when the user distribution is <i>non-uniform</i> . 10 interferers, CGA beamforming, Elliptical channel	95
6.16 BER vs. E_b/N_0 of MSINR based Beamformer-Rake when the user distribution is <i>uniform</i> . 5 interferers, M-CFA beamforming, Circular channel	96
6.17 BER vs. E_b/N_0 of MSINR based Beamformer-Rake when the user distribution is <i>non-uniform</i> . 5 interferers, M-CFA beamforming, Circular channel	96
6.18 BER vs. E_b/N_0 of MSINR based Beamformer-Rake when the user distribution is	

	<i>uniform</i> . 10 interferers, M-CFA beamforming, Circular channel	96
6.19	BER vs. E_b/N_0 of MSINR based Beamformer-Rake when the user distribution is <i>non-uniform</i> . 10 interferers, M-CFA beamforming, Circular channel	96
6.20	BER vs. E_b/N_0 of MSINR based Beamformer-Rake when the user distribution is <i>uniform</i> . 5 interferers, M-CFA beamforming, Elliptical channel	97
6.21	BER vs. E_b/N_0 of MSINR based Beamformer-Rake when the user distribution is <i>non-uniform</i> . 5 interferers, M-CFA beamforming, Elliptical channel	97
6.22	BER vs. E_b/N_0 of MSINR based Beamformer-Rake when the user distribution is <i>uniform</i> . 10 interferers, M-CFA beamforming, Elliptical channel	97
6.23	BER vs. E_b/N_0 of MSINR based Beamformer-Rake when the user distribution is <i>non-uniform</i> . 10 interferers, M-CFA beamforming, Elliptical channel	97
6.24	BER vs. E_b/N_0 comparison between CGA & M-CFA. Beamformer-Rake receiver, <i>uniform</i> user distribution. 5 interferers, Circular channel	98
6.25	BER vs. E_b/N_0 comparison between CGA & M-CFA. Beamformer-Rake receiver, <i>non-uniform</i> user distribution. 5 interferers, Circular channel	98
6.26	BER vs. E_b/N_0 comparison between CGA & M-CFA. Beamformer-Rake receiver, <i>uniform</i> user distribution. 10 interferers, Circular channel	98
6.27	BER vs. E_b/N_0 comparison between CGA & M-CFA. Beamformer-Rake receiver, <i>non-uniform</i> user distribution. 5 interferers, Circular channel	98
6.28	BER vs. E_b/N_0 comparison between CGA & M-CFA. Beamformer-Rake receiver, <i>uniform</i> user distribution. 5 interferers, Elliptical channel	99
6.29	BER vs. E_b/N_0 comparison between CGA & M-CFA. Beamformer-Rake receiver, <i>non-uniform</i> user distribution. 5 interferers, Elliptical channel	99
6.30	BER vs. E_b/N_0 comparison between CGA & M-CFA. Beamformer-Rake receiver, <i>uniform</i> user distribution. 10 interferers, Elliptical channel	99
6.31	BER vs. E_b/N_0 comparison between CGA & M-CFA. Beamformer-Rake receiver, <i>non-uniform</i> user distribution. 5 interferers, Elliptical channel	99
6.32	Performance comparison of different algorithms to solve GE. Beamformer-Rake, 5 interferers, CGA beamforming, Circular channel	100
6.33	Performance comparison of different algorithms to solve GE. Beamformer-Rake, 10 interferers, CGA beamforming, Circular channel	100
6.34	Performance comparison of different algorithms to solve GE. Beamformer-Rake, 5 interferers, CGA beamforming, Elliptical channel	100
6.35	Performance comparison of different algorithms to solve GE. Beamformer-Rake, 5 interferers, CGA beamforming, Elliptical channel	100
6.36	Performance comparison between MSNR & MSINR beamforming. Beamformer-Rake, 5 interferers, uniform user distribution, Circular channel	102
6.37	Performance comparison between MSNR & MSINR beamforming. Beamformer-Rake, 5 interferers, non-uniform user distribution, Circular channel	102
6.38	Performance comparison between MSNR & MSINR beamforming. Beamformer-Rake, 10 interferers, uniform user distribution, Circular channel	102
6.39	Performance comparison between MSNR & MSINR beamforming. Beamformer-Rake, 10 interferers, non-uniform user distribution, Circular channel	102
6.40	Performance comparison between MSNR & MSINR beamforming. Beamformer-Rake, 5 interferers, uniform user distribution, Elliptical channel	103
6.41	Performance comparison between MSNR & MSINR beamforming. Beamformer-Rake,	

5 interferers, non-uniform user distribution, Elliptical channel	103
6.42 Performance comparison between MSNR & MSINR beamforming. Beamformer-Rake, 10 interferers, uniform user distribution, Elliptical channel	103
6.43 Performance comparison between MSNR & MSINR beamforming. Beamformer-Rake, 10 interferers, non-uniform user distribution, Elliptical channel	103
7.1 MMSE based Beamformer-Rake receiver for WCDMA uplink	110
7.2 Performance comparison between MMSE and MSINR based Beamformer-Rake receivers in terms of BER vs. E_b/N_0 . There are 5 interferers. The user distribution is uniform. The multipath environment is defined by the vehicular channel	113
7.3 Performance comparison between MMSE and MSINR based Beamformer-Rake receivers in terms of BER vs. E_b/N_0 . There are 5 interferers. The user distribution is non-uniform. The multipath environment is defined by the vehicular channel	113
7.4 Performance comparison between MMSE and MSINR based Beamformer-Rake receivers in terms of BER vs. E_b/N_0 . There are 10 interferers. The user distribution is uniform. The multipath environment is defined by the vehicular channel	114
7.5 Performance comparison between MMSE and MSINR based Beamformer-Rake receivers in terms of BER vs. E_b/N_0 . There are 10 interferers. The user distribution is non-uniform. The multipath environment is defined by the vehicular channel	114
7.6 Spatial Aliasing vs. Diversity Gain. There are 5 interferers. The user distribution is uniform. The multipath environment is defined by the vehicular channel	116
7.7 Spatial Aliasing vs. Diversity Gain. There are 5 interferers. The user distribution is non-uniform. The multipath environment is defined by the vehicular channel	116
7.8 Spatial Aliasing vs. Diversity Gain. There are 10 interferers. The user distribution is uniform. The multipath environment is defined by the vehicular channel	117
7.9 Spatial Aliasing vs. Diversity Gain. There are 10 interferers. The user distribution is non-uniform. The multipath environment is defined by the vehicular channel	117
8.1 A simple OFDM transmitter	120
8.2 16QAM signal constellation diagram for a 64-sub-carrier OFDM system with a two-ray multipath channel, the second ray being 6 dB lower than the first one. No equalization is performed	123
8.3 16QAM signal constellation diagram for a 64-sub-carrier OFDM system with a two-ray multipath channel, the second ray being 6 dB lower than the first one. One tap equalization is at the output of FFT for individual sub-carriers	124
8.4 Proposed beamforming scheme	125
8.5 Frame structure of the OFDM system	126
8.6 MSE in AWGN environment for sub-carrier no.1	128
8.7 Beam pattern for various sub-carriers	129
8.8 BER in AWGN environment	130
8.9 Magnitude response of the COST-207 TU channel model	131
8.10 Magnitude response of the IMT2000 Indoor A channel model	131
8.11 Performance of the sub-band beamforming scheme in COST-207 TU channel condition	132

8.12	Performance of the sub-band beamforming scheme in IMT2000 Indoor A channel condition	133
8.13	VIPER measurement system	134
8.14	Layout of the VIPER outdoor measurement	135
8.15a	Magnitude response of the vector channel of the desired user for snapshot 6	136
8.15b	Magnitude response of the vector channel of the desired user for snapshot 25	136
8.16	Performance of the beamforming scheme for various sub-band sizes in the measured channel	137
8.17	Comparison of performance for RLS and LMS	138
9.1	Flowchart of the alternate linear Lagrange multiplier method	143
9.2	MSE for the linear Lagrange multiplier methods. Linear Lagrange I is the simplified alternative algorithm and Linear Lagrange II is the simplified original algorithm. The SNR = 10 dB, $\mu = 0.001$	144
9.3	Tracking Property of the proposed linear adaptive algorithm. The AOA changes by 0.1° at each snapshot. SNR = 0 dB, SIR = 6.99 dB, $f = 0.75$, $\mu = 0.03$	145
9.4	Flowchart of the linear power method	147
9.5	Flowchart of the alternate linear generalized Lagrange multiplier method	148
A.1	Sample beam pattern for the simple null-steering scheme	152
A.2	Sample beam pattern for the MSINR scheme	153
B.1	MSINR based Beamformer-Rake receiver for WCDMA uplink. The weight vector is computed based on DPCCH only	154
B.2	MSINR based Beamformer-Rake receiver for WCDMA uplink. CGA is utilized for MSINR beamforming The weight vector is computed based on DPCCH only	155
B.3	MSINR based Beamformer-Rake receiver for WCDMA uplink. Modified CFA is utilized for MSINR beamforming The weight vector is computed based on DPCCH only	155
C.1	Structure I 2-D diversity combiner	157
C.2	Structure II 2-D diversity combiner	158

List of Tables

4.1	3G data rate requirements	40
4.2	WCDMA key technical characteristics	43
4.3	Uplink data rate vs. spreading factor	46
4.4	Mapping of $z_v(n)$	52
4.5	Parameters of WCDMA spreading and modulation at the uplink	52
5.1	Computational complexity of algorithms to solve the SE	69
5.2	Circular channel parameters	71
5.3	Elliptical channel parameters	71
5.4	Simulation parameters for MSNR based beamforming	71
6.1	MSINR based Beamformer-Rake details	93
7.1	Vehicular channel	112
7.2	Simulation parameters for MSINR vs. MMSE beamforming criterion for Beamformer-Rake.....	112
7.3	Simulation parameters for spatial aliasing vs. diversity gain	115
7.4	Vehicular channel	115
8.1	Output SIR at AWGN environment	129
8.2	COST-207 TU channel	131
8.3	Parameters of vector channel model	131
8.4	IMT2000 Indoor A channel	131

Chapter 1

Introduction

1.1 Introduction

A Beamformer-Rake [1] receiver is a concatenation of a beamformer [2] and a Rake receiver [3], [4]. This provides a higher degree of freedom since the signal can be processed in both the temporal and the spatial domains. The signal processing of the Beamformer-Rake combats against the Multiple Access Interference (MAI) and mitigates fading. Wireless service providers throughout the world are working to introduce the third generation (3G) [5] cellular service that will provide higher data rates and better spectral efficiency. Wideband Code Division Multiple Access (WCDMA) [6], [7], [8], [9], [10] has been widely accepted as one of the air interfaces for 3G. A Beamformer-Rake receiver can be an effective solution to provide the receivers enhanced capabilities needed to achieve the required performance of a WCDMA system. One of the objectives of this research is to develop and study different Beamformer-Rake receiver structures that are suitable for WCDMA systems and investigate their performance under different operating conditions. The majority of the beamforming techniques employed for performing the spatial processing at the Beamformer-Rake receiver in this work are based on solving the *Eigenvalue Problem* [11]. The key objective of this dissertation is to investigate different computationally simple algorithms for solving the Eigenvalue problem and at the same time propose and develop additional low-complexity innovative techniques. Orthogonal Frequency Division Multiplexing (OFDM) [12] is a multi-carrier technique that has recently received considerable attention for high speed wireless communication. We propose a simple pilot symbol assisted frequency domain beamforming technique for OFDM receivers and investigate its performance for different channel conditions.

The dissertation is organized as follows. The rest of this chapter is devoted to relevant literature survey. Chapter 2 introduces the fundamental concept of spatial and temporal processing and the idea of Beamformer-Rake receivers. Chapter 3 is devoted towards different beamforming criteria that can be employed in a CDMA based cellular environment and an OFDM system. Chapter 4 describes the physical layer of the WCDMA system as well as the current status of the deployment of 3G systems around the world.

Chapter 5 presents different adaptive algorithms to solve the Simple Eigenvalue problem (SE) [11] resulting from the Maximum Signal to Noise Ratio (MSNR) [13] criterion based beamforming. We develop a Beamformer-Rake receiver for the WCDMA system that utilizes MSNR based Eigen-Beamforming for spatial processing. Simulations results that show the performance of the Beamformer-Rake receiver as well as compare the different adaptive algorithms are presented.

The different techniques to perform beamforming based on the Maximum Signal to Interference and Noise Ratio (MSINR) [2] criterion in a Code Division Multiple Access (CDMA) system is introduced in Chapter 6. This chapter also describes several adaptive algorithms to implement the Eigen-Beamforming. The Adaptive Matrix Inversion (AMI) method, a new adaptive algorithm to solve the Generalized Eigenvalue problem (GE) [11] is proposed. We also develop several Beamformer-Rake receivers based on MSINR Eigen-Beamforming for the WCDMA system. Simulation results that compare the performance of the different receivers are presented. The performance of the proposed AMI method is also compared with other existing algorithms.

Chapter 7 is devoted to the Pilot Symbol Assisted (PSA) [14], [15] Beamformer-Rake receiver. Simulation results that compare this receiver with MSINR based Beamformer-Rake receiver are presented. This chapter concludes with a discussion on the merits of spatial diversity gain [13]. A PSA based frequency domain beamforming technique for the OFDM system is proposed in Chapter 8. The concept of sub-band beamforming scheme is demonstrated for different multipath propagation conditions. We also employ measured vector channels to investigate the performance of this scheme. Chapter 9 concludes this dissertation. A brief summary of the contribution and future direction of the research is outlined. We point out further developments of the solution to the Eigenvalue problem. A list of publications based on the research presented in this dissertation is also provided.

There are three appendices at the end of the report. Appendix A discusses the concept of beamforming in a flat fading channel that consists of components with multiple distinct Angle of Arrivals [2]. This also discusses the significance (or the lack of it) of beam pattern [2] in such a scenario. Appendix B provides block diagram of Beamformer-Rake receivers that employ the control channel signals only to compute the weight vectors. Appendix C discusses 2-D receivers based on conventional diversity combining [16]. We introduce two different structures for such receivers and establish their equivalence with the help of analysis.

1.2 Literature Survey

The term adaptive antenna has been used in the literature since the late 50's and early 60's [17], [18], [19], [20], [21], [22]. A multitude of different adaptive antenna techniques have been proposed in the last four decades or so. In this section we present a literature survey of adaptive antennas. Vector channel models [16] are required to investigate the performance of a receiver equipped with adaptive antenna processing. Therefore we also provide a literature survey on the topic of vector channels. This section concludes with a survey of different aspects of the OFDM [12] system including the adaptive antenna array techniques that are suitable for OFDM.

A null-steering beamformer is used to cancel a plane wave coming from a particular direction by placing a null at the Angle of Arrival (AOA) of that plane wave in the beam pattern. One of the earliest schemes [23] proposed to achieve this by estimating the signal arriving from a known direction by steering a conventional beam in the direction of the source and then subtracting the output of this from each antenna element. Although this process is very effective in canceling strong interference, the scheme becomes unwieldy as the number of interfering signals grows. Therefore null steering based on constraints was proposed in [24]. The basic idea is to form a beam with unity gain in the direction of the desired user and nulls in the direction of the interferers [24], [25], [26] (see Section 2.3.1 for an example of this scheme). This beamformer does not minimize the uncorrelated noise at the output of the beamformer. This was achieved in [27]. Null steering schemes towards known locations have been also shown to be effective in a transmit beamforming array to minimize the interference towards other co-channel mobiles in a cellular system [28].

The null-steering schemes do not maximize the output Signal to Noise Ratio (SNR). A beamformer that maximizes the SNR and at the same time tends to minimize the interference was therefore proposed by various researchers [29]-[32]. This beamformer termed as the optimal beamformer maximizes the Signal to Interference and Noise Ratio (SINR) at the output of the beamformer. The optimum beamforming technique can be attributed to [33] whose early work by finding the Maximum Likelihood (ML) estimate of the power of the desired signal led to its development. The optimum beamformer is often time termed as the Minimum Variance Distortionless Response (MVDR) Beamformer. In mobile communications literature, the optimal beamformer is often referred to as the optimal combiner. Discussion on the use of the optimal combiner to cancel interferences and to improve the performance of mobile communications systems can be found in [34]-[37].

A beamformer that utilizes a reference signal to calculate the weights was proposed in [17]. The beamformer utilizes the Wiener solution arising from the Minimum Mean Squared Error (MMSE) criterion. Further analysis of this technique can be found in [38], [39], [40], and [32]. This scheme was also shown to be effective in acquiring a weak signal in the presence of strong jammers in [41] (see an example of this in Section 3.5). The MMSE beamformer was compared to an MVDR beamformer in [42]. Similar study in a mobile communication environment based on simulation was performed in [43]. The study of reference based beamforming for mobile communications system have also been reported in [44]-[47].

Beam-space processing is a two stage scheme where the first stage takes the array signals as input and produces a set of multiple outputs, which are then weighted and combined to produce the array output. Since beam-space beamforming is not very closely related to the research work presented in this dissertation, only references [39, 48-55] are provided here for interested readers. As the signal bandwidth increases and the narrowband assumption no longer holds, a Tapped Delay Line (TDL) structure or a lattice structure can be an effective solution. We will just present some pertinent references [56-63] here. The application of TDL structure for broadband beamforming in mobile communication environment has been reported in [44], [64], [65].

In a frequency domain beamformer, signals from each element are transformed into the frequency domain using the FFT and each frequency bin is processed by a narrow-band processor structure. In a way this is similar to the beamforming scheme we propose for the OFDM system in Chapter 8. The frequency domain beamformer can be suboptimal if the signals in different frequency bin are independent. Trade-offs and comparison with time domain beamforming have been presented in [66]. The advantage of the frequency-domain method for bearing estimation is discussed in [67], and the advantage for correlated data is considered in [68].

Estimation of Direction of Arrival (DOA) is one of the major branches of adaptive beamforming. Spectral estimation technique is one of the oldest methods for DOA estimation. Bartlett method is probably the most elementary method for spectral estimation. This method involves weighting the signals from all the antenna elements and finding the average power at different directions. The application of the Bartlett method to the mobile communications environment has been investigated in [69]. Finding the ML estimate of the direction can improve the resolution of the direction finding technique [70] over the Bartlett method. The application of linear prediction [71], Maximum Entropy Method (MEM) [72] and Maximum Log-likelihood Method (MLM) [70] has also been investigated.

The DOA estimate techniques based on the Eigenstructure methods are to some extent similar in principle to the beamforming techniques employed in our research. The basic idea is to utilize the structure of the received signal covariance matrix which can be partitioned into two orthogonal subspaces corresponding to the directional signal and the noise. The Eigenstructure methods try to find an eigenvector that is in the noise subspace and then search for directions for which the steering vector is orthogonal to this eigenvector. The Eigenstructure methods have been investigated in details in [73-81]. The MUSIC method and its several variations are probably the most investigated of the Eigenstructure based DOA estimate techniques. The spectral MUSIC estimates the noise space by employing the Eigen-decomposition of the estimated array covariance matrix [82] or the singular value decomposition of the data covariance matrix [83]. The application of MUSIC for mobile communications has been investigated in [84]. A variation of MUSIC termed as the Root-MUSIC is applicable to Uniform Linear Array (ULA) [85] and has better performance compared to the MUSIC. There are other variations of the MUSIC like the constrained MUSIC [83] and beam-space MUSIC [86], [87]. There have been also investigations of the min-Norm method [88], [89] and the CLOSEST method [90].

ESPRIT [91] is a computationally efficient and robust method of DOA estimation that employs two identical arrays so that the second element of each pair is displaced by the same distance and in the same direction relative to the first element. Different variations of the ESPRIT algorithm can be found in [92-99]. The application of ESPRIT in estimating the DOA at the reverse link of CDMA cellular system has been reported in [100]. WSF is another DOA estimation method that has been widely investigated [101], [102].

The optimal beamforming techniques mentioned a little earlier requires the estimate of the inverse interference and noise covariance matrix. The Sample Matrix Inversion (SMI) makes a running estimate of the matrix and utilizes matrix inversion lemma to get a simple estimate of the inverse. The SMI method is well described in [30], [103], and [104].

The Least Mean Squared (LMS) algorithm [105] is the most computationally simple algorithm to find the weight vector that satisfies the MMSE beamforming criterion. Ever since the publication of their seminal paper by Windrow *et. al* [17], the LMS has been the subject of numerous research investigations. There are different variations of the LMS algorithm, the unconstrained LMS [106-112], sign algorithm LMS [113], [114], normalized LMS [115-118] and the constrained LMS [119-

[121] are to name a few. The LMS algorithm is not a very robust algorithm in a fast fading channel. This fact was demonstrated in [122] in the context of spatial equalization.

The convergence of LMS is very slow when the signal covariance matrix (the pertinent matrix in the Wiener solution) has a large spread in its Eigenvalue. The recursive Least Square (RLS) algorithm [105] avoids this at the cost of higher computational complexity. The details of RLS algorithm and its employment in adaptive beamforming can be found in [123-130]. Simulation study has shown the RLS algorithm to be superior to the LMS and the SMI algorithms for flat fading under mobile communications environment [131]. The capacity gain with an RLS based adaptive array at the reverse link of the CDMA system has been reported in [132].

The Constant Modulus Algorithm (CMA) is a gradient based blind adaptive technique. The CMA is widely attributed to [133] and [134]. The main disadvantage of this method is its slow convergence. Faster converging CMA namely the Orthogonalized CMA [135] and Least Squares CMA (LSCMA) [136], [137] have been proposed in the literature. The development and analysis of CMA is described in detail in [138].

Adaptive beamforming based on the optimal or MSINR criterion can lead to a Generalized Eigenvalue problem (GE) [1]. The Generalized Power Method (GPM) [11] is probably the most common method to solve the GE. However the high computational complexity of the GPM makes it unsuitable for real time implementation. Computationally simple algorithms like the Generalized Lagrange Multiplier method (GLM) [139] and the Adaptive Inversion Method [140], [141] have been proposed. In Chapter 6 we will derive the AMI method and investigate its performance.

The conventional (MSNR criterion based) beamforming can be implemented by solving for a Simple Eigenvalue problem (SE) [142]. The Power method [11] can be used to solve the SE. The Conjugate Gradient Method has been proposed to implement the MSNR based beamforming [142-144]. The Lagrange multiplier method has also been proposed as a low complexity solution to the SE [145]. The power method has been simplified in [146] to reduce the computational complexity. An alternate method applying the Lagrange multiplier to solve the GE has been proposed in [147]. A similar technique has been proposed in [148] to solve the SE.

A Rake receiver is used in a CDMA system to exploit the multipath diversity. Combining the adaptive antenna array with the Rake structure, a Beamformer-Rake receiver was proposed [36],

[149]. This receiver utilizes the Code Filtering Approach (CFA) [1] to formulate the GE required to perform MSINR based beamforming. The system capacity improvement for this receiver is analyzed in [37], [150], and [151]. Kwon *et. al*, [139] proposed an alternative technique to the CFA to form the Generalized Eigenvalue problem. Another alternative to CFA was proposed by [152]. This method termed as the Code Gated Algorithm (CGA) employs a combination of high-pass and low-pass filter and form the GE with the signals at the output of these filters. A Beamformer-Rake receiver that utilizes the LMS algorithm to perform MMSE based beamforming was proposed in [14]. A detailed study of this structure for the WCDMA system can be found in [15]. A thorough analysis of a Beamformer-Rake receiver that performs optimal and conventional combining in both the spatial and temporal domain can be found in [153]. Performance of the receiver at the uplink of a WCDMA system is also reported in that study.

It is essential to have vector channel models [16] in order to investigate the performance of a receiver equipped with spatio-temporal processing. Vector channel models describe the temporal or spectral parameters like power delay profile, Doppler spread as well as spatial parameters like AOA distribution, angle spread. Geometrically based vector channel models define a region in space where the objects are distributed and the distribution of these objects. The objects are responsible for scattering and/or reflection. Typically a multipath signal is viewed as a single bounce from the transmitter to the receiver. Therefore these models are often termed as Geometrically Based Single Bounce (GBSB) models [154], [155]. Circular channel model [156-159] is a popular model to describe the macro-cellular environment. In a circular channel model the transmitter is surrounded by local scatterers that are distributed within a circle centered on the transmitter. Typical urban and bad urban models are special cases of the circular channel model [160-162]. The elliptical channel model [16], [154], [155] is a typical GBSB model to describe the microcellular environment. The objects are uniformly distributed within an ellipse and the transmitter and the receiver are located at the foci of the ellipse. The maximum delay defines the boundary of the ellipse. The elliptical model provides a much greater angle spread than the previously mentioned models. There are other geometrical models that can be found in the literature [163], [164]. There is also a separate class of vector channel models known as the statistical vector channel model that can be found in the literature [156], [161], [165]- [168]. A special statistical channel model based on the Jakes' model [156], [168] can be employed to generate the complex coefficient of a resolvable multipath as a summation of a number of unresolvable components. This model provides very good control over the angle spread of the unresolvable components.

The concept of frequency division multiplexing for multi-carrier transmission can be traced back to the 60s [169]. The patent for OFDM was issued in the beginning of 1970 [170]. In [171], it was demonstrated that the Discrete Fourier Transform (DFT) can be applied for efficient modulation and demodulation of an OFDM system. OFDM was studied during the 80s for high speed modems [172]. The research on OFDM gained momentum in the 90s. The loss of orthogonality due to Doppler spread has been analyzed in [173], [174]. The effects of Inter Carrier Interference (ICI) and Inter Symbol Interference (ISI) and techniques to combat these detrimental phenomena have been investigated in [175-180]. An adaptive antenna array has been proposed to increase the capacity of an OFDM based system [181], [182]. Co-channel interference (CCI) cancellation with the aid of an MMSE based adaptive antenna array has been demonstrated in [183]. Combined diversity and beamforming have been shown to be effective to combat ICI and CCI in a slow varying channel [184]. Time domain beamforming for an OFDM receiver based on LMS driven MMSE beamforming has been proposed in [185]. MMSE based adaptive antenna has also been proposed [186] to suppress the delayed signal and Doppler shifted signal. The concept of sub-band beamforming for OFDM system has been put forward independently by [187] and [188].

Chapter 2

Fundamental Concepts of Space Time Processing

2.1 Introduction

The capacity of a cellular system is limited by two different phenomena, namely multipath fading and multiple access interference (MAI). A Two Dimensional (2-D) receiver [1], [15] combats both of these by processing the signal both in the spatial and temporal domain. An ideal 2-D receiver would perform joint space-time processing. But this will provide optimum performance at the cost of high computational complexity. In this chapter we will introduce the idea of a computationally simpler technique termed as a Concatenated Space Time Processor (CSTP) [13].

Adaptive antenna arrays can be used to combat either fading or MAI with the employment of spatial processing only. Since the users of a cellular system transmit from different spatial locations, the received signal from each user has a unique spatial signature associated with it. Adaptive antenna arrays [2] can exploit this spatial property of the signal to reduce the MAI by performing beamforming. The beamformer may be a very practical solution to improve the performance of a Code Division Multiple Access (CDMA) system which is designed to operate in co-channel interference. The capacity of a CDMA system can be effectively increased with a small reduction in the co-channel interference levels. This is a marked contrast from Time Division Multiple Access (TDMA) systems which do not benefit as much from a small reduction in interference [138]. Adaptive antenna array can also attain diversity gain [16] if the received signals at the different antenna elements are relatively uncorrelated. The spatial diversity gain can help mitigate multipath fading. The opportunity to employ temporal diversity processing is an inherent advantage of a CDMA system. In a CDMA system, Rake [3] receivers are used to combat the fading by processing the different time resolvable copies of the received signal in the temporal domain. The CSTP cascades an antenna array with a Rake receiver to take advantage of both the antenna array and a Rake receiver. In a CSTP the output of a spatial processor is fed into a succeeding temporal processor or it can be the other way around [15].

In this chapter we will discuss a special class of CSTP popularly known as a Beamformer-Rake [1]. A Beamformer-Rake is a concatenation of a beamformer with a temporal Rake. We will employ this

structure in most of the cases throughout this report. In Appendix C we will briefly discuss 2-D diversity combiner which is a concatenation of a conventional spatial diversity combiner [16] with a Rake structure. This chapter begins with a discussion on antenna arrays and the fundamental concepts of beamforming. The description of temporal processing in the form of Rake receiver comes next. We conclude with a discussion on Beamformer-Rake and the potential of performance improvement with the application of such receiver.

2.2 Antenna Array

An antenna array consists of a set of antenna elements that are spatially distributed at known locations with reference to a common fixed point [189], [190]. The antenna elements can be arranged in various geometries. Some of the popular geometrical configurations are Linear, Circular and Planar. In a linear array, the centers of the elements of the array are aligned along a straight line. In case of a circular array, the centers of the elements lie on a circle. For a planar array configuration, the centers of the array lie on a single plane. Both the linear and circular array are obviously special cases of the planar array.

The radiation pattern of an array is determined by the radiation pattern of the individual elements, their orientation and relative positions in space, and the amplitude and the phase of the feeding current [189]. If each element of the array is an isotropic point source, the radiation pattern of the array will depend solely on the geometry and feeding current of the array. In that case the radiation pattern is commonly known as the *array factor*. If each of the elements of the array is similar but non-isotropic, by the principle of pattern multiplication [2], the radiation pattern can be computed as a product of the array factor and the individual element pattern [191].

2.2.1 Uniform Linear Array

If the spacing between the elements of a linear array is equal, it is known as Uniform Linear Array (ULA). Figure 2.1 shows an N element ULA. The spacing between the array elements is d and a plane wave arrives at the array from a direction θ off the array *broadside*. The array broadside is perpendicular to the line containing the center of the elements. The angle θ measured clockwise from the array broadside is called Direction of Arrival (DOA) or the Angle of Arrival (AOA) of the received signal.

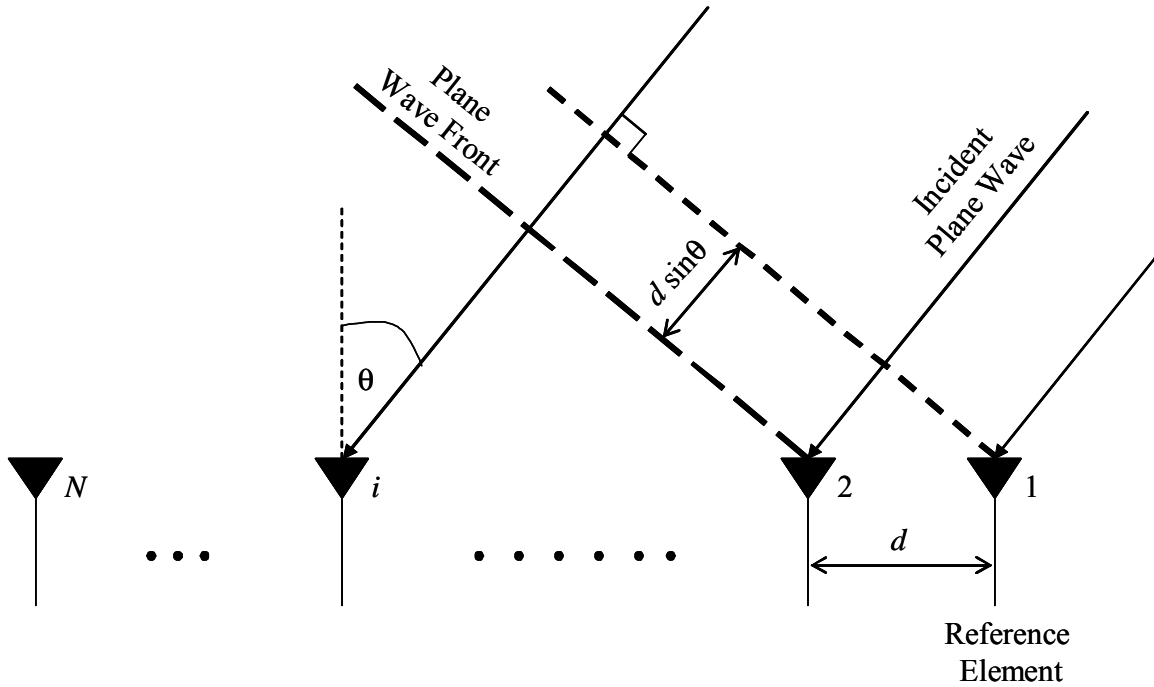


Figure 2.1: Plane wave incident on a ULA with an AOA of θ

The received signal at the first element can be written as [189]

$$\tilde{x}_1(t) = A_1(t) \cos\{2\pi f_c t + \gamma(t) + \beta\}, \quad (2.1)$$

where,

$A_1(t)$ is the amplitude of the signal

f_c is the carrier frequency

$\gamma(t)$ is the information

β is the random phase

Note that the complex envelope of the signal at the first element is given by

$$x_1(t) = A_1(t) e^{j\{\gamma(t) + \beta\}} \quad (2.2)$$

Let us assume that the signals originate far away from the array and the plane wave associated with the signal advances through a non-dispersive medium that only introduces propagation delay. Under these circumstances, the signal at any other element can be represented by a time advanced or time-delayed version of the signal at the first element. Referring to Figure 2.1, the wave front impinging on the first element travels an additional $d \sin \theta$ distance to arrive at the second element. The time delay due to this additional propagation distance is given by

$$\tau = \frac{d \sin \theta}{c}, \quad (2.3)$$

where c is the velocity of light.

So the received signal at the second element is given by

$$\begin{aligned} \tilde{x}_2(t) &= \tilde{x}_1(t - \tau) \\ &= A_1(t - \tau) \cos\{2\pi f_c(t - \tau) + \gamma(t - \tau) + \beta\} \end{aligned} \quad (2.4)$$

If the carrier frequency f_c is large compared to the bandwidth of the impinging signal, the signal may be treated as quasi-static during time intervals of order τ and we can write

$$\tilde{x}_2(t) = A(t) \cos\{2\pi f_c t - 2\pi f_c \tau + \gamma(t) + \beta\} \quad (2.5)$$

Thus the complex envelope of the signal at the second antenna can be written as

$$\begin{aligned} x_2(t) &= A(t) e^{j\{-2\pi f_c \tau + \gamma(t) + \beta\}} \\ &= x_1(t) e^{j\{-2\pi f_c \tau\}} \end{aligned} \quad (2.6)$$

It is thus evident from Equation 2.6 that the time delay of the signal can now be represented by a phase shift. From Equations 2.3 and 2.6, we can write

$$\begin{aligned} x_2(t) &= x_1(t) e^{j\left\{-2\pi f_c \frac{d \sin \theta}{c}\right\}} \\ &= x_1(t) e^{-j\left\{2\pi \frac{d}{\lambda} \sin \theta\right\}} \end{aligned} \quad (2.7)$$

Therefore the complex envelope of the received signal at the i^{th} ($i = 1, 2, \dots, N$) element can be expressed as

$$x_i(t) = x_1(t) e^{-j\left\{2\pi \frac{d}{\lambda} (i-1) \sin \theta\right\}} \quad (2.8)$$

Let us define a column vector whose each element contains the received signal at the corresponding array element. Therefore the received signal vector is defined as

$$\underline{x}(t) = [x_1(t) \quad x_2(t) \quad \dots \quad x_N(t)]^T, \quad (2.9)$$

where T represents transpose.

We can also define

$$\underline{a}(\theta) = \left[1 \quad e^{-j\left\{2\pi \frac{d}{\lambda} \sin \theta\right\}} \quad \dots \quad e^{-j\left\{2\pi \frac{d}{\lambda} (N-1) \sin \theta\right\}} \right]^T \quad (2.10)$$

$\underline{a}(\theta)$ is known as the array response vector or the steering vector of an ULA. The array response vector is a function of the AOA, individual element response, the array geometry and the signal frequency. We will assume that for the range of operating carrier frequency, the array response vector does not change. Since we have already fixed the geometry (Uniform Linear Array) and the individual element response (identical isotropic elements), the array response vector is a function of the AOA only. The received signal vector can now be written in a compact vector form as

$$\underline{x}(t) = \underline{a}(\theta)x(t) \quad (2.11)$$

We would like to point out that so far we have assumed that the bandwidth of the impinging signal is much smaller than the reciprocal of the propagation time across the array. This assumption, commonly known as the *narrowband assumption* [2] for the signal, made it possible to represent the propagation delay within the elements of the array by phase shifts in the signal. Although the narrowband model is exact for sinusoidal signals, this is usually a good approximation for a situation where the bandwidth of the signal is very small compared to the inverse of the propagation time across the array. Any deviation from the narrowband model is detrimental to the performance of a narrowband beamformer usually manifesting as a limit in the ability to null interferers [138]. In such a scenario, a wideband beamformer [2], [189] must be used (see section 1.2 for more references). Throughout this research we will assume that the WCDMA signal satisfies the narrowband assumption. We provide with a justification next.

The delay the wave front experiences to propagate from the first element to the N^{th} element is given by

$$\tau_{\max} = \frac{(N-1)d \sin \theta}{c} \quad (2.12)$$

If the spacing between the elements is half the carrier wavelength,

$$\begin{aligned} \tau_{\max} &= \frac{(N-1)\frac{\lambda}{2}}{c} ; \quad \max(\sin \theta) = 1 \\ &= \frac{(N-1)\frac{c}{2f_c}}{c} = \frac{(N-1)}{2f_c} \end{aligned} \quad (2.13)$$

If there are 4 elements and the carrier frequency is 2 GHz, $\tau_{\max} = \frac{3}{2 \times 2000 \times 10^6}$ seconds.

So for the WCDMA signal which has a bandwidth of 5 MHz, the ratio of the reciprocal of the maximum delay and the signal bandwidth is given by

$$\begin{aligned}\chi_{\max} &= \frac{3 \times 5 \times 10^6}{2 \times 2000 \times 10^6} \\ &= 0.0037\end{aligned}$$

Therefore the narrowband assumption holds for WCDMA signal.

2.3 Beamformer

Beamforming is the most common spatial processing technique that an antenna array can utilize. In a cellular system, the desired and the interfering signals originate from different spatial locations. This spatial separation is exploited by a beamformer which can be regarded as a spatial filter separating the desired signal from the interference. The signals from different antenna elements are weighted and summed to “optimize” the quality of the signal. Figure 2.2 illustrates the idea of a narrowband [2], [189] beamformer. With the proper selection of beamforming criterion, it is possible to *point* the beam towards the direction of the desired user and/or place nulls in the direction of the interferers.

If we have K total signals with distinct Angle of Arrival (AOA) impinging on an antenna array consisting of N elements, the received signal vector can be written as

$$\underline{x}(t) = \sum_{i=1}^K s_i(t) \underline{a}(\theta_i) + \underline{n}(t), \quad (2.14)$$

where $s_i(t)$ is the i^{th} signal with an AOA of θ_i , $\underline{a}(\theta_i)$ is the $N \times 1$ antenna response vector for the AOA of θ_i and $\underline{n}(t)$ is the thermal noise vector. The output of the antenna array is given by

$$y(t) = \underline{w}^H(t) \underline{x}(t) \quad (2.15)$$

Here $\underline{w} = [w_1 \ w_2 \ \dots \ w_N]^T$ is the $N \times 1$ weight vector and H denotes Hermitian transpose. The weight vector is chosen to optimize some beamforming criterion. Popular adaptive beamforming techniques include Minimum Mean Square Error (MMSE) [2], Maximum Signal to Interference and Noise Ratio (MSINR) [2], Maximum Signal to Noise Ratio (MSNR) [192], Constant Modulus (CMA) [138], Maximum Likelihood (ML) [2], etc. We will discuss some of these beamforming criteria in Chapter 3.

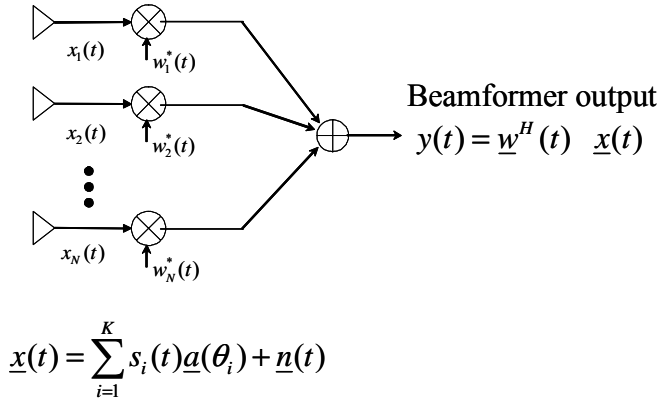


Figure 2.2a: Beamformer principle

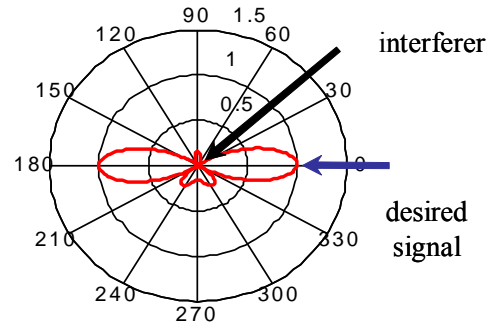


Figure 2.2b: Typical array gain pattern

2.3.1 Example of a Simple Beamforming (Null-Steering) with ULA

We will use a very simple example to demonstrate the principle of beamforming. Let us assume that the desired users signal is coming from the broadside of the ULA so that its AOA is 0° . Let us also assume that there is an interfering signal being received with an AOA of 45° . The array response vector for the desired user is given by

$$\underline{a}_{desired} = \underline{a}(0) = \begin{bmatrix} 1 \\ 1 \end{bmatrix}. \quad (2.16)$$

Similarly, the array response vector of the interferer is given by

$$\underline{a}_{int} = \underline{a}\left(\frac{\pi}{4}\right) = \begin{bmatrix} 1 \\ e^{-j2\pi \times \frac{1}{2} \sin\left(\frac{\pi}{4}\right)} \end{bmatrix} = \begin{bmatrix} 1 \\ e^{-j\frac{\pi}{\sqrt{2}}} \end{bmatrix} = \begin{bmatrix} 1 \\ -0.6057 - j0.7957 \end{bmatrix} \quad (2.17)$$

A beamformer will try to increase the gain in the direction of the desired user and at the same time will try to minimize the gain in the direction of the interferer. So an *ideal weight vector* will satisfy the following criterion:

$$\begin{aligned} \underline{w}^H \underline{a}_{desired} &= 1 \\ \underline{w}^H \underline{a}_{int} &= 0 \end{aligned} \quad (2.18)$$

We can solve Equation 2.18 to get

$$\underline{w} = \begin{bmatrix} 0.5 - j0.2478 \\ 0.5 + j0.2478 \end{bmatrix}.$$

The beamformer response (analogous to frequency response of an FIR filter) to a particular AOA θ is given by

$$g(\theta) = \underline{w}^H \underline{a}(\theta) \quad (2.19)$$

The beam pattern is defined as the magnitude of $g(\theta)$, i.e.

$$G(\theta) = |g(\theta)| \quad (2.20)$$

The beam pattern which describes the array gain versus AOA for a particular weight vector is in many ways analogous to the magnitude response of an FIR filter. The beam pattern for the above example is illustrated in Figure 2.3. As we can clearly observe, the beamformer has unity gain for the desired user and a null at the direction of the interferer. Since the beamformer can place nulls in the direction of the interfering user, it is often time referred to as null steering beamformer (see section 1.2) in the literature. Note that this elementary beamforming will work only if the total number of discrete signals is equal to or less than the number of elements. In fact a beamformer with N elements can steer $N - 1$ nulls which makes it unsuitable for a CDMA cellular environment. When the number of incident signals exceeds the number of antenna elements, the array is called overloaded. However the processing gain of the CDMA receiver is a big ally against the overloading of an array and spatial diversity gain can improve the performance the antenna array.

We can also make the following observations from the simple beamforming example

- Even though we have placed a null at the direction of the interferer, the antenna gain is not maximized at the direction of the desired user. So we can employ more refined beamforming criterion. We will discuss some of these beamforming criteria in the next chapter.
- We have implicitly assumed that we have apriori knowledge of the array response vectors corresponding to different users. In an urban cellular environment, each resolvable multipath may be comprised of several unresolved components coming from significantly different angles. In such case, it is not possible to associate a discrete AOA with a signal impinging the antenna array and the knowledge of the array response vector may not be very reliable. It is also necessary to estimate the AOA to find the array response vector. But one of the key assumptions all high resolution AOA estimation techniques require is that the number of signal wave fronts including co-channel interference signals must be less than the number of elements in the array. This is not a very realistic scenario for a

commercial CDMA system. Eigen-Beamforming techniques, discussed in the latter sections, can be an effective solution since they do not need apriori knowledge of the array response vectors, i.e. there is no need to explicitly estimate the AOAs.

We have used the beam pattern to illustrate the working principle of the elementary null-steering beamformer. However one should not put too much importance on the beam pattern as it only describes the magnitude response of the beamformer and does not provide any information of the phase. The weight vector is intended to satisfy a particular beamforming criterion. A MSINR weight vector for example, will maximize the output SINR and the beam pattern may not show a high gain at the AOA of the desired user or a null at the AOA of the interferer. This is especially true in a multipath environment when the array response vector is replaced by the composite channel vector (see Appendix A for more details)

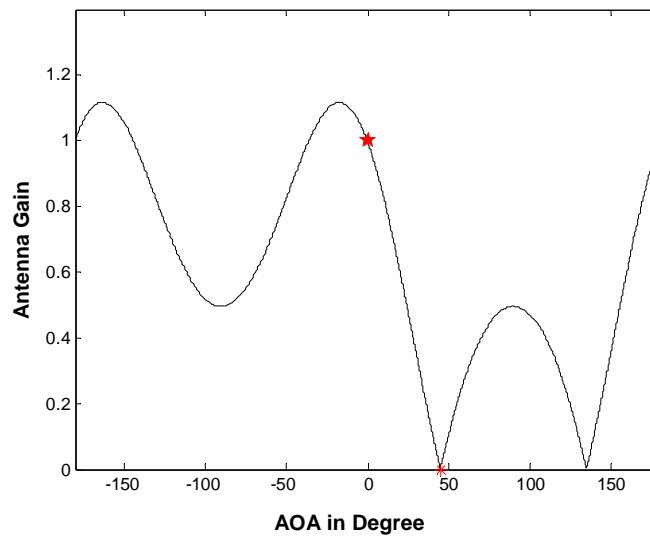


Figure 2.3: Beam pattern for the elementary beamformer. The AOA of the desired user is 0° and the AOA of the interferer is 45° .

2.4 Array Ambiguity

Let us consider the array response vector of a ULA given by Equation 2.10. It is obvious that any two AOAs θ_1 and θ_2 related as $\theta_2 = \pi - \theta_1$ will have the same array response vector i.e. $\underline{a}(\theta_1) = \underline{a}(\theta_2)$. As a result it is impossible for a ULA to distinguish between the desired signal coming from the direction θ_1 and an interfering signal coming from the direction θ_2 . This ambiguity makes it

impossible to place a null in the direction of the interferer without nulling the desired signal itself. Any linear array suffers from this ambiguity although the relation between the ambiguous AOAs depends on the inter-element spacing. This ambiguity can be avoided if sectorization [3] is employed and/or the individual elements are not isotropic. Throughout this report we will assume that the cellular system employs a 3 sector per cell arrangement which is a valid assumption for WCDMA systems.

2.5 Spatial Sampling Theorem

Theorems applied to the FIR filter in the time domain may sometimes also be applied to an ULA in the spatial domain because of the analogous relation between an FIR filter and an ULA [189]. In the time/frequency domain, the Nyquist sampling theorem [4] states that for a bandlimited signal with highest frequency f , the signal is uniquely determined by its discrete time samples if the sampling rate is equal to or greater than $2f$. If the sampling rate is less than $2f$, there will be aliasing. Similarly to avoid spatial aliasing, the beamformer must satisfy the following criterion [138], [189]

$$d \leq \frac{\lambda}{2}. \quad (2.21)$$

This is known as the Nyquist sampling theorem in the spatial domain. Therefore to perform beamforming without spatial aliasing, the element spacing of the array must be less than or equal to half of the carrier wavelength. (Note that the ambiguity resulting from the spatial aliasing is different from the ambiguity we mention in section 2.4.) However the element spacing cannot be made arbitrarily small because of mutual coupling effects between elements. As a result, in a practical beamformer, the antenna elements are spaced close to half wavelength so that the spatial aliasing is avoided and the mutual coupling effect is minimized as well. For the beamformers employed in this report, we assume that the element spacing of the ULA is at half of the carrier wavelength unless explicitly mentioned otherwise.

2.6 Spatial Diversity Gain

The adaptive antenna array can achieve spatial diversity and mitigate multipath fading. This is in addition to the interference cancellation attained from steering beams towards the desired user and/or steering nulls in the direction of interferers. The signal envelopes observed across the elements of an antenna array should have very little cross-correlation in order to achieve diversity gain. As a result, if the signal at one of the elements is going through a deep fade, it is highly unlikely that the signals at

the other elements are encountering that at the same time. So there is nearly always good signal reception on one of the antenna elements. Therefore combining the signals from various elements will increase the SNR and the fidelity of the received signal. This gain in SNR is termed as the spatial diversity gain. The spatial diversity gain depends mainly on two factors [16]. They are cross-correlation of the fading envelopes across the elements of the array and the mean power level of the signal. The lower the cross-correlation the lower the chances of the signals across various elements encountering simultaneous fades and therefore higher the diversity gain is. If the mean power level of the signals at the different elements is not equal, the element at higher power will dominate the combined output. It will be difficult to improve the SNR when the stronger branch is going through a deep fade. As a result the diversity gain is higher when the signals are received with equal mean power level on various antenna elements.

Ideally, a *diversity combiner* would need zero cross-correlation between signals across elements. The elements may be required to be separated by distance that is on the order of several carrier wavelengths to ensure low cross-correlation between signals across elements. Therefore the elements of a diversity combiner are not usually ‘Nyquist-spaced’. The spacing between the elements depends on the angle spread of the channel. The higher the angle spread, smaller the element spacing can be. So there is an obvious trade-off between the diversity gain and spatial aliasing while deciding on the inter-element spacing of an adaptive antenna array. We will discuss attaining spatial diversity gain at the cost of spatial aliasing in Chapter 7.

2.7 Temporal Processing: Rake Receiver for CDMA

In a frequency selective channel, there are multiple replicas (that are resolvable in time) of the transmitted signal at the receiver, traversing different multipath. These multiple copies can be combined to improve the signal to noise ratio (SNR) at the receiver. Since the signals are coming from different paths, they encounter independent fading. This means that if one of the paths is undergoing a deep fade, it is very unlikely that the signals from the other paths are also encountering fading. As a result the receiver still has a good chance to attain acceptable fidelity. In a CDMA system the receiver can employ multiple correlators to separate the multiple copies of the signal and mitigate fading. This receiver, commonly known as a Rake receiver [3], has been extensively employed by the second generation CDMA based cellular systems like the IS-95. Temporal processing by the Rake receiver lets the CDMA system exploit multipath diversity and makes it inherently resistant to fading. There are different techniques that can be applied to combine the output

of the correlators. If the combining weights are matched to the discrete channel gain coefficients corresponding to the respective multipath components, it is called Maximal Ratio Combining (MRC). MRC is a coherent combining scheme. For non-coherent combining, all the weights can be set equal and this is termed as Equal Gain Combining (EGC). Both the MRC and the EGC are intended to improve SNR. However it is also possible to set the combining weights such that SINR instead of SNR is maximized.

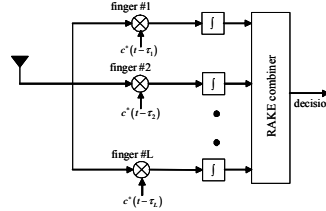


Figure 2.4: Rake receiver

2.8 Beamformer-Rake Receiver

A Beamformer-Rake [1] cascades a beamformer with Rake reception to process the signal both in the spatial and the temporal domain. For each finger of the temporal Rake processor, there is a beamformer to improve the fidelity of the signal of that particular branch. Figure 2.5 illustrates the structure and operating principle of a Beamformer-Rake. At the front end of the receiver is an antenna array. The signals from the array are fed into a set of spatial combiners that perform beamforming for different multipath and each weight vector accentuates the signal from a particular multipath component of the desired user. A temporal combiner follows the spatial combiner where the contribution from different multipath (from their corresponding spatial combiner) is combined to exploit the multipath diversity.

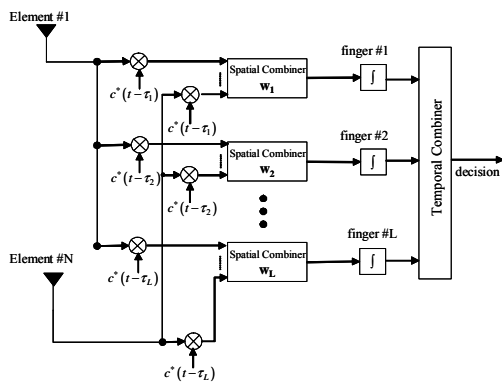


Figure 2.5a: Beamformer-Rake structure

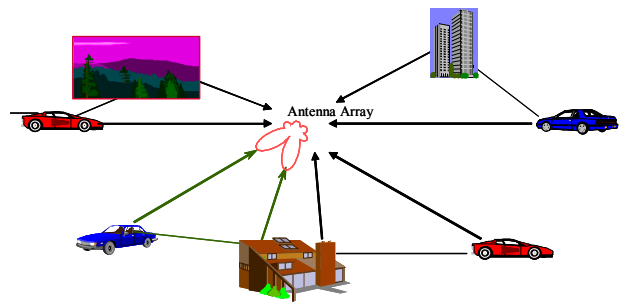


Figure 2.5b: Different weight vector accentuates different multipath component of the desired user

Chapter 2 Fundamental Concepts of Space Time Processing

Let us present an example of the performance dividends of a Beamformer-Rake receiver compared to a correlation receiver equipped with spatial processing only and a conventional Rake receiver that is equipped with temporal processing only. MSINR beamforming criterion is exploited in all the spatial processing whereas MRC is employed in the temporal domain combining. (*We will discuss MSINR based beamforming in chapter 3. It is sufficient to know at this point that MSINR beamforming takes the interferers into account to evaluate the weight vectors.*) We will not overly emphasize the simulation environment at this point. We will encounter the same scenario in the latter chapters and will describe the simulation scenario in detail. There are 6 users uniformly distributed within a sector of $[-60^\circ \ 60^\circ]$. In the case of the uniform user distribution all the users are operating at the same average received power level whereas for the non-uniform user distribution, the interferer closest to the desired user operates at a higher received power level. This particular user with higher data rate has a lower spreading factor (which is 4 as opposed to 32 for rest of the users) compared to the other 5 users. It also has two data channels while the other users have one data channels only. The multipath propagation condition is described by the vehicular channel (see Chapter 7) which represents a channel with small angle spread and several relatively strong multipath components. In the Bit Error Rate (BER) vs. E_b/N_0 curves of Figure 2.6, solid lines represent the case where the user distribution is uniform. We can see that temporal processing offers similar benefit compared to the spatial processing. This is because even though the rake receiver experiences signal degradation from MAI, there are several strong multipath components to provide temporal diversity. For the simple correlation receiver, the spatial processing reduces the MAI significantly even if there is no temporal diversity to be gained. A Beamformer-Rake receiver still outperforms both of them since the temporal processor of the 2-D receiver experiences less interference than the simple Rake Receiver.

Now let us consider the case where one of interferers is operating at a higher data rate and therefore higher power level. This is known as the near-far problem [9]. Referring to Figure 2.6, we see that there is very little degradation in the performance of the spatial processor. Since the beamformer employs the MSINR criterion, it takes the effect of the interference into account. As a result it steers beam towards the desired user and at the same time ensures that the strong interferer is nulled somewhat. However the near-far effect from the strong interferer affects the Rake receiver severely and we see drastic degradation in the performance of the temporal processor. The Beamformer-Rake receiver does not suffer any significant performance degradation because the spatial processing shields the temporal processor from the near-far problem.

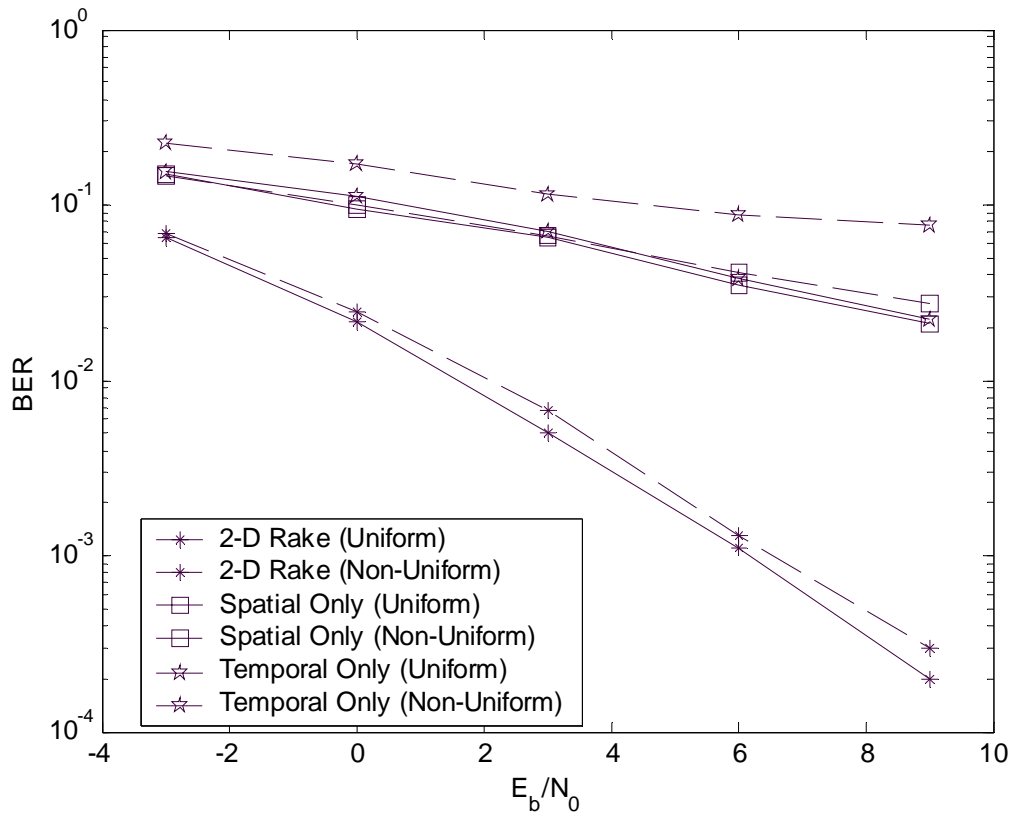


Figure 2.6: Performance comparison among various receivers under different user distribution

The previous example illustrates the performance improvement that can be achieved with the application of a Beamformer-Rake which enjoys the collective benefit of the temporal and spatial processing and none of their individual weaknesses. In the subsequent chapters we will investigate a variety of Beamformer-Rake receivers and demonstrate their performance under different operating conditions.

Chapter 3

Beamforming Criteria

3.1 Introduction

In this chapter we describe different techniques that can be applied for beamforming in a CDMA based cellular environment and an OFDM system. The three beamforming criteria discussed in this chapter are the Maximum Signal to Noise Ratio (MSNR), the Maximum signal to Interference and Noise Ratio (MSINR) and the Minimum Mean Square Error (MMSE). The chapter starts with the formulation of the MSNR solution as a Simple Eigenvalue problem (SE). We then go on to discuss the MSINR beamforming criterion and formulate that as a Generalized Eigenvalue problem (GE). The MMSE based beamforming comes next. We end the chapter with a comparison between MSINR and MMSE beamforming for a simple scenario and a discussion on the estimation of second order statistics for beamforming.

3.2 MSNR Beamforming

The MSNR beamforming criterion as the name suggests is intended to maximize the Signal to Noise Ratio (SNR) at the output of the beamformer. In the literature, it is often termed as the conventional beamformer (see section 1.2 for detail references). The weight vector that maximizes the SNR is the *principal eigenvector* of the covariance matrix of the desired signal. If the interference and noise is *spatially white*, this is the optimum beamforming.

3.2.1 Maximizing the Signal to Noise Ratio

Let us consider the case of maximizing the Signal to Noise Ratio (SNR) of the desired signal in *white* noise. . The received signal can be written as

$$\underline{x} = \underline{s} + \underline{n}. \tag{3.1}$$

Here \underline{s} and \underline{n} are the $N \times 1$ desired signal vector and complex additive Gaussian noise vector respectively with N being the number of antenna elements. The noise is zero mean and the covariance is given by

Chapter 3 Beamforming Criteria

$$\underline{\underline{R}}_{nn} = E[\underline{n}(t)\underline{n}^H(t)] = \sigma_n^2 I_N, \quad (3.2)$$

where σ_n^2 is the noise variance. Equation 3.2 implies that the noise is spatially white. Let us for the time being further assume that the noise is temporally white also so that

$$E[\underline{n}(t_1)\underline{n}^H(t_2)] = \sigma_n^2 I_N \delta(t_1 - t_2) \quad (3.3)$$

Now the power of the desired signal at the output of the beamformer, assuming that the signal is a zero mean stationary process, is given by

$$\begin{aligned} P_s &= E\left(\|\underline{w}^H \underline{s}\|^2\right) \\ &= E\left(\underline{w}^H \underline{s} \underline{s}^H \underline{w}\right) \\ &= \underline{w}^H E\left(\underline{s} \underline{s}^H\right) \underline{w} \\ \Rightarrow P_s &= \underline{w}^H \underline{\underline{R}}_{ss} \underline{w} \end{aligned} \quad (3.4)$$

Here $\underline{\underline{R}}_{ss} = E\left(\underline{s} \underline{s}^H\right)$ is the covariance matrix of the desired signal vector \underline{s} and \underline{w} is the $N \times 1$ antenna weight vector.

Similarly, the power of the noise at the output of the beamformer is

$$\begin{aligned} P_n &= E\left(\|\underline{w}^H \underline{n}\|^2\right) \\ &= \underline{w}^H \underline{\underline{R}}_{nn} \underline{w} \\ &= \sigma_n^2 \underline{w}^H \underline{w} \end{aligned} \quad (3.5)$$

Therefore the SNR at the beamformer output is given by

$$SNR = \frac{\underline{w}^H \underline{\underline{R}}_{ss} \underline{w}}{\sigma_n^2 \underline{w}^H \underline{w}} \quad (3.6)$$

To find the optimum weight vector that maximizes the SNR, we take the derivative of the right hand side of Equation 3.6 with respect to \underline{w}^H and set it equal to a null vector. Therefore we get,

$$\begin{aligned} \frac{\left(\underline{w}^H \underline{w}\right) \underline{\underline{R}}_{ss} \underline{w} - \left(\underline{w}^H \underline{\underline{R}}_{ss} \underline{w}\right) \underline{w}}{\left(\underline{w}^H \underline{w}\right)^2} &= \underline{0} \\ \Rightarrow \underline{\underline{R}}_{ss} \underline{w} &= \left[\frac{\underline{w}^H \underline{\underline{R}}_{ss} \underline{w}}{\underline{w}^H \underline{w}} \right] \underline{w} \end{aligned} \quad (3.7)$$

Chapter 3 Beamforming Criteria

The value of $\frac{\underline{w}^H \underline{R}_{ss} \underline{w}}{\underline{w}^H \underline{w}}$ is bounded by the minimum and the maximum eigenvalue of the symmetric matrix \underline{R}_{ss} [2], the maximum eigenvalue λ_{\max} satisfying

$$\underline{R}_{ss} \underline{w} = \lambda_{\max} \underline{w} \quad (3.8)$$

is the maximum value of the SNR. The eigenvector \underline{w}_{MSNR} corresponding to λ_{\max} is the optimum weight vector that maximizes the SNR at the output of the antenna array.

So, the MSNR solution for the optimum weight vector is given by the principal eigenvector (the eigenvector corresponding to the maximum eigenvalue) of the following Simple Eigenvalue problem (SE):

$$\underline{R}_{ss} \underline{w}_{MSNR} = \lambda \underline{w}_{MSNR} \quad (3.9)$$

This type of MSNR based beamforming is often known as *Eigen-Beamforming* for obvious reason.

If we could assign a single AOA θ_d to the desired signal, the desired signal vector can be written as

$$\underline{s}(k) = d(k) \underline{a}(\theta_d), \quad (3.10)$$

where d is the desired symbol, k is the sample index and $\underline{a}(\theta_d)$ is the array response vector for an AOA of θ_d . So we can write

$$\underline{R}_{ss} = E\left(\|d\|^2\right) \underline{a}(\theta_d) \underline{a}^H(\theta_d). \quad (3.11)$$

So from Equation 3.8, we can write

$$E\left(\|d\|^2\right) \underline{a}(\theta_d) \underline{a}^H(\theta_d) \underline{w}_{MSNR} = \lambda_{\max} \underline{w}_{MSNR} \quad (3.12)$$

By defining $\zeta = \frac{E\left(\|d\|^2\right) \underline{a}^H(\theta_d) \underline{w}_{MSNR}}{\lambda_{\max}}$, the MSNR weight vector is given by

$$\underline{w}_{MSNR} = \zeta \underline{a}(\theta_0). \quad (3.13)$$

A similar expression can be derived for a scenario when a resolvable path is a summation of several unresolvable paths with distinct AOAs. The array response vector is replaced by the channel vector (see Appendix A for a definition of channel vector).

Equation 3.13 makes sense intuitively. Since there is no particular directivity or spatial structure associated with the noise, co-phasing the received signals from different antenna elements will maximize the SNR. It also suggests that MSNR beamforming could be implemented with the help of any high resolution direction finding (DF) technique [69-104]. However DF techniques are not applicable for a large number of propagation conditions. Moreover the direction finding techniques usually require that the number of signal wave fronts including the co-channel interference signals be less than the number of antenna elements in the antenna array [1]. This is not a realistic scenario for a commercial, especially CDMA based, cellular system.

3.2.2 Alternate SE for MSNR Beamforming

Observation of Equation 3.9 indicates that we will need an estimate of the covariance matrix of the desired signal, $\underline{\underline{R}}_{ss}$, to perform the Eigen-Beamforming. However it may be difficult to separate the signal from the noise to form an estimate of $\underline{\underline{R}}_{ss}$ and *if we could separate the signal from the noise, we might not require beamforming*. However there is an alternative technique that would not require estimating the desired signal covariance matrix. If the desired signal is independent of the noise, the received signal covariance matrix can be written as

$$\underline{\underline{R}}_{xx} = \underline{\underline{R}}_{ss} + \sigma_n^2 I_N \quad (3.14)$$

So the Received Signal to Noise Ratio is given by

$$RSNR = 1 + SNR \quad (3.15)$$

It is obvious from Equation 3.15 that maximizing the RSNR will maximize the SNR. If we follow the same procedure detailed by Equation 3.4 to 3.9 we get that the weight vector that maximizes the SNR is given by the principal eigenvector of the following SE:

$$\underline{\underline{R}}_{xx} \underline{w}_{MSNR} = \lambda' \underline{w}_{MSNR} \quad (3.16)$$

The principal eigenvector of the covariance matrix $\underline{\underline{R}}_{xx}$ constitutes a single dimensional signal and noise subspace. The remaining eigenvectors corresponding to $N-1$ equal eigenvalues constitute a non-unique orthonormal basis to the noise-only subspace which is orthogonal to the signal and noise subspace. So by applying the weight, the beamformer takes a projection of the signal to a subspace (the signal and noise subspace) that is orthogonal to the noise-only subspace.

If the noise is stronger than the desired signal, the maximum eigenvalue does not correspond to the desired signal and as a result the principal eigenvector of Equation 3.16 is not the MSNR weight vector. However in a CDMA environment, such a scenario is not very likely to occur because of the processing gain and the power control mechanism. The CDMA receivers are equipped with a bank of correlators and the output of the correlators contain the narrowband desired signal and in-band interference and noise (typically not very large compared to the desired signal because of the CDMA processing gain). Therefore the covariance matrix can be formed at the output of the CDMA correlators to formulate the required SE for the MSNR solution.

In the previous analysis we have rather conveniently consolidated the entire undesired signal as noise and assumed it to be white. We could split the noise component of Equation 3.1 into two different components so that

$$\underline{n} = \underline{n}' + \underline{i}, \quad (3.17)$$

where \underline{n}' is spatially and temporally white noise and \underline{i} is the interference. In this scenario if the interference is white, MSNR weight is the optimum weight vector. But if the interference is not white, the eigenvector corresponding to the maximum eigenvalue of the received signal does not correspond to the MSNR weight vector. However this is a moot point since the spatial structure of the interference requires to be taken into account and the optimum weight vector will be the weight that maximizes the Signal to Interference and Noise Ratio (SINR). We will discuss maximum SINR (MSINR) based Eigen-Beamforming a little later in this chapter.

3.2.3 Phase Ambiguity in Eigen-Beamforming

Before we move on to other beamforming techniques, we would like to point out a potential drawback of Eigen-Beamforming techniques commonly known as the phase ambiguity. Since the beamformer is intended to maximize the SNR (or the SINR as we will see shortly), there is no constraint on the beamformer to preserve the phase of the signal. The MSNR weight vector

maximizes the SNR $\frac{\underline{w}^H \underline{R} \underline{w}}{\sigma_n^2 \underline{w}^H \underline{w}}$ and is the principal eigenvector of the SE given by Equation 3.9

The SNR at the output of the beamformer is given by

$$SNR_{\max} = \frac{\underline{w}_{MSNR}^H \underline{R} \underline{w}_{MSNR}}{\sigma_n^2 \underline{w}_{MSNR}^H \underline{w}_{MSNR}} \quad (3.18)$$

Let us see what the SNR would be if the beamformer employs a weight vector $\hat{w} = \rho \underline{w}_{MSINR}$ where ρ is a complex scalar. The SNR at the output of the beamformer is given by

$$\begin{aligned}
 SNR' &= \frac{\hat{w}^H \underline{R}_{ss} \hat{w}}{\sigma_n^2 \hat{w}^H \hat{w}} \\
 &= \frac{(\rho \underline{w}_{MSINR})^H \underline{R}_{ss} (\rho \underline{w}_{MSINR})}{\sigma_n^2 (\rho \underline{w}_{MSINR})^H (\rho \underline{w}_{MSINR})} \\
 &= \frac{|\rho|^2 \underline{w}_{MSINR}^H \underline{R}_{ss} \underline{w}_{MSINR}}{\sigma_n^2 |\rho|^2 \underline{w}_{MSINR}^H \underline{w}_{MSINR}} \\
 &= \frac{\underline{w}_{MSINR}^H \underline{R}_{ss} \underline{w}_{MSINR}}{\sigma_n^2 \underline{w}_{MSINR}^H \underline{w}_{MSINR}} \\
 &= SNR_{\max}
 \end{aligned} \tag{3.19}$$

Therefore the weight vector \hat{w} also maximizes the SNR and there is no way to guarantee that the solution of the SE will preserve the phase. Similar phase ambiguity is present for MSINR based Eigen-beamforming. As a result Eigen-Beamforming is applicable where

- there is no phase modulation
- non-coherent detection is possible
- pilot assisted coherent detection is possible

Since the WCDMA uplink has pilot symbols in the DPCCH, it is possible to perform Eigen-Beamforming at the WCDMA reverse link.

3.3 MSINR Beamforming

In this section we introduce the idea of Eigen-Beamforming resulting from the Maximum Signal to Interference and Noise Ratio (MSINR) criterion for beamforming. In the literature, it is often termed as the optimal beamformer (see section 1.2 for detail references). In the previous section we discussed the MSNR beamforming criterion which is optimum only if the interference and noise is *spatially white*. In a WCDMA system, the users will have different data rate i.e. different spreading factors. At the same time they will have different target Bit Error Rate (BER). As a result some of the higher data rate users might be required to operate at a higher power level compared to their lower data rate counterparts and the interference is not spatially white. Under these operating conditions, the MSINR beamforming is the optimum beamforming criterion. Unlike the MSNR beamforming criterion that leads to a simple eigenvalue problem, the MSINR beamforming results in a Generalized Eigenvalue problem (GE). In addition to the signal covariance matrix, the interference and noise covariance

matrix becomes a factor in order to *fine tune* the weight according to the spatial distribution of the interference and noise.

3.3.1 Maximizing the Signal to Interference and Noise Ratio

Let us write the received signal vector as

$$\underline{x} = \underline{s} + \underline{u}, \quad (3.20)$$

where \underline{s} is the desired signal and \underline{u} is the undesired signal which comprises of interference and thermal noise.

The power of the desired signal at the output of the antenna array after combining is given by Equation 3.4 which is repeated for convenience,

$$P_s = \underline{w}^H \underline{R}_{ss} \underline{w} \quad (3.21)$$

Here $\underline{R}_{ss} = E(\underline{s} \underline{s}^H)$ is the covariance matrix of the desired signal vector \underline{s} .

Similarly, the power of the undesired signal at the output of the antenna array is

$$P_u = E(\|\underline{w}^H \underline{u}\|^2) = \underline{w}^H \underline{R}_{uu} \underline{w} \quad (3.22)$$

with $\underline{R}_{uu} = E(\underline{u} \underline{u}^H)$ being the covariance matrix of the interference and noise signal vector \underline{u} .

So the output Signal to Interference and Noise Ratio (SINR) is

$$SINR_{out} = \frac{\underline{w}^H \underline{R}_{ss} \underline{w}}{\underline{w}^H \underline{R}_{uu} \underline{w}} \quad (3.23)$$

To find the optimum weight vector that maximizes the output SINR, we have to take the derivative of the right hand side of Equation 3.23 with respect to \underline{w}^H and set it equal to a null vector. Therefore,

$$\underline{R}_{ss} \underline{w} = \left(\frac{\underline{w}^H \underline{R}_{ss} \underline{w}}{\underline{w}^H \underline{R}_{uu} \underline{w}} \right) \underline{R}_{uu} \underline{w} \quad (3.24)$$

The value of $\frac{\underline{w}^H \underline{R}_{ss} \underline{w}}{\underline{w}^H \underline{R}_{uu} \underline{w}}$ is bounded by the minimum and the maximum eigenvalue of the symmetric

matrix $\underline{R}_{uu}^{-1} \underline{R}_{ss}$ [2]. The maximum eigenvalue λ_{max} satisfying

$$\underline{\underline{R}}_{uu}^{-1} \underline{\underline{R}}_{ss} \underline{w} = \lambda_{\max} \underline{w} \quad (3.25)$$

is the optimum (maximum) value of the SINR. The eigenvector \underline{w}_{MSINR} corresponding to λ_{\max} is the optimum weight vector that maximizes the SINR at the output of the antenna array.

So, the MSINR solution for the optimum weight vector is given by the principal eigenvector (the eigenvector corresponding to the maximum eigenvalue) of the following Generalized (or joint) Eigenvalue problem (GE):

$$\underline{\underline{R}}_{ss} \underline{w}_{MSINR} = \lambda \underline{\underline{R}}_{uu} \underline{w}_{MSINR} . \quad (3.26)$$

We can observe that the covariance matrix of the interference and noise signal has been introduced in the Eigen-Equation to take the spatial structure of the undesired signal into account. The matrix $\underline{\underline{R}}_{uu}$ can be regarded as an operator modifying the weight vector that one would otherwise obtain from solving a simple eigenvalue problem like $\underline{\underline{R}}_{ss} \underline{w} = \lambda \underline{w}$. The MSINR beamforming can be viewed as a technique that maximizes the SNR for *spatially colored* noise, or the MSINR beamforming can be regarded as a special case of MSINR beamforming for spatially white noise.

As discussed in the previous section, if we could assign a single AOA θ_d to the desired signal, the covariance matrix of the desired signal can be written as

$$\underline{\underline{R}}_{ss} = E\left(\|d\|^2\right) \underline{a}(\theta_d) \underline{a}^H(\theta_d), \quad (3.27)$$

So from Equation 3.26, we can write

$$\underline{\underline{R}}_{uu}^{-1} \left\{ E\left(\|d\|^2\right) \underline{a}(\theta_d) \underline{a}^H(\theta_d) \underline{w}_{MSINR} \right\} = \lambda_{\max} \underline{w}_{MSINR} \quad (3.28)$$

By defining $\xi = \frac{E\left(\|d\|^2\right) \underline{a}^H(\theta_d) \underline{w}_{MSINR}}{\lambda_{\max}}$, the MSINR weight vector is given by

$$\underline{w}_{MSINR} = \xi \underline{\underline{R}}_{uu}^{-1} \underline{a}(\theta_0). \quad (3.29)$$

Once again we can observe that the interference and noise covariance matrix modifying the MSINR weight to compute the MSINR weight. The expression for the weight vector can be easily extended for a scenario when a resolvable path is a summation of several unresolvable paths with distinct AOAs.

3.3.2 Maximizing the Received Signal to Interference and Noise Ratio

If the desired signal is independent of the interference and noise, the received signal covariance matrix can be written as

$$\underline{R}_{xx} = \underline{R}_{ss} + \underline{R}_{uu} \quad (3.30)$$

The Received Signal to Interference and Noise Ratio (RSINR) becomes

$$RSINR = 1 + SINR \quad (3.31)$$

So maximizing RSINR amounts to maximizing SINR and we will end up with the same set of weights. As a result we will not distinguish between the MSINR and the Maximum RSINR (MRSINR) criterion. However let us formally state the MRSINR beamforming criterion as

The MRSINR solution for the optimum weight vector is given by the principal eigenvector (the eigenvector corresponding to the maximum eigenvalue) of the following Generalized (or joint) Eigenvalue problem (GE):

$$\underline{R}_{xx} \underline{w}_{MRSINR} = \lambda \underline{R}_{uu} \underline{w}_{MRSINR} \quad (3.32)$$

Equation 3.32 offers us another insight to the property of the optimum weight vector for colored noise. In case of the MSNR based Eigen-Beamforming (the solution of the Simple Eigenvalue problem), the objective is to split the *eigenspace* [193] of the received signal covariance matrix into two orthogonal subspaces and then find the eigenvector that defines the subspace (signal and noise subspace) orthogonal to the noise only subspace and corresponds to the desired signal. The two subspaces in the case of the MRSINR beamforming (or equivalently MSINR beamforming) are orthogonal to each other with respect to the covariance matrix of the interference and noise signal. This permits the adjustment of the weight vector according to the spatial signature of the undesired signal.

3.4 MMSE Beamforming Criterion

The Minimum Mean Squared Error (MMSE) criterion intends to find a weight vector that will minimize the Mean Squared Error (MSE) between the combined signal and some desired (or reference) signal. The error signal can be defined as [2]

$$e(k) = d(k) - \underline{w}^H \underline{x}(k), \quad (3.33)$$

Chapter 3 Beamforming Criteria

where d is the reference signal, \underline{w} is the antenna weight vector, \underline{x} is the received signal vector at the antenna array, k is the sample index.

So the MSE is given by

$$J = E\left[\|e(k)\|^2\right] \quad (3.34)$$

Here E denotes the ensemble expectation operator.

Thus we can rewrite Equation 3.33 the following way.

$$\begin{aligned} J &= E\left[\|d(k) - \underline{w}^H \underline{x}(k)\|^2\right] \\ &= E\left[\{d(k) - \underline{w}^H \underline{x}(k)\}\{d(k) - \underline{w}^H \underline{x}(k)\}^*\right] \\ &= E\left[\|d(k)\|^2 - d(k)\underline{x}^H(k)\underline{w} - d^*(k)\underline{w}^H \underline{x}(k) + \underline{w}^H \underline{x}(k)\underline{x}^H(k)\underline{w}\right] \\ &= E\left[\|d(k)\|^2\right] - \underline{r}_{xd}^H \underline{w} - \underline{w}^H \underline{r}_{xd} + \underline{w}^H \underline{\underline{R}}_{xx} \underline{w} \end{aligned} \quad (3.35)$$

where, $\underline{\underline{R}}_{xx} = E\left[\underline{x}(k)\underline{x}^H(k)\right]$ is the covariance matrix of the received signal and $\underline{r}_{xd} = E\left[\underline{x}(k)d^*(k)\right]$ is the cross-correlation vector between the received signal vector \underline{x} and the reference signal d .

The MSE J is minimized when the gradient vector $\nabla(J)$ is equal to a null vector. Now the gradient vector is defined as

$$\nabla(J) = 2 \frac{\partial}{\partial \underline{w}^*} \quad (3.36)$$

where $\frac{\partial}{\partial \underline{w}^*}$ is the conjugate derivative with respect to vector \underline{w} .

So we can write

$$\begin{aligned} \nabla(J) \Big|_{\underline{w}_{MMSE}} &= \underline{0} \\ -2\underline{r}_{xd} + 2\underline{\underline{R}}_{xx} \underline{w}_{MMSE} &= \underline{0} \end{aligned} \quad (3.37)$$

Thus we arrive at the well-known Wiener-Hopf equation [8]

$$\underline{\underline{R}}_{xx} \underline{w}_{MMSE} = \underline{r}_{xd} \quad (3.38)$$

We can premultiply Equation 3.38 by $\underline{\underline{R}}_{xx}^{-1}$ and get

$$\underline{w}_{MMSE} = \underline{\underline{R}}_{xx}^{-1} \underline{r}_{xd} \quad (3.39)$$

The above solution for MMSE weight is often called the Wiener solution [2].

If the desired signal is uncorrelated with the interference and noise,

$$\underline{\underline{R}}_{xx} = \underline{\underline{R}}_{ss} + \underline{\underline{R}}_{uu}, \quad (3.40)$$

Now if the desired signal had a single AOA θ_d associated with it and the reference signal was the actual desired signal,

$$\begin{aligned} \underline{\underline{R}}_{ss} &= E\left(\|d\|^2\right) \underline{a}(\theta_d) \underline{a}^H(\theta_d) \\ \underline{\underline{R}}_{xd} &= E\left(\|d\|^2\right) \underline{a}(\theta_d) \end{aligned} \quad (3.41)$$

By applying *Woodbury's Identity* [2], we get

$$\underline{\underline{R}}_{xx}^{-1} = \left\{ \frac{1}{1 + E\left(\|d\|^2\right) \underline{a}^H(\theta_d) \underline{\underline{R}}_{uu}^{-1} \underline{a}(\theta_d)} \right\} \underline{\underline{R}}_{uu}^{-1} \quad (3.42)$$

So the MMSE weight is given by

$$\underline{w}_{MMSE} = \chi \underline{\underline{R}}_{uu}^{-1} \underline{a}(\theta_0), \quad (3.43)$$

$$\text{where } \chi = \left\{ \frac{E\left(\|d\|^2\right)}{1 + E\left(\|d\|^2\right) \underline{a}^H(\theta_d) \underline{\underline{R}}_{uu}^{-1} \underline{a}(\theta_d)} \right\} \quad (3.44)$$

By comparing Equation 3.43 with Equation 3.29, we observe that the MMSE weight vector differs from the MSINR weight vector by a scalar. Since the SINR at the output of the beamformer does not depend on the scalar, *the MMSE weight vector in fact maximizes SINR.*

3.5 Comparison of MSINR and MMSE Beamforming for a Simple Scenario

In this section we compare the performance of the MSINR and MMSE beamforming for a simple scenario. The signal transmitted by the desired user is corrupted by two interferers and thermal noise at the receiver which is equipped with a 4 element ULA with half wavelength spacing between the omni directional elements. It is assumed that the receiver can perform coherent detection.

3.5.1 Simulation Environment

The desired user transmits 8ms long slots of QPSK symbols. 7ms of the slot contains actual QPSK symbol that represents the ON time. The remaining 1ms is the OFF period when no signal is

transmitted. This OFF period is to facilitate the estimation of interference and noise covariance matrix to perform MSINR based Eigen-Beamforming. At a sampling rate of 25 KHz, there are 25 samples of interference and noise signal. If one sample is used to represent one transmitted symbol, the ON period consists of 175 symbols/samples. Unless explicitly mentioned otherwise, all the statistics is estimated for 25 samples. So for the MMSE beamforming, it is assumed that there are 25 known pilot symbols at the beginning of each slot.

The location of the desired user is at 30^0 with respect to the receiver array broadside. The two interferers are located at 60^0 and -60^0 respectively. The interference is assumed to be wideband zero mean white Gaussian Noise. The only channel impairment is Additive White Gaussian Noised (AWGN). There are no reflectors or scatterers assumed to be present so that there is no angle spread and the position of the transmitters directly translates to AOA.

3.5.2 Estimation of Second Order Statistics for Beamforming:

The MSINR weight vector is computed by employing the GE given by Equation 3.32. Let us assume for the time being that we can solve the GE. We will discuss the different algorithms to solve the GE in Chapter 6. The required covariance matrices are estimated as an average over a block of data so that

$$\begin{aligned}\hat{\underline{\underline{R}}}_{xx} &= \frac{1}{N_{off}} \sum_{l=0}^{N_{off}-1} \underline{x}(l) \underline{x}^H(l) \\ \hat{\underline{\underline{R}}}_{uu} &= \frac{1}{N_{off}} \sum_{l=N_{on}}^{N_{on}+N_{off}-1} \underline{x}(l) \underline{x}^H(l)\end{aligned}\tag{3.45}$$

Here $\underline{x}(l)$ is the received signal vector, N_{on} and N_{off} are the number of samples in the ON and OFF period respectively.

The MMSE weight vector is estimated by applying the Wiener solution given in Equation 3.39. The estimate of the received signal covariance matrix, $\hat{\underline{\underline{R}}}_{xx}$, is computed according to Equation 3.45. The cross-correlation vector is estimated as

$$\hat{\underline{r}}_{xd} = \frac{1}{N_{off}} \sum_{l=0}^{N_{off}-1} \underline{x}(l) d^*(l),\tag{3.46}$$

where $d^*(l)$ is the conjugate of the known pilot sample.

For the given simulation scenario, the interfering signals are independent of each other and thermal noise. Each interfering signal can be associated with a discrete AOA. As a result, the actual Interference and Noise covariance matrix is given by

$$\underline{\underline{R}}_{uu} = \sum_{i=0}^1 \sigma_i^2 \underline{a}(\theta_i) \underline{a}^H(\theta_i) + \sigma_n^2 I \quad (3.47)$$

Here σ_i^2 is the received signal power of the i^{th} interferer, $\underline{a}(\theta_i)$ is the array response vector of the i^{th} interferer with an AOA of θ_i , σ_n^2 is the variance of the zero mean thermal noise. Since the desired signal has a discrete AOA and it is independent of the interfering signals as well as the noise, the actual received signal covariance matrix is given by

$$\underline{\underline{R}}_{xx} = \underline{\underline{R}}_{uu} + \sigma_d^2 \underline{a}(\theta_d) \underline{a}^H(\theta_d) \quad (3.48)$$

where σ_d^2 is the power of the desired signal, $\underline{a}(\theta_d)$ is the array response vector of the desired signal with an AOA of θ_d and $\underline{\underline{R}}_{uu}$ is the interference and noise covariance matrix as given by Equation 3.47.

For an AOA of 30° , the array response vector of the desired user is given by $[1 \ -0.993 - j0.0376 \ 0.9972 + j0.0751 \ -0.9936 - j0.11263]^T$. If we estimate the exact interference and noise covariance matrix with Equation 3.47, we can compute the actual MSINR weight by employing Equation 3.29. This actual MSINR weight is employed to generate the base-line performance curves. For comparison purposes, we also simulate the performance of a single antenna receiver that has no spatial processing capability.

3.5.3 Simulation Results

Figures 3.1 and 3.2 show the beam patterns for different levels of interference. The MSINR and MMSE beam patterns based on the matrix estimates are very similar to the beam pattern of the MSINR weight computed with exact knowledge of the desired signal AOA and the covariance matrix of the interference and noise signal. The Figures 3.3 to 3.6 show the BER for different interference power level. The single antenna receiver without spatial processing has unacceptable performance. There is a large improvement in performance if beamforming is employed. We can observe that the performance of the MMSE and MSINR beamforming based on the estimated covariance matrices are very similar. Also there is very little degradation compared to the performance of the beamformer that employs the actual MSINR weight.

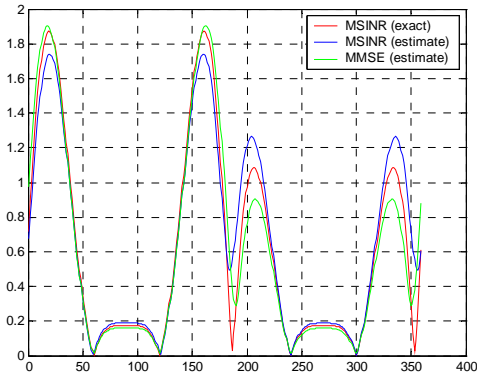


Figure 3.1: Examples of beam pattern. The desired user is at 30° . The interferers are at 60° and -60° (300°) respectively. Both the interferers are being received at 20 dB higher power level than the desired user.

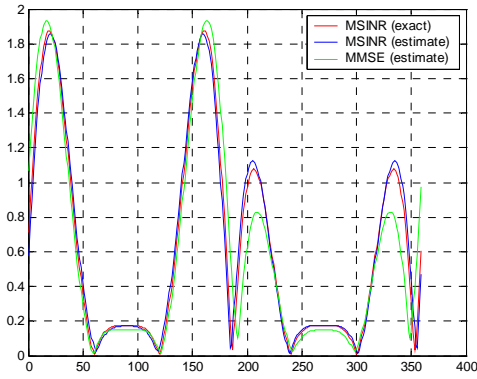


Figure 3.2: Examples of beam pattern. The desired user is at 30° . The interferers are at 60° and -60° (300°) respectively. Both the interferers are being received at 10 dB higher power level than the desired user.

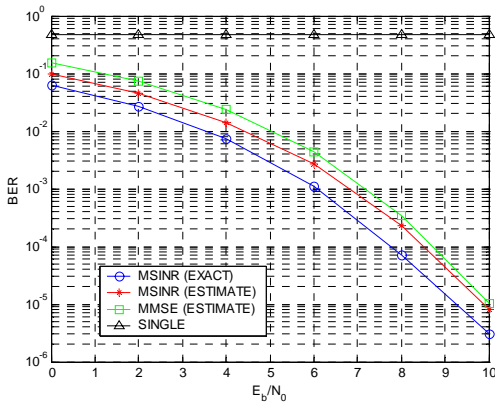


Figure 3.3: BER vs. E_b/N_0 . Both the interferers are being received at 20 dB higher power level than the desired signal.

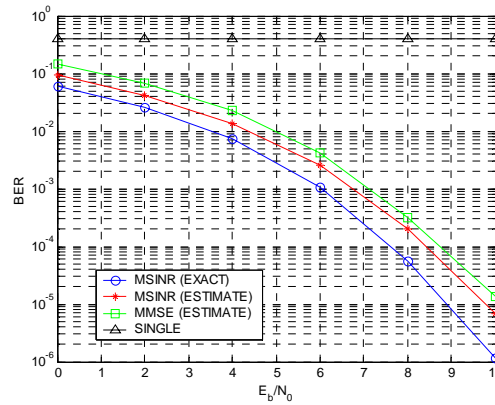


Figure 3.4: BER vs. E_b/N_0 . Both the interferers are being received at 10 dB higher power level than the desired signal.

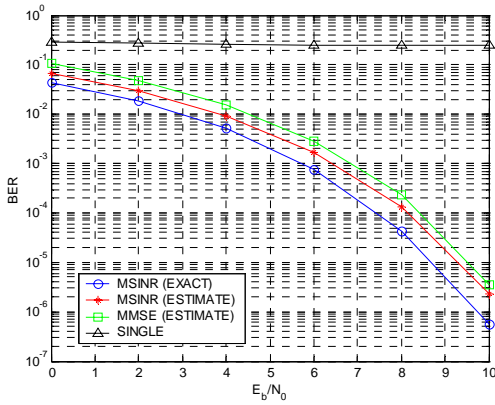


Figure 3.5: BER vs. E_b/N_0 . Both the interferers are being received at equal power level compared to the desired signal.

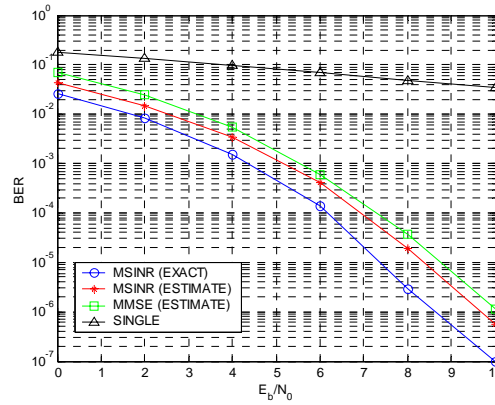


Figure 3.6: BER vs. E_b/N_0 . Both the interferers are being received at 10 dB lower power level than the desired signal.

The final set of simulation results shown in Figures 3.7 and 3.8 demonstrate the effect of sample size on the performance of the beamforming. We can observe that for both the beamforming criteria, the performance gets better with the increase in sample size. This is expected since the ensemble average provides a better estimate for larger number of samples. We can observe big gain in performance as the sample size increases from 10 to 15 and also from 15 to 20. However the performance does not improve significantly by increasing the sample size from 20 to 25. Therefore there is an optimum number of samples for an accurate estimate of the statistics required for beamforming and for this scenario it can be taken as 20 or 25. The simulations were conducted for static channel condition and in a time varying environment the coherence time [3], defined as the length of time for which the signal retains strong correlation, has to be considered also. The block must contain adequate number of samples for a reliable ensemble average and at the same time it must be small enough so that the channel does not change significantly within the block.

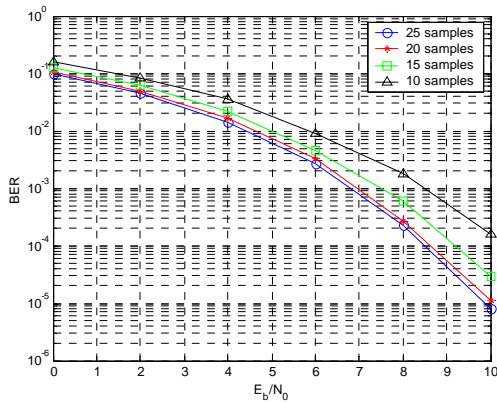


Figure 3.7: BER vs. E_b/N_0 for MSINR beamforming. Both the interferers are being received at 20 dB higher power level than the desired signal. Different number of samples are being used to compute the required statistics.

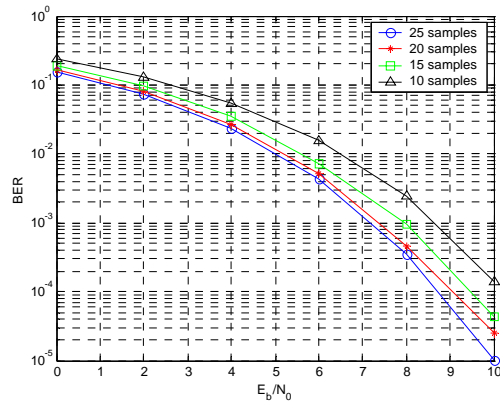


Figure 3.8: BER vs. E_b/N_0 for MMSE beamforming. Both the interferers are being received at 20 dB higher power level than the desired signal. Different number of samples are being used to compute the required statistics.

Chapter 4

WCDMA

4.1 Introduction

In this chapter we briefly discuss the different generations of cellular standards and the migration from the circuit switched voice traffic oriented older generation wireless networks to the coming third generation cellular systems that will employ packet switched networking techniques to deal with the increased demand for wireless data services. The chapter begins with a brief discussion of the first and second generation cellular systems. Then we outline the migration towards the third generation systems and discuss the key requirements of the next generation cellular systems. We then proceed to discuss the key aspects of the physical layer of the uplink of WCDMA [6], [7], potentially the most popular of the third generation standards. The chapter concludes with a discussion on the current status of the deployment of the third generation cellular systems around the world.

4.2 Cellular Standards: From 1G to 3G

The goal for the next generation of mobile communication systems is to seamlessly provide a wide variety of communication services to anybody, anywhere, anytime. The intended services for next generation mobile phone users include services like transmitting high speed data, video and multimedia traffic as well as voice signals. The technology needed to tackle the challenges to make these services available is popularly known as the Third Generation (3G) Cellular Systems. The first generation systems are represented by the analog mobile systems designed to carry the voice application traffic. Their subsequent digital counterparts are known as second generation cellular systems. Third generation systems mark a significant leap, both in applications and capacity, from the current second generation standards. Whereas the current digital mobile phone systems are optimized for voice communications, 3G communicators are oriented towards multimedia message capability.

4.2.1 First Generation (1G) Cellular Systems

The first generation cellular systems generally employ analog Frequency Modulation (FM) techniques. The Advanced Mobile Phone System (AMPS) is the most notable of the first generation

systems. AMPS was developed by the Bell Telephone System. It uses FM technology for voice transmission and digital signaling for control information. Other first generation systems include Narrowband AMPS (NAMPS), Total Access Cellular System (TACS) and Nordic Mobile Telephone System (NMT-900). All the first generation cellular systems employ Frequency Division Multiple Access (FDMA) with each channel assigned to a unique frequency band within a cluster of cells. The first generation networks are based on circuit switched technique.

4.2.2 Second Generation (2G) Cellular Systems

The rapid growth in the number of subscribers and the proliferation of many incompatible first generation systems were the main reason behind the evolution towards second generation cellular systems. Second generation systems take advantage of compression and coding techniques associated with digital technology. All the second generation systems employ digital modulation schemes. Multiple access techniques like Time Division Multiple Access (TDMA) and Code Division Multiple Access (CDMA) are used along with FDMA in the second generation systems. Second generation cellular systems include United States Digital Cellular (USDC) standards IS-54 and IS-136, Global System for Mobile communications (GSM), Pacific Digital Cellular (PDC) and cdmaOne based IS-95A/IS-95B. Like their first generation counterparts, the 2G networks are also circuit switched.

4.2.3 Transition towards 3G: 2.5G Cellular Systems

The demand for wireless data services has resulted in transition towards packet switched networks. The so called 2.5 G cellular systems are currently being employed to facilitate the move from the circuit switched 2G cellular networks to the next generation packet based network. Two major 2.5G cellular systems currently being deployed are General Packet Radio Service (GPRS) and Enhanced Data-rates for Global Evolution (EDGE).

The General Packet Radio Service (GPRS) is a value added service that allows information to be sent and received across a mobile telephone network. It supplements today's circuit switched data and short message service. GPRS is based on standardized open interfaces and therefore interworks with existing circuit-switched services. Since GPRS is a packet switched technology, bandwidth is only utilized during data transmission and is shared between all subscribers. This allows operators to offer billing on a usage basis rather than on connection time. Users are therefore always connected and

only charged for data transfer. This makes GPRS ideally suited to bursty traffic transmission, and opens the door to a world of new services previously impractical over mobile networks.

Enhanced Data-rates for Global Evolution (EDGE) is a Third Generation (3G) compliant high-speed wireless data and Internet access technology that offers economies of scale. EDGE is a standardized set of improvements to the GSM radio interface. It defines a new modulation and new radio protocols that bring higher maximum data rates and increased spectral efficiency. EDGE is applicable to both GPRS traffic (EGPRS) and circuit switched data traffic (ECSD). EDGE can be integrated into existing GSM networks by the installation of new transceivers or new base stations. EDGE can also be applied to TDMA (D-AMPS/IS-136) networks by the addition of a complete EGPRS overlay. In the GSM context, EDGE is considered part of the 2G+/2.5G evolution, whereas for the TDMA community, it is sometimes termed as a 3G technology.

4.2.4 Third Generation Cellular Systems

Third generation cellular systems are being designed to support wideband services like high speed Internet access, video and high quality image transmission with the same quality as the fixed networks. The primary requirements of the next generation cellular systems are [5], [194]:

- Voice quality comparable to Public Switched Telephone Network (PSTN).
- Support of high data rate. The following table shows the data rate requirement of the 3G systems

Table 4.1: 3G data rate requirements

Mobility Needs	Minimum Data Rate
Vehicular	144 kbps
Outdoor to indoor and pedestrian	384 kbps
Indoor Office	2 Mbps

- Support of both packet-switched and circuit-switched data services.
- More efficient usage of the available radio spectrum
- Support of a wide variety of mobile equipment
- Backward Compatibility with pre-existing networks and flexible introduction of new services and technology
- An adaptive radio interface suited to the highly asymmetric nature of most Internet communications: a much greater bandwidth for the downlink than the uplink.

Research efforts have been underway for more than a decade to introduce multimedia capabilities into mobile communications. Different standard agencies and governing bodies have been responsible for the efforts to integrate a wide variety of proposals for third generation cellular systems. Three different 3G standards emerged as the solution for the next generation cellular systems. They are WCDMA, CDMA2000, and UWC-136.

WCDMA employs CDMA air interface with the GSM based networks. CDMA2000 is a multi-carrier CDMA standard and is a natural progression of the CDMA based 2G standard IS-95. UWC-136, a TDMA based standard, was proposed to upgrade the existing TDMA based 2G networks. However recent developments suggest that UWC-136 will not come into service in practice. The following figure, adopted from [5], shows the evolution of third generation cellular systems:

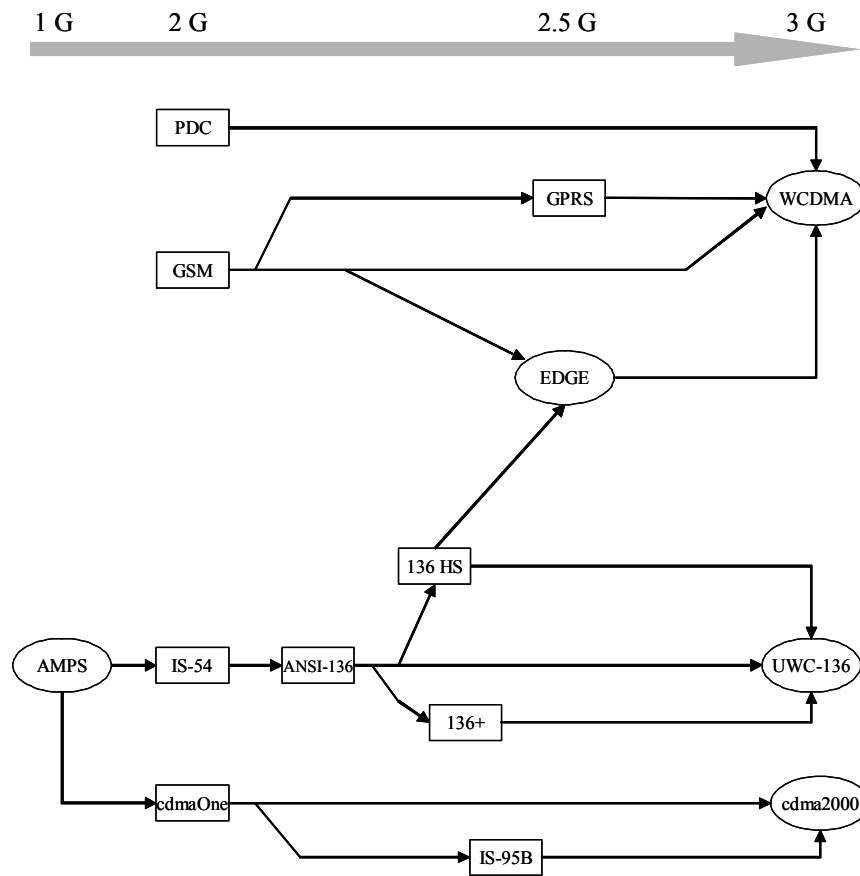


Figure 4.1: Evolution towards 3G

References [5] and [8-10] provide further discussion on the evolution of third generation cellular systems.

4.3 WCDMA: Air Interface for 3G

One of the most popular approaches to 3G is to combine a Wideband CDMA (WCDMA) air interface with the fixed network of GSM. Several proposals supporting WCDMA were submitted to the International Telecommunication Union (ITU) and its International Mobile Telecommunications for the year 2000 (IMT2000) initiative for 3G. The organizations who merged their various WCDMA proposals include Japan's Association of Radio Industry and Business (ARIB), Alliance for Telecommunications Industry Solutions (ATIS), T1P1 and European Telecommunications Standards Institute (ETSI) through its Special Mobile Group (SMG). The standard that emerged is based on ETSI's Universal Mobile Telecommunication System (UMTS) and is commonly known as UMTS Terrestrial Radio Access (UTRA) [5]. This standard is intended to take advantage of the WCDMA radio techniques without ignoring the numerous advantages of the already existing GSM networks. The access scheme for UTRA is Direct Sequence Code Division Multiple Access (DS-SS). The information is spread over a band of approximately 5 MHz. This wide bandwidth is the reason for the name Wideband CDMA or WCDMA. There are two different modes namely Frequency Division Duplex (FDD) and Time Division Duplex (TDD). For the FDD mode, the uplink and downlink transmissions employ two separated frequency bands for this duplex method. A pair of frequency bands with specified separation is assigned for a connection. In the TDD duplex mode, uplink and downlink transmissions are carried over the same frequency band by using synchronized time intervals. Thus time slots in a physical channel are divided into transmission and reception part. Since different regions have different frequency allocation schemes, the capability to operate in either FDD or TDD mode allows for efficient utilization of the available spectrum.

The two dimensional (2-D) receivers described in this report are tailored for a WCDMA system operating in the FDD mode. So all the physical layer description provided in this chapter holds for the FDD mode only.

4.3.1 WCDMA Key Features

The key operational features of the WCDMA radio interface are listed below [9], [10]:

- Support of high data rate transmission: 384 kbps with wide area coverage, 2 Mbps with local coverage.
- High service flexibility: support of multiple parallel variable rate services on each connection.
- Both Frequency Division Duplex (FDD) and Time Division Duplex (TDD).

- Built in support for future capacity and coverage enhancing technologies like adaptive antennas, advanced receiver structures and transmitter diversity.
- Support of inter frequency hand over and hand over to other systems, including hand over to GSM.
- Efficient packet access.

4.3.2 WCDMA Key Technical Characteristics

The following table shows the key technical features of the WCDMA radio interface:

Table 4.2: WCDMA key technical characteristics

Multiple Access Scheme	DS-CDMA
Duplex Scheme	FDD/TDD
Packet Access	Dual mode (Combined and dedicated channel)
Multi-rate/Variable rate scheme	Variable spreading factor and multi-code
Chip Rate	3.84 Mcps
Carrier Spacing	4.4-5.2 MHz (200 kHz carrier raster)
Frame Length	10 ms
Inter Base Station Synchronization	FDD: No accurate synchronization needed
Channel Coding Scheme	Convolutional Code (rate 1/2 and 1/3)

The chip rate may be extended to two or three times the standard 3.84 Mcps to accommodate for data rates higher than 2 Mbps. The 200 kHz carrier raster has been chosen to facilitate coexistence and interoperability with GSM.

4.4 WCDMA Physical Layer at the Uplink

This section provides a layer 1 (also termed as physical layer) description of the radio access network of a WCDMA system operating in the FDD mode. The spreading and modulation operation for the Dedicated Physical Channels (DPCH) at the reverse link is illustrated in detail. The uplink data structure for the DPCHs is described and the spreading and scrambling codes used in the uplink are investigated. The spreading modulation and data structure for forward link DPCH, Physical Random Access channel (PRACH), Synchronization Channel (SCH), etc. are described in detail in [5] and [6] along with those of the uplink DPCHs.

4.4.1 Physical Channel Structure

WCDMA defines two dedicated physical channels in both links:

- Dedicated Physical Data Channel (DPDCH): to carry dedicated data generated at layer 2 and above.
- Dedicated Physical Control Channel (DPCCH): to carry layer 1 control information.

Each connection is allocated one DPCCH and zero, one or several DPDCHs. In addition, there are common physical channels defined as:

- Primary and secondary Common Control Physical Channels (CCPCH) to carry downlink common channels
- Synchronization Channels (SCH) for cell search
- Physical Random Access Channel (PRACH)

The spreading and modulation for the DPDCH and the DPCCH the uplink are described in the following two subsections.

4.4.1.1 Uplink Spreading and Modulation

In the uplink the data modulation of both the DPDCH and the DPCCH is Binary Phase Shift Keying (BPSK). The modulated DPCCH is mapped to the Q-channel, while the first DPDCH is mapped to the I-channel. Subsequently added DPDCHs are mapped alternatively to the I or the Q-channel. Spreading Modulation is applied after data modulation and before pulse shaping. The spreading modulation used in the uplink is dual channel QPSK. Spreading modulation consists of two different operations. The first one involves replacing each data symbol by a number of chips given by the spreading factor. The second operation is scrambling where a complex valued scrambling code is applied to the chips. The bandwidth of the signal spread signal becomes 3.84 Mcps. Figure 4.2 shows the spreading and modulation for an uplink user. The uplink user has a single DPDCH only.

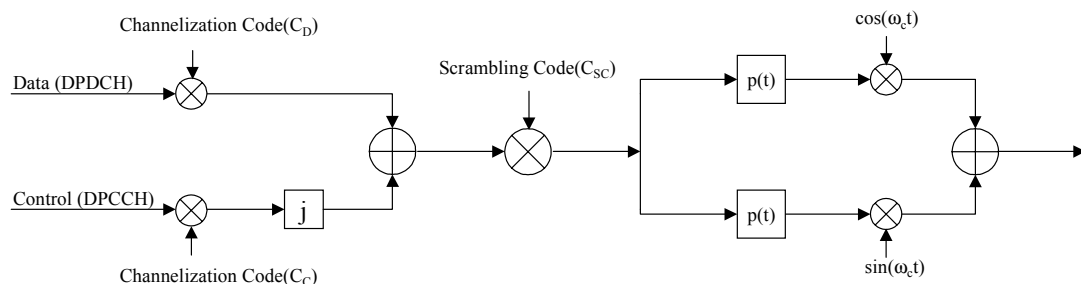


Figure 4.2: Uplink spreading and modulation

The bipolar data symbols on I and Q branches are independently multiplied by different channelization codes. The channelization codes are known as Orthogonal Variable Spreading Factor (OVSF) codes. OVSF codes are discussed in section 4.4.1.3. The resultant signal is multiplied by a complex scrambling code. The complex scrambling code is a unique signature of the mobile station. Next, the scrambled signal is pulse shaped. Square-Root Raised Cosine filters with roll-off factor of 0.22 are employed for pulse shaping. The pulse shaped signal is subsequently upconverted as shown in Figure 4.2. The application of a complex scrambling code with spreading modulation as described above is sometimes termed as Hybrid Phase Shift Keying (HPSK). HPSK reduces the peak-to-average power of the mobile station by generating the complex scrambling sequence in a special way [195]. The generation of complex scrambling code is discussed in section 4.4.1.4. The spreading factor for the control channel is always set at the highest value which is 256. The channelization code of the control channel is always a sequence of 256 ones.

4.4.1.2 Uplink Frame Structure

Figure 4.3 shows the principal frame structure of the uplink dedicated physical channels. Each frame of 10 ms is split into 15 slots. Each slot is of length 2560 chips, corresponding to one power control period. The super frame length is 720 ms; i.e. a super frame corresponds to 72 frames. Pilot bits assist coherent demodulation and channel estimation. TFCI stands for transport format combination indicator and is used to indicate and identify several simultaneous services. Feedback Information (FBI) bits are to be used to support techniques requiring feedback. TPC which stands for transmit power control is used for power control purposes. The exact number of bits of these different uplink DPCCH fields is given in [7].

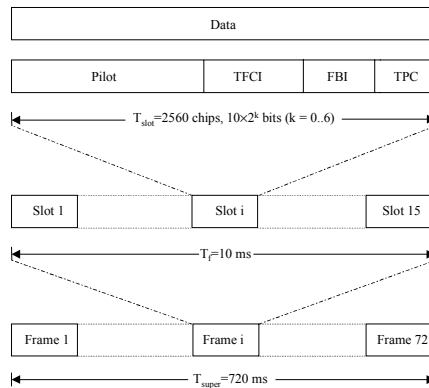


Figure 4.3: Frame structure for uplink DPDCH/DPCCH

The parameter k in Figure 4.3 determines the number of bits in each slot. It is related to spreading factor (SF) of the physical channel as

$$SF = \frac{256}{2^k} \quad (4.1)$$

The spreading factor thus may range from 256 down to 4. The spreading factor is selected according to the data rate. The following table shows the spreading factor and the number of data channel for the different data rates at the WCDMA uplink.

Table 4.3: Uplink data rate vs. spreading factor

Data rate (kbps)	Data channel spreading factor	Number of data channels
12.2	64	1
64	16	1
144	8	1
384	4	1
768	4	2
2048	4	6

4.4.1.3 Uplink Channelization Codes

The most important purpose of the channelization codes is to help preserve orthogonality among different physical channels of the uplink user. As mentioned in section 4.4.1.1, OVSF codes are employed as uplink spreading codes. OVSF codes can be explained using the code tree shown in Figure 4.4. The subscript here gives the spreading factor and the argument within the parenthesis provides the code number for that particular spreading factor.

Each level in the code tree defines spreading codes of length SF, corresponding to a particular spreading factor of SF. The number of codes for a particular spreading factor is equal to the spreading factor itself. All the codes of the same level constitute a set and they are orthogonal to each other. Any two codes of different levels are orthogonal to each other as long as one of them is not the mother of the other code. For example the codes $c_{16}(2)$, $c_8(1)$ and $c_4(1)$ are all mother codes of $c_{32}(3)$ and hence are not orthogonal to $c_{32}(32)$.

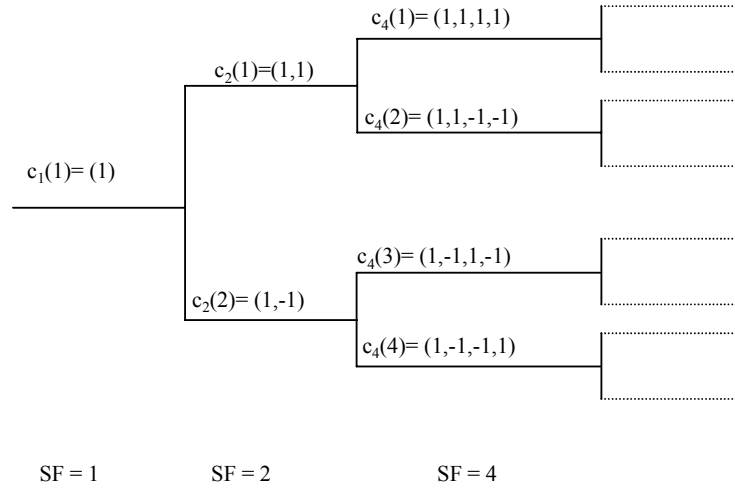


Figure 4.4: Code-tree for generation of OVSF codes

The generation method of OVSF can be explained with the help of the following matrix equations:

$$\begin{aligned}
 [c_1(1)] &= 1; & \begin{bmatrix} c_2(1) \\ c_2(2) \end{bmatrix} &= \begin{bmatrix} c_1(1) & c_1(1) \\ c_1(1) & \overline{c_1(1)} \end{bmatrix} = \begin{bmatrix} 1 & 1 \\ 1 & -1 \end{bmatrix} \\
 & & \bullet & \\
 & & \bullet & \\
 \begin{bmatrix} c_N(1) \\ c_N(2) \\ \cdot \\ \cdot \\ c_N(N-1) \\ c_N(N) \end{bmatrix} &= \begin{bmatrix} c_{N/2}(1) & \overline{c_{N/2}(1)} \\ c_{N/2}(1) & \overline{c_{N/2}(1)} \\ \cdot & \cdot \\ \cdot & \cdot \\ c_{N/2}(N/2) & \overline{c_{N/2}(N/2)} \\ c_{N/2}(N/2) & \overline{c_{N/2}(N)} \end{bmatrix}
 \end{aligned} \tag{4.2}$$

In the above matrix notation, an over bar indicates binary complement (e.g. $\overline{1} = -1$ and $\overline{-1} = 1$) and N is an integral power of two.

The OVSF codes do not have a single, narrow auto-correlation peak as shown in figure 4.5. As a consequence code-synchronization may become difficult. OVSF codes exhibit perfect orthogonality only at zero lags and even this does not hold for partial-sequence cross-correlation. As a result the advantage of using OVSF codes could be lost when all the users are not synchronized to a single time base or when significant multipath is present.

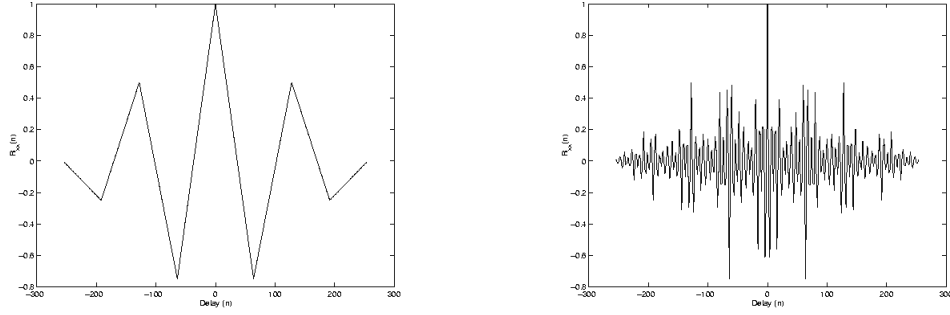


Figure 4.5: Auto-correlation for two OVSF codes of SF=256

A sequence of 256 ones, which is the first code at the code tree for a spreading factor of 256, is used to spread the DPCCH. The first DPDCH is spread by the code number $(SF/4+1)$ where SF is the spreading factor for the data channel. As for example, the 5th code is used for spreading the first DPDCH for a spreading factor of 16. So the spreading code for the first DPDCH is always a repetition of $\{1, 1, -1, -1\}$. Subsequently added DPDCHs for multi-code transmission are spread by codes in ascending order starting from code number 2 excepting the code used for the first DPDCH. Code selection in this orderly manner along with the proper choice of scrambling code increases the spectral efficiency by limiting the diagonal transitions in the signal constellation [194]. This also results into efficient use of the power amplifier [195]. We should mention that for multi-code transmission, the spreading factor is limited to 4 only.

4.4.1.4 Uplink Scrambling Codes

Uplink Scrambling codes help maintain separation among different mobile stations. Either short or long scrambling codes can be used in the uplink. Short scrambling codes are recommended for base stations equipped with advanced receivers employing multiuser detection or interference cancellation. In this report, we used long scrambling codes for the simulations.

Scrambling codes (both short and long) can be defined with the help of the following equation

$$C_{sc} = C_1(w_1 + jw_2C_2')$$
(4.3)

Here, C_1 is a real chip rate code, C_2' is a decimated version of a real chip rate code C_2 .

The usual decimation factor is 2 so that,

$$C_2'(2k) = C_2'(2k+1) = C_2(2k)$$
(4.4)

w_1 is a repetition of $\{1\ 1\}$ at the chip rate and w_2 is a repetition of $\{1\ -1\}$ at the chip rate
 So we can write

$$C_{sc} = C_1 + jw_2C_1C_2' \tag{4.5}$$

The following block diagram shows the implementation of Equation 4.5. All the additions and multiplications are performed in modulo 2 arithmetic.

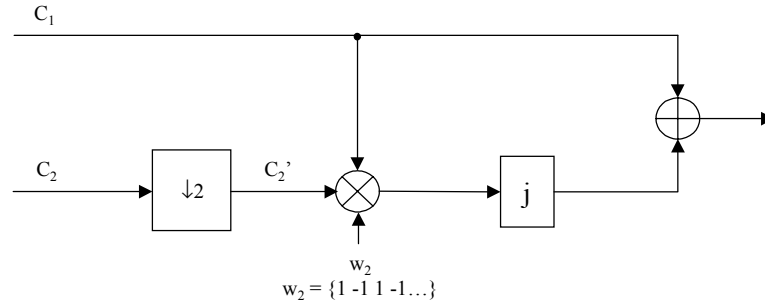


Figure 4.6: Generation of scrambling codes

The WCDMA standard defines a period of 10 ms or 1 frame for the period of the scrambling codes.

4.4.1.4.1 Uplink Long Scrambling Codes:

Long scrambling codes are constructed as described in section 4.4.1.4. The real chip rate codes C_1 and C_2 are formed as the position wise modulo 2 sum of 38400 chip segments of two binary m sequences. The binary m sequences are generated from two generator polynomials of degree 25. This is explained in detail below following the discussion in [6]

Two binary sequences x and y are generated using the generator polynomials $X^{25} + X^3 + 1$ and $X^{25} + X^3 + X^2 + X + 1$ respectively. The resulting sequence constitutes segments of a set of Gold sequences. Let $n_{23}.....n_0$ be the 24 bit binary representation of the scrambling code number n (decimal). In the binary representation, n_0 is the least significant bit (LSB). The x sequence depends on the choice of the scrambling code number and is thus denoted as x_n . Furthermore, let $x_n(i)$ and $y(i)$ denote the i^{th} symbol of the sequences x_n and y respectively. The m sequences are constructed the following way

The Initial conditions are set:

$$\begin{aligned} x_n(0) = n_0, x_n(1) = n_1, \dots, x_n(22) = n_{22}, x_n(23) = n_{23}, x_n(24) = 1 \\ y(0) = y(1) = \dots, y(23) = y(24) = 1 \end{aligned} \quad (4.6)$$

Then subsequent symbols are generated recursively according to:

$$\begin{aligned} x_n(i + 25) = \langle x_n(i + 3) + x_n(i) \rangle_{\text{mod } 2}, i = 0, 1, \dots, 2^{25} - 27 \\ y(i + 25) = \langle y(i + 3) + y(i + 2) + y(i + 1) + y(i) \rangle_{\text{mod } 2}, i = 0, 1, \dots, 2^{25} - 27 \end{aligned} \quad (4.7)$$

The real chip rate code $C_{1,n}$ and $C_{2,n}$ for the n th scrambling code are defined as

$$\begin{aligned} C_{1,n} = \{ \langle x_n(0) + y(0) \rangle_{\text{mod } 2}, \langle x_n(1) + y(1) \rangle_{\text{mod } 2}, \dots, \langle x_n(N-1) + y(N-1) \rangle_{\text{mod } 2} \} \\ C_{2,n} = \left\{ \begin{array}{l} \langle x_n(M) \rangle_{\text{mod } 2} \\ \langle +y(M) \rangle_{\text{mod } 2} \end{array} \right\}, \left\{ \begin{array}{l} \langle x_n(M+1) \rangle_{\text{mod } 2} \\ \langle +y(M+1) \rangle_{\text{mod } 2} \end{array} \right\}, \dots, \left\{ \begin{array}{l} \langle x_n(M+N-1) \rangle_{\text{mod } 2} \\ \langle +y(M+N-1) \rangle_{\text{mod } 2} \end{array} \right\} \end{aligned} \quad (4.8)$$

The generation of the codes $C_{1,n}$ and $C_{2,n}$ are explained in the next figure [6]

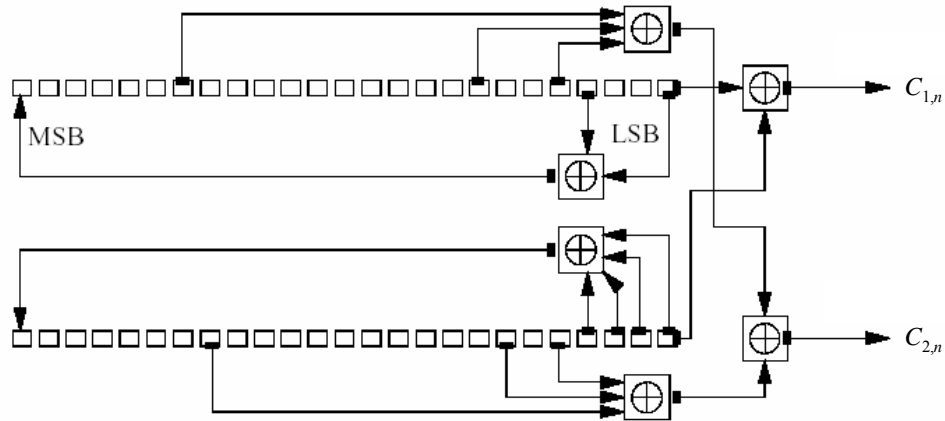


Figure 4.7: Uplink long scrambling code generator

The scrambling codes are designed so that they have very low cross-correlation among them. This ensures good Multiple Access Interference (MAI) rejection capability.

4.4.1.4.2 Uplink Short Scrambling Codes

The short scrambling codes are also generated in the same way as described in section 4.4.1.4. Here the real and imaginary parts of the complex spreading codes, C_1 and C_2 respectively, are taken from a

family of periodically extended $S(2)$ codes. The uplink short codes $S_v(n)$, $n=0,1,\dots,255$, of length 256 chips are obtained as the one chip periodic extension of $S(2)$ sequences of length 255 [6]. So $S_v(0)=S_v(255)$. Figure 4.8 shows the generation of uplink short scrambling codes.

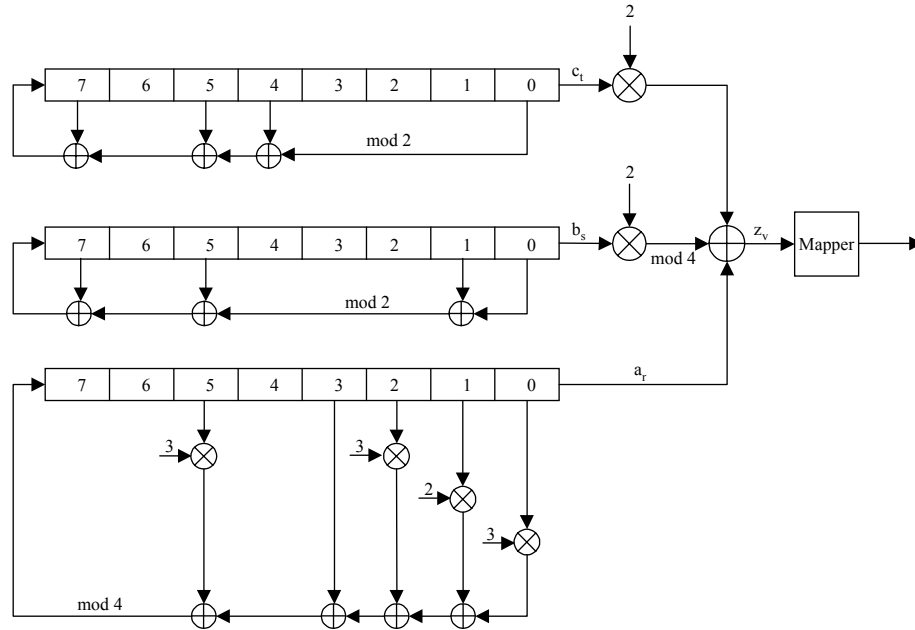


Figure 4.8: Uplink short scrambling code generator

The quaternary sequence $z_v(n)$, $0 \leq v \leq 16777216$, of length 255 is generated by the modulo 4 summation of the quaternary sequence $a_r(n)$ and the two binary sequences $b_s(n)$ and $c_t(n)$, i.e.

$$z_v(n) = \langle a_r(n) + 2b_s(n) + 2c_t(n) \rangle_{\text{mod } 4} \quad n = 0, 1, \dots, 254 \quad (4.9)$$

The user index v determines the indexes r , s and t in the following way

$$\begin{aligned} v &= r + 2^8 \cdot s + 2^{16} \cdot t \\ r &= 0, 1, \dots, 254, \quad s = 0, 1, \dots, 254, \quad t = 0, 1, \dots, 254 \end{aligned} \quad (4.10)$$

The values of the indexes s and t are converted to 8-bit binary and used as the initial states at the respective registers. The value of the index r is transformed to an 8-bit word before being used as the initial state at the generator. The transformation is given by:

$$a_r(0) = \langle 2v_r(0) + 1 \rangle_{\text{mod } 4} \quad (4.11)$$

$$a_r(n) = \langle 2v_r(n) \rangle_{\text{mod } 4} \quad n = 1, 2, \dots, 7 \quad (4.12)$$

Figure 4.9 shows the initial conditions at the shift registers.

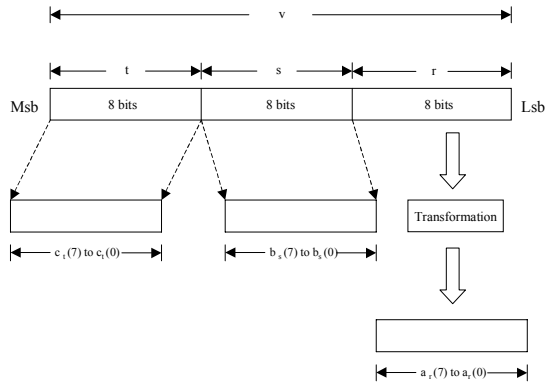


Figure 4.9: Initial conditions at the shift registers

The sequence $z_v(n)$ is mapped to $S_v(n)$ according to the following table. The real and imaginary parts of $S_v(n)$ are the sequences $C_1(n)$ and $C_2(n)$ respectively.

Table 4.4: Mapping of $z_v(n)$

$z_v(n)$	$S_v(n)$
0	$+1+j$
1	$-1+j$
2	$-1-j$
3	$+1-j$

4.4.1.5 Summary of WCDMA Uplink Modulation

We can summarize the discussion on the modulation applied to the dedicated physical channels in the following table

Table 4.5: Parameters of WCDMA spreading and modulation at the uplink

Spreading Modulation	Dual Channel QPSK for UL
Data Modulation	BPSK for UL
Channelization	OVSF codes
Scrambling	Complex Scrambling
Frame Length	10 ms
Chip Rate	3.84 Mcps
Pulse Shaping	Raised Cosine with 0.22 roll off

4.4.2 Channel Coding

The main purpose of channel coding is to selectively introduce redundancy into the transmitted data and improve the wireless link performance in the process [3]. Channel codes can be used to detect as well as correct errors. The WCDMA systems have provision for both error detection and error correction. Channel coding scheme at the WCDMA system is a combination of error detection, error correction, along with rate matching, interleaving and transport channels mapping onto/splitting from physical channels [196]. This section gives a brief description on the error detection and error correction schemes recommended for the WCDMA systems.

4.4.2.1 Error Detection

Error detection is provided by a Cyclic Redundancy Check (CRC) code. The CRC is 24,16,8 or 0 bits. The entire transmitted frame is used to compute the parity bits. Any of the following cyclic generator polynomials can be used to construct the parity bits:

$$\begin{aligned}
 g_{24}(D) &= D^{24} + D^{23} + D^6 + D^5 + D + 1 \\
 g_{16}(D) &= D^{16} + D^{12} + D^5 + D + 1 \\
 g_8(D) &= D^8 + D^7 + D^4 + D^3 + D + 1
 \end{aligned}
 \tag{4.13}$$

A detailed description of the error detection scheme is given in [196].

4.4.2.2 Error Correction

Two alternative error correction schemes have been specified for the WCDMA system. They are Convolutional Coding and Turbo Coding. For standard services that require BER up to 10^{-3} , which is the case for voice applications, convolutional coding is to be applied. The constraint length for the proposed convolutional coding schemes is 9. Both rate 1/2 and 1/3 convolutional coding have been specified. For high-quality services that require BER from 10^{-3} to 10^{-6} , turbo coding is required. The feasibility of applying 4-state Serial Concatenated Convolutional Code (SCCC) has been investigated by different standardization bodies. Reference [196] provides a detailed description of the error correction coding schemes along with rate matching, interleaving and transport channel mapping.

For the simulations performed for this report, we did not employ any error detection or error correction schemes.

4.5 Deployment Status of 3G around the World^{[197], [198]}

This section presents 3G activities that are taking place in major parts of the world. This will illuminate highlights regarding 3G deployments and provide a clear view about the developments and key issues that face the 3G systems. Different geographically important regions for 3G perspectives are addressed and these include USA, Europe, Asia, South America and Australia.

4.5.1 Status of 3G in the USA

The deployment of 3G cellular systems in the USA faces two major obstacles: legacy problem arising from a multitude of already existing 2G networks and the availability (or the lack of) RF spectrum. The existing networks are a major factor in determining what path the carriers will choose to get to 3G. As per present-day status, WCDMA and CDMA2000 are the two realistic options. While WCDMA is a natural progression of GSM networks, CDMA2000 builds on standards currently using CDMA technology. The US currently has six major carriers or wireless service providers (Verizon, Sprint, Cingular, AT& T Wireless, Nextel, VoiceStream) and between them they have three different 2G cellular standards (CDMA, TDMA and GSM). This means that the 3G in the U.S. may be heading towards both WCDMA and CDMA 2000 for the next generation of mobile applications.

Shortage of spectrum may seriously undermine 3G implementation in the US. The frequency band between 2520 to 2670 MHz has already been identified for 3G. However this means that the big six carriers will have an average of somewhere between 25 MHz and 35 MHz of spectrum. In marked contrast, the big European carriers have about 90 MHz. As a result many feel that the US currently does not have adequate spectrum for a full-fledged nationwide implementation of 3G mobile services. The FCC has been discussing the possible allocation of the 1710-1755 band, primarily used by the U.S. Department of Defense, and the 2110-2150 band which is used by schools and health care centers. Both the US army and the Navy have refused to move into another frequency band. They maintain that altering the frequency of the military equipments could be a security risk and this migration will not be a speedy process. The Air Force has however indicated that it will handover its portion of the spectrum for \$3.2 billion, which it claims is necessary to relocate its air-to-ground satellite communication system. Schools and health care centers have also balked at moving because of potentially enormous costs. As a result the FCC is struggling to find suitable spectrum for 3G services and recently postponed the designation of spectrum for 3G. This can significantly delay the rollout of 3G in the US.

Hoping to be the first to implement 3G in the U.S., several of the major carriers have been conducting field trials on the CDMA 2000 1XRTT. It appears that although most of the carriers have not decided on a particular standard yet, they do have some interim plans to speed up their network until they decide which third generation wireless solution they will eventually pursue. Several of the US carriers have significant stakeholder in European and Japanese carriers who have already adopted WCDMA as their 3G standard. They wield a significant influence on their US affiliates and may be the deciding factor in choosing the standard for the next generation cellular network in the US.

Sprint PCS whose network is solely CDMA based, has decided to go with the CDMA2000 standard. During the middle of March 2001, Sprint announced that it would roll out its 3G technology in four phases. The first phase of the deployment will be to migrate to a CDMA2000 network, which will double the Sprint PCS network's capacity for voice communications, increase data transmission speeds from 14.4Kbps to 144Kbps. Companies supporting Sprint PCS' 3G migration include Lucent Technologies, Motorola, Nortel Networks, and Qualcomm.

AT&T Wireless, who has about 18 percent of the wireless market in the U.S, is the only carrier in the US to date that has officially stated that it will migrate to WCDMA. The company's Japanese affiliate NTT DoCoMo, who is a 16% stakeholder, had a big part in its decision-making. AT&T Wireless' plan is to begin overlaying GSM/GPRS on its TDMA network this year and is on schedule to begin introducing 2.5G services. Nokia Networks will provide AT&T Wireless with GPRS-ready 850 and 1900 MHz radio network systems designed for seamless evolution to 3G.

Verizon Wireless (which has a 27 percent share of the wireless market) is upgrading its network with interim technologies compatible with CDMA2000. The carrier has already upgraded its network to support next generation technology for enhanced wireless voice capacity in parts of Metro New York and Northern New Jersey. Lucent Technologies has a three-year, \$5 billion deal with Verizon Wireless to supply 3G mobile telephony equipment. Verizon is also conducting trials with Ericsson handsets for using CDMA2000. British worldwide carrier Vodafone, which owns about 45% of Verizon, has recently announced that it would encourage Verizon to switch to WCDMA and as of now, it appears Verizon Wireless eventually will use a WCDMA network standard for 3G wireless services.

VoiceStream, who are backed by the big European carrier Deutsche Telekom, will probably be also migrating towards WCDMA. VoiceStream currently owns 6 percent market share in the US. Given

this scenario, WCDMA appears to have won at least 51% of the US market share. Cingular (with about 21% of the US market share) probably faces the toughest road to 3G, because its network is part TDMA and part GSM. During the middle of March 2001, the company announced its plan to roll out the 2.5G data service GPRS. The company plans to roll out the service first in California, Nevada, and Washington, followed by regions in the southeastern United States. Since GPRS is based on GSM networks, Cingular appears to be leaning towards WCDMA. This overwhelming majority of WCDMA may force Nextel (9 percent market share) to also choose WCDMA, although the company is currently conducting tests on CDMA 2000 1XRTT.

4.5.2 Status of 3G in Europe

The deployment of 3G services in Europe seems to be significantly ahead than that in the US. Since GSM was the prevalent 2G standard in Europe, the WCDMA based 3G standard was supported by the European carriers from the very beginning of the 3G standardization process. The spectrum for the 3G has been already auctioned at different European countries and the carriers have paid approximately US\$126 billion on wireless licenses.

The largest of European service providers, Britain based Vodafone, had announced that commercial 3G services would be launched in the second half of 2002. However recent development suggests that they are slowing the rollout of its infrastructure for 3G networks in the UK and other European countries and its launch of 3G services could slip to the middle of 2003. Recently British Telecommunications also indicated that it would delay the rollout of its first 3G service on Britain's Isle of Man due to a software bug in equipment that made the cell-to-cell handover of calls unreliable. Nortel and NEC have contracts with B-T to supply 3G equipments.

4.5.3 Status of 3G in the South America

Most Latin American countries, except for the large countries like Brazil and Argentina, probably will not roll out 3G services anytime soon. Telesp Celular, Brazil's largest mobile operator, and Lucent recently announced a \$130 million contract to introduce the first 3G mobile network in Brazil. They are going with the interim CDMA 2000 based 1XRTT. On the other hand, Telemar, the biggest fixed operator in Brazil, is planning on launching a GSM based GPRS service with the help from Nokia. This is a strong indication that WCDMA could be the next generation technology chosen by the company. Argentina is in the process of auctioning the spectrum for 3G and the Argentine

government expects to raise between \$500 million and \$600 million from the auction. Current 2G services in Argentina include CDMA, GSM and TDMA. As a result, the country could be heading towards both WCDMA and CDMA2000.

4.5.4 Status of 3G in Asia¹

4.5.4.1 3G in Korea

All of the second generation cellular systems in Korea are based on IS95 CDMA technology. As a result, it seems that selecting CDMA2000 is a natural migration from 2 G to 3 G. However, all of the major service providers in Korea insisted deployment of third generation systems based on WCDMA because they wanted global roaming throughout the Asian area where most of the 2 G networks are based on GSM. Meanwhile, Korean government wanted to keep both WCDMA and CDMA2000 as standards for 3G. Finally, Korean government has selected two service providers, SKIMT and KTicomm, as WCDMA based service providers and one consortium consisting of LG Telecomm, Hanaro, and PowerComm as CDMA2000 based service providers.

Three major wireless service providers, SK Telecomm, KT, and LG Telecomm, are now providing CDMA 1x based services in limited areas. The biggest service carrier, SK Telecomm, who has about 50 percent of wireless market in Korea, is the first in the world to offer 3G services to its customers and provides the highest data rate in the world at 144kbps, based on Qualcomm's CDMA2000 technology. SKIMT, which merged to SK Telecomm, could not deploy its WCDMA IMT-2000 third generation wireless service before the start of 2002 Soccer World Cup co-host by Japan and Korea as it had originally promised. However, the company has further plans to launch commercial service of a CDMA-IMT 2000 service as a third-generation CDMA2000 1X-EV-DO (Evolution Data Only). KTicomm, the second largest wireless carrier in Korea, is in the selection process for infrastructure equipments supplier in order to place orders for WCDMA based wireless network equipments. The company is planning on deploying its WCDMA based wireless services by the end 2002 as the company promised.

However, there is skepticism about deploying WCDMA based wireless networks in Korea. Qualcomm disclosed that the company would not be able to make the chip sets MSM6500 and MSM6600, which are core chip sets to support roaming between second and third generation and between CDMA2000 and WCDMA based networks, available to the public until 2003. If Korean

¹ The author would like to thank K.K. Bae for his contributions

government requires service providers to support roaming between heterogeneous networks such as 2G and 3G, and CDMA2000 based and WCDMA based networks, and even requires dual mode handset, the deployment of 3G wireless services will be significantly delayed.

4.5.4.2 3G in Japan

The deployment of 3G WCDMA based services in Japan is significantly ahead of that of the USA and is competing with European companies. Two wireless carriers acquired license for WCDMA based 3G services and one carrier acquired for CDMA2000 based 3G services. NTT DoCoMo conducted trial WCDMA based 3G services called FOMA to 4500 subscribers in Tokyo, Kawasaki, and Yokohama on May 30, 2001. The trial service was conducted for four months with expected maximum data rate at 384 kbps. NTT DoCoMo has started providing commercial services in limited areas, and is planning on expanding services to nationwide in 2003.

4.5.4.3 3G in China

Most of the current second generation networks in China are GSM based. China Mobile, China's largest mobile service provider uses GSM technology. China Unicom, China's sole CDMA service provider and the second largest, is making headway in offering CDMA 2000 service aiming at 78 million subscribers, which accounts for a market share of 30 percent, over the next five years. The company made contracts for CDMA mobile equipments with Lucent Technology and Motorola for US\$400 million each, with Nortel Networks for US\$275 million, and with Samsung and Ericsson for US\$200 million each.

4.5.4.3 3G in India

India plans to use CDMA2000 technology as the 3G standard.

4.5.5 Status of 3G in Australia

Hutchison Telecom made a contract with Ericsson for third generation network in Australia under a \$435 million contract marking Ericsson's first 3G project in Australia. Ericsson will provide a radio access network, IP core network and transmission technologies. Also included in the contract are advanced network management systems, network operations, mobile Internet application platforms and terminals.

Chapter 5

Eigen-Beamforming based on MSNR Criterion

5.1 Introduction

In this chapter we investigate several computationally simple adaptive algorithms for solving the Simple Eigenvalue problem resulting from the Maximum Signal to Noise Ratio (MSNR) beamforming criterion. We compare the different algorithms in terms of their computational complexity. A Beamformer-Rake receiver employing the MSNR beamforming criterion is developed for the WCDMA reverse link. We conclude the chapter with simulation results that show the performance of the different algorithms when this receiver operates under various propagation and MAI conditions.

5.2 Adaptive Algorithms to Solve the Simple Eigenvalue Problem

There are several algorithms that can be applied to solve the simple eigenvalue problem. In this section we will discuss some of these techniques in detail. The algorithms discussed in this section are

- Power Method
- Lagrange Multiplier Method
- Conjugate Gradient Method

We will provide flowcharts of the algorithms. Simple and efficient numerical methods are required to solve the SE for practical implementation. Therefore we will estimate the computational complexity of each of these algorithms.

5.2.1 Metric for Computational Complexity

Before we start discussion on the adaptive algorithms to solve the simple eigenvalue problem, we need to define a metric or unit to measure the computational complexity of a particular algorithm.

Let us consider the scalar multiplication of two $N \times 1$ vectors complex vectors \underline{x} and \underline{y} where

$$\underline{x} = \left[x_{real}^1 + j x_{imag}^1 \quad x_{real}^2 + j x_{imag}^2 \quad \dots \quad \dots \quad x_{real}^N + j x_{imag}^N \right]^T \text{ and}$$

$$\underline{y} = \left[y_{real}^1 + j y_{imag}^1 \quad y_{real}^2 + j y_{imag}^2 \quad \dots \quad y_{real}^N + j y_{imag}^N \right]^T$$

Now a scalar multiplication will yield

$$\underline{x}^H \underline{y} = \sum_{i=1}^N \left\{ \left(x_{real}^i y_{real}^i + x_{imag}^i y_{imag}^i \right) + j \left(x_{imag}^i y_{real}^i - x_{real}^i y_{imag}^i \right) \right\} \quad (5.1)$$

So N Complex Multiplications (CM) and $N-1$ Complex Additions (CA) are required to perform such an operation. Since CA is easier to implement than CM, we will use CM as a measure of computational load. Let us define $O(\eta N)$ to be the metric of computational complexity which represents η times N number of CM. Throughout this report, we will use $O(\eta N)$ as the unit to measure the computational complexity of an algorithm.

5.2.2 Power Method

The power method [11] is probably the most well-known method to solve the simple eigenvalue problem. This technique is defined by the following simple update equation:

$$\underline{w}(i+1) = \frac{1}{\lambda(i)} \underline{R}_{ss}(k) \underline{w}(i), \quad (5.2)$$

where the eigenvalue is calculated at each iteration as

$$\lambda(i) = \frac{\underline{w}^H(i) \underline{R}_{ss}(k) \underline{w}(i)}{\underline{w}^H(i) \underline{w}(i)}. \quad (5.3)$$

Here i is the index of iteration for each snapshot (sample) index k .

In the limit $i \rightarrow \infty$, the estimated eigenvalue eigenvector pair converges to the true quantities.

In a time varying environment the covariance matrix is estimated as [1]

$$\underline{R}_{ss}(k) = f \underline{R}_{ss}(k-1) + \underline{s}(k) \underline{s}^H(k) \quad (5.4)$$

where f is a forgetting factor between 0 and 1.

Since, it is the eigenvector not the eigenvalue that is of real concern for performing the beamforming, we can write down the following set of equations for the modified power method where a single iteration of the power method is applied during each snapshot.

$$\begin{aligned}\underline{q}(k+1) &= \underline{\underline{R}}_{ss}(k)\underline{w}(k) \\ \underline{w}(k+1) &= \frac{\underline{q}(k+1)}{\|\underline{q}(k+1)\|}\end{aligned}\tag{5.5}$$

Note that the iteration index i reduces to the snapshot index k . Also we do not need to calculate the corresponding eigenvalue which is just a real scalar. We observe that the computation complexity of the power method is $O(N^2 + N)$ where N is the number of elements. We would require another $O(1.5N^2)$ for updating the covariance matrix.

We still have to choose an initial condition for the power iteration. Any signal in the N dimensional signal space can be expressed as a linear combination of the eigenvectors or the natural bases so that

$$\underline{s} = \sum_{i=0}^{N-1} a_i \underline{q}_i\tag{5.6}$$

Here $\underline{q}_0, \underline{q}_1, \underline{q}_2, \dots, \underline{q}_{N-1}$ are the eigenvectors corresponding to the eigenvalues $\lambda_0 > \lambda_1 \geq \lambda_2, \dots, \lambda_{N-1}$. As long as $a_0 \neq 0$ for the initial condition, the power method will converge. In order to guarantee a very fast convergence, it is better to have an initial guess that is *rich* in the direction of \underline{q}_0 i.e. when a_0 is large compared to the other coefficients. The signal at the output of the CDMA correlator has such property because of the processing gain. As a result $\underline{w}(0) = \frac{\underline{s}(0)}{\|\underline{s}(0)\|}$ is a good starting point for iterative algorithms to solve the SE. Here $\underline{s}(0)$ is the first sample of the signal vector at the output of the despreader. We are going to utilize this initial condition in the adaptive algorithms to solve the SE as well as the generalized eigenvalue problem arising from MSINR based Eigen-Beamforming described in this dissertation.

If we employ the instantaneous estimate of the covariance matrices so that $\underline{\underline{R}}_{ss}(k) = \underline{s}(k)\underline{s}^H(k)$, the power method can be described by the following set of equations

$$\begin{aligned}y(k) &= \underline{w}^H(k)\underline{s}(k) \\ \underline{q}(k+1) &= y^*(k)\underline{s}(k) \\ \underline{w}(k+1) &= \frac{\underline{q}(k+1)}{\|\underline{q}(k+1)\|}\end{aligned}\tag{5.7}$$

This reduces the computational complexity of the power method to $O(3N)$. However our investigation showed that there is a stiff performance penalty associated with this simplification and consequently we did not employ this simplification when presenting the final simulation results. However we have pointed out another linearization of the power method in the Section 9.3.1.2 of Chapter 9.

5.2.3 Lagrange Multiplier Method

The Lagrange multiplier method computes the optimum weight vector by treating the Simple Eigenvalue problem as a constrained maximization problem [145]. The goal is to find a weight vector \underline{w} that maximizes $\underline{w}^H \underline{R}_{ss} \underline{w}$ subject to the constraint $\underline{w}^H \underline{w} = 1$. So, we can introduce the following functional

$$J(\underline{w}) = \underline{w}^H \underline{R}_{ss} \underline{w} + \gamma(1 - \underline{w}^H \underline{w}), \quad (5.8)$$

where γ is the Lagrange multiplier for the constraint $\underline{w}^H \underline{w} = 1$.

We will try to maximize the functional $J(\underline{w})$ subject to the constraint $\underline{w}^H \underline{w} = 1$. If the method of steepest ascent is employed to iteratively find the weight vector \underline{w} that maximizes $J(\underline{w})$, we can write

$$\underline{w}(k+1) = \underline{w}(k) + \frac{1}{2} \mu \underline{\nabla}(k) \quad (5.9)$$

Here, μ is a positive real constant which is chosen for the convergence of the adaptive procedure and $\underline{\nabla}$ is the gradient vector of the functional $J(\underline{w})$ with respect to \underline{w}^H (sometimes termed as the conjugate derivative). So, the weight update equation becomes

$$\underline{w}(k+1) = \underline{w}(k) + \mu \left[\underline{R}_{ss}(k) - \gamma(k) \underline{I} \right] \underline{w}(k) \quad (5.10)$$

Here, \underline{I} is the $N \times N$ identity matrix. Note that since Equation 5.10 represents a geometric series, μ must satisfy the following criterion for the absolute convergence of the weight vector \underline{w}

$$0 < \mu < \frac{2}{\lambda_0 - \lambda_i}, \quad i = 1, 2, \dots, N-1 \quad (5.11)$$

where $\lambda_0 \geq \lambda_1 \geq \dots \geq \lambda_{N-1}$ are the eigenvalues of the covariance matrix \underline{R}_{ss} .

Since the constraint must be satisfied at each iteration, we can employ the expression given by Equation 5.10 to $\underline{w}^H(k+1)\underline{w}(k+1)=1$. By recognizing the fact that $\underline{w}^H(k)\underline{w}(k)=1$ also, we can write the following solution for $\gamma(k)$ [145]:

$$\gamma(k) = \frac{b - \sqrt{b^2 - ac}}{a} \quad (5.12)$$

where,

$$\begin{aligned} a &= \mu, \quad b = 1 + \mu \underline{w}^H(k) \underline{\underline{R}}_{ss}(k) \underline{w}(k) \\ c &= \mu \underline{w}^H(k) \underline{\underline{R}}_{ss}^2(k) \underline{w}(k) + 2 \underline{w}^H(k) \underline{\underline{R}}_{ss}(k) \underline{w}(k) \end{aligned} \quad (5.13)$$

The signal covariance matrix can be estimated as Equation 5.4 which is repeated here

$$\underline{\underline{R}}_{ss}(k) = f \underline{\underline{R}}_{ss}(k-1) + \underline{s}(k) \underline{s}^H(k) \quad (5.14)$$

As stated before, $\underline{w}(0) = \frac{\underline{s}(0)}{\|\underline{s}(0)\|}$ is a very good initial guess at the beginning of the iteration. The

weight vector $\underline{w}(k)$ is normalized at the end of each iteration. Figure 5.1 illustrates the flowchart of the Lagrange multiplier algorithm:

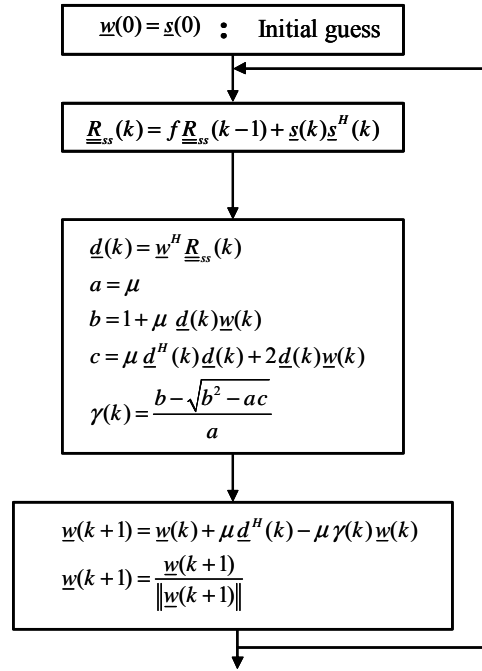


Figure 5.1: Flowchart of the Lagrange multiplier method

We can observe that the Lagrange multiplier method takes about $O(2N^2 + 4.5N)$ computations for each iteration. Thus the computational complexity is quadratic with the number of antenna elements. We can reduce the computational complexity and make it linear with the number of antenna elements by using the instantaneous signal vectors only to estimate the signal covariance matrix [145] so that $\underline{\underline{R}}_{ss}(k) = \underline{s}(k)\underline{s}^H(k)$.

The weight update equation becomes

$$\underline{w}(k+1) = [1 - \mu\gamma(k)]\underline{w}(k) + \mu y^*(k)\underline{s}(k) \quad (5.15)$$

where,

$$\gamma(k) = \frac{b - \sqrt{b^2 - ac}}{a} \quad (5.16)$$

$$a = \mu, b = 1 + \mu |y(k)|^2, c = |y(k)|^2 \left\{ \mu \|\underline{s}(k)\|^2 + 2 \right\}, y(k) = \underline{w}^H(k)\underline{s}(k) \quad (5.17)$$

At the beginning of the iteration, $\underline{w}(0) = \frac{\underline{s}(0)}{\|\underline{s}(0)\|}$ is still applied as an initial guess and the weight vector

$\underline{w}(k)$ is still normalized at the end of each iteration.

The flowchart of the simplified Lagrange multiplier method is shown next:

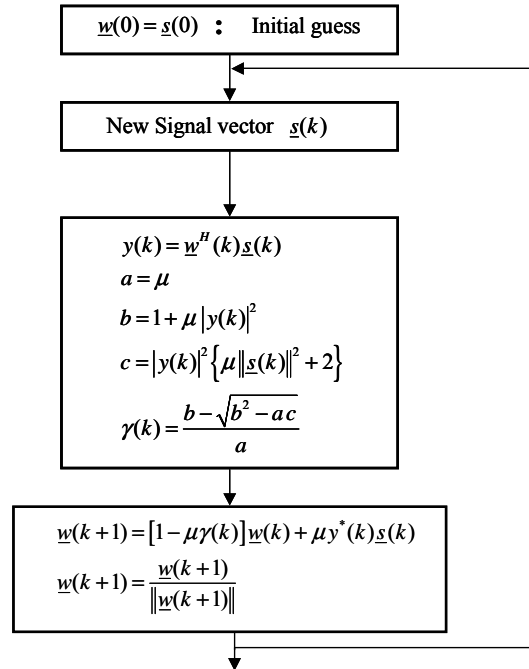


Figure 5.2: Flowchart of the simple linear Lagrange multiplier method

The simplified Lagrange multiplier method has $O(4N)$ computational complexity. So the computational complexity has been reduced significantly and linearized. The method of Lagrange multiplier can be utilized to develop an alternate algorithm that also has linear computational complexity. We derive this method in Section 9.3.1.1.

5.2.4 Conjugate Gradient Method

The Conjugate Gradient Method (CGM) [11] is a well-known method to solve matrix equations of the form $\underline{A}\underline{x} = \underline{y}$ where the matrix \underline{A} and the excitation vector \underline{y} are known. The CGM was modified in [142], [143] based on the fact that the solution to the Simple Eigenvalue problem maximizes the Rayleigh quotient of the covariance matrix at each snapshot. It was proposed that the weight can be updated by the following equation:

$$\underline{w}(i+1) = \underline{w}(i) + p(i)\underline{v}(i). \quad (5.18)$$

The adaptive gain $p(i)$ for the i^{th} iteration is determined so that it maximizes the following functional, which is the aforementioned Rayleigh quotient, at each snapshot $k = 1, 2, \dots$

$$J(\underline{w}(i)) = \frac{\underline{w}^H(i)\underline{R}_{ss}(k)\underline{w}(i)}{\underline{w}^H(i)\underline{w}(i)}, \quad (5.19)$$

with the constraint $\underline{w}^H(i)\underline{w}(i) = 1$. Here i is the iteration number in a given snapshot. The functional $J(\underline{w}(i))$ is maximized as the iteration proceeds $i = 1, 2, \dots$ for each snapshot k . The iteration continues as the functional converges to its maximum at each snapshot and the weight is updated at each iteration by Equation 5.18.

Now the adaptive gain $p(i)$ that maximizes (or minimizes) $J(\underline{w}(i))$ must satisfy the following condition:

$$\frac{\partial}{\partial p(i)} [J(\underline{w}(i+1))] = 0 \quad (5.20)$$

So from Equations 5.18 and 5.19 and by realizing the fact that $\underline{w}^H(i)\underline{w}(i) = 1$, we can write [142]

$$p(i) = \frac{-B \pm \sqrt{B^2 - 4AC}}{2A}, \quad (5.21)$$

where,

$$\begin{aligned}
 A &= b(i) \operatorname{Re}[c(i)] - d(i) \operatorname{Re}[a(i)] \\
 B &= b(i) - \lambda(i) d(i) \\
 C &= \operatorname{Re}[a(i)] - \lambda(i) \operatorname{Re}[c(i)]
 \end{aligned} \tag{5.22}$$

and

$$\begin{aligned}
 \lambda(i) &= \underline{w}^H(i) \underline{R}_{ss}(k) \underline{w}(i) \\
 a(i) &= \underline{w}^H(i) \underline{R}_{ss}(k) \underline{v}(i), \quad b(i) = \underline{v}^H(i) \underline{R}_{ss}(k) \underline{v}(i) \\
 c(i) &= \underline{w}^H(i) \underline{v}(i), \quad d(i) = \underline{v}^H(i) \underline{v}(i)
 \end{aligned} \tag{5.23}$$

Here $\operatorname{Re}[\cdot]$ is the real part of the complex quantity. Note that the negative sign in Equation 5.21 gives the adaptive gain $p(i)$ that maximizes the Rayleigh quotient (whereas the positive sign corresponds to the one that minimizes).

Obviously we still have to determine the search direction vector $\underline{v}(i)$ for the i^{th} iteration. The search direction vector is determined so that it is *conjugate* with the search direction vector at the previous iteration with respect to the covariance matrix $\underline{R}_{ss}(k)$. Consequently the search direction vector is updated according to the following equation:

$$\underline{v}(i+1) = \underline{r}(i+1) + \beta(i) \underline{v}(i) \tag{5.24}$$

Here \underline{r} is the residue vector representing the instantaneous error and is updated by

$$\underline{r}(i+1) = \lambda(i+1) \underline{w}(i+1) - \underline{R}_{ss}(k) \underline{w}(i+1) \tag{5.25}$$

where the maximum eigenvalue is updated by

$$\lambda(i+1) = \underline{w}^H(i+1) \underline{R}_{ss}(k) \underline{w}(i+1) \tag{5.26}$$

The scalar quantity $\beta(i)$ is given by

$$\beta(i) = - \frac{\underline{r}^H(i+1) \underline{R}_{ss}(k) \underline{v}(i)}{\underline{v}^H(i) \underline{R}_{ss}(k) \underline{v}(i)} \tag{5.27}$$

It was proposed in [142], [143] to run a single iteration of the CGM at each snapshot so that the iteration index i becomes the snapshot index k and the resulting algorithm was termed as the Modified

CGM (MCGM). The weight vector is normalized at the end of each iteration (snapshot) and to begin the procedure the following initial conditions are used:

$$\begin{aligned}
 \underline{w}(0) &= \frac{\underline{s}(0)}{\|\underline{s}(0)\|} \\
 \lambda(0) &= \underline{w}^H(0) \underline{\underline{R}}_{ss}(0) \underline{w}(0) \\
 \underline{v}(0) &= \underline{r}(0) = \lambda(0) \underline{w}(0) - \underline{\underline{R}}_{ss}(0) \underline{w}(0)
 \end{aligned} \tag{5.28}$$

The following figure shows the flowchart of the MCGM

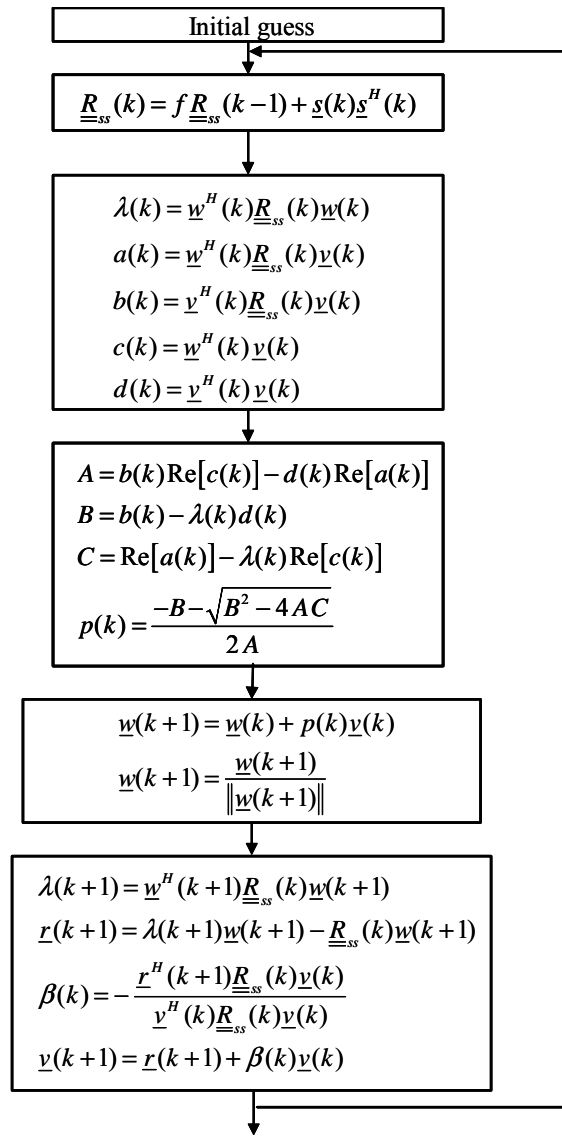


Figure 5.3: Flowchart of the modified conjugate gradient method

It is obvious that we need to perform a lot of matrix multiplications and as a result the computational complexity is quadratic with the number of antenna elements. We can observe that the computational load at $O(4N^2 + 10.5N)$ is very high and may be quite unacceptable for practical implementation. We can use the instantaneous estimate $\underline{\underline{R}}_{ss}(k) = \underline{s}(k)\underline{s}^H(k)$ as we did in the previous section for the Lagrange multiplier method. This will reduce the computational complexity at the cost of some performance degradation [142]. The following flowchart shows the simplified MCGM:

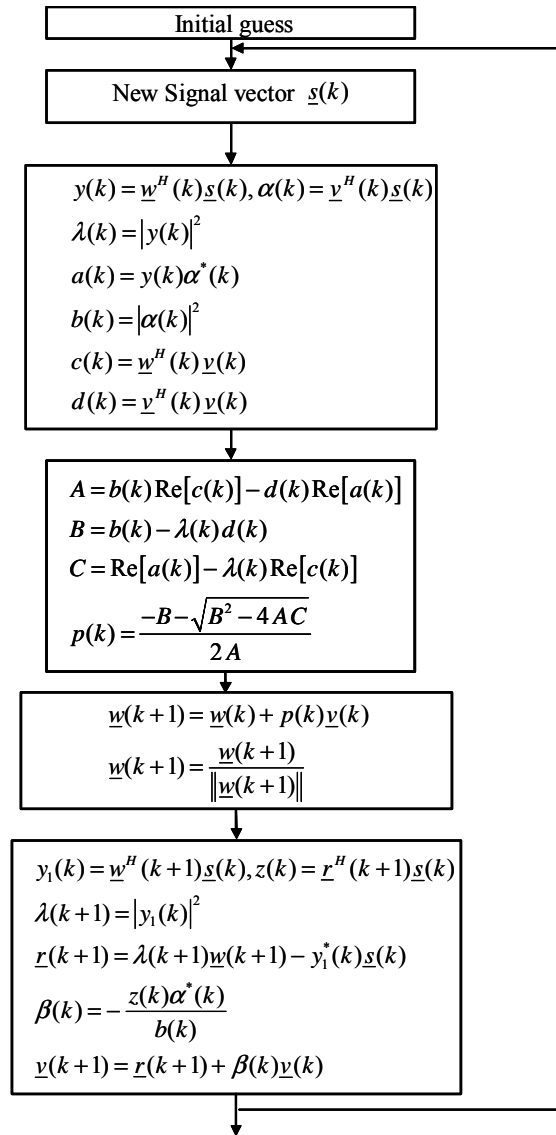


Figure 5.4: Flowchart of the linear modified conjugate gradient method

The computational complexity of the linear MCGM is still quite high at $O(9.5N)$.

5.2.5 Summary of the Algorithms

The following table compares the different algorithms in terms of their computational complexity

Table 5.1: Computational complexity of algorithms to solve the SE

Algorithm	Computational Complexity
Power Method	$O(N^2 + N)$
Lagrange Multiplier Method	$O(2N^2 + 4.5N)$
Linear Lagrange Multiplier Method	$O(4N)$
Modified Conjugate Gradient Method	$O(4N^2 + 10.5N)$
Linear Modified Conjugate Gradient Method	$O(9.5N)$

5.3 Block Processing for Slow Varying Environment

If the channel is changing slowly, tracking the changes becomes relatively easy and it is not necessary to update the weight at each sample. A single set of weight vector for a block of L samples, the value of L depending on the coherence time of the channel, can be sufficient. The covariance matrix can be estimated by averaging over L samples so that

$$\hat{\underline{R}}_{\underline{x}\underline{x}}(i) = \frac{1}{L} \sum_{l=N_{start}^i}^{N_{start}^i+L-1} \underline{x}(l) \underline{x}^H(l) \quad (5.29)$$

Here i is the block index, N_{start}^i is the sample index of the first sample of the i^{th} block. For such a scenario, it may be more efficient to generate a single set of weight for the block of L samples with the power method. Because of the fast convergence property of the power method it will require very few iterations (in most cases two or three) to compute a sufficiently accurate weight vector.

5.4 MSNR Based Beamformer-Rake Receiver for WCDMA Uplink

In this section we propose a MSNR based Beamformer-Rake receiver which is applicable in the reverse link of a WCDMA system. The proposed receiver is shown in Figure 5.5. In WCDMA uplink, the transmission format for a frame in the data channels is conveyed by the Transport Format Combination Indicator (TFCI) symbols of the corresponding Dedicated Physical Control Channel (DPCCH) frame. Therefore the weight vectors of the data and control channel have to be computed separately. First the control channel signal is combined and decoded. Once the number of data channel and the spreading codes for the DPDCHs are known, the receiver can despread the DPDCHs

and compute the weight vector for the data channel. For the simulations performed in this report, we operate on the data channel only and assume that we already know the transmission format at the data channel. Calculated weights at the end of a DPCCH slot are used to form the beam for the data symbols of the corresponding DPDCH slots and as the initial weights for the weight estimate in the next DPCCH slot. For a practical implementation, the pilot symbols of the DPCCH have to be utilized to synchronize the signal to the reference (first) antenna element. After that we have to ensure that the computed weight vector has a real scalar as the first element so that there is no phase ambiguity resulting from the Eigen-beamforming.

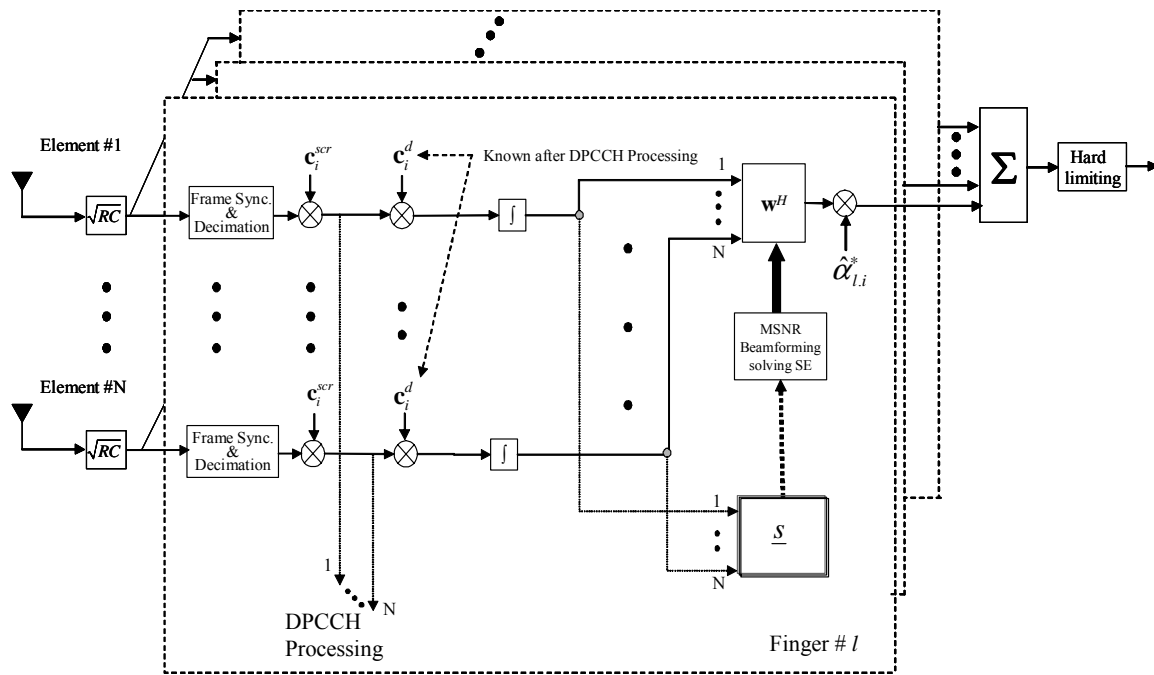


Figure 5.5: MSNR based Beamformer-Rake receiver for WCDMA uplink

The beamforming operation is followed by temporal processing where the spatially combined signals from different multipath are combined. We propose Maximal Ratio Combining (MRC) at the temporal domain. Since the WCDMA uplink has pilot symbols at the DPCCH, coherent combining is feasible. For the simulations conducted in this report, we assume that we have perfect channel estimation.

5.5 Simulation Results

In this section we present simulation results that illustrate and compare the performance of different algorithms for MSNR beamforming. We employ the Beamformer-Rake receiver described in the previous section in both the microcellular and macrocellular environment. We employ the circular and the elliptical channel models respectively to describe the multipath propagation condition. The channel parameters are described in Tables 5.2 and 5.3 respectively. We assume that we have 3 sectors per cell so that the users are uniformly distributed within $[-60^{\circ} \ 60^{\circ}]$. The desired user always has a spreading factor of 32. The simulation parameters are described in Tables 5.4. We employ two types of spatial distribution for the users based on the received power level of the individual users. The first one is the uniform distribution where all the users having spreading factor of 32 for their single DPDCH are uniformly distributed in angle across the sector. Signals from all the users are received at equal mean power level. We term the second distribution as non-uniform where all the users except for the one closest to the desired user have spreading factor of 32 for their DPDCHs. The remaining user is a high data rate user whose DPDCH has a spreading factor of 4. The received power level of this user is proportionately higher to compensate for the lower spreading gain. The users are still uniformly distributed across the sector.

Table 5.2: Circular channel parameters

Number of Resolvable Multipath	6
Separation between TX and RX	8 km
Doppler Spread	177 Hz (100 kmph at 2 GHZ)
Maximum Relative Delay	8 μ sec (32 chips)

Table 5.3: Elliptical channel parameters

Number of Resolvable Multipath	6
Doppler Spread	177 Hz (100 kmph at 2 GHZ)
Separation between TX and RX	800 m
Maximum Relative Delay	2 μ sec (8 chips)

Table 5.4: Simulation Parameters for MSNR based beamforming

Type of Receiver	Beamformer-Rake
Beamforming Technique	MSNR based Eigen-Beamforming
Algorithms to Solve SE	Power Method, Lagrange Multiplier Method, MCGM
Antenna Elements	4 element ULA with half wavelength spacing bet ⁿ omni elements
Temporal Combining	Maximal Ratio Combining (MRC) from 4 fingers
Vector Channel	Circular & Elliptical Channel Model (see Table 5.2& 5.3)
Number of Interferers	5 and 10
User Distribution	Uniform and Non-uniform

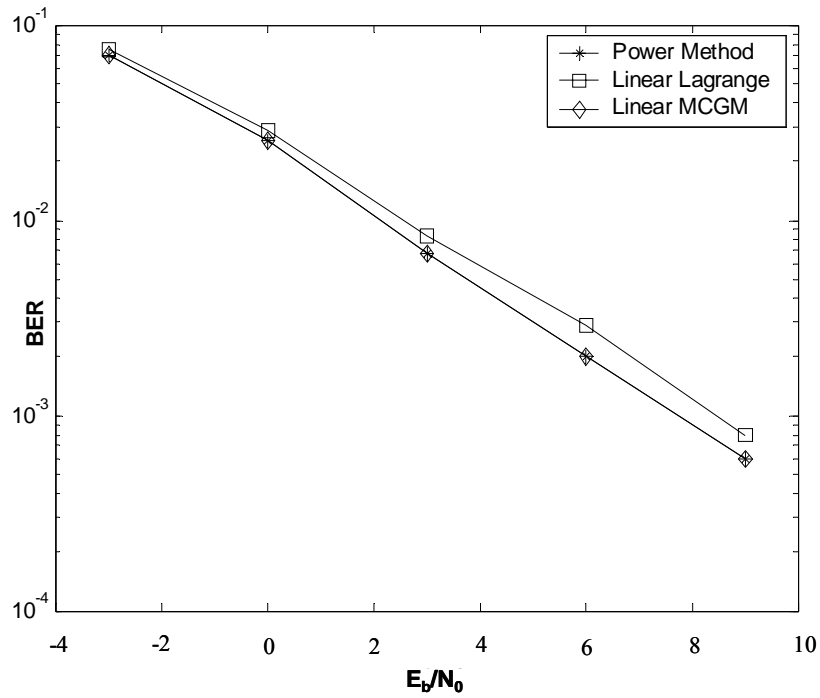


Figure 5.6: BER vs. E_b/N_0 performance of the MSNR based Beamformer-Rake receiver. There are 5 interferers. The user distribution is *uniform*. Three different algorithms are applied to solve the Simple Eigenvalue Problem. Circular channel model describes the propagation condition.

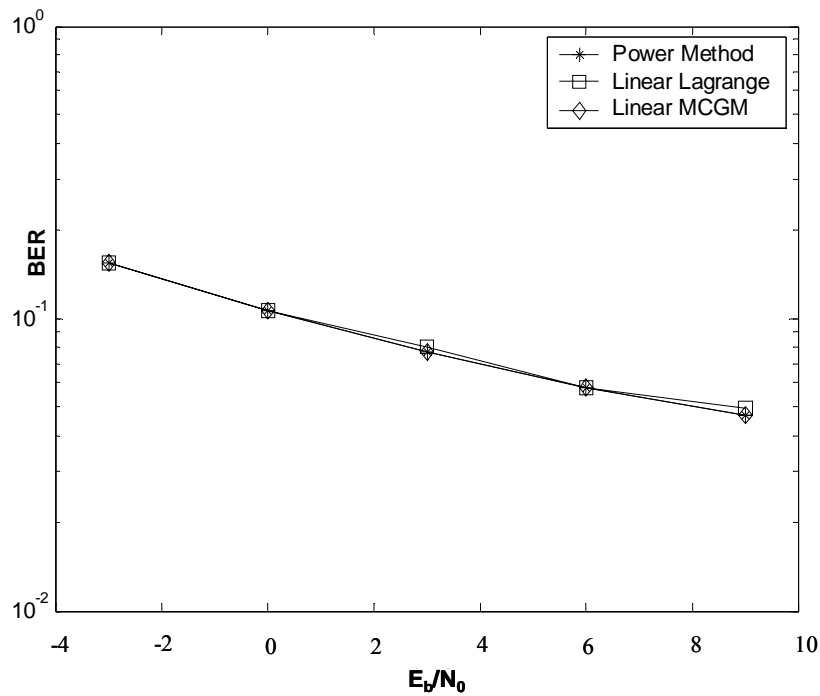


Figure 5.7: BER vs. E_b/N_0 performance of the MSNR based Beamformer-Rake receiver. There are 5 interferers. The user distribution is *non-uniform*. Three different algorithms are applied to solve the Simple Eigenvalue Problem. Circular channel model describes the propagation condition.

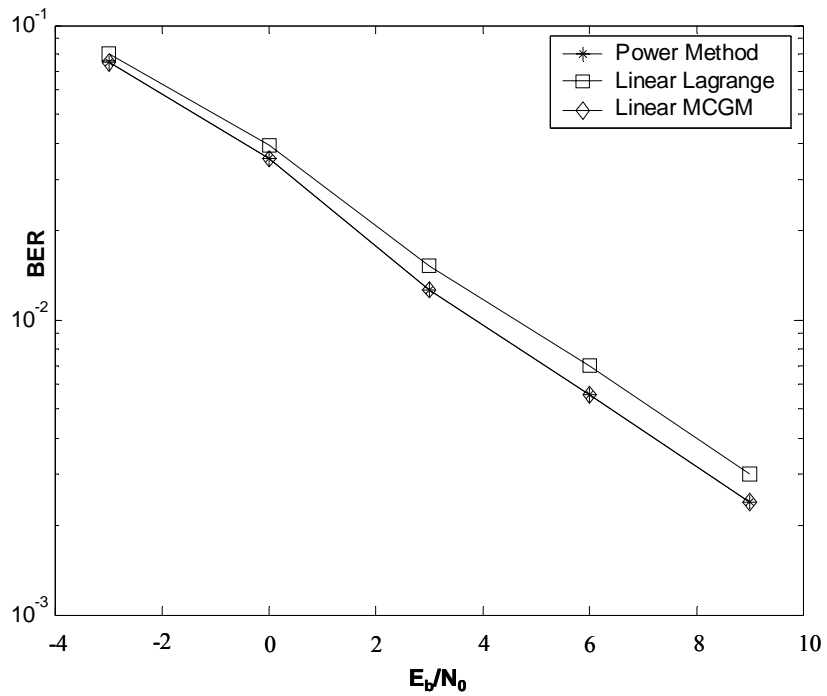


Figure 5.8: BER vs. E_b/N_0 performance of the MSNR based Beamformer-Rake receiver. There are 10 interferers. The user distribution is *uniform*. Three different algorithms are applied to solve the Simple Eigenvalue Problem. Circular channel model describes the propagation condition.

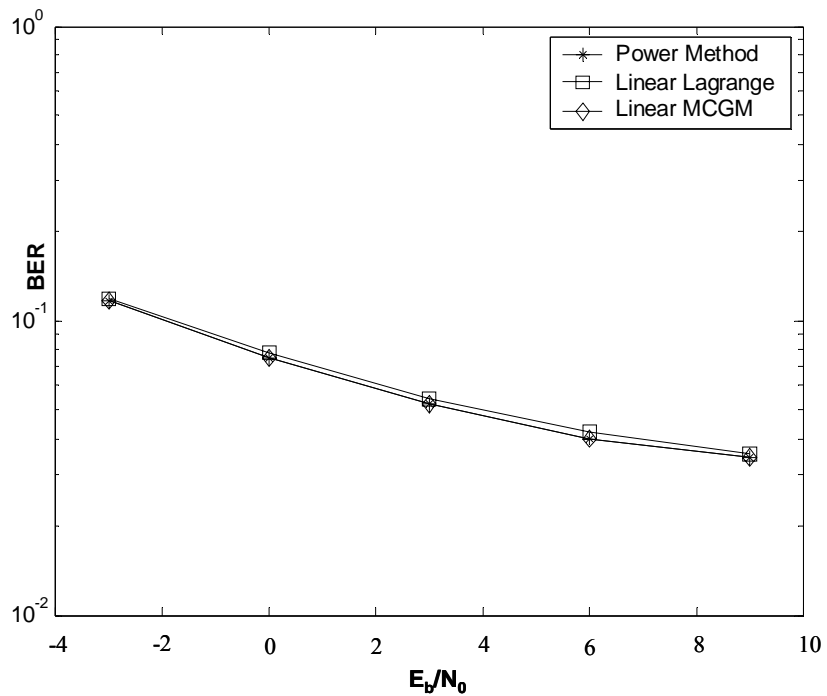


Figure 5.9: BER vs. E_b/N_0 performance of the MSNR based Beamformer-Rake receiver. There are 10 interferers. The user distribution is *non-uniform*. Three different algorithms are applied to solve the Simple Eigenvalue Problem. Circular channel model describes the propagation condition.

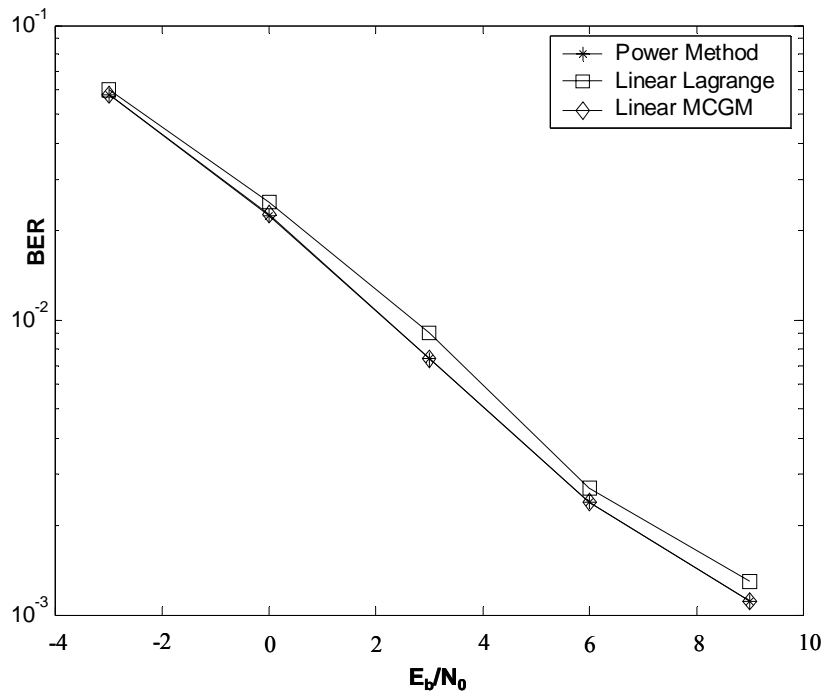


Figure 5.10: BER vs. E_b/N_0 performance of the MSNR based Beamformer-Rake receiver. There are 5 interferers. The user distribution is *uniform*. Three different algorithms are applied to solve the Simple Eigenvalue Problem. Elliptical channel model describes the propagation condition.

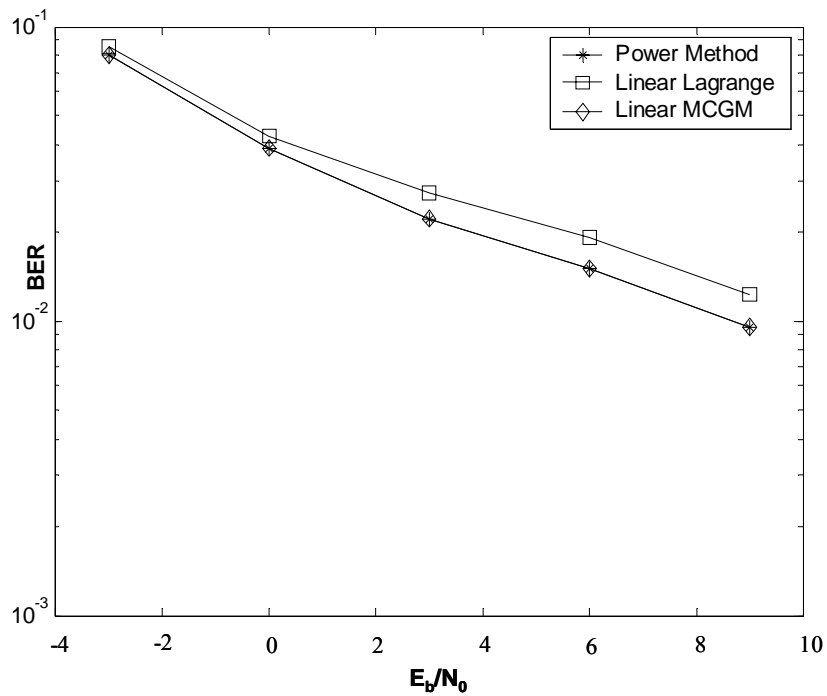


Figure 5.11: BER vs. E_b/N_0 performance of the MSNR based Beamformer-Rake receiver. There are 5 interferers. The user distribution is *non-uniform*. Three different algorithms are applied to solve the Simple Eigenvalue Problem. Elliptical channel model describes the propagation condition.

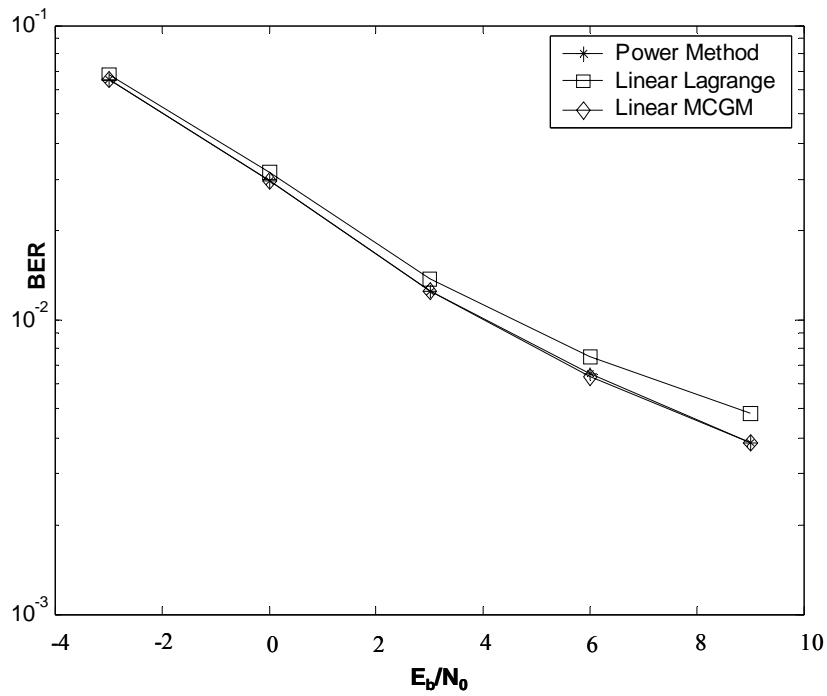


Figure 5.12: BER vs. E_b/N_0 performance of the MSNR based Beamformer-Rake receiver. There are 10 interferers. The user distribution is *uniform*. Three different algorithms are applied to solve the Simple Eigenvalue Problem. Elliptical channel model describes the propagation condition.

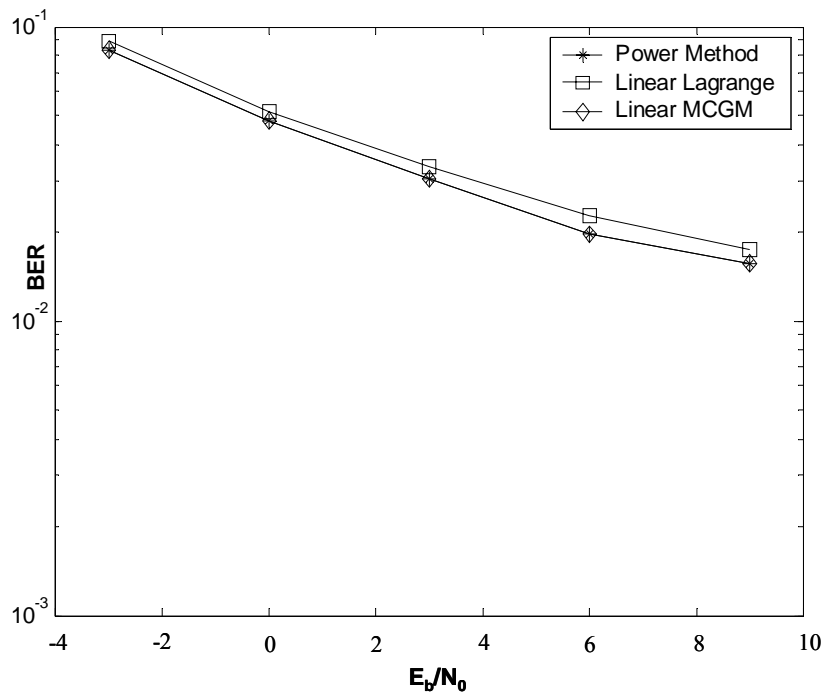


Figure 5.13: BER vs. E_b/N_0 performance of the MSNR based Beamformer-Rake receiver. There are 10 interferers. The user distribution is *non-uniform*. Three different algorithms are applied to solve the Simple Eigenvalue Problem. Elliptical channel model describes the propagation condition.

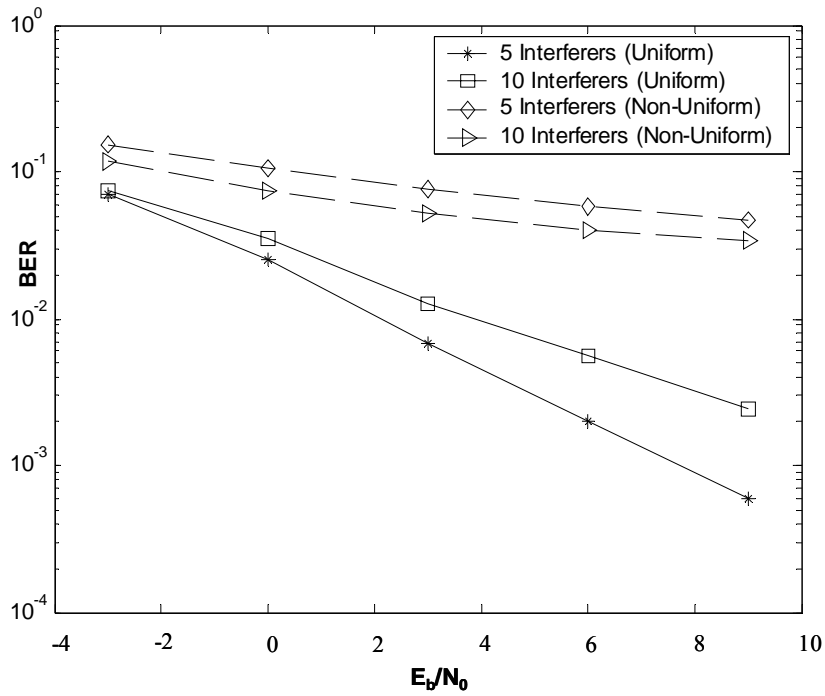


Figure 5.14: BER vs. E_b/N_0 performance of the Power method for a MSNR based Beamformer-Rake receiver. There are 5 & 10 interferers. The solid and the dashed curves represent uniform and non-uniform user distributions respectively. Circular channel model describes the propagation condition.

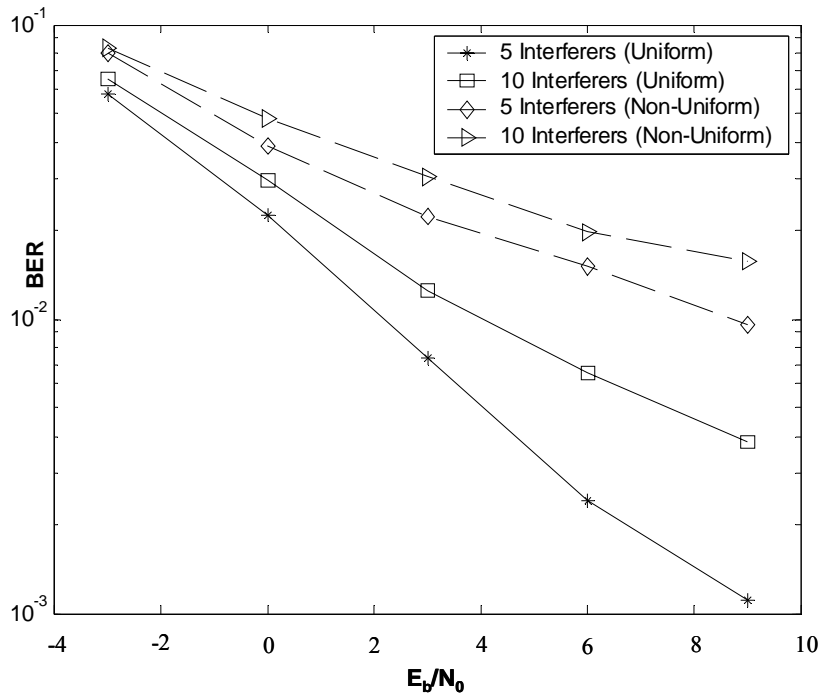


Figure 5.15: BER vs. E_b/N_0 performance of Power method for a MSNR based Beamformer-Rake. There are 5 & 10 interferers. Solid and dashed curves represent uniform and non-uniform user distributions respectively. Elliptical channel describes the propagation condition.

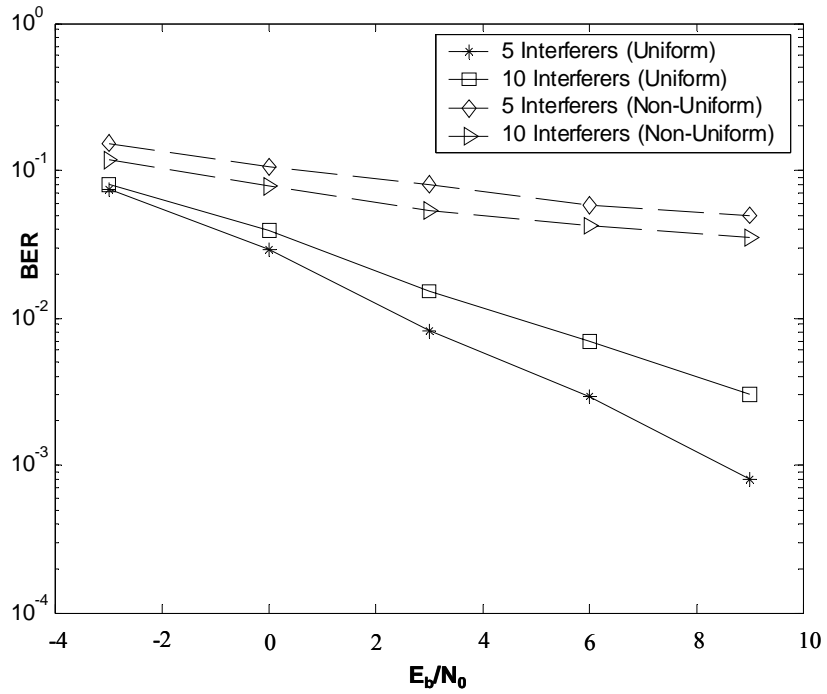


Figure 5.16: BER vs. E_b/N_0 performance of linear Lagrange multiplier method for a MSNR based Beamformer-Rake. There are 5 & 10 interferers. Solid and dashed curves represent uniform and non-uniform user distributions respectively. Circular channel describes the propagation condition.

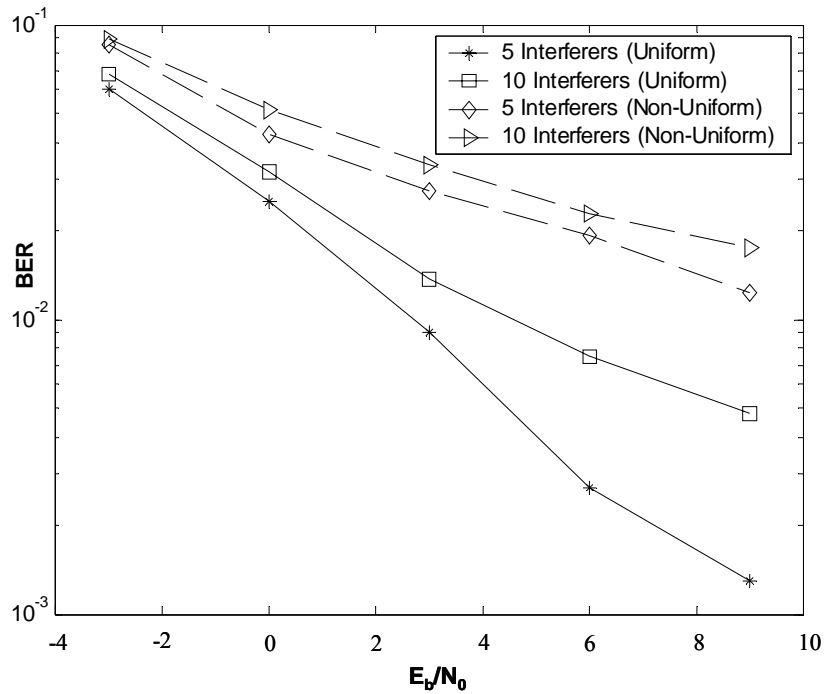


Figure 5.17: BER vs. E_b/N_0 performance of linear Lagrange multiplier method for a MSNR based Beamformer-Rake. There are 5 & 10 interferers. Solid and dashed curves represent uniform and non-uniform user distributions respectively. Elliptical channel describes the propagation condition.

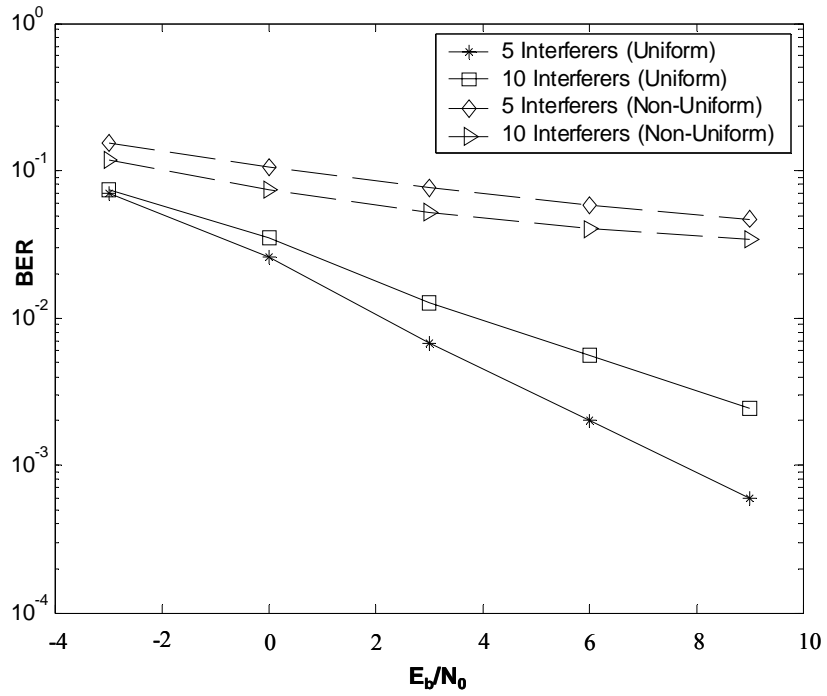


Figure 5.18: BER vs. E_b/N_0 performance of the linear MCGM for a MSNR based Beamformer-Rake. There are 5 & 10 interferers. Solid and dashed curves represent uniform and non-uniform user distributions respectively. Circular channel describes the propagation condition.

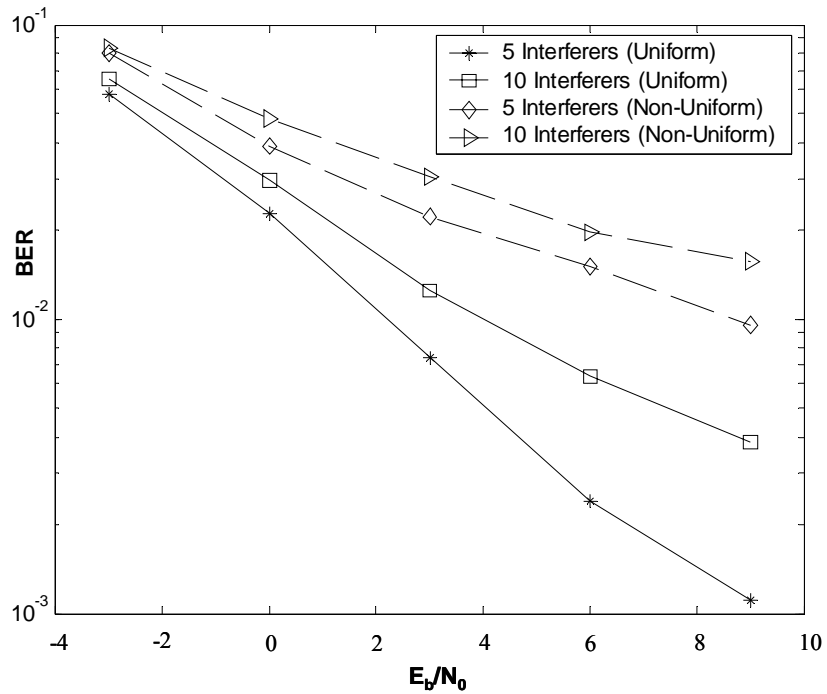


Figure 5.19: BER vs. E_b/N_0 performance of the linear MCGM for a MSNR based Beamformer-Rake. There are 5 & 10 interferers. Solid and dashed curves represent uniform and non-uniform user distributions respectively. Circular channel describes the propagation condition.

We can observe the following points from the simulation results presented from Figures 5.6 to 5.19:

- All the algorithms have almost similar performance when applied to a MSNR based Beamformer-Rake receiver. The Linear Lagrange Multiplier method performs a little poorer than the Power method and the Linear Modified Conjugate Gradient method. We can infer that there is very little penalty associated with employing the linear algorithms to solve the simple eigenvalue problem.
- The presence of a strong interferer drastically degrades the performance. This is not surprising since the MSNR beamforming criterion assumes that the interference and noise is spatially white and this does not hold when the signals from different users are not received at an equal average power level. As a result the temporal Rake experiences near-far problem.
- In the presence of a strong interferer the performance of the receiver is poorer when we have 5 interferers than the case of 10 interferers when the propagation model is described by the circular channel model. The circular model has a narrow angle spread. As a result the signal coming from a particular user is confined within a narrow region. But in the case of elliptical channel, the signals from different users can come from a much wider angle spread. As a result the spatial whiteness is more likely for the elliptical channel. At the same time, a strong signal coming from a very specific narrow region can dominate the spatial structure of the interference and noise when we have fewer interfering signals. Therefore when the propagation condition is described by the circular channel model and there is a strong interferer present, the performance of the receiver is poorer than when we have 5 interferer rather than 10 interferers.

The adverse effect of uneven power distribution among the received signals can be better coped with beamforming criterion that takes the spatial structure of the interference and noise into account. This leads us to Maximum Signal to Noise Ratio (MSINR) beamforming criterion which was described in Chapter 3. We will investigate computationally simple techniques to implement MSINR beamforming in the next chapter.

Chapter 6

Eigen-Beamforming based on MSINR Criterion

6.1 Introduction

In this chapter we describe efficient adaptive algorithms to solve the Generalized Eigenvalue problem resulting from the Maximum Signal to Interference and Noise Ratio (MSINR) beamforming criterion. The chapter starts with the formulation of the GE for the CDMA systems. We then go on to discuss various algorithms to solve the GE. Beamformer-Rake receivers based on the MSINR spatial processing are proposed for the WCDMA reverse link. We present simulation results that show the performance of these receivers under various propagation and MAI conditions. We compare the performance of different MSINR beamforming techniques as well as the performance of the different algorithms to solve the GE. We also compare the MSINR based Beamformer-Rake with the MSNR based Beamformer-Rake in terms of BER performance under different operating conditions.

6.2 MSINR Beamforming for CDMA Systems

There are different techniques to exploit the MSINR beamforming criterion in a CDMA system. The processing gain of a CDMA correlation operation is usually utilized to set up the Generalized Eigenvalue problem. In this section we will describe three different techniques, namely Code Filtering Approach (CFA), Modified CFA and Code Gated Algorithm (CGA).

6.2.1 Code Filtering Approach (CFA)

The code filtering approach (CFA) was proposed in [1]. The basic idea is to form the covariance matrices required for the MSINR criterion with help of CDMA despreading.

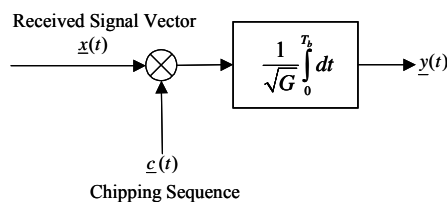


Figure 6.1: CDMA despreading

With reference to Figure 6.1, we can write that,

$$\begin{aligned}
 \underline{\underline{R}}_{xx} &= E[\underline{x}(m)\underline{x}^H(m)] \\
 &= E[\{\underline{s}(m) + \underline{u}(m)\}\{\underline{s}(m) + \underline{u}(m)\}^H] \\
 &= E[\underline{s}(m)\underline{s}^H(m)] + E[\underline{u}(m)\underline{u}^H(m)] + E[\underline{s}(m)\underline{u}^H(m)] + E[\underline{u}(m)\underline{s}^H(m)]
 \end{aligned} \tag{6.1}$$

Now if the desired signal and the interference and noise signal are independent, the last two terms of Equation 6.1 goes away. So we have,

$$\underline{\underline{R}}_{xx} = \underline{\underline{R}}_{ss} + \underline{\underline{R}}_{uu} \tag{6.2}$$

Similarly,

$$\underline{\underline{R}}_{yy} = G\underline{\underline{R}}_{ss} + \underline{\underline{R}}_{uu} \tag{6.3}$$

So from Equations 6.2 and 6.3 we have

$$\underline{\underline{R}}_{ss} = \frac{1}{G-1}(\underline{\underline{R}}_{yy} - \underline{\underline{R}}_{xx}) \tag{6.4}$$

and

$$\underline{\underline{R}}_{uu} = \frac{1}{G-1}(G\underline{\underline{R}}_{xx} - \underline{\underline{R}}_{yy}) \tag{6.5}$$

Thus we can estimate the covariance matrices of the desired signal and the interference and noise signal from Equations 6.4 and 6.5 respectively. Obviously we still need to solve the GE.

6.2.2 Modified CFA (M-CFA)

Let us revisit the GE resulting from the MSINR criterion,

$$\underline{\underline{R}}_{ss} w_{MSINR} = \lambda \underline{\underline{R}}_{uu} w_{MSINR} \tag{6.6}$$

Now if we replace $\underline{\underline{R}}_{ss}$ and $\underline{\underline{R}}_{uu}$ by the expressions given in Equations 6.4 and 6.5, we get

$$\begin{aligned}
 \frac{1}{G-1}(\underline{\underline{R}}_{yy} - \underline{\underline{R}}_{xx}) w_{MSINR} &= \frac{\lambda}{G-1}(G\underline{\underline{R}}_{xx} - \underline{\underline{R}}_{yy}) w_{MSINR} \\
 \Rightarrow \underline{\underline{R}}_{yy} w_{MSINR} &= \left(\frac{\lambda G + 1}{1 + \lambda}\right) \underline{\underline{R}}_{xx} w_{MSINR}
 \end{aligned} \tag{6.7}$$

So we can write

$$\underline{\underline{R}}_{yy} \underline{w}_{MSINR} = \lambda' \underline{\underline{R}}_{xx} \underline{w}_{MSINR} \quad (6.8)$$

Thus we do not have to form the covariance matrices of the desired signal and the interference and noise signal explicitly. We can form the covariance matrices at the input and the output of the CDMA correlator and still formulate the MSINR based GE. This modification of the CFA was proposed by Kwon *et. al.* [139]. They argued that the CFA for MSINR beamforming tends to maximize the following functional which is the SINR at the beamformer output

$$SINR_{out} = \frac{\underline{w}^H \underline{\underline{R}}_{ss} \underline{w}}{\underline{w}^H \underline{\underline{R}}_{uu} \underline{w}} \quad (6.9)$$

By utilizing the expressions given by Equations 6.4 and 6.5, it is straight forward to show that [139]

$$\frac{\underline{w}^H \underline{\underline{R}}_{yy} \underline{w}}{\underline{w}^H \underline{\underline{R}}_{xx} \underline{w}} = G - \frac{G-1}{SINR_{out} + 1} \quad (6.10)$$

Obviously, $\underline{\underline{R}}_{xx}$ has to be full rank so that $\underline{w}^H \underline{\underline{R}}_{xx} \underline{w} \neq 0$ for any $\underline{w} \neq 0$.

So, any weight vector that maximizes the functional $\frac{\underline{w}^H \underline{\underline{R}}_{yy} \underline{w}}{\underline{w}^H \underline{\underline{R}}_{xx} \underline{w}}$, eventually maximizes

$$SINR_{out} = \frac{\underline{w}^H \underline{\underline{R}}_{ss} \underline{w}}{\underline{w}^H \underline{\underline{R}}_{uu} \underline{w}}.$$

Hence if $G > 1$ (which is always true for CDMA systems), the optimum weight vector for MSINR solution can be found as the principal eigenvector of the GE of Equation 6.8.

6.2.3 Code Gated Algorithm

The Code Gated Algorithm (CGA) [152] is a technique that maximizes the Received Signal to Interference and Noise Ratio (RSINR). As explained in Chapter 3, maximizing the Received Signal to Interference and Noise Ratio (RSINR) is equivalent to maximizing the SINR. When the received signal is multiplied by the chipping sequence (spreading code) of the desired user in a CDMA receiver, the despread signal consists of a narrowband desired signal in wideband interference and noise. The data can be filtered to form an estimate of the received signal and the interference and noise signal [152]. This is shown in Figure 6.2. Note that the processing gain G is assumed to be absorbed appropriately during the filtering operation.

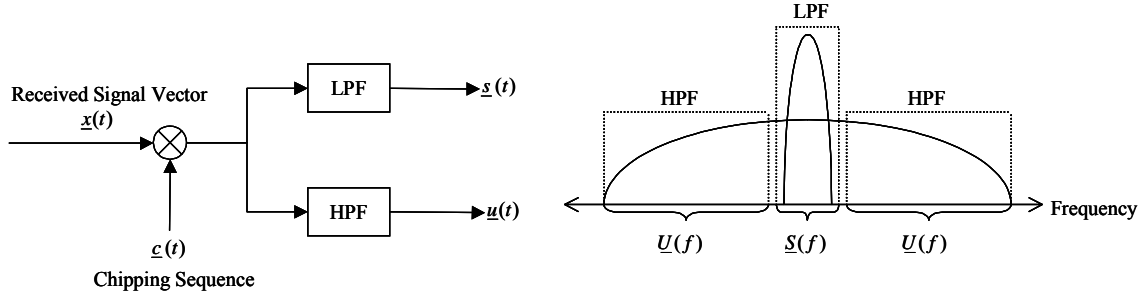


Figure 6.2: The concept of CGA

6.3 Adaptive Algorithms to solve the GE

In this section we describe several adaptive algorithms that can be employed to solve the generalized eigenvalue problem. We start with a description of the well known Generalized Power Method (GPM) [11]. The computationally simpler Generalized Lagrange Multiplier method (GLM) [139] is described next. We then propose a new algorithm termed as the Adaptive Matrix Inversion (AMI) [140] method. The AMI is also linearized [141] to reduce the computational complexity.

6.3.1 Generalized Power Method

The generalized power method utilizes the property of a positive semi-definite matrix to reduce the generalized eigenvalue problem to a simple eigenvalue problem. The power method described in Chapter 5 is then applied to solve the problem. The interference and noise covariance matrix can be decomposed [199] in the following way

$$\underline{\underline{R}}_{uu} = \underline{\underline{R}} \underline{\underline{R}}^H \quad (6.11)$$

Here $\underline{\underline{R}}$ is the Cholesky factor [199] of the matrix $\underline{\underline{R}}_{uu}$. So we can rewrite the GE as

$$\underline{\underline{R}}^{-1} \underline{\underline{R}}_{ss} (\underline{\underline{R}}^{-1})^H \underline{\underline{R}}^H \underline{\underline{w}} = \lambda \underline{\underline{R}}^H \underline{\underline{w}} \quad (6.12)$$

Let us define the following quantities,

$$\begin{aligned} \underline{\underline{R}}^{-1} \underline{\underline{R}}_{ss} (\underline{\underline{R}}^{-1})^H &= \underline{\underline{\mathfrak{R}}} \\ \underline{\underline{R}}^H \underline{\underline{w}} &= \underline{\underline{\mathcal{W}}} \end{aligned} \quad (6.13)$$

Therefore Equation 6.12 can be rewritten as the following SE

$$\underline{\Re} \underline{\varpi} = \lambda \underline{\varpi} \quad (6.14)$$

The power method outlined in Chapter 5 can be employed to solve the equivalent simple eigenvalue problem of Equation 6.14. The actual weight vector can be found after solving the following triangular system

$$\underline{R}^H \underline{w} = \underline{\varpi} \quad (6.15)$$

We can update the relevant matrices at each snapshot of the signal and iterate the GPM once per snapshot to estimate the weight. However it is evident that the GPM involves a lot of computation (e.g. Cholesky factorization requires computational complexity of $O(N^3/3)$ [199]) and consequently may not be practical for real time implementation. So we need algorithms that are less burdensome in terms of computational load. One such algorithm is the generalized Lagrange multiplier method.

6.3.2 Generalized Lagrange Multiplier Method

The Lagrange multiplier method computes the optimum weight vector by treating the Generalized Eigenvalue problem as a constrained maximization problem. The goal is to find a weight vector \underline{w} that maximizes $\underline{w}^H \underline{R}_{ss} \underline{w}$ subject to the constraint $\underline{w}^H \underline{R}_{uu} \underline{w} = 1$ [139]. Note that the constraint has changed from the simple Lagrange multiplier method described in Section 5.2.3. We can introduce the following functional

$$J(\underline{w}) = \underline{w}^H \underline{R}_{ss} \underline{w} + \beta(1 - \underline{w}^H \underline{R}_{uu} \underline{w}) \quad (6.16)$$

where β is the Lagrange multiplier for the constraint $\underline{w}^H \underline{R}_{uu} \underline{w} = 1$. To find the weight vector that maximizes $J(\underline{w})$, the steepest ascent method can be utilized and the recursion can be written as

$$\underline{w}(k+1) = \underline{w}(k) + \frac{1}{2} \mu \underline{\nabla}(k) \quad (6.17)$$

where $\underline{\nabla}(k)$ is the gradient vector of $J(\underline{w})$ with respect to \underline{w}^H which can be written as

$$\underline{\nabla}(k) = 2 \left[\underline{R}_{ss} \underline{w} - \beta \underline{R}_{uu} \underline{w} \right]. \quad (6.18)$$

Substituting the value of $\underline{\nabla}(k)$ in Equation 6.17, we have

$$\underline{w}(k+1) = \underline{w}(k) + \mu \left[\underline{R}_{ss} \underline{w} - \beta \underline{R}_{uu} \underline{w}(k) \right]. \quad (6.19)$$

In Equation 6.19, we need to find the Lagrange multiplier β for each updating. If $\underline{w}^H \underline{R}_{uu} \underline{w} = 1$, the value of β must satisfy

$$\underline{w}^H (k+1) \underline{R}_{uu} \underline{w}(k+1) = 1 \quad (6.20)$$

It provides the following equation of β :

$$\begin{aligned} \mu \underline{w}^H \underline{R}_{ss}^3 \underline{w} \beta^2 - \underline{w}^H (2 \underline{R}_{uu}^2 + \mu \underline{R}_{ss} \underline{R}_{uu}^2 + \mu \underline{R}_{uu}^2 \underline{R}_{ss}) \underline{w} \beta + \mu \underline{w}^H \underline{R}_{ss} \underline{R}_{uu} \underline{R}_{ss} \underline{w} \\ + \underline{w}^H \underline{R}_{uu} \underline{R}_{ss} \underline{w} + \underline{w}^H \underline{R}_{ss} \underline{R}_{uu} \underline{w} = 0 \end{aligned} \quad (6.21)$$

where $\underline{w} = \underline{w}(k)$. By solving the quadratic equation for β shown in Equation 6.21, we can determine the Lagrange multiplier required for the updating of weight given by Equation 6.19. Unfortunately, we can see that there are a lot of matrix multiplications to be performed resulting in high computational complexity.

Instead of directly solving Equation 6.21, we can modify it to reduce computational complexity. Replacing \underline{R}_{uu} and \underline{R}_{ss} with instantaneous estimates $\underline{u} \underline{u}^H$ and $\underline{s} \underline{s}^H$, respectively, the Lagrange multiplier β can be found as [139]

$$\beta = \frac{b - \sqrt{b^2 - ac}}{a} \quad (6.22)$$

where

$$a = \mu |\delta|^2 \alpha^2; b = |\delta|^2 \alpha + \mu \alpha \operatorname{Re}(\xi \delta z^*); c = \mu |\xi|^2 |z|^2 + 2 \operatorname{Re}(\xi \delta z^*) \quad (6.23)$$

and

$$\alpha = \underline{u}^H \underline{u}, \xi = \underline{u}^H \underline{x}, \delta = \underline{w}^H \underline{u}, z = \underline{w}^H \underline{x}. \quad (6.24)$$

With the value of β from Equation 6.22, the weight update equation can be written as

$$\underline{w}(k+1) = \underline{w}(k) + \mu \left[\underline{x}(k) \underline{x}^H(k) \underline{w}(k) - \beta \underline{u}(k) \underline{u}^H(k) \underline{w}(k) \right]. \quad (6.25)$$

Note that \underline{u} is the sampled sequence at the chip rate, while \underline{x} is the despread sequence at the symbol rate. Since the weight vector is updated at the symbol rate, the signal vector \underline{u} has to be down sampled at the symbol rate.

The following figure shows the flowchart of the Lagrange Multiplier method:

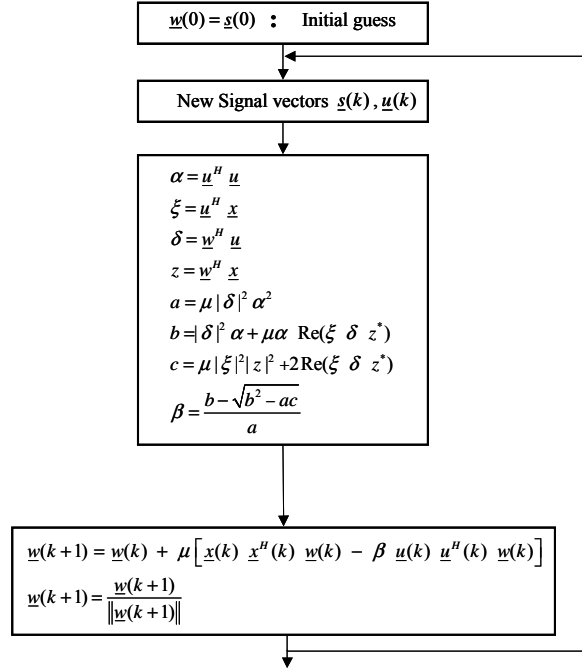


Figure 6.3: Flowchart of the GLM

We can observe that the computational complexity of the GPM is $O(7.5N)$. The Lagrange multiplier algorithm has been employed [147] to derive an alternate algorithm for solving the GE. This technique utilizes the fact that the Lagrange multiplier β , in Equations 6.16 and 6.19 is the largest eigenvalue of the GE. We provide a brief derivation of this method in Section 9.3.1.3.

6.3.3 Adaptive Matrix Inversion (AMI)

In this section we will propose a new algorithm to solve the generalized eigenvalue problem. We term this new method as Adaptive Matrix Inversion Method (AMI)[140], [141]. We begin the adaptive matrix inversion method by splitting the interference and noise covariance matrix $\underline{\underline{R}}_{uu}$ so that

$$\underline{\underline{R}}_{uu} = \underline{\underline{R}}_{uu}^O + \underline{\underline{R}}_{uu}^D. \quad (6.26)$$

$\underline{\underline{R}}_{uu}^D$ denotes a matrix whose diagonal elements are identical to those of $\underline{\underline{R}}_{uu}$ and off-diagonal elements are zero and $\underline{\underline{R}}_{uu}^O$ represents a matrix whose diagonal elements are zero and off-diagonal elements are identical to those of $\underline{\underline{R}}_{uu}$.

So we can write the GE as

$$\underline{\underline{R}}_{ss} \underline{w} = \lambda (\underline{\underline{R}}_{uu}^D + \underline{\underline{R}}_{uu}^O) \underline{w}. \quad (6.27)$$

Now by rearranging the terms of Equation 6.27, we get

$$(\underline{\underline{R}}_{uu}^D)^{-1} (\underline{\underline{R}}_{ss} - \lambda \underline{\underline{R}}_{uu}^O) \underline{w} = \lambda \underline{w} \quad (6.28)$$

We propose the following weight update equation

$$\underline{w}(k+1) = \frac{\{ \underline{\underline{R}}_{uu}^D(k) \}^{-1} [\underline{\underline{R}}_{ss}(k) - \lambda(k) \underline{\underline{R}}_{uu}^O(k)] \underline{w}(k)}{\lambda(k)} \quad (6.29)$$

By recognizing the fact that $\underline{\underline{R}}_{uu}^O(k) = \underline{\underline{R}}_{uu}(k) - \underline{\underline{R}}_{uu}^D(k)$, we can write the weight update equation as,

$$\underline{w}(k+1) = \underline{w}(k) + \frac{\{ \underline{\underline{R}}_{uu}^D(k) \}^{-1} [\underline{\underline{R}}_{ss}(k) - \lambda(k) \underline{\underline{R}}_{uu}(k)] \underline{w}(k)}{\lambda(k)} \quad (6.30)$$

Note that the left multiplication by $\{ \underline{\underline{R}}_{uu}^D(k) \}^{-1}$ amounts to element-by-element division of each element of the $N \times 1$ right vector by the diagonal element of the matrix $\underline{\underline{R}}_{uu}$. We can calculate the eigenvalue $\lambda(k)$ during each iteration as

$$\lambda(k) = \frac{\underline{w}^H(k) \underline{\underline{R}}_{ss}(k) \underline{w}(k)}{\underline{w}^H(k) \underline{\underline{R}}_{uu}(k) \underline{w}(k)} \quad (6.31)$$

The covariance matrices are updated according to the following equations:

$$\begin{aligned} \underline{\underline{R}}_{ss}(k) &= f \underline{\underline{R}}_{ss}(k-1) + \underline{s}(k) \underline{s}^H(k) \\ \underline{\underline{R}}_{uu}(k) &= f \underline{\underline{R}}_{uu}(k-1) + \underline{u}(k) \underline{u}^H(k) \end{aligned} \quad (6.32)$$

At the beginning, $\underline{w}(0) = \underline{s}(0)$ is used as an initial guess.

If the interference and noise is spatially white,

$$\underline{\underline{R}}_{uu}(k) = \sigma_u^2(k) I_N ; \underline{\underline{R}}_{uu}^O(k) = \underline{\underline{0}}_{N \times N} ; \{ \underline{\underline{R}}_{uu}^D(k) \}^{-1} = \frac{1}{\sigma_u^2(k)} I_N \quad (6.33)$$

So Equation 6.29 reduces to

$$\begin{aligned} \underline{w}(k+1) &= \frac{\frac{1}{\sigma_u^2(k)} I_N \left[\underline{R}_{ss}(k) - \lambda(k) \underline{0}_N \right] \underline{w}(k)}{\lambda(k)} \\ &= \frac{I_N \left[\underline{R}_{ss}(k) \right] \underline{w}(k)}{\sigma_u^2(k) \lambda(k)} \\ \Rightarrow \underline{w}(k+1) &= \frac{1}{\lambda'(k)} \underline{R}_{ss}(k) \underline{w}(k); \lambda'(k) = \sigma_u^2(k) \lambda(k) \end{aligned} \quad (6.34)$$

Similarly,

$$\begin{aligned} \lambda(k) &= \frac{\underline{w}^H(k) \underline{R}_{ss}(k) \underline{w}(k)}{\sigma_u^2(k) \underline{w}^H(k) \underline{w}(k)} \\ \Rightarrow \lambda'(k) &= \frac{\underline{w}^H(k) \underline{R}_{ss}(k) \underline{w}(k)}{\underline{w}^H(k) \underline{w}(k)} \end{aligned} \quad (6.35)$$

So as the GE reduces to an SE the AMI reduces to the Power method.

The flowchart of the AMI method is shown in the next Figure. As we can observe that the AMI requires a lot of matrix multiplications which may make its implementation in real time burdensome.

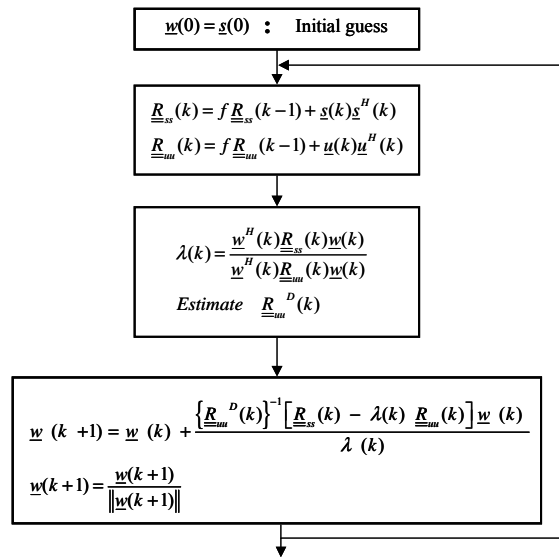


Figure 6.4: Flowchart of the AMI

We can reduce the computational complexity of the algorithm by utilizing the expressions of the covariance matrices given in Equation 6.32. Let us redefine Equation 6.31 as

$$\lambda(k) = \frac{\lambda_{num}(k)}{\lambda_{den}(k)} \quad (6.36)$$

Here,

$$\begin{aligned} \lambda_{num}(k) &= \underline{w}^H(k) \underline{\underline{R}}_{ss}(k) \underline{w}(k) \\ &= \underline{w}^H(k) \left[f \underline{\underline{R}}_{ss}(k-1) + \underline{s}(k) \underline{s}^H(k) \right] \underline{w}(k) \\ &= f \underline{w}^H(k) \underline{\underline{R}}_{ss}(k-1) \underline{w}(k) + \underline{w}^H(k) \underline{s}(k) \underline{s}^H(k) \underline{w}(k) \\ \Rightarrow \lambda_{num}(k) &\approx f \underline{w}^H(k-1) \underline{\underline{R}}_{ss}(k-1) \underline{w}(k-1) + \underline{w}^H(k) \underline{s}(k) \underline{s}^H(k) \underline{w}(k) \end{aligned} \quad (6.37)$$

Now if we define $\alpha(k) = \underline{s}^H(k) \underline{w}(k)$, we can write

$$\lambda_{num}(k) = f \lambda_{num}(k-1) + |\alpha(k)|^2 \quad (6.38)$$

Similarly,

$$\lambda_{den}(k) = f \lambda_{den}(k-1) + |\beta(k)|^2 \quad (6.39)$$

where, $\beta(k) = \underline{u}^H(k) \underline{w}(k)$

Now let us simplify Equation 6.30. We will start by rewriting Equation 6.30 as

$$\underline{w}(k+1) = \underline{w}(k) + \underline{z}(k) \quad (6.40)$$

Here,

$$\underline{z}(k) = \frac{\left\{ \underline{\underline{R}}_{uu}^D(k) \right\}^{-1} \left[\underline{\underline{R}}_{ss}(k) - \lambda(k) \underline{\underline{R}}_{uu}(k) \right] \underline{w}(k)}{\lambda(k)} \quad (6.41)$$

Now,

$$\begin{aligned} \underline{z}(k) &= \frac{\left\{ \underline{\underline{R}}_{uu}^D(k) \right\}^{-1} \left[\underline{\underline{R}}_{ss}(k) - \lambda(k) \underline{\underline{R}}_{uu}(k) \right] \underline{w}(k)}{\lambda(k)} \\ &= \frac{\left\{ \underline{\underline{R}}_{uu}^D(k) \right\}^{-1} \left[f \underline{\underline{R}}_{ss}(k-1) + \underline{s}(k) \underline{s}^H(k) - \lambda(k) \left\{ f \underline{\underline{R}}_{uu}(k-1) + \underline{u}(k) \underline{u}^H(k) \right\} \right] \underline{w}(k)}{\lambda(k)} \end{aligned}$$

$$\Rightarrow \underline{z}(k) = \left\{ \underline{R}_{uu}^D(k) \right\}^{-1} \begin{bmatrix} \frac{1}{\lambda(k)} \left\{ f \underline{R}_{ss}(k-1) \underline{w}(k) + \underline{s}(k) \underline{s}^H(k) \underline{w}(k) \right\} \\ -f \underline{R}_{uu}(k-1) \underline{w}(k) - \underline{u}(k) \underline{u}^H(k) \underline{w}(k) \end{bmatrix} \quad (6.42)$$

We can define

$$\begin{aligned} \underline{v}(k) &= f \underline{R}_{ss}(k-1) \underline{w}(k) + \underline{s}(k) \underline{s}^H(k) \underline{w}(k) \approx f \underline{R}_{ss}(k-1) \underline{w}(k-1) + \underline{s}(k) \underline{s}^H(k) \underline{w}(k) \\ &= f \underline{v}(k-1) + \alpha(k) \underline{s}(k) \end{aligned} \quad (6.43)$$

Initial guess: $\underline{v}(0) = \alpha(0) \underline{s}(0)$

Similarly,

$$\begin{aligned} \underline{y}(k) &= f \underline{R}_{uu}(k-1) \underline{w}(k) + \underline{u}(k) \underline{u}^H(k) \underline{w}(k) \\ &\approx f \underline{y}(k-1) + \beta(k) \underline{u}(k) \end{aligned} \quad (6.44)$$

Initial guess: $\underline{y}(0) = \beta(0) \underline{u}(0)$

So, we can write,

$$\underline{z}(k) = \left\{ \underline{R}_{uu}^D(k) \right\}^{-1} \begin{bmatrix} \frac{1}{\lambda(k)} \underline{v}(k) - \underline{y}(k) \end{bmatrix} \quad (6.45)$$

Note that the multiplication by $\left\{ \underline{R}_{uu}^D(k) \right\}^{-1}$ amounts to dividing the elements of an $N \times 1$ vector element by element by the elements of a vector $\underline{d}(k)$ which can be computed as

$$\underline{d}(k) = f \underline{d}(k-1) + \underline{u}(k) \cdot \text{conj}(\underline{u}(k)). \quad (6.46)$$

At the beginning, $\underline{w}(0) = \underline{s}(0)$ is used as an initial guess.

The simplified AMI is illustrated in the next flowchart. We can observe that the computational complexity of the linear AMI is $O(8.5N)$ which is a little higher than the same of the generalized Lagrange multiplier method. However we will show a little later that the linear AMI provides better performance compared to the GLM.

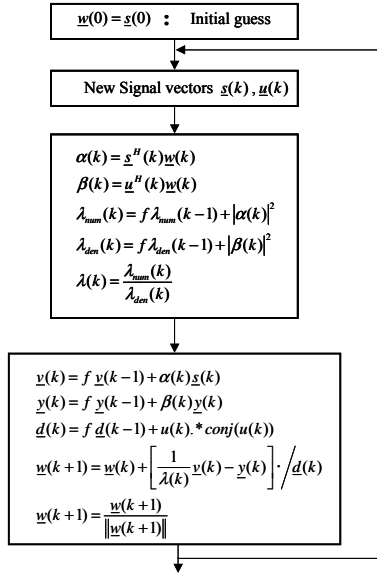


Figure 6.5: Flowchart of the linear AMI

6.4 MSINR based Beamformer-Rake receiver for WCDMA uplink

In this section we will put forward two Beamformer-Rake receivers for the WCDMA uplink. Both the receivers employ the MSINR beamforming criterion. They utilize the CGA and the modified CFA techniques to perform the spatial beamforming operations. The proposed receivers are shown in the following two figures.

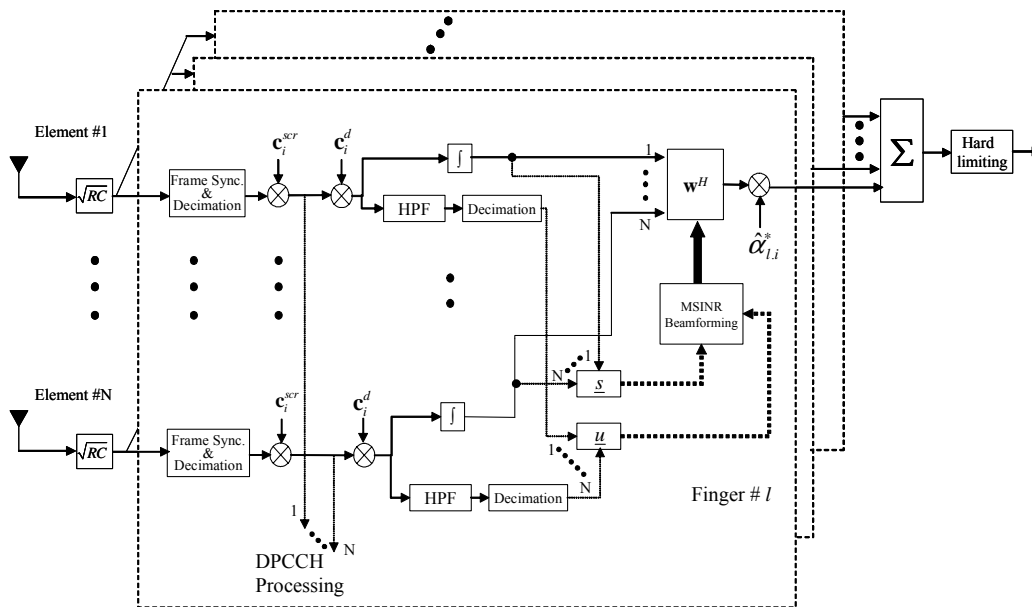


Figure 6.6: CGA based Beamformer-Rake receiver for WCDMA uplink

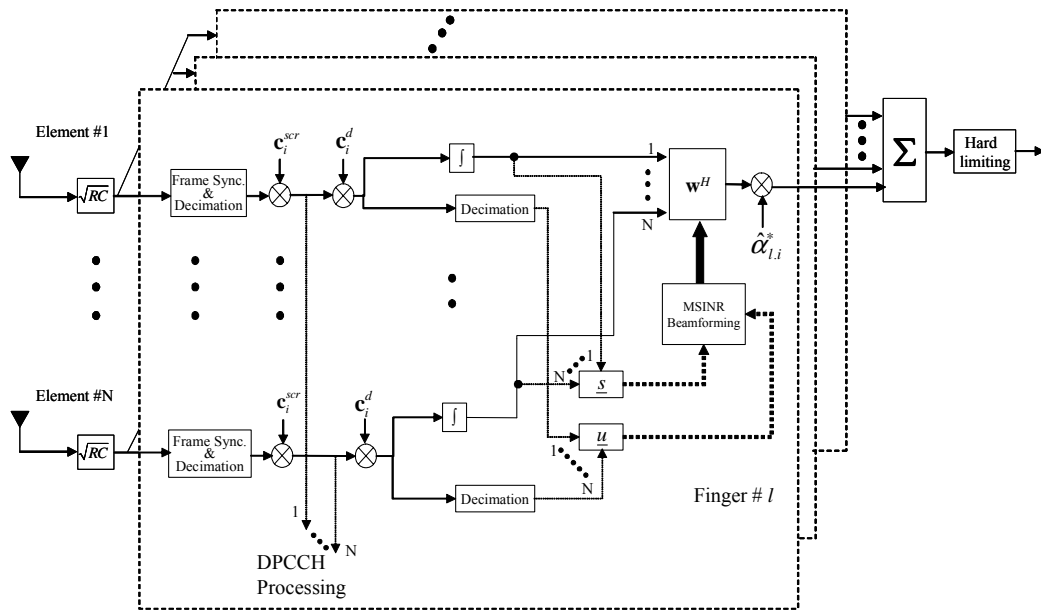


Figure 6.7: Modified CFA based Beamformer-Rake receiver for WCDMA uplink

As mentioned in the previous chapter, the transmission format for a WCDMA uplink frame in the data channels is conveyed by the TFCI symbols of the corresponding DPCCH frame. Therefore we compute the weight vector of the data and control channel separately. This is similar to the MSNR based Beamformer-Rake receiver. Note that the signal at the input of the despreader needs to be decimated down to symbol level before forming the matrix that corresponds to the interference and noise signal. This is essential to reduce the number of operations. For our simulations, we operate on the data channel only and assume that we already know the transmission format at the data channel. Calculated weights at the end of a DPCCH slot are used to form the beam for the data symbols of the corresponding DPDCH slots and as the initial weights for the weight estimate in the next DPCCH slot. Both the receivers employ a 4 element ULA with half wavelength spacing between the omnidirectional elements.

The beamforming operation is followed by temporal processing where the spatially combined signals from different multipath are combined. The receiver has 4 fingers to exploit the multipath diversity. We employ Maximal Ratio Combining (MRC) at the temporal domain. The underlying assumption is that the spatial processing has mitigated the MAI sufficiently so that maximizing the SNR in the temporal domain will suffice. Since the WCDMA uplink has pilot symbols at the DPCCH, coherent combining is feasible. For the simulations conducted, we assume that we have perfect channel estimation.

6.5 Simulation Environment

We employed the two different MSINR based Beamformer-Rake receivers described in the previous section. They utilize the CGA and the modified CFA to perform beamforming in the spatial domain. The details of the 2-D receivers employed are shown in Table 6.1.

Table 6.1: MSINR based Beamformer-Rake details

Type of Receiver	Beamformer-Rake
Beamforming Techniques	CGA based MSINR and modified CFA based MSINR
Algorithms to Solve GE	GPM, AMI, Linear AMI and GLM
Antenna Elements	4 element ULA with half wavelength spacing bet ⁿ omni elements
Temporal Combining	Maximal Ratio Combining (MRC) from 4 fingers

We essentially utilize the same simulation environment that we employed for the MSNR based Beamformer-Rake receivers in Chapter 5. The essential points are reiterated below:

- There are 5 and 10 interferers distributed uniformly within $[-60^\circ 60^\circ]$ along with the desired user who is in the middle of all the users. The uniform distribution indicates all the users including the desired user have spreading factor of 32 at their data channels. The non-uniform distribution represents one interferer located closest to the desired user with a data channel spreading factor of 4. (The details can be found in Section 5.5.)
- The Circular and Elliptical channel models, representing macro-cellular and micro-cellular environments respectively, describes the propagation conditions. (The details of the channel models can be found in Tables 5.2 and 5.3)

6.6 Simulation Results for the MSINR Beamforming for the Beamformer-Rake

In this section we will present simulation results that illustrate the performance of the MSINR beamforming technique for the Beamformer-Rake receiver. We will compare the performance of the different algorithms to solve the Generalized Eigenvalue problem. We will show that the Code gated Algorithm and the modified Code Filtering Approach provide the same performance regardless of the algorithm applied to solve the GE. The simulation environment was discussed in the previous section. The BER vs. E_b/N_0 performance will be used to compare the different receiver structures as well as the beamforming techniques and iterative algorithms for solving the GE.

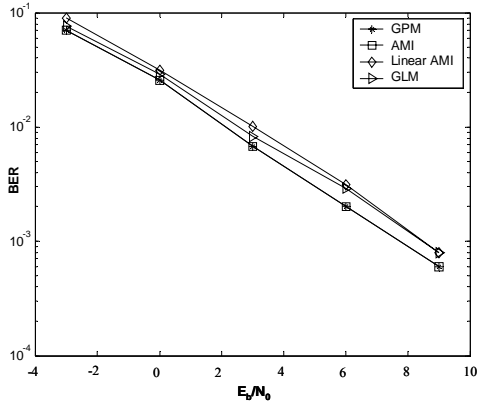


Figure 6.8: BER vs. E_b/N_0 of MSINR based Beamformer-Rake when the user distribution is *uniform*. 5 interferers, CGA beamforming, Circular channel.

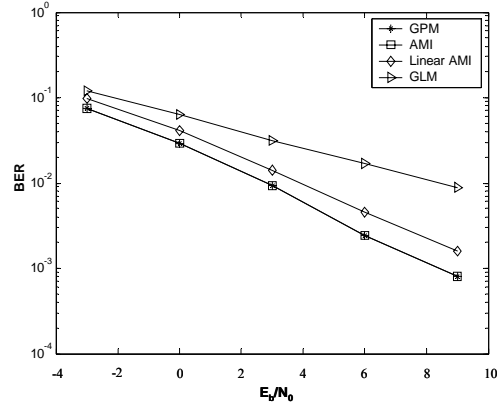


Figure 6.9: BER vs. E_b/N_0 of MSINR based Beamformer-Rake when the user distribution is *non-uniform*. 5 interferers, CGA beamforming, Circular channel.

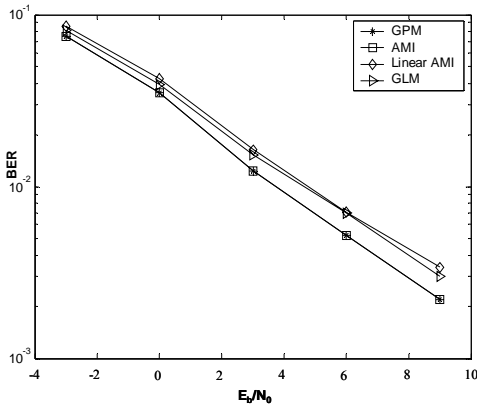


Figure 6.10: BER vs. E_b/N_0 of MSINR based Beamformer-Rake when the user distribution is *uniform*. 10 interferers, CGA beamforming, Circular channel.

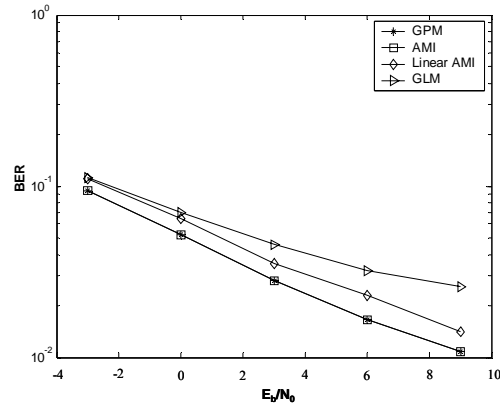


Figure 6.11: BER vs. E_b/N_0 of MSINR based Beamformer-Rake when the user distribution is *non-uniform*. 10 interferers, CGA beamforming, Circular channel.

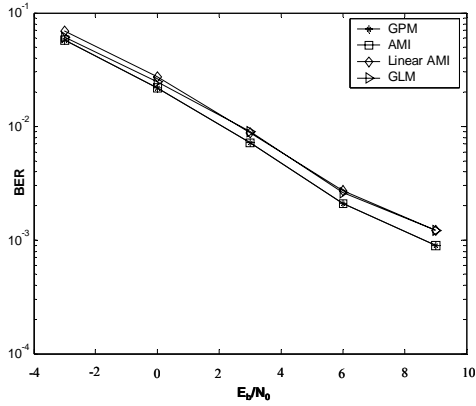


Figure 6.12: BER vs. E_b/N_0 of MSINR based Beamformer-Rake when the user distribution is *uniform*. 5 interferers, CGA beamforming, Elliptical channel.

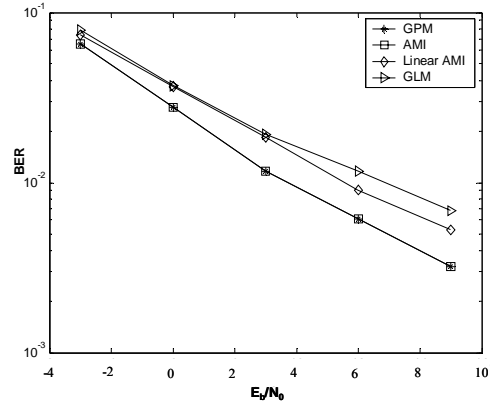


Figure 6.13: BER vs. E_b/N_0 of MSINR based Beamformer-Rake when the user distribution is *non-uniform*. 5 interferers, CGA beamforming, Elliptical channel.

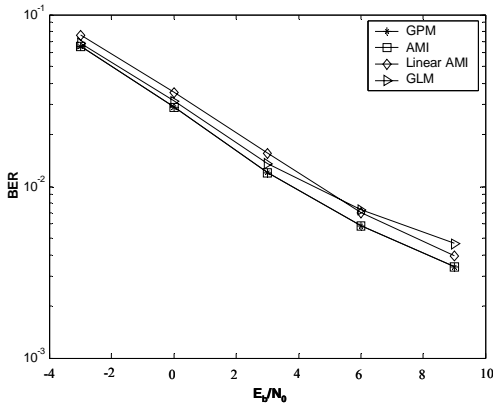


Figure 6.14: BER vs. E_b/N_0 of MSINR based Beamformer-Rake when the user distribution is *uniform*. 10 interferers, CGA beamforming, Elliptical channel.

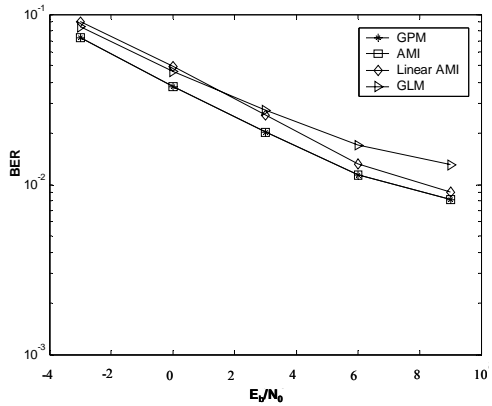


Figure 6.15: BER vs. E_b/N_0 of MSINR based Beamformer-Rake when the user distribution is *non-uniform*. 10 interferers, CGA beamforming, Elliptical channel.

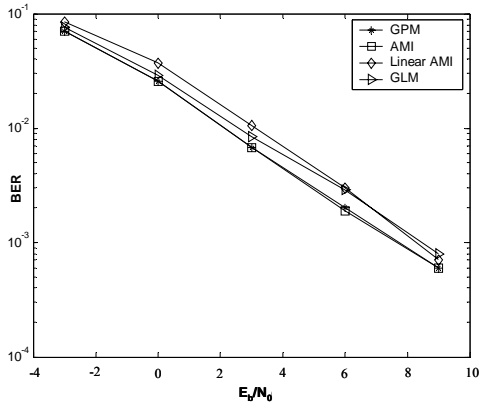


Figure 6.16: BER vs. E_b/N_0 of MSINR based Beamformer-Rake when the user distribution is *uniform*. 5 interferers, M-CFA beamforming, Circular channel.

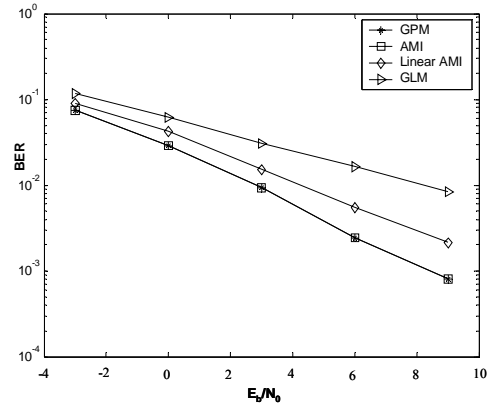


Figure 6.17: BER vs. E_b/N_0 of MSINR based Beamformer-Rake when the user distribution is *non-uniform*. 5 interferers, M-CFA beamforming, Circular channel.

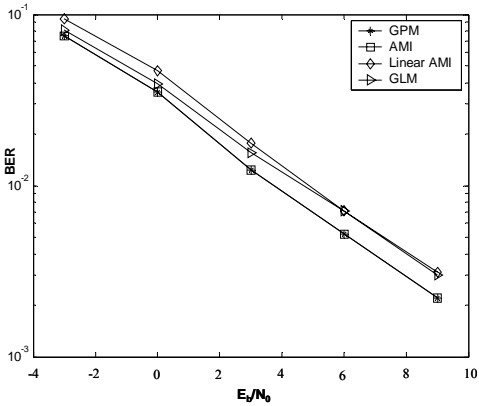


Figure 6.18: BER vs. E_b/N_0 of MSINR based Beamformer-Rake when the user distribution is *uniform*. 10 interferers, M-CFA beamforming, Circular channel.

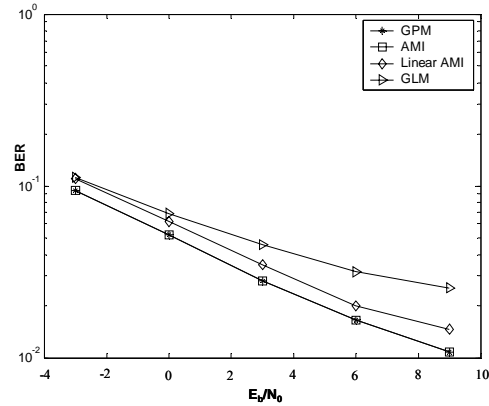


Figure 6.19: BER vs. E_b/N_0 of MSINR based Beamformer-Rake when the user distribution is *non-uniform*. 10 interferers, M-CFA beamforming, Circular channel.

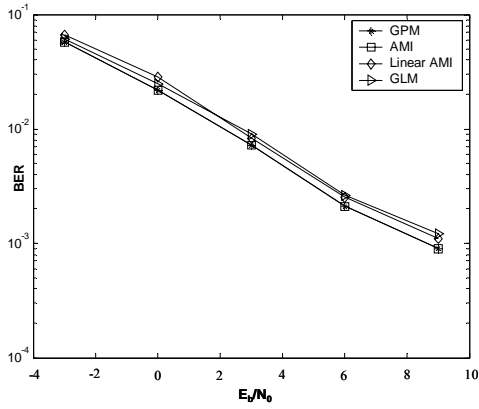


Figure 6.20: BER vs. E_b/N_0 of MSINR based Beamformer-Rake when the user distribution is *uniform*. 5 interferers, M-CFA beamforming, Elliptical channel.

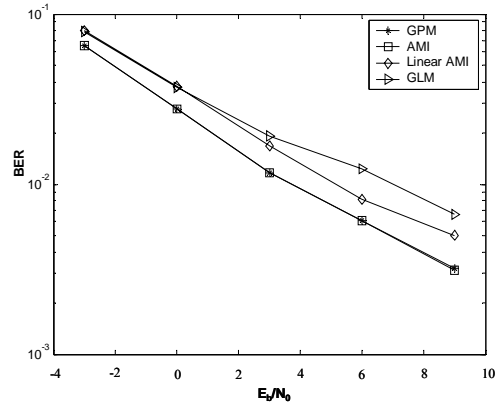


Figure 6.21: BER vs. E_b/N_0 of MSINR based Beamformer-Rake when the user distribution is *non-uniform*. 5 interferers, M-CFA beamforming, Elliptical channel.

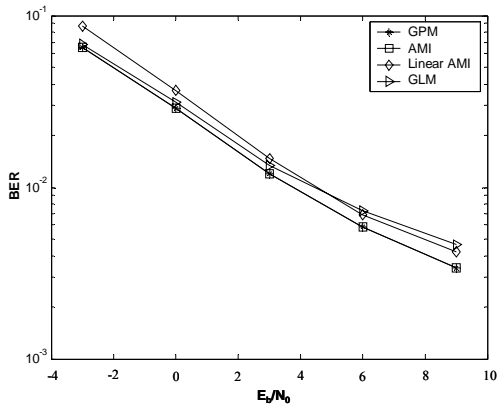


Figure 6.22: BER vs. E_b/N_0 of MSINR based Beamformer-Rake when the user distribution is *uniform*. 10 interferers, M-CFA beamforming, Elliptical channel.

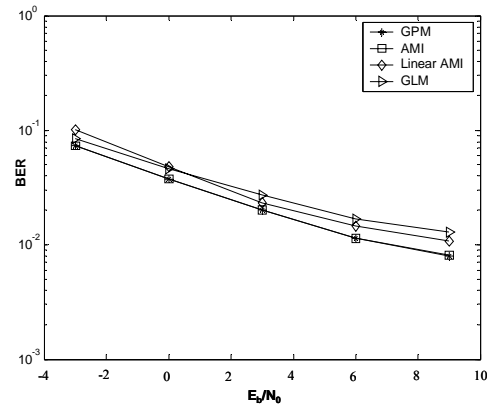


Figure 6.23: BER vs. E_b/N_0 of MSINR based Beamformer-Rake when the user distribution is *non-uniform*. 10 interferers, M-CFA beamforming, Elliptical channel.

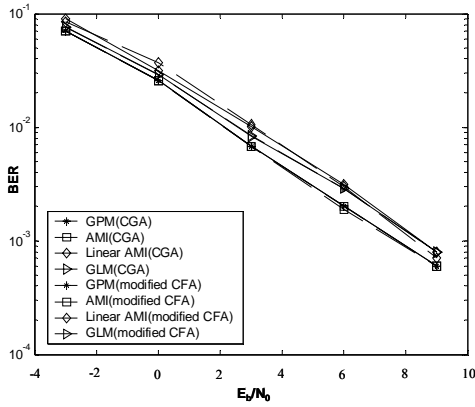


Figure 6.24: BER vs. E_b/N_0 comparison between CGA & M-CFA. Beamformer-Rake receiver, *uniform* user distribution. 5 interferers, Circular channel.

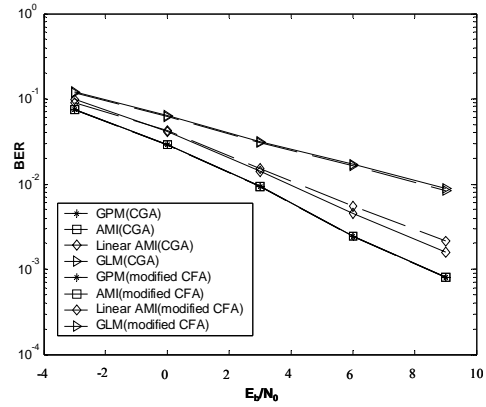


Figure 6.25: BER vs. E_b/N_0 comparison between CGA & M-CFA. Beamformer-Rake receiver, *non-uniform* user distribution. 5 interferers, Circular channel.

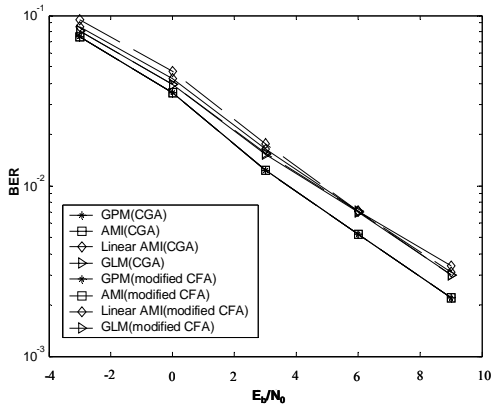


Figure 6.26: BER vs. E_b/N_0 comparison between CGA & M-CFA. Beamformer-Rake receiver, *uniform* user distribution. 10 interferers, Circular channel.

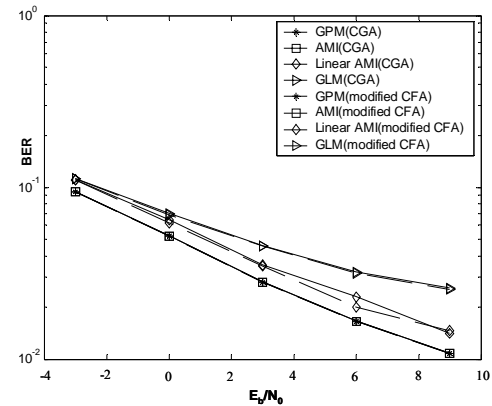


Figure 6.27: BER vs. E_b/N_0 comparison between CGA & M-CFA. Beamformer-Rake receiver, *non-uniform* user distribution. 10 interferers, Circular channel.

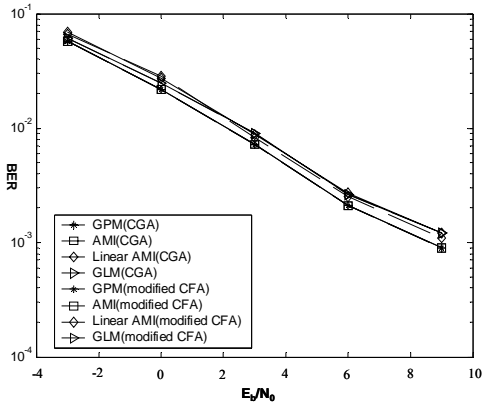


Figure 6.28: BER vs. E_b/N_0 comparison between CGA & M-CFA. Beamformer-Rake receiver, *uniform* user distribution. 5 interferers, Elliptical channel.

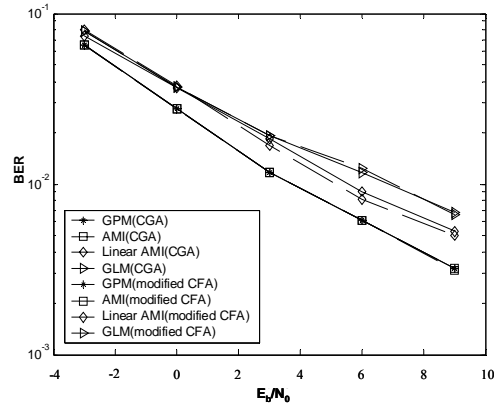


Figure 6.29: BER vs. E_b/N_0 comparison between CGA & M-CFA. Beamformer-Rake receiver, *non-uniform* user distribution. 5 interferers, Elliptical channel.

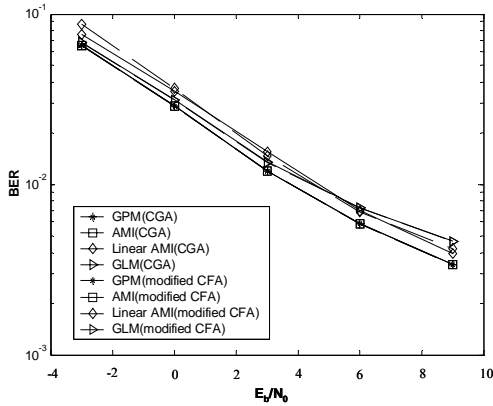


Figure 6.30: BER vs. E_b/N_0 comparison between CGA & M-CFA. Beamformer-Rake receiver, *uniform* user distribution. 10 interferers, Elliptical channel.

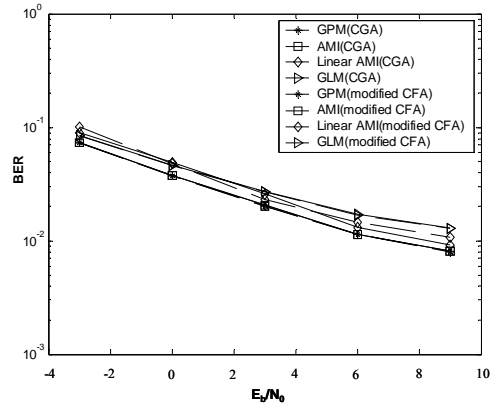


Figure 6.31: BER vs. E_b/N_0 comparison between CGA & M-CFA. Beamformer-Rake receiver, *non-uniform* user distribution. 10 interferers, Elliptical channel.

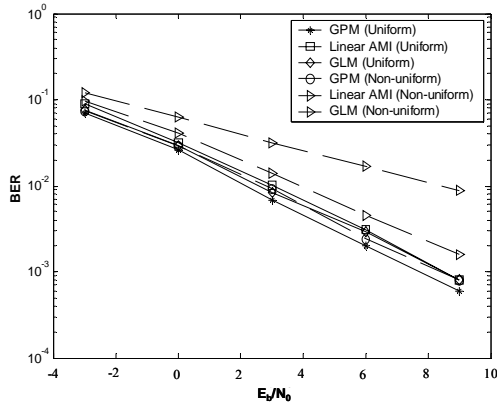


Figure 6.32: Performance comparison of different algorithms to solve GE. Beamformer-Rake, 5 interferers, CGA beamforming, Circular channel.

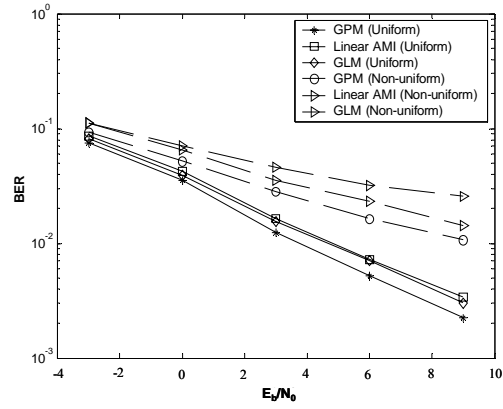


Figure 6.33: Performance comparison of different algorithms to solve GE. Beamformer-Rake, 10 interferers, CGA beamforming, Circular channel.

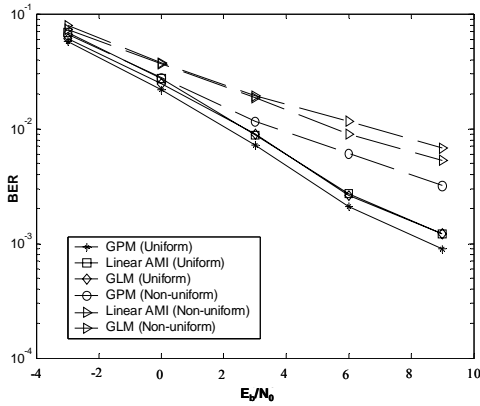


Figure 6.34: Performance comparison of different algorithms to solve GE. Beamformer-Rake, 5 interferers, CGA beamforming, Elliptical channel.

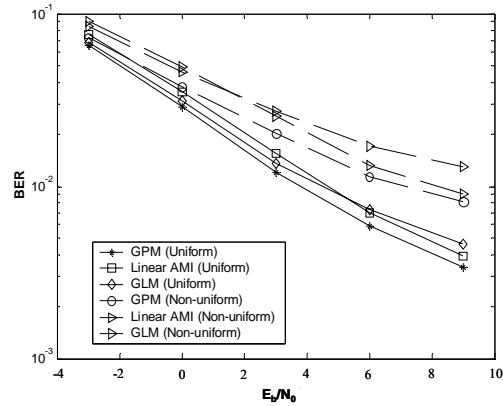


Figure 6.35: Performance comparison of different algorithms to solve GE. Beamformer-Rake, 10 interferers, CGA beamforming, Elliptical channel.

We can make the following conclusions from the simulation results (Figures 6.8 to 6.35)

- When applied to a Beamformer-Rake receiver, the CGA and the modified CFA provide the same BER vs. E_b/N_0 performance.
- The Adaptive Matrix Inversion method performs the same as the Generalized Power method.
- There is very little penalty associated with linearizing the AMI. Although the difference is a little more visible when there is a strong interferer present. Since both the covariance matrices are factors during the estimation of the weight vector, the consequence of the approximation is more pronounced when the interference is no longer spatially white (i.e. no longer of the structure $\underline{R}_{uu} = \sigma_u^2 I_N$).
- The performance of the linear AMI is similar to the Generalized Lagrange Multiplier method when the user distribution is uniform.
- The linear AMI outperforms the GLM significantly for non-uniform user distribution i.e. when one of the interferers is much stronger than the other interferers. The GLM uses the instantaneous estimates of the covariance matrices. As a result the effect of this approximation is more prominent when both the matrices are vital for the estimation of the weight vector i.e. the case when the interference and noise is no longer spatially white because of the presence of a strong interference.

6.7 Comparison of MSINR and MSNR Beamforming Techniques for Beamformer-Rake

In the next few Figures, we are going to present a comparison between the MSNR and MSINR beamforming techniques. The results will demonstrate the superiority of the MSINR beamforming technique. The vector channel models are still described by Tables 5.2, 5.3. The Code Gated Algorithm was selected to perform the MSINR beamforming. We still employ Beamformer-Rake receivers that utilize the MSINR and MSNR beamforming criteria to perform the spatial processing. Since the Adaptive Matrix Inversion algorithm exhibited similar performance to the Generalized Power method, we excluded the AMI to make the BER graphs a little more readable.

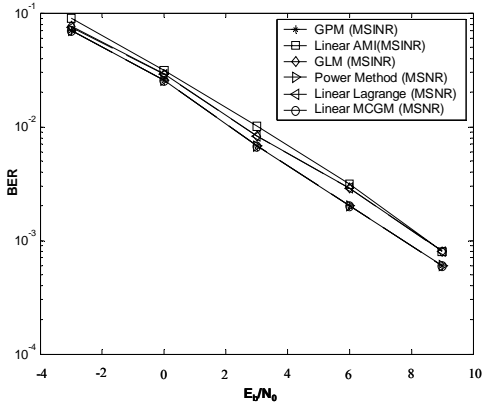


Figure 6.36: Performance comparison between MSNR & MSINR beamforming. Beamformer-Rake, 5 interferers, uniform user distribution, Circular channel.

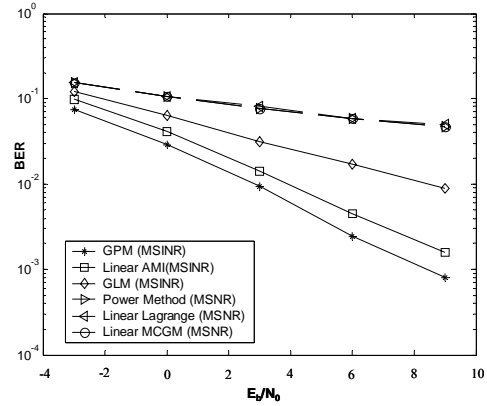


Figure 6.37: Performance comparison between MSNR & MSINR beamforming. Beamformer-Rake, 5 interferers, non-uniform user distribution, Circular channel.

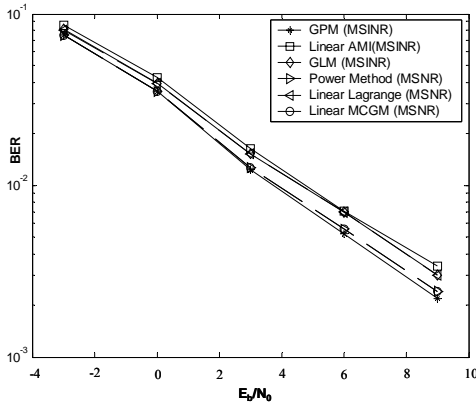


Figure 6.38: Performance comparison between MSNR & MSINR beamforming. Beamformer-Rake, 10 interferers, uniform user distribution, Circular channel.

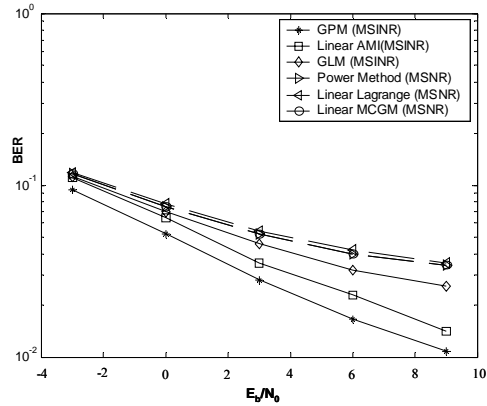


Figure 6.39: Performance comparison between MSNR & MSINR beamforming. Beamformer-Rake, 10 interferers, non-uniform user distribution, Circular channel.

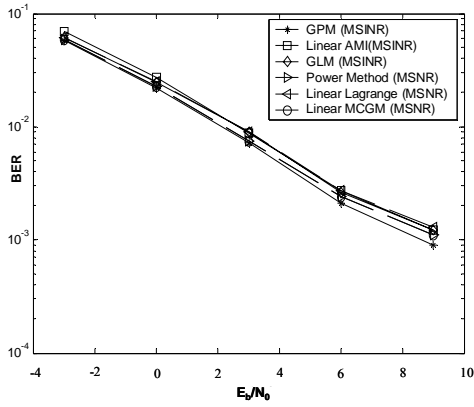


Figure 6.40: Performance comparison between MSNR & MSINR beamforming. Beamformer-Rake, 5 interferers, uniform user distribution, Elliptical channel.

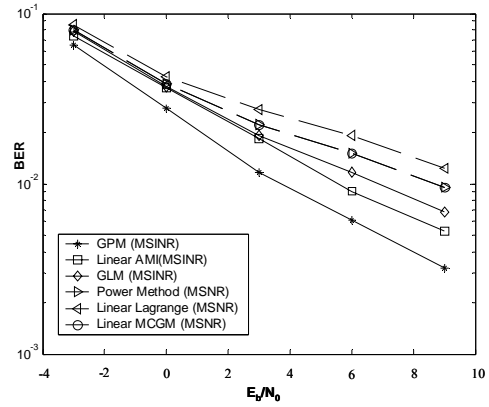


Figure 6.41: Performance comparison between MSNR & MSINR beamforming. Beamformer-Rake, 5 interferers, non-uniform user distribution, Elliptical channel.

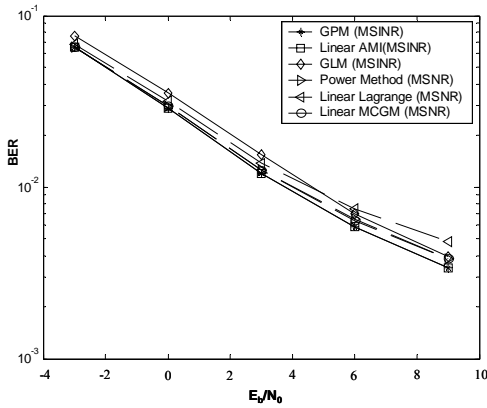


Figure 6.42: Performance comparison between MSNR & MSINR beamforming. Beamformer-Rake, 10 interferers, uniform user distribution, Elliptical channel.

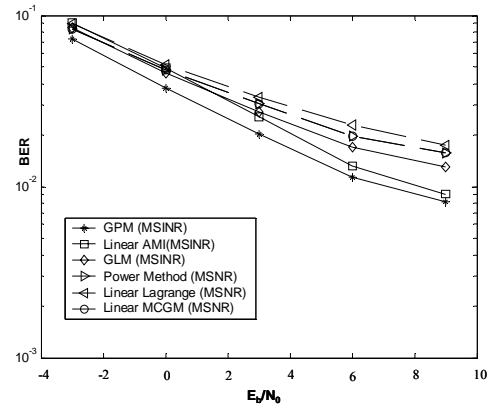


Figure 6.43: Performance comparison between MSNR & MSINR beamforming. Beamformer-Rake, 10 interferers, non-uniform user distribution, Elliptical channel.

Let us highlight the significant facts of the comparison between MSINR and MSINR beamforming techniques:

- The Beamformer-Rake receivers perform the same for both the Circular and Elliptical channel as long as all the signals are received at the same average power level. This is to be expected, because under the condition of spatial whiteness of the interference and noise, the MSINR beamforming criterion reduces to the MSNR criterion. Therefore there is no advantage to be achieved from the MSINR beamforming.
- In the presence of strong interferer, the MSINR based 2-D receiver outperforms the same based on the MSNR criterion. In this scenario, the MSNR is not the optimum beamforming criterion anymore. The spatial structure of the colored interference and noise has to be taken into account to estimate the optimum beamformer weight vectors. The MSNR Eigen-Beamforming does exactly that by introducing the interference and noise covariance matrix into the Eigen-equation. The MSINR based beamformers can protect the temporal Rake structure better from the near-far situation.
- The difference in performance is less significant in the case of the Elliptical channel environment. This is because the Elliptical channel with its much wider angle spread is more conducive to maintaining the spatial whiteness of the interference and noise signal.

Although we have demonstrated the superiority of the MSINR based beamforming, the importance and the applicability of the MSNR beamforming should not be dismissed. In the simulations conducted, we have assumed that the interferer with a lower spreading factor is allowed to raise its power level proportionately to compensate for the lower spreading gain. However in an actual system the power control mechanism will maintain some sort of parity between the mean power levels of the received signal and will not allow the near-far system to occur. At the same time, if the mobile station with a higher data rate (low spreading factor) is required to transmit at a very high power level, the coverage area for high data rate service will be very small due to the power constraint. Since the higher data rate user may not require real-time service, an acceptable level of performance could be achieved by transmitting at a lower power level and employing some form of Automatic Repeat Request (ARQ) scheme. The MSINR based beamforming allows for better flexibility on the power control scheme, but the MSNR based beamforming has the advantage of reduced complexity in the receiver design and less computational burden for estimating the weights.

Chapter 7

Beamformer-Rake based on MMSE Criterion

7.1 Introduction

The Beamformer-Rake receivers we have discussed so far employ Eigen-Beamforming technique based on the MSNR and MSINR criterion. In this chapter we will introduce a Beamformer-Rake receiver that employs the Minimum Mean Square Error (MMSE) [2] criterion to perform the spatial processing. The MMSE beamforming technique, as explained in Chapter 3 requires known data and uses that as a reference to generate the error to be minimized. The receiver still employs the MRC at the temporal domain. The chapter begins with a discussion of the Direct Matrix Inversion (DMI) technique for the Wiener solution. We also briefly layout the steepest descent method and outline the well known Least Mean Square (LMS) approach for solving the MMSE problem. We propose a Beamformer-Rake receiver for the WCDMA uplink that employs Pilot Symbol Assisted (PSA) [14], [15] MMSE based beamforming technique. This section concludes with a performance comparison of this Beamformer-Rake with the MSINR based Beamformer-Rake receiver described in the previous chapter. The last section of this chapter provides a discussion on the importance of spatial diversity gain. We provide simulation results that show that achieving diversity gain is more important than maintaining Nyquist spacing between the elements of an adaptive antenna array at the presence of a large number of co-channel interferers.

7.2 MMSE Beamforming Criterion

The Minimum Mean Squared Error (MMSE) weight vector is given by the Wiener solution (see Chapter 3 for a detailed discussion)

$$\underline{w}_{MMSE} = \underline{R}_{xx}^{-1} \underline{r}_{xd}, \quad (7.1)$$

where \underline{R}_{xx}^{-1} is the inverse of the covariance matrix, $\underline{R}_{xx} = E[\underline{x}(k)\underline{x}^H(k)]$, of the received signal vector \underline{x} and $\underline{r}_{xd} = E[\underline{x}(k)d^*(k)]$ is the cross-correlation vector between the received signal vector \underline{x} and the reference signal d .

7.2.1 Direct Matrix Inversion (DMI)

The received signal matrix can be estimated by using an L sample rectangular averaging window as

$$\hat{\underline{\underline{R}}}_{xx}(k) = \frac{1}{L} \sum_{l=k-L+1}^k \underline{x}(l) \underline{x}^H(l) \quad (7.2)$$

Here $\underline{x}(l)$ is collected sample of the received signal over a block of L samples. Similarly, the cross-correlation vector can be estimated as

$$\hat{\underline{r}}_{xd}(k) = \frac{1}{L} \sum_{l=k-L+1}^k \underline{x}(l) d^*(l) \quad (7.3)$$

where $\underline{x}(l)$ is collected samples of the received signal, $d^*(l)$ is the conjugate of the actual sample sent. As before the estimation is performed over a block of L samples. The DMI [15] involves computing the inverse of the estimated received signal matrix $\hat{\underline{\underline{R}}}_{xx}$ and then calculate the MMSE weight vector by applying the Wiener solution. Based on the estimates of Equation 7.2 and 7.3, the MMSE weight can be computed as

$$\underline{w}_{MMSE}(k+1) = \hat{\underline{\underline{R}}}_{xx}^{-1}(k) \underline{r}_{xd}(k) \quad (7.4)$$

Since matrix inversion requires a lot of computation, the inverse can be computed according to the following *rank 1* update:

$$\underline{\underline{R}}_{xx}^{-1}(k) = \underline{\underline{R}}_{xx}^{-1}(k-1) - \frac{\underline{\underline{R}}_{xx}^{-1}(k-1) \underline{x}(k) \underline{x}^H(k) \underline{\underline{R}}_{xx}^{-1}(k-1)}{1 + \underline{x}^H(k) \underline{\underline{R}}_{xx}^{-1}(k-1) \underline{x}(k)} \quad (7.5)$$

$$\underline{\underline{R}}_{xx}^{-1}(0) = \frac{1}{\epsilon} I, \quad \epsilon > 0$$

The update according to Equation 7.5 is termed as the Sample Matrix Inversion (SMI) [103], [104] technique. Each iteration of Equation 7.5 requires computational complexity on the order of $O(3.5N^2 + N)$.

If the channel does not change very rapidly, it may not be necessary to estimate and update the weight for each sample and a single set of weight for a block of L samples may be adequate. For such a scenario, the received signal covariance matrix and cross-correlation vector can be estimated only once by averaging over the entire block of samples. We can then employ the Cholesky [11] or LDL^T

[199] factorization of $\hat{\underline{\underline{R}}}_{xx}$ and the Forward-Backward solve [199] technique to get the MMSE weight. This procedure is outlined in the following set of Equations.

$$\begin{aligned}\hat{\underline{\underline{R}}}_{xx}(i) &= \frac{1}{L} \sum_{l=N_{start}^i}^{N_{start}^i+L-1} \underline{x}(l) \underline{x}^H(l) \\ \hat{\underline{r}}_{xd}(i) &= \frac{1}{L} \sum_{l=N_{start}^i}^{N_{start}^i+L-1} \underline{x}(l) d^*(l)\end{aligned}\tag{7.6}$$

$$\hat{\underline{\underline{R}}}_{xx}(i) = \hat{\underline{\underline{R}}}(i) \hat{\underline{\underline{R}}}^H(i)\tag{7.7}$$

$$\hat{\underline{\underline{R}}}(i) \underline{y}(i) = \hat{\underline{r}}_{xd}(i)\tag{7.8}$$

$$\hat{\underline{\underline{R}}}^H(i) \underline{w}_{MMSE}(i) = \underline{y}(i)$$

Here i is the block index, N_{start}^i is the sample index of the first sample of the i^{th} block and $\hat{\underline{\underline{R}}}(i)$ is the Cholesky factor of $\hat{\underline{\underline{R}}}_{xx}(i)$. Equation 7.8 defines the Forward-Backward solve method. Note the computational savings due to the triangular structure of $\hat{\underline{\underline{R}}}(i)$.

Before we leave the topic of DMI, we would like to point out an enhancement to DMI which is commonly referred to as the Diagonal Loading (DL) [200] technique. A diagonal loading factor [200] is introduced in the Wiener solution to prevent singularity due to matrix inversion so that

$$\underline{w}_{MMSE} = \left[\hat{\underline{\underline{R}}}_{xx} + \gamma I \right]^{-1} \hat{\underline{r}}_{xd}\tag{7.9}$$

Here γ is the diagonal loading factor and we have ignored the indices for block and sample for the sake of convenience. In a practical system the adaptive antenna array will always operate in the presence of thermal noise and as a result the received signal covariance matrix will almost always be full rank. However the value of γ can be chosen according to the Interference to Noise Ratio (INR) to provide performance enhancement [201]. Obviously this means that the INR has to be known *a priori* or can be determined.

7.2.2 Method of Steepest Descent

The method of steepest descent provides a computationally simple alternative to DMI. This is the exact opposite of the steepest ascent method applied in the Lagrange multiplier methods for solving the Eigenvalue problem. The steepest ascent method intends to find the maxima of a functional

whereas the method of steepest descent aims towards reaching the minima of a functional. The procedure is outlined below [105], [189]:

1. Begin with an initial guess ($k = 0$, k being the index of iteration) for the weight vector \underline{w} as $\underline{w}(0)$. Typically, $\underline{w}(0)$ is set equal to a column vector of an $N \times N$ identity matrix.
2. Using the present estimate of the weight vector $\underline{w}(k)$ (the initial guess $\underline{w}(0)$ for $k = 0$), compute the gradient vector $\nabla\{J(k)\}$ for the k^{th} iteration.
3. Compute the next estimate of the weight vector $\underline{w}(k+1)$ by making a change in the present estimate (initial guess for $k = 0$) in a direction opposite to that of the gradient vector.
4. Go back to step 2 and repeat the process.

Successive adjustments to the weight vector in the direction of the negative of the gradient vector should eventually lead to the minimum mean squared error J_{\min} , at which the weight vector is the optimum weight vector \underline{w}_{MMSE} .

If $\underline{w}(k)$ denotes the estimate of the weight vector at the k^{th} iteration, the next estimate of the weight vector for the $(k+1)^{\text{th}}$ iteration, $\underline{w}(k+1)$, is estimated according to the following simple recursion:

$$\underline{w}(k+1) = \underline{w}(k) + \frac{1}{2}\mu[-\nabla\{J(k)\}], \quad (7.10)$$

where μ is a small positive constant, often termed as the step size. Now,

$$\nabla\{J(k)\} = -2\underline{r}_{xd} + 2\underline{R}_{xx}\underline{w}(k) \quad (7.11)$$

So the weight update equation becomes

$$\underline{w}(k+1) = \underline{w}(k) + \mu[\underline{r}_{xd} - \underline{R}_{xx}\underline{w}(k)] \quad (7.12)$$

If we apply the definitions of the covariance matrix and the correlation vector, the gradient vector during each iteration can be computed as

$$\begin{aligned} \nabla\{J(k)\} &= -2\left[E\{\underline{x}(k)d^*(k)\} - E\{\underline{x}(k)\underline{x}^H(k)\}\underline{w}(k)\right] \\ &= -2E\left\{\underline{x}(k)\left[d^*(k) - \underline{x}^H(k)\underline{w}(k)\right]\right\} \\ &= -2E\left\{\underline{x}(k)\left[d(k) - \underline{w}^H(k)\underline{x}(k)\right]^*\right\} \\ &= -2E\left\{\underline{x}(k)e^*(k)\right\} \end{aligned} \quad (7.13)$$

So we can write the weight update equation as

$$\underline{w}(k+1) = \underline{w}(k) + \mu E\{\underline{x}(k)e^*(k)\} \quad (7.14)$$

Equations 7.12 and 7.14 are the mathematical formulation of the steepest descent method.

7.2.3 Least Mean Square (LMS) algorithm

It is obvious that an exact measurement of the gradient vector $\nabla\{J(k)\}$ as well as a judicious choice of the step size μ is required for the convergence of the steepest descent method to the optimum MMSE weight vector. However Equation 7.11 indicates that an exact measurement of the gradient vector requires prior knowledge of the covariance matrix of the received signal and the correlation vector between the received signal vector and the reference signal. As a result the gradient vector must be measured from the observed data. The Least Mean Square (LMS) algorithm proposes a very simple instantaneous estimate [105] of the gradient vector so that

$$\hat{\nabla}\{J(k)\} = -2\underline{x}(k)e^*(k). \quad (7.15)$$

The weight update equation for the LMS algorithm becomes

$$\underline{w}(k+1) = \underline{w}(k) + \mu \underline{x}(k)e^*(k). \quad (7.16)$$

The following two equations thus define the LMS algorithm:

$$\begin{aligned} e(k) &= d(k) - \underline{w}^H(k)\underline{x}(k) \\ \underline{w}(k+1) &= \underline{w}(k) + \mu \underline{x}(k)e^*(k) \end{aligned} \quad (7.17)$$

We can observe that the LMS has a computational complexity of $O(2N)$. This low computational complexity is the most attractive feature of the LMS algorithm. The response of the LMS algorithm is determined by the following three principal factors [105]

- The step-size
- The size of the weight vector
- Eigen-value distribution of the received signal covariance matrix

The LMS algorithm is described in detail in [105], [17].

We have shown in a previous study [202], [203] that the LMS is not a very suitable algorithm for spatial processing in a Beamformer-Rake receiver. One of the reasons for this is the eigenvalue distribution of the covariance matrix of the received signal. Since the control channel has a large processing gain (because of a spreading factor of 256) the covariance matrix has a large dominant

eigenvalue (corresponding to the desired signal) followed by quite small eigenvalues (corresponding to interference and noise). The LMS algorithm has difficulty to converge in such a scenario [105]. Also it has been shown [122] that the LMS based MMSE beamforming is not a very robust technique in a fast fading channel. Therefore we propose a Beamformer-Rake receiver for WCDMA uplink that computes the MMSE weight vector by employing the DMI technique outlined in section 7.2.1.

7.3 Pilot Symbol Assisted DMI-based Beamformer-Rake Receiver for WCDMA

The Wiener solution requires a reference signal to compute the cross correlation vector. Since, WCDMA specifies pilot symbols at the DPCCH, we can employ a Beamformer-Rake receiver that computes the optimum MMSE weight for its spatial processing with the help of the pilot symbols. This type of beamforming technique is sometimes termed as the Pilot Symbol Assisted (PSA) [14] beamforming. Figure 7.1 shows the PSA based Beamformer-Rake receiver for the WCDMA uplink. It employs the DMI technique to compute the set of weight vector required for the spatial processing.

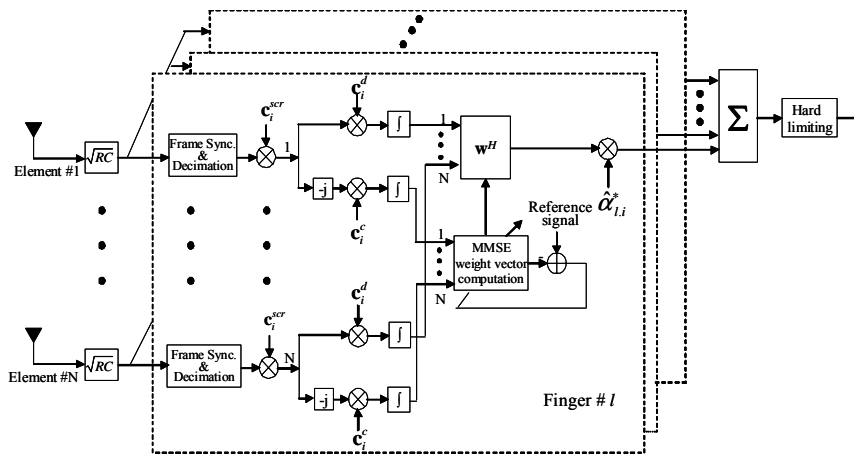


Figure 7.1: MMSE based Beamformer-Rake receiver for WCDMA uplink

The received signal from a particular multipath is descrambled with the appropriate scrambling code of the desired user. The control channel signal is despread from the chip level to the symbol level. The despread control signal from all the antenna elements is employed to evaluate and update the MMSE weight vector for the particular multipath. Calculated weights for the i^{th} DPCCH slot are used to form the beam for the data symbols of the corresponding DPDCH slots. The weight vectors for the i^{th} DPCCH slot is calculated from the despread pilot symbols of the $(i-1)^{\text{th}}$, i^{th} and $(i+1)^{\text{th}}$ DPCCH

slots. The number of pilot symbols in WCDMA DPCCH slot varies from 4 to 6 depending on the data rate. This is the reason for employing samples from three slots so that there are sufficient samples for collecting the required statistics. However for the simulations conducted, we assume that all 10 symbols of a DPCCH slot are known pilot symbols. The beamforming operation is followed by temporal processing where the spatially combined signals from different multipath are combined with MRC. Since the WCDMA uplink has pilot symbols at the DPCCH, coherent combining is feasible. We assume that we have perfect channel estimation for the simulations conducted.

7.4 Performance Comparison with MSINR Beamforming

In this section we will compare the performance of the MMSE based Beamformer-Rake receiver with that of an MSINR based Beamformer-Rake receiver. Pilot Symbol Assisted DMI technique is employed to compute the set of MMSE weight vector. The modified CFA is employed to perform MSINR beamforming. We use the linear AMI algorithm developed in Section 6.3.3 to solve the generalized eigenvalue problem. Note that the DMI based receiver uses the DPCCH only to compute the weight vectors and employ those weight vectors to combine the DPDCH. Therefore for fair comparison, we employ the DPCCH only to calculate the weight vector for the MSINR based receiver. This is different from the receivers described in Chapters 5 and 6. We have provided the block diagram of Beamformer-Rake receivers that employ the DPCCH only to compute the weight vectors in Appendix B. Figure B.3 shows the block diagram of the Beamformer-Rake receiver employed in this study. For the simulations conducted, even though we used the control channel only to compute the weight vectors, we assumed that the TFCI bits were decoded without any error.

We assume a three sector per cell configuration so that the users are located within $[-60^\circ \ 60^\circ]$. The receivers operate in an outdoor vehicular environment and the multipath propagation conditions are given by the vehicular channel described in Table 7.1. We assume that all four resolvable multipath components are within 30° of the angle spread with respect to the central arriving angle of the transmitted signal. Using the Jakes' model [156], the complex amplitude of the l^{th} resolvable multipath component on the n^{th} antenna can be represented as [168]

$$h_{l,n}(t) = \frac{\sqrt{\bar{P}_l}}{\sqrt{M}} \sum_{m=0}^{M-1} e^{j \left[2\pi f_d \cos(\Phi_{l,m})t + \phi_{l,m} + \frac{2\pi}{\lambda_c} d_n \sin(\theta_{l,m}) \right]} \quad (7.18)$$

where \bar{P}_l is the average power received for the l^{th} path (taken from Table 7.1 for the simulations), M is the number of scatterers composing each resolvable path, f_d is the maximum Doppler frequency,

$\phi_{l,m}$ is a uniformly distributed random phase, $\Phi_{l,m}$ is the random angle of departure relative to the motion of the mobile of each multipath, d_n is the distance between the n^{th} antenna element and the reference antenna, λ_c is the carrier wavelength, and $\theta_{l,m}$ is the angle of arrival of each scattered replica with respect to the array broadside. Moreover, we assume that $\theta_{l,m}$ is uniformly distributed between $[\Theta_l - \frac{\Delta_l}{2}, \Theta_l + \frac{\Delta_l}{2}]$, where Θ_l and Δ_l are the central angle of arrival and the angle spread of the l^{th} resolvable multipath, respectively. Table 7.1 shows the parameters used for generating the complex coefficients of the vehicular channel model for our study. The simulation parameters are summarized in Table 7.2. The spatial distributions of the users are the uniform and non-uniform distributions described in Section 5.5.

Table 7.1: Vehicular channel

Jakes Model Parameters		Power Delay Profile	
f_d	223 Hz (120 Km/hr at 2 GHz)	Relative Delay (ns)	Average Power (dB)
M	20	0	0
Δ	5^0	260	-3
Φ	$0^0 \sim 360^0$	521	-6
ϕ	$0^0 \sim 360^0$	781	-9
d_n/λ	$0.5n$		

Table 7.2: Simulation parameters for MSINR vs. MMSE beamforming for Beamformer-Rake

Type of Receiver	Beamformer-Rake
Spatial Processing Technique	MMSE
Antenna Elements	4 element ULA
Temporal Combining	Maximal Ratio Combining (MRC) from 4 fingers
Vector Channel	Vehicular Channel (see Table 7.1)
Number of Interferers	5 and 10

The following four figures compare the performance of the MMSE and MSINR beamforming for Beamformer-Rake receiver application. We can observe that the performance of the MSINR and MMSE based Beamformer-Rake is very close. This is in agreement with the theoretical equivalence shown in chapter 3. However the MMSE based beamforming does provide small improvement in performance. This is largely due to the fact that the MMSE weight vector for a slot is computed with samples from that slot as well as with samples from the previous and next slots and we assume that all the DPCH symbols are known pilot. DMI requires a lot of operations and the computational complexity is quadratic. As we mentioned previously in Section 7.2.2, computationally simple algorithm like the LMS does not perform satisfactorily in this environment. At the same time linear AMI is one of the several computationally simple algorithms to perform MSINR based beamforming

and there is very little penalty associated with choosing a linear complexity algorithm. Therefore, the MSINR based beamforming seems to be the better option.

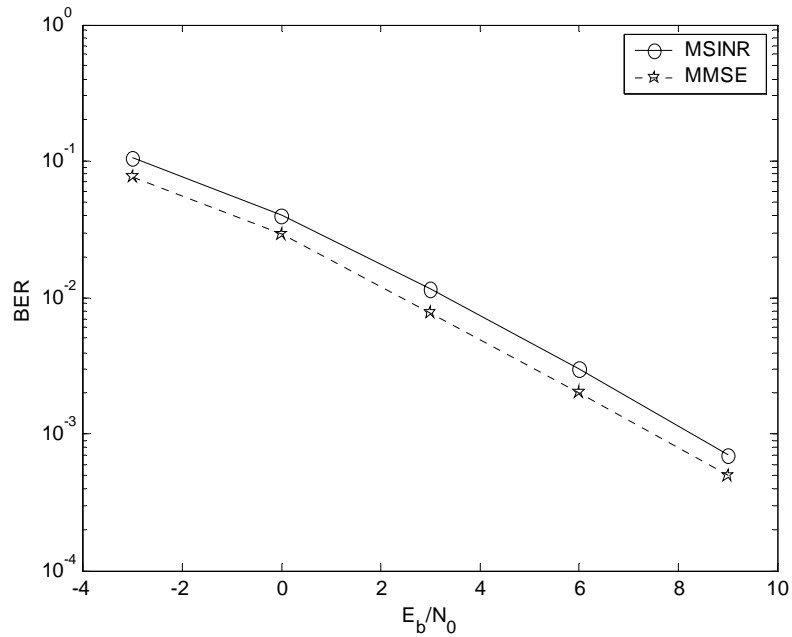


Figure 7.2: Performance comparison between MMSE and MSINR based Beamformer-Rake receivers in terms of BER vs. E_b/N_0 . There are 5 interferers. The user distribution is uniform. The multipath environment is defined by the vehicular channel.

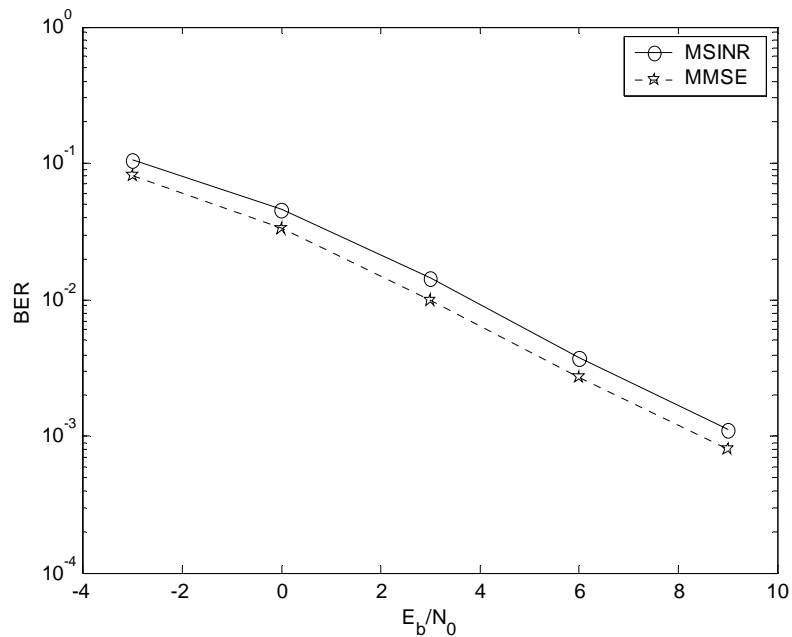


Figure 7.3: Performance comparison between MMSE and MSINR based Beamformer-Rake receivers in terms of BER vs. E_b/N_0 . There are 5 interferers. The user distribution is non- uniform. The multipath environment is defined by the vehicular channel.

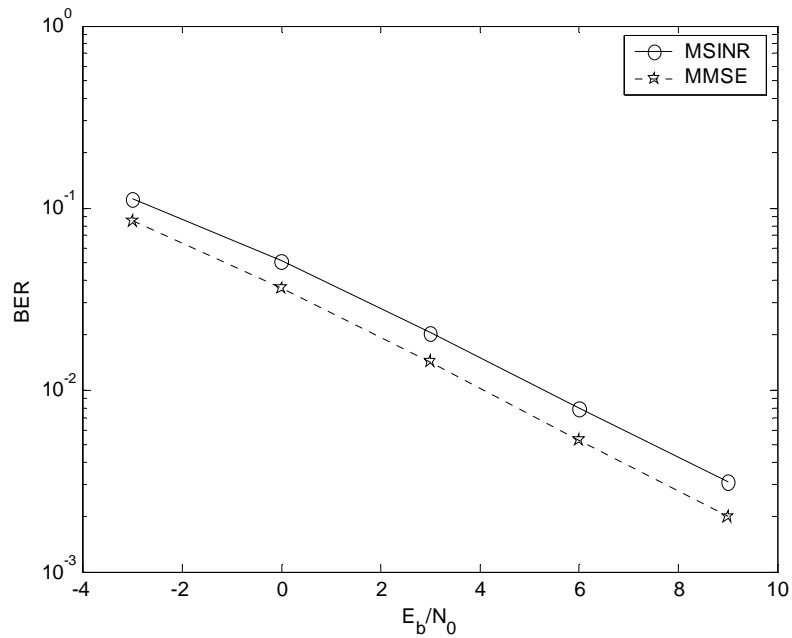


Figure 7.4: Performance comparison between MMSE and MSINR based Beamformer-Rake receivers in terms of BER vs. E_b/N_0 . There are 10 interferers. The user distribution is uniform. The multipath environment is defined by the vehicular channel.

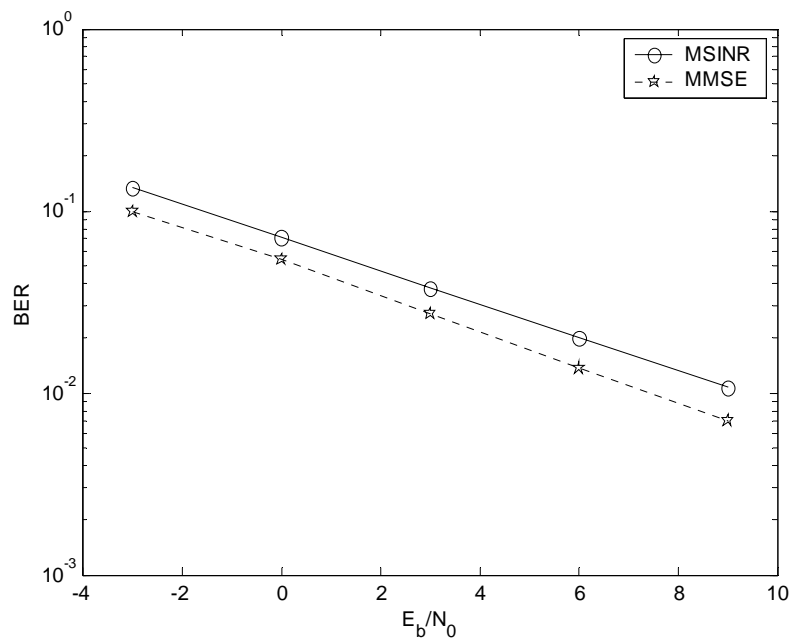


Figure 7.5: Performance comparison between MMSE and MSINR based Beamformer-Rake receivers in terms of BER vs. E_b/N_0 . There are 10 interferers. The user distribution is non-uniform. The multipath environment is defined by the vehicular channel.

7.5 Diversity Gain vs. Spatial Aliasing

The Nyquist sampling theorem states that in order to avoid spatial aliasing the spacing between the elements of an antenna array has to be less than or equal to half the carrier wavelength. However in order to get diversity gain, correlation across the signals at different antenna elements has to be low. As a result, the elements are often required to be not *Nyquist-spaced* and because of the larger spacing there is spatial aliasing and grating lobes [191] that are generated in the beam-pattern. However the loss due to spatial aliasing can be offset by the diversity gain. In a wireless system where the number of co-channel interferers is larger than the number of elements of a practical antenna array, we can not perform explicit null-steering. As a result the advantage of beamforming is lost to some extent. In this situation it is essential to attain diversity gain, even at the cost of spatial aliasing if necessary. This fact will be demonstrated with the aid of simulation in this section

7.5.1 Simulation Results: Spatial Aliasing vs. Diversity Gain

We equip the Beamformer-Rake receivers with two different 4 element ULA. For one array the spacing between the elements is half the carrier wavelength. For the other ULA the spacing between the elements is 10 times the carrier wavelength to ensure diversity gain in a channel with very small angle spread. Both the antenna array performs MMSE based spatial combining. The simulation parameters are described in Table 7.3. The spatial distributions of the users are similar to that described in Section 5.5. The vehicular channel of Table 7.4 describes the propagation condition

Table 7.3: Simulation parameters for spatial aliasing vs. diversity gain

Type of Receiver	Beamformer-Rake
Beamforming Criterion	MMSE
Antenna Elements	4 element ULA with spacing of $\lambda/2$ and 10λ
Temporal Combining	Maximal Ratio Combining (MRC) from 4 fingers
Vector Channel	Vehicular Channel (see Table 7.4)
User Distribution	Uniform and Non-Uniform (see Section 5.5)

Table 7.4: Vehicular channel

Jakes Model Parameters		Power Delay Profile	
f_d	223 Hz (120 Km/hr at 2 GHz)	Relative Delay (ns)	Average Power (dB)
M	20	0	0
Δ	5^0	260	-3
Φ	$0^0 \sim 360^0$	521	-6
ϕ	$0^0 \sim 360^0$	781	-9
d_n/λ	$0.5n$ & $10n$		

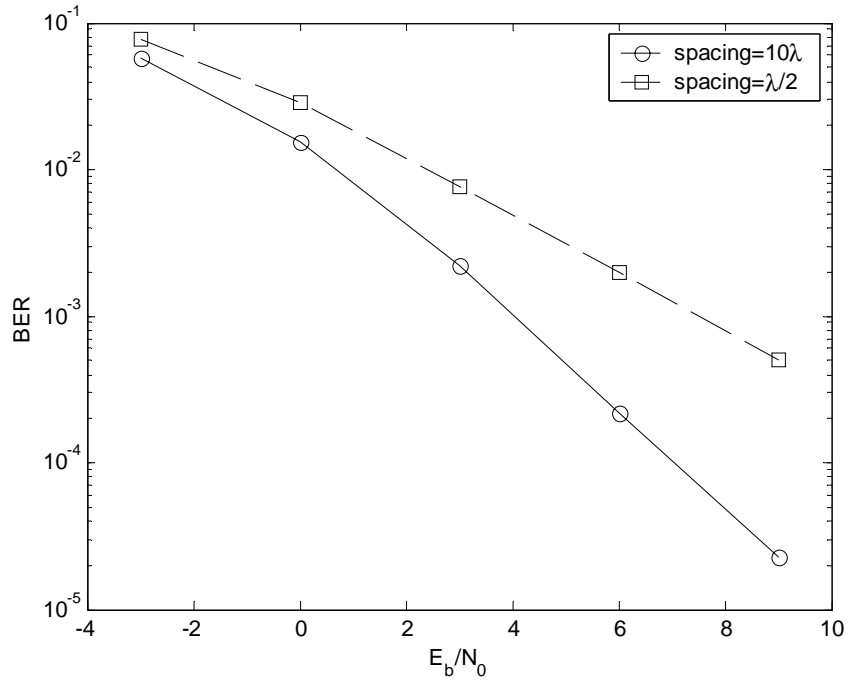


Figure 7.6: Spatial Aliasing vs. Diversity Gain. There are 5 interferers. The user distribution is uniform. The multipath environment is defined by the vehicular channel.

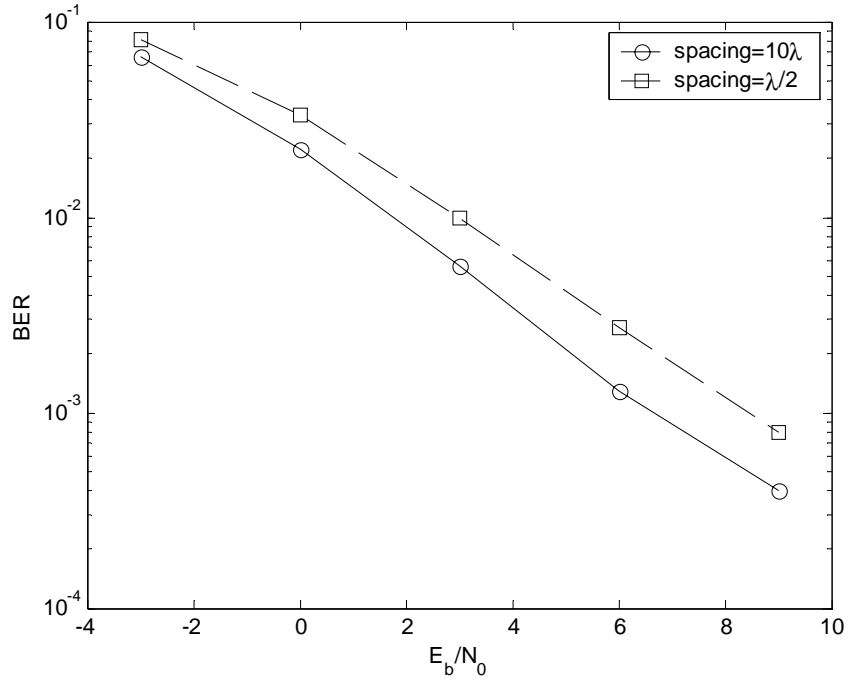


Figure 7.7: Spatial Aliasing vs. Diversity Gain. There are 5 interferers. The user distribution is non-uniform. The multipath environment is defined by the vehicular channel.

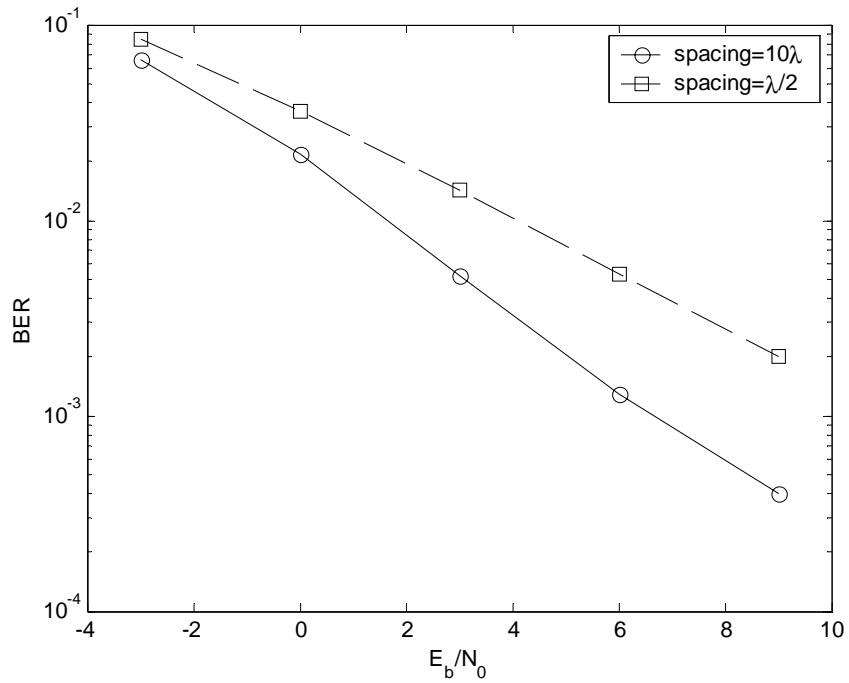


Figure 7.8: Spatial Aliasing vs. Diversity Gain. There are 10 interferers. The user distribution is uniform. The multipath environment is defined by the vehicular channel.

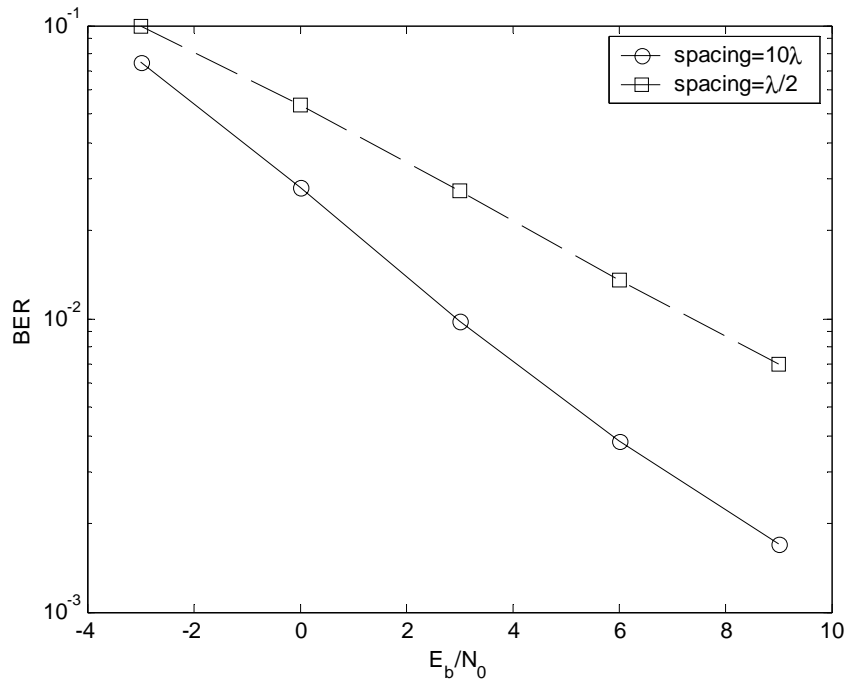


Figure 7.9: Spatial Aliasing vs. Diversity Gain. There are 10 interferers. The user distribution is non-uniform. The multipath environment is defined by the vehicular channel.

We can clearly observe the benefit of spatial diversity. The performance gain shown demonstrates that it is not essential to maintain Nyquist spacing among elements of an adaptive antenna array when the number of co-channel interferers exceeds the number of elements and the angle spread of the channel is very narrow. It is better to achieve diversity gain even at the cost of the spatial aliasing to cope with the overloading of the array.

Chapter 8

Beamforming for OFDM Systems

8.1 Introduction

Orthogonal Frequency Division Multiplexing (OFDM) [12] is a multi-carrier technique that has recently received considerable attention for high speed wireless communication. In this chapter we will develop a simple pilot symbol assisted frequency domain beamforming technique for the OFDM receiver. The weight vector estimated with the proposed scheme cancels strong interference and minimizes channel impairments. Interference rejection from beamforming can enable more than one pair of nodes of an *ad hoc* network to share the same channel. This can potentially increase the system throughput of the ad hoc networks which are mainly based on Collision Sense Multiple Access (CSMA) [204] techniques. The chapter begins with a brief description of the fundamental concept of an OFDM system. The beamforming scheme is explained next and we investigate different aspects of the beamforming technique in a simple AWGN environment. The concept of sub-band beamforming is demonstrated by employing two multipath channels with contrasting frequency response in the next section. The final section investigates the performance of the proposed beamforming scheme for vector channel based on actual measurement data. The applicability of computationally simple LMS algorithm instead of the RLS algorithm is also investigated in this section.

8.2 Fundamental concepts of OFDM

OFDM has been accepted as the standard for Digital Audio Broadcast (DAB) [205] and Digital Video Broadcast (DVB) [206] in Europe. It has also been established as one of the techniques for the IEEE 802.11a wireless LAN standard [207]. OFDM has emerged as one of the primary candidates for the Fourth Generation (4G) wireless communication systems and high speed ad hoc wireless networks. The basic principle of OFDM is to split the data into multiple parallel streams and employ orthogonal sub-carriers to each of these streams [12]. The sub-carriers are allowed to overlap but they are still *mathematically orthogonal* [4] to each other. This makes the OFDM spectrally efficient compared to a conventional multi-carrier system. Each OFDM symbol consists of a sum of sub-carriers that are modulated by PSK or QAM. The k^{th} sample of an OFDM symbol can be written as

$$x_k = \sum_{m=0}^{M-1} X_m e^{j\frac{2\pi km}{M}}, \quad 0 \leq k \leq M-1 \quad (8.1)$$

where M is the number of sub-carriers and X_m is the data symbol, PSK or QAM modulated, on the m^{th} sub-carrier.

Equation 8.1 is identical to the expression of an M point Inverse Discrete Fourier Transform (IDFT). Therefore the sub-carrier multiplexing can be efficiently performed with the help of Inverse Fast Fourier Transformation (IFFT) operation. This is one of the most attractive features of OFDM since the transmitter can multiplex data symbols onto sub-carriers by employing the computationally efficient IFFT operation. Therefore the frequency division multiplexing can be achieved by baseband processing rather than band-pass filtering. Figure 8.1 shows a simple OFDM transmitter. Obviously an OFDM receiver can perform the demodulation with a simple Fast Fourier Transform (FFT) operation. This eliminates the banks of sub-carrier oscillators and coherent demodulators required by conventional frequency division multiplexing systems [12].

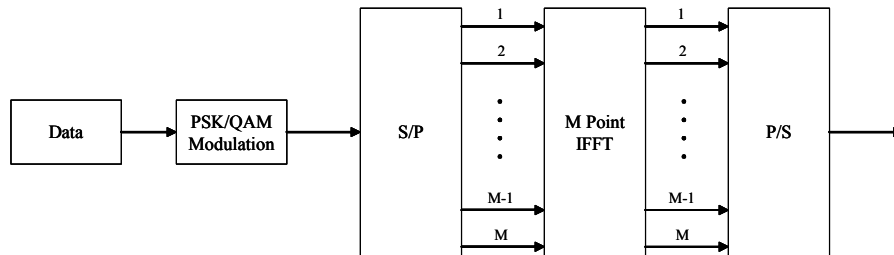


Figure 8.1: A Simple OFDM transmitter

8.3 Inter Symbol Interference in OFDM

The basic principle of OFDM involves splitting a high rate data stream into M streams of lower data rate streams that are transmitted simultaneously over the same number of sub-carriers. The lower data rate streams have M times the symbol duration compared to the original data stream. This reduces the ratio of the relative delay spread to the symbol duration by the same factor and diminishes the multipath dispersion in an OFDM system. The ISI can be completely eliminated by introducing a guard time, longer than the delay spread [12], for each OFDM symbol. The OFDM symbol is cyclically extended during the guard time in order to eliminate the Inter Carrier Interference (ICI). ICI

is the cross-talk between the sub-carriers which is detrimental to the orthogonality of between the sub-carriers. The cyclic extension is an overhead to the system and reduces the system throughput. For the simulations conducted, *we employed cyclic extensions to eliminate the loss of orthogonality between sub-carriers*. References [12] and [208] provide detailed discussion on the topic of ISI and ICI.

8.4 Spectrum Shaping of OFDM

There are several signal processing techniques that can be applied to make the out of band spectrum of an OFDM signal reduce rapidly. Windowing of individual symbols is one method that ensures that the amplitude goes smoothly to zero at the symbol boundaries [12]. This reduces the sidelobe levels and lends better spectral property to the OFDM signal. Raised Cosine window is one of the most commonly used windows. A Raised Cosine function is defined as

$$\begin{aligned} \omega(t) &= 0.5 + 0.5 \cos\left(\pi + \frac{\pi t}{\alpha T_s}\right) & 0 \leq t \leq \alpha T_s \\ &= 1 & \alpha T_s \leq t \leq T_s \\ &= 0.5 + 0.5 \cos\left(\frac{\pi(t - T_s)}{\alpha T_s}\right) & T_s \leq t \leq (1 + \alpha)T_s \end{aligned} \quad (8.2)$$

Here T_s is the symbol duration and α is the roll-off factor. Conventional filtering techniques can also be applied instead of time domain windowing in order to reduce out of band spectrum. However, from an implementation viewpoint windowing is an order of magnitude less complex than the filtering [12]. For the simulations conducted, we did not apply any spectrum shaping techniques since there were no adjacent channel users.

8.5 Frequency Domain Beamformer for OFDM receiver²

Multipath propagation causes data symbols on each sub-carrier to encounter different amplitude and phase responses. As a result, even when individual sub-carriers experience flat channel response, the channel can still be frequency-selective from the whole signal spectrum perspective. Consequently a conventional OFDM receiver requires one-tap equalizers for each sub-carrier to minimize the channel distortion. In this section, we propose a novel OFDM adaptive beamforming technique that eliminates the equalization at the output of the FFT operation [187]. This is achieved by grouping adjacent sub-carriers into sub-bands and employing separate weight vector for each of the sub-bands. The number

² The author would like to thank B. L. P. Cheung for his contributions

of sub-carriers in a sub-band depends on the coherence bandwidth [9], the bandwidth for which the signal retains strong correlation, of the channel.

Let us assume that each OFDM symbol is transmitted through a multipath channel with L resolvable multipaths and the receiver is equipped with a uniformly spaced linear array (ULA) consisting of N elements. Using the narrowband model assumption, the k^{th} sample at the n^{th} antenna element can be expressed as

$$r_{k,n} = \sum_{l=0}^{L-1} h_{k,l} x_k e^{-j \frac{2\pi}{\lambda_c} (n-1)d \sin \theta_{k,l}} + \eta_{k,n} \quad (8.3)$$

where d is the antenna spacing, λ_c is the wavelength of the carrier, $\theta_{k,l}$ is the angle of arrival (AOA) with respect to the array broadside for the l^{th} path of the channel impulse response at time k , $h_{k,l}$ is the complex random variable for the l^{th} path of the channel impulse response at time k , and $\eta_{k,n}$ is the additive white Gaussian noise (AWGN) at the n^{th} antenna element at time k . Let us for the time being assume that the AOA does not change with time so that it is a function of l only. If we let $\omega_n(\theta_l)$ be the phase shift of the received signal from the l^{th} path at the antenna element n with respect to the received signal at the reference antenna element, Equation 8.3 can be rewritten as

$$r_{k,n} = \sum_{l=0}^{L-1} h_{k,l} x_k e^{-j \omega_n(\theta_l)} + \eta_{k,n} \quad (8.4)$$

where

$$\omega_n(\theta_l) = \frac{2\pi}{\lambda_c} (n-1)d \sin \theta_l \quad (8.5)$$

We assume that the guard time is longer than the delay spread so that ISI can be completely eliminated. The demodulated symbol on the m^{th} sub-carrier at the output of FFT at the n^{th} antenna element can be written as [187]

$$\begin{aligned} Y_{m,n} &= \sum_{k=0}^{M-1} \sum_{l=0}^{L-1} X_k H_l(m-k) e^{-j \left(\frac{2\pi k l}{M} + \omega_n(\theta_l) \right)} + N_{m,n} \\ &= \left[\sum_{l=0}^{L-1} H_l(0) e^{-j \left\{ \frac{2\pi m l}{M} + \omega_n(\theta_l) \right\}} \right] X_m + \sum_{k \neq m} \sum_{l=0}^{L-1} X_k H_l(m-k) e^{-j \left\{ \frac{2\pi k l}{M} + \omega_n(\theta_l) \right\}} + N_{m,n} \\ \Rightarrow Y_{m,n} &= \alpha_{m,n} X_m + \beta_{m,n} + N_{m,n}, \quad 0 \leq m \leq M-1 \end{aligned} \quad (8.6)$$

where $N_{m,n}$ is the AWGN noise on the m^{th} sub-carrier at the n^{th} antenna element, $\alpha_{m,n}$ is the multiplicative distortion caused by the channel at the m^{th} sub-carrier at the n^{th} antenna element, $\beta_{m,n}$ is the ICI term, and $H_l(m-k)$ is the FFT of a time-variant multipath channel $h_{k,l}$, which is defined as

$$H_l(m-k) = \frac{1}{M} \sum_{n=0}^{M-1} h_{k,l} e^{-j \frac{2\pi n(m-k)}{M}} \quad (8.7)$$

If we assume that the multipath channel is time-invariant over one OFDM symbol duration, $H_l(m-k)$ in Equation 8.7 becomes zero and thus there is no ICI. In this case, Equation 8.6 contains only the multiplicative distortion whose effect can be visualized in a signal constellation diagram. Figure 8.2 shows a 16QAM signal constellation diagram at one of the antennas of the receiver for a 64-subcarrier OFDM system for a two-ray multipath channel. The delay spread of the channel is less than the guard time so that there is no ISI. We assume that the power of the second path is 6 dB lower than the first one and no noise is present at the receiver front end. The multiplicative distortion moves some of the signal points over the decision boundaries and results in significant degradation in the BER performance.

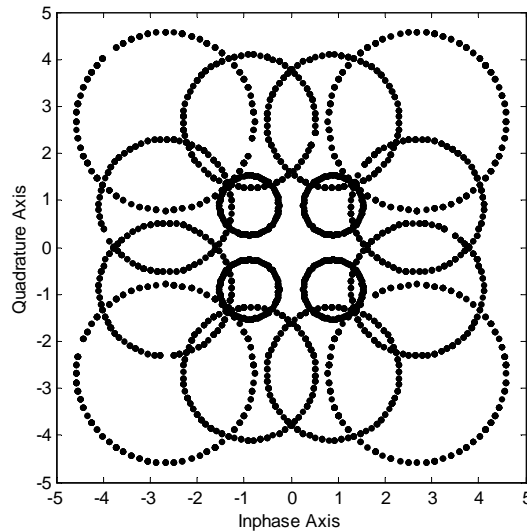


Figure 8.2: 16QAM signal constellation diagram for a 64-subcarrier OFDM system with a two-ray multipath channel, the second ray being 6 dB lower than the first one. No equalization is implemented

The multiplicative distortion $\alpha_{m,n}$ can be eliminated by using a one-tap equalizer [207] at the n^{th} sub-carrier. For the case in Figure 8.3, one-tap equalizers [207] based on the zero-forcing criterion are

implemented on individual sub-carriers at the output of the FFT. No distortion is observed in the signal constellation diagram since the multiplicative distortion is compensated by the one-tap equalizers. Therefore in a conventional OFDM receiver, channel equalization is usually employed at the FFT output to correct the amplitude and phase distortion caused by the multipath distortion.

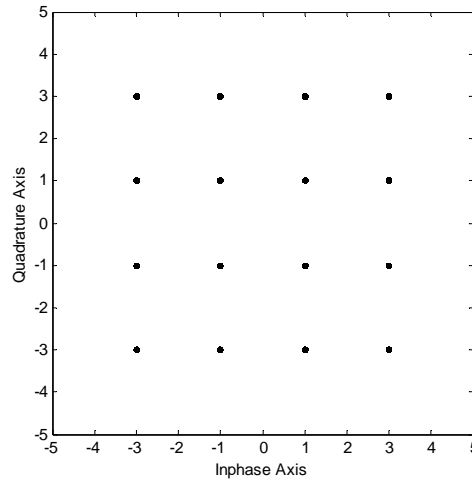


Figure 8.3: 16QAM signal constellation diagram for a 64-subcarrier OFDM system with a two-ray multipath channel, the second ray being 6 dB lower than the first one. One-tap equalization is implemented at the output of FFT for individual sub-carriers.

However, the multiplicative distortion $\alpha_{m,n}$ contains $\omega_n(\theta_l)$, which provides the AOA information for beamforming. *Thus equalization should not be performed at this stage if we want to retain the AOA information.* Instead, the multiplicative distortion is left with the demodulated symbol so that the beamformer can steer the beam towards the desired user. Employing the proper beamforming criterion, the beamformer will be able to minimize the effect of $\alpha_{m,n}$ when the adaptive algorithm converges. Therefore the weight vectors cancel interference and at the same time perform equalization. Since the multiplicative distortion may be fairly distinctive across the spectrum, a single beamformer with one set of weight vector will not be able to perform optimum combining for all sub-carriers. Therefore, symbols on individual sub-carriers should ideally be processed by their own beamformers. In this way, each beamformer has its own set of weight vector which combines the demodulated symbols on its corresponding sub-carrier in an optimal way. If $\alpha_{m,n} \approx \alpha_{m+1,n} \approx \dots \approx \alpha_{m+p-1,n}$, all p sub-carriers can be processed by the same beamformer and the computational load is reduced. We term this group of sub-carriers a sub-band. It is obvious that the

size of the sub-band, i.e. the value of p , depends on the coherence bandwidth of the channel. We have implicitly assumed that the spectral property of the interferer remains the same across the whole spectrum. If that is not the case, the size of the sub-band may be limited by the interfering signal. A beamforming scheme based on the concept of sub-band beamforming is shown in the next figure.

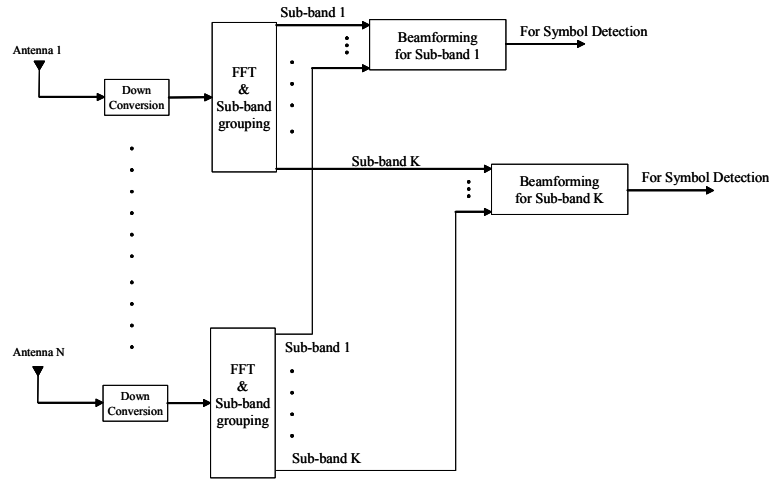


Figure 8.4: Proposed beamforming scheme

8.6 Simulation Study of the Proposed Beamforming Scheme

In this section we will show simulation results that illustrate the concept of sub-band beamforming and investigate different aspect of the technique.

8.6.1 Description of the OFDM System

The OFDM system has a data rate of 20 Mbps. We employ 16-QAM modulation scheme which means that the bandwidth of the OFDM signal is 5 MHz. The number of sub-carriers for each OFDM symbol is 512. The beamforming scheme requires pilot symbols as reference signal. While inserting pilot symbols into the data stream, one has to consider the coherence time [3] of the channel. We have to ensure that there are enough pilot symbols within the coherence time of the channel to estimate the required statistics. At the same time, since we are computing separate weight vector for each sub-band, there should be an adequate number of pilot symbols for each sub-band. However the pilot symbols are an overhead for the system and it should not reduce the throughput significantly. We define a transmitted frame which consists of 107 OFDM symbols. The first 12 symbols are known pilot symbols which are used to compute the initial weight vectors based on the Recursive Least

Square (RLS) [105] technique. There are 88 data symbols during which we switch to the decision-directed RLS algorithm to update the weight vector for tracking the time-variant channel. In order to facilitate the tracking and to keep the MSE at a low level, we insert 7 more pilot symbols at equal interval during the data portion of the frame. (We will ignore these pilot symbols while investigating the beamforming scheme in an AWGN environment.) Figure 8.5 illustrates the frame structure of the OFDM system.

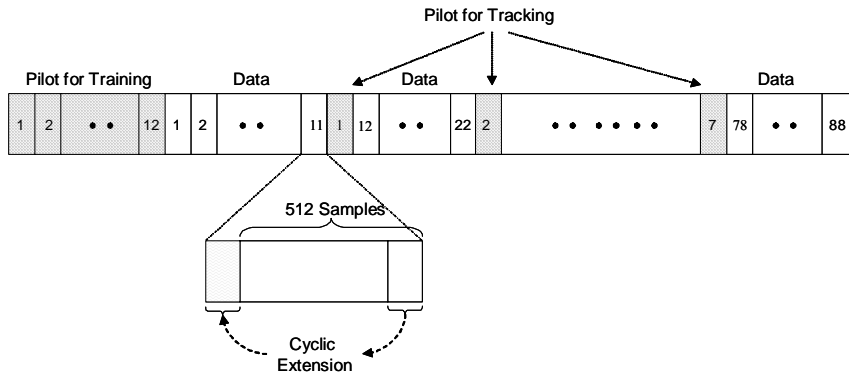


Figure 8.5: Frame structure of the OFDM system

8.6.2 Recursive Least Square Algorithm

We employ the Recursive Least Square (RLS) algorithm to ensure that the computed weight vector converges within the first 12 pilot symbols. In this section we will briefly describe the well known Recursive Least Square (RLS) algorithm to compute and update the weight vector. The weight vector is intended to minimize a cost function consisting of the sum of squares over a time window. The error signal is defined as [105]

$$e(i) = d(i) - \underline{w}^H \underline{x}(i), \tag{8.8}$$

where d is the reference signal, \underline{w} is the antenna weight vector, \underline{x} is the received signal vector at the antenna array, i is the sample index and H denotes Hermitian transpose. An exponential windowing is applied to define the cost function so that

$$J(k) = \sum_{i=1}^k \lambda^{k-i} |e(i)|^2 \tag{8.9}$$

Here $0 \leq \lambda \leq 1$ is a positive constant known as the forgetting factor. This determines how quickly the previous data samples are *de-emphasized*. In a stationary environment, all samples past and present

should have equal weight and λ is set to 1. In a time varying environment λ is close to but less than 1. Usually the faster the channel conditions change, the smaller the value of λ is. Note that the cost function is different from that of an MMSE case where the cost function is the ensemble average of the squared errors. The RLS algorithm can be obtained from minimizing Equation 8.9 by expanding the magnitude squared and by applying the matrix inversion lemma [105]. The RLS algorithm can be described by the following few steps [105]:

$$\begin{aligned}
 \underline{\kappa}(k) &= \frac{\underline{\underline{P}}(k)\underline{x}(k)}{\lambda + \underline{x}^H(k)\underline{\underline{P}}(k)\underline{x}(k)} \\
 e(k) &= d(k) - \underline{w}^H(k)\underline{x}(k) \\
 \underline{w}(k+1) &= \underline{w}(k) + e^*(k)\underline{\kappa}(k) \\
 \underline{\underline{P}}(k+1) &= \lambda^{-1}\underline{\underline{P}}(k) - \lambda^{-1}\underline{\kappa}(k)\underline{x}^H(k)\underline{\underline{P}}(k)
 \end{aligned} \tag{8.10}$$

The initial value for $\underline{\underline{P}}(k)$ is set as $\underline{\underline{P}}(0) = \Upsilon I_{N \times N}$, where Υ is a large positive constant and $I_{N \times N}$ is the $N \times N$ identity matrix with N being the number of antenna elements. The convergence of RLS algorithm is typically an order of magnitude faster than the LMS algorithm [105]. The RLS algorithm was chosen for this reason so that the beamforming scheme requires very few pilot symbols to converge. However the computational complexity of the RLS algorithm for each iteration is $O(4N^2 + 4N)$ which is much higher than that of the LMS.

8.6.3 Simulation in Simple AWGN Environment

Let us first employ the beamforming scheme in a very simple scenario where the only channel impairment is AWGN. The receiver is equipped with a four element ULA with half carrier wavelength of spacing between the elements. The elements are assumed to be omni-directional. The desired signal is corrupted by two interferers and thermal AWGN. The interfering signal is complex wideband white Gaussian noise. The interfering signals are uncorrelated from the desired signal and have similar wideband spectral property of the desired signal in the band of interest. So this can be regarded as a simplified model for representing the MAI. The desired user is transmitted from the spatial location of 0° with respect to the array broadside. Two interfering signals whose received powers are 6 dB higher than the desired signal originate at 60° and -60° . Note that this is significantly different from the simulation environment employed to evaluate the performance of the 2-D receivers. In such a scenario, there were more interferers than the number of antenna elements and after the processing gain, all the interfering signals were weaker than the desired signal. However in this case, the number of interfering signals is less than the number of antenna elements and our

objective is to cancel or null the interferers that are significantly stronger than the desired signal. Such interferers are common in a military environment and are often termed as jammers. We have mentioned in the introductory section that one of the targeted applications for this beamforming scheme could be to increase the system throughput of an ad hoc network by enabling more than one pair of nodes to share the same channel. In an ad hoc network there is no centralized power control. If the transmitting node of the latter pair is closer to the receiving node of the original pair, it can create near-far scenario. As a result the beamformer must be able to cancel a few interfering signals that are much stronger than the desired signal.

Since the channel is not time varying, we do not insert any pilot symbols in the middle of the OFDM frame. Obviously we still have the first 12 symbols as known pilot symbols to aid the convergence of the adaptive algorithm. In this simple environment, we would require only one set of weight vector to process all the sub-carriers i.e. the size of the sub-band is 512 sub-carriers. For the simulations conducted we used samples from a randomly chosen sub-carrier to compute the weight vector. The forgetting factor λ of the RLS algorithm is set at 1. Figure 8.6 shows the Mean Square Error (MSE) at the output of the beamformer for the 1st sub-carrier for two different input SNR levels. We can observe that the MSE converges within the first 12 pilot symbols. The steady state MSE for an SNR of 20 dB settles below 10^{-2} (-20 dB). Similarly, the steady state MSE for 10 dB input SNR is lower than 10^{-1} (-10dB). This is a clear indication that the interference has been cancelled successfully. We can also observe that the MSE is similar when each sub-carrier is processed by its own weight vector.

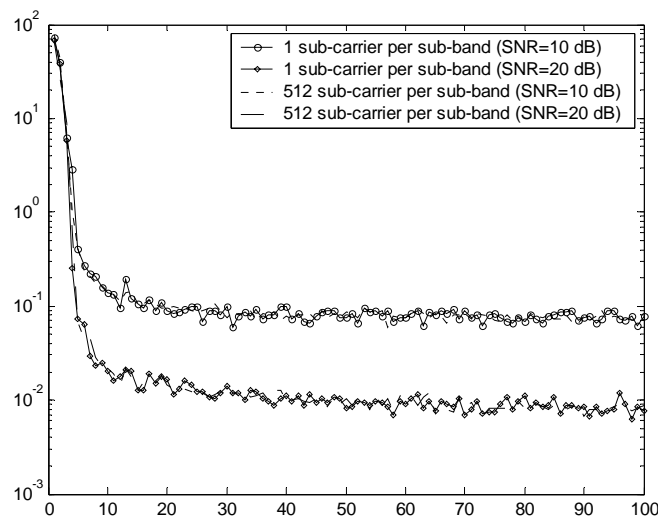


Figure 8.6: MSE in AWGN environment for sub-carrier no. 1

Table 8.1 shows the Signal to Interference Ratio (SIR) at the output of the beamformer and demonstrates that the interference has been cancelled effectively. Also the average and the minimum SIR are similar regardless of the number of weight vectors applied to combine the signal at different sub-carriers. This is consistent with the behavior of the MSE observed previously.

Table 8.1 Output SIR at AWGN environment

1 sub-carrier per sub-band				512 sub-carrier per sub-band			
Avg. SIR for SNR=10 dB	Min. SIR for SNR=10 dB	Avg. SIR for SNR=20 dB	Min. SIR for SNR=20 dB	Avg. SIR for SNR=10 dB	Min. SIR for SNR=10 dB	Avg. SIR for SNR=20 dB	Min. SIR for SNR=20 dB
52.5 dB	44.8 dB	59.8 dB	53.6 dB	51.5 dB	44.9 dB	58.7 dB	54.1 dB

The beam pattern can be an important tool to investigate the performance of the beamforming scheme in this simple scenario. Since there is no multipath and the objective is to cancel interference, we should be able to notice high gain at the direction of the desired user and deep nulls at the directions of the interfering signals. Figure 8.7 illustrate the beam pattern for three different sub-carriers when we compute separate weight vectors for different sub-carriers. The input SNR is 10 dB. All the beam patterns are very similar which is what we would expect in an AWGN environment. We can observe the nulls at -60° and 60° which are the locations of the interferers. Also the gain at the desired user's location (0°) is approximately equal to one. The beam pattern when only one weight is used is also plotted in Figure 8.7 and we can observe its similarity with the other three beam patterns.

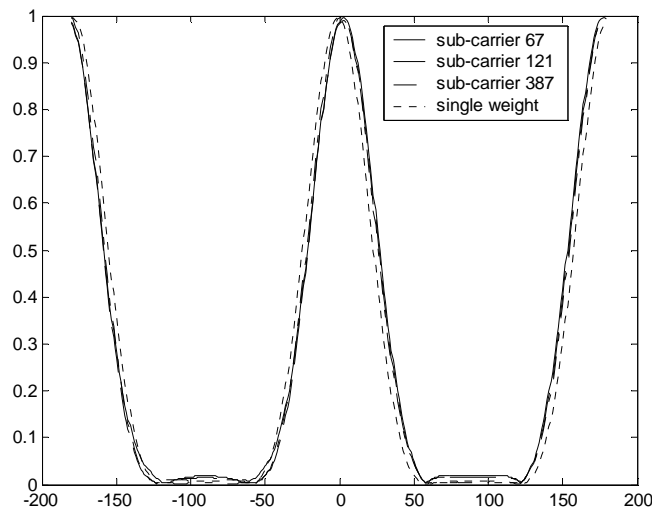


Figure 8.7: Beam pattern for various sub-carriers

Based on the discussions so far, we can infer that the BER does not depend on the number of weight vectors employed for this simple simulation scenario. This is evident from the BER plot shown in Figure 8.8.

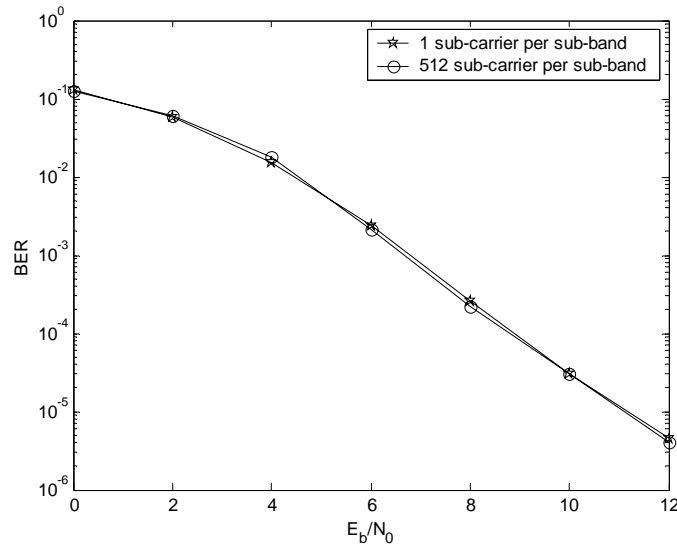


Figure 8.8: BER in AWGN environment

8.6.4 Simulation in Frequency Selective Multipath Channel

We apply our proposed beamforming scheme to two different multipath environments. The objective is to demonstrate that a number of sub-carriers, composing a sub-band, can be processed by a single set of weights and that the number of sub-carriers per sub-band can vary with the frequency selective nature of the channel. The desired user is once again at 0° with respect to the array broadside. There are two interferers located at 30° and -60° and are being received at 13 dB and 6 dB higher power level than the desired user respectively. The receiver is equipped with an 8 omni-element ULA.

The first channel employed is the COST-207 six-tap typical urban (TU) channel [209], which is defined by the power delay profile of Table 8.2. We assume that all six resolvable multipath components are within 30° with respect to the central arriving angle of the transmitted signal. The vector model based on Jakes' model described in Chapter 7 is employed to generate the complex amplitude of the resolvable multipath components for different antenna elements. The different parameters of Jakes' model for COST-207 model are defined in Table 8.3. This channel is extremely frequency selective as we can observe from Figure 8.9. The second channel employed is the IMT2000

indoor A channel [194] described by the power delay profile of Table 8.4. This channel has a fairly flat response (see Figure 8.10) with a much higher angle spread. We assume that the resolvable multipath components are within 60° with respect to the central arriving angle of the transmitted signal. The parameters of the vector channel model for the indoor channel are also shown in Table 8.3.

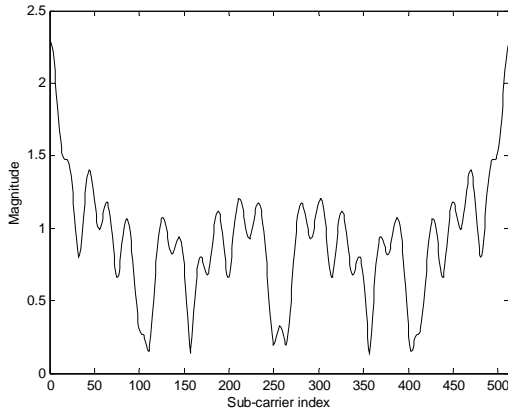


Figure 8.9: Magnitude response of the COST-207 TU channel model

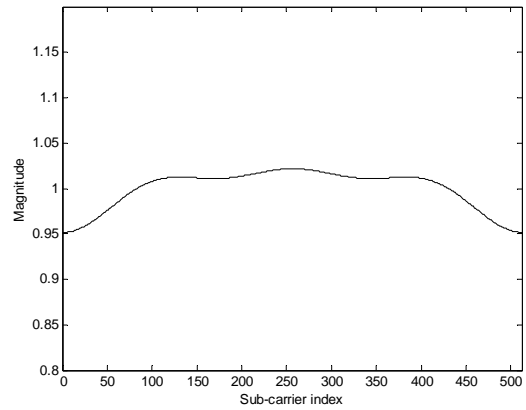


Figure 8.10: Magnitude response of the IMT2000 Indoor A channel model

Table 8.2: COST-207 TU channel

Tap number	1	2	3	4	5	6
Delay (μs)	0.0	0.2	0.5	1.6	2.3	5.0
Frac. power	0.19	0.38	0.24	0.09	0.06	0.04

Table 8.3: Parameters of vector channel model

Doppler spread, f_d	10 Hz
Number of local scatterers, M	20
Angle spread, Δ	10° (COST-207), 60° (IMT2000)
Angle of departure, Φ	$0^\circ \sim 360^\circ$
Random phase, ϕ	$0^\circ \sim 360^\circ$
Normalized distance of element from reference, d_n/λ	$0.5n$

Table 8.4: IMT2000 Indoor A channel

Relative Delay (ns)	Average Power (dB)
0	0
50	-3
110	-10
170	-18
290	-26
310	-32

Figure 8.11 show the BER performance of the sub-band beamforming scheme for the COS-207 TU channel condition. The baseline performance curve is generated for the case when there is a weight vector for each sub-carrier i.e. the size of the sub-band is only one sub-carrier. When the size of the sub-band is increased from one, the weight vector is computed for the first sub-carrier of the sub-band and that weight is employed to combine all the sub-carriers of that particular sub-band. We can observe that the performance of the beamforming scheme is similar when the size of the sub-band is either two sub-carriers or one sub-carrier. However when four sub-carriers are grouped together to form a sub-band the performance starts to deteriorate. Therefore for an extremely frequency selective channel like the COST-207 TU channel, the size of the sub-band is limited to only two sub-carriers. However by computing 256 weight vectors rather than 512 weight vectors, the computational load is reduced by a factor of two. This also means that the number of known QAM symbols can be halved in the OFDM pilot symbols and the system throughput can be increased by a reduction of the overhead.

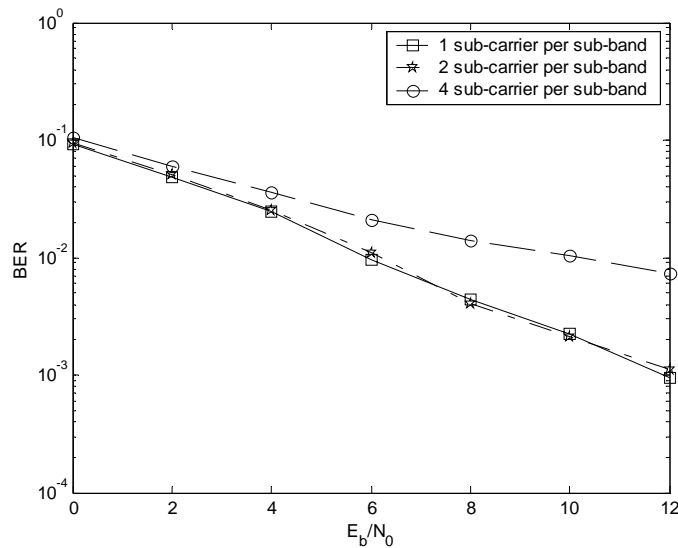


Figure 8.11: Performance of the sub-band beamforming scheme in COST-207 TU channel condition

Figure 8.12 shows the BER performance of the beamforming scheme for the IMT2000 indoor A channel condition. The baseline performance curve is once again generated for the case when the size of the sub-band is only one sub-carrier. The performance does not diminish significantly when 8 sub-carriers are grouped together to form a sub-band. The performance does not change even when the size of the sub-band is increased from 8 to 32 sub-carriers. However the performance deteriorates to

some extent as the size of the sub-bands become 64. We can see that the BER becomes unacceptable for sub-band size larger than 64. Based on these observations we can conclude that at least 32 sub-carriers can be grouped to form a sub-band and we would require only 16 weight vectors. In such a scenario only 32 out of the 512 QAM symbols in a OFDM pilot symbol needs to be known. The larger size of the sub-band for the IMT2000 is expected because the channel is fairly flat compared to the COST-207 TU channel. As a result the number of sub-carriers that experience similar channel response is much larger and consequently a single weight can serve a larger number of sub-carriers.

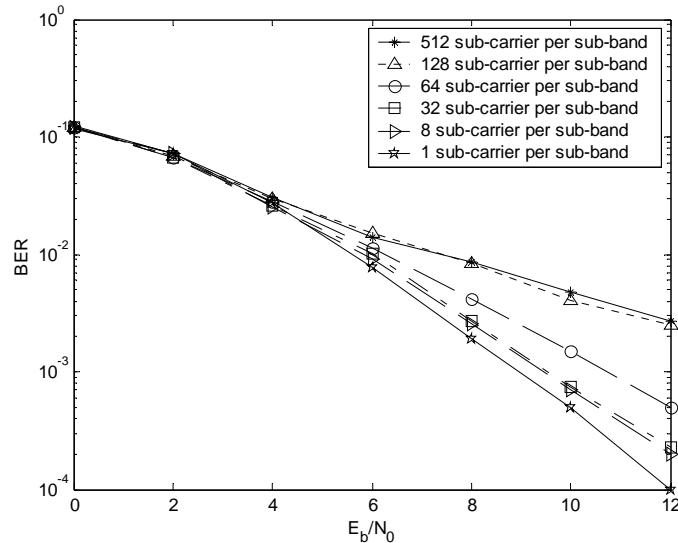


Figure 8.12: Performance of the sub-band beamforming scheme in IMT2000 Indoor A channel condition

The previous example of the beamforming in two channels with widely different coherence bandwidth demonstrates the concept of sub-band beamforming. We have established that the size of the sub-band varies according to the channel condition. Therefore it is necessary to determine the optimum size of the sub-band before the system can begin operation.

8.7 Performance in Vector Channel based on Measurement Data³

In this section we are going to employ the beamforming scheme in an environment where the propagation condition is described by vector channel based on actual measurement data. Measurements were performed using Virginia Tech's wideband, vector channel measurement system. The VIPER (vector impulse response) system [210] simultaneously measures channels between a transmitter antenna and up to four receiver antennas. The measurement system transmitter uses an

³ The author would like to thank Raqibul Mostafa, Bill Newhall and James Hicks for their contributions.

FPGA programmed to produce a 1023-chip length PN sequence clocked at 80 Mcps. The PN sequence bi-phase modulates the 2050 MHz carrier, and the resultant signal is amplified and transmitted using a single antenna. The receiver down converts signals with bandwidths up to 400 MHz and samples up to four channels at 1 Gsps. Snapshots of signals are stored in RAM and processed in software. Figure 8.13 [211] shows the block diagram of the VIPER measurement system.

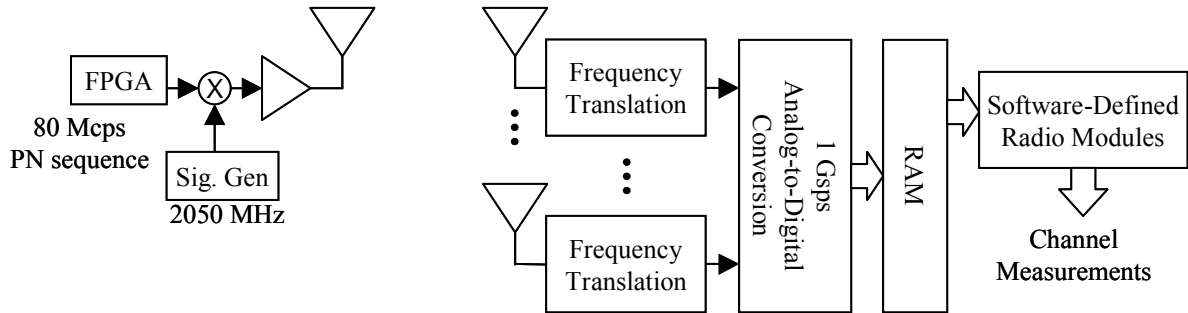


Figure 8.13: VIPER measurement system

Power-delay profiles are computed and used to approximate the channel impulse responses. A cross-correlation function is calculated between the received signal and the transmitted signal (known by the receiver) to produce the power-delay profile, resulting in knowledge of strength and delay characteristics of multipath components for each channel.

The wideband measurements were performed on the Virginia Tech campus in an area with dense buildings and other obstructions. Figure 8.14 shows a map of the plaza, which is bordered by four buildings of stone construction reaching heights of two stories or greater. The obstructions within the plaza consist of vestibules and skylights constructed of concrete, metal, and glass. Pedestrian traffic in the area was very low during measurements. Two one receiver location and two transmitter locations were used. The locations were chosen such that the line-of-sight path between the transmitter and receiver was blocked by multiple obstructions.

The receiver antenna was a four-element, linear array of vertical monopoles with quarter-wavelength spacing. The transmitter antenna was an end-fed dipole oriented vertically throughout the measurements. Transmitter-receiver separation was approximately 210 feet; for this distance, a transmit power of 1 dBm was used. The two transmitter positions are separated by approximately 30°.

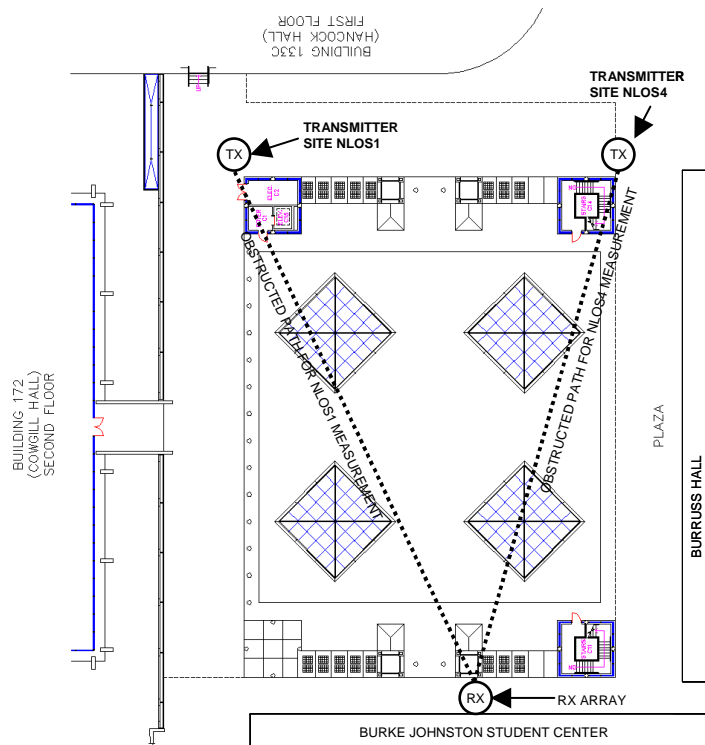


Figure 8.14: Layout of the VIPER outdoor measurement⁴

Measurements were performed with the receiver array was held stationary. While the receiver was logging signal data, the transmitter antenna was moved throughout an extent of approximately five wavelengths about the defined transmitter location. This movement enabled recording of small-scale fading of multipath at the receiver without including large scale effects. The collected snapshots when the transmitter was at position NLOS4 were used to represent the propagation channel for the desired user. The collected snapshots when the transmitter was at position NLOS1 were employed to describe the channel for the interfering source.

The channel frequency response for the desired user for two different snapshots is shown in Figure 8.15. We can observe the channel response is moderate. The channel has a wide angle spread resulting from the rich scattering environment and as a result we observe that there is large variation in the channel response across the antenna elements.

⁴ The author would like to thank Mike Hill for providing the layout of the plaza

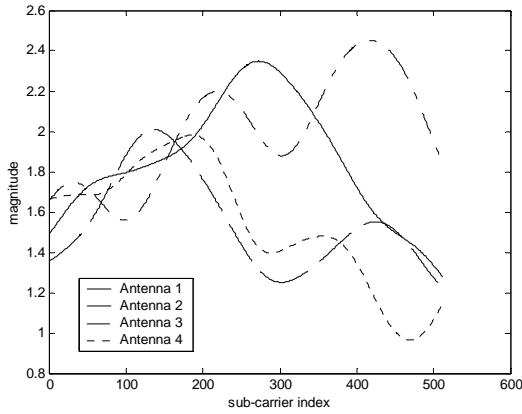


Figure 8.15a: Magnitude response of the vector channel of the desired user for snapshot 6

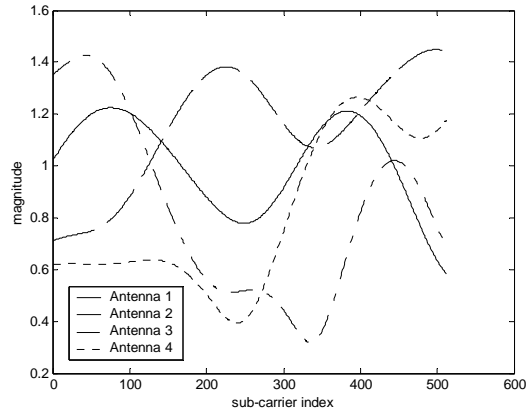


Figure 8.15b: Magnitude response of the vector channel of the desired user for snapshot 25

Let us present the performance of the proposed beamforming scheme in this channel environment. The desired user employs the OFDM system described in Section 8.5.1. The interfering signal is a complex wideband Gaussian random signal. The received power of the interfering signal is 6 dB higher than the desired signal. Figure 8.16 shows the performance of the beamforming scheme in terms of BER for different sizes of the sub-bands. We can observe that there is very little performance degradation as long as the size of the sub-band is kept to 8 sub-carriers. There is a large performance degradation when 16 sub-carriers are grouped together to form a sub-band and we can clearly observe an error floor. The performance deteriorates further for a sub-band size of 32 sub-carriers and the error floor is noticeable even at a very low SNR. Thus we can conclude that for this particular environment, the optimum size of a sub-band is 8 sub-carriers.

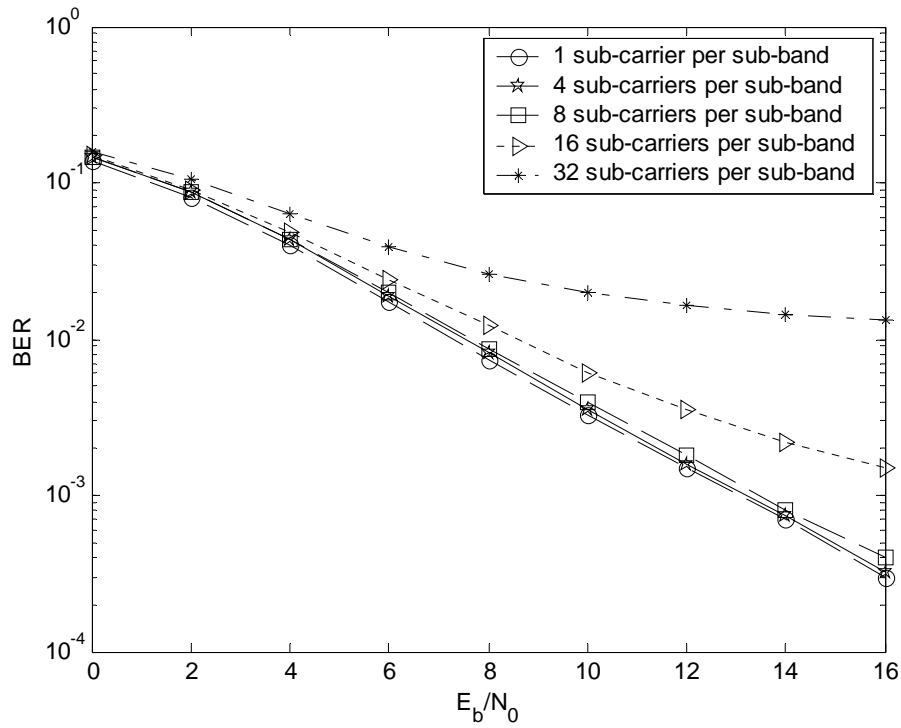


Figure 8.16: Performance of the beamforming scheme for various sub-band sizes in measured channel

The choice of RLS algorithm for computing the weight vectors and then for tracking in a decision directed mode is based on its good convergence property. However the RLS algorithm is fairly complex in terms of its computational complexity and the number of operations required is quadratic with the number of antenna elements (see Section 8.5.2). Therefore, once the initial weight vectors are computed, it may be possible to employ a computationally simple algorithm to update the weights. We investigated the applicability of the LMS [105] algorithm for tracking. The LMS requires a lot less operations compared to the RLS algorithm and the computational complexity is linear with the number of antenna elements (see Section 7.2.2). Figure 8.17 shows the performance of the beamforming scheme when the LMS algorithm is applied for tracking the channel and updating the weight vectors after the first 12 pilot symbols. The step size for the LMS algorithm is 0.001. The size of the sub-band is 8 sub-carriers. We observe that there is some performance degradation (about 2 dB at a BER of 10^{-3}) when we employ the LMS algorithm. However, the reduction in computational complexity may justify this slight performance degradation.

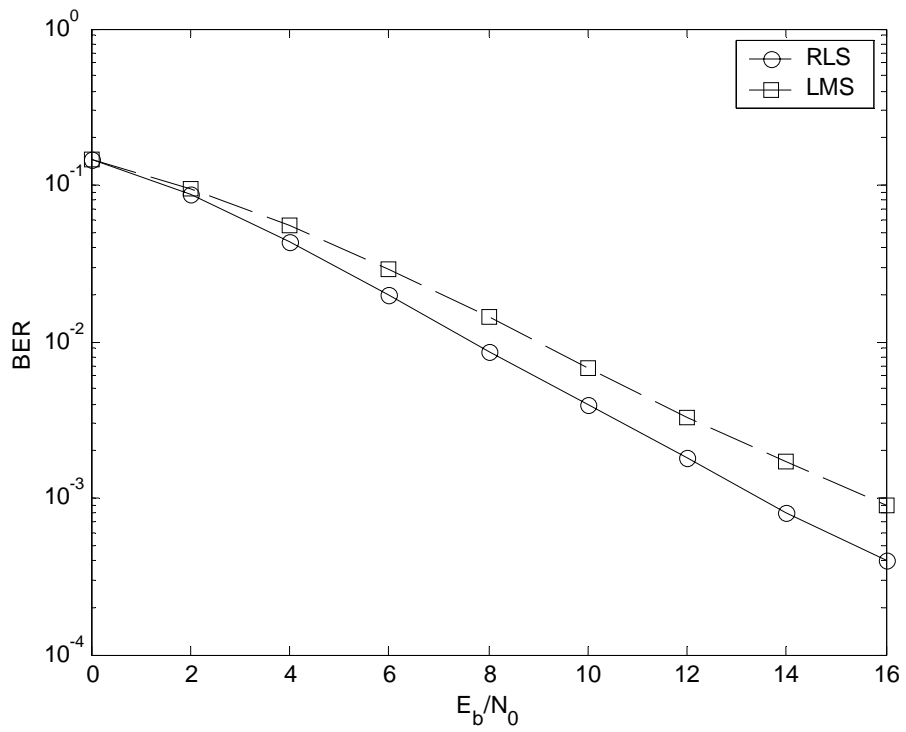


Figure 8.17: Comparison of performance for RLS and LMS

Chapter 9

Conclusions and Future Works

9.1 Conclusions

In this dissertation we have achieved the following

- We investigated different beamforming techniques that are applicable to the 3G CDMA systems and OFDM based wireless systems.
- We developed a Beamformer-Rake that utilizes the MSNR beamforming for spatial processing. This receiver is suitable for the WCDMA base station.
- We thoroughly investigated different algorithms for solving the Simple Eigenvalue problem required to perform MSNR based Eigen-Beamforming. We compared the different algorithms in terms of computational complexity. The performance of these algorithms when applied to a Beamformer-Rake was investigated for various conditions at the reverse link of a WCDMA system.
- We proposed several Beamformer-Rake receivers that employ the MSINR beamforming. These receivers are suitable for the WCDMA base station.
- We comprehensively described different algorithms to solve the Generalized Eigenvalue problem required to perform MSINR based beamforming.
- We proposed a completely new low-complexity algorithm to solve the Generalized Eigenvalue problem. We compared this method with existing ones in terms of computational complexity. The performance of this algorithm compared to other existing algorithms when applied to a Beamformer-Rake operating at the uplink of a WCDMA system was investigated for various operating conditions. We also compared the performance of different MSINR based Beamformer-Rake receivers.
- We compared the performance of the MSNR beamforming with that of MSINR beamforming in the context of Beamformer-Rake receivers.
- We proposed a Pilot Symbol Assisted DMI based Beamformer-Rake and compared its performance with that of a MSINR based Beamformer-Rake.
- We described two different structures of 2-D diversity combiners and showed their equivalence with the aid of analysis.

- We demonstrated the importance of spatial diversity gain in a CDMA based cellular environment.
- We proposed a new frequency domain beamforming scheme for the OFDM system and demonstrated the concept of sub-band beamforming for various propagation conditions.
- We investigated the performance of the proposed OFDM beamforming scheme in vector channel based on actual measurement data.

9.2 List of Publications

Here is a list of publications resulting from the work presented in this dissertation:

- **F. Alam**, D. Shim, and B. D. Woerner “Solution of the Simple Eigenvalue Problem for Beamforming in WCDMA System,” for submission to IEEE Transaction on Wireless Communications, October 2002.
- **F. Alam**, R. Mostafa, W. Newhall, B. L. P. Cheung, B. D. Woerner, and J. H. Reed, “Pilot Symbol Assisted Frequency Domain Beamforming for OFDM System,” for submission to IEEE Transaction on Wireless Communications, November 2002.
- **F. Alam**, D. Shim, and B. D. Woerner “Solution of the Generalized Eigenvalue Problem for Beamforming in WCDMA System,” for submission to IEEE Transaction on Vehicular Technology, November 2002.
- **F. Alam**, D. Shim, and B. D. Woerner, “A New Adaptive Algorithm for MSNR Beamforming in WCDMA System,” submitted to IEEE Vehicular Technology Conference 2003, Korea, April 2003.
- **F. Alam**, and B. D. Woerner, “Beamforming vs. Diversity Combining for Third Generation CDMA System,” submitted to the 5th International Conference on Computer and Information Technology, ICCIT 2002, Dhaka, Bangladesh, Dec. 2002.
- **F. Alam**, R. Mostafa, B. L. P. Cheung, B. D. Woerner and J. H. Reed, “Frequency Domain Beamforming for OFDM System in Practical Multipath Channel,” accepted for presentation in the 2nd International Conference on Electrical and Computer Engineering (ICECE), Dhaka, Bangladesh, Dec. 2002.
- B. L. P. Cheung, **F. Alam**, J. H. Reed, and B. D. Woerner, “New Adaptive Beamforming Algorithms for OFDM systems,” in the Proceedings of the 14th Annual International Conference on Wireless Communications, vol. 1, pp. 71-75, Calgary, Alberta, Canada, July 2002.

- **F.Alam**, D.Shim, and B.D. Woerner, “Comparison of Low Complexity Algorithms for MSNR Beamforming,” in the proceedings of IEEE Vehicular Technology Conference, vol. 4, pp. 1776-1780, Birmingham, Alabama, USA, May 2002.
- **F.Alam**, D.Shim, and B.D. Woerner, “A New Low-Complexity Beamformer-Rake Receiver for WCDMA,” in the proceedings of IEEE International Conference on Communications, ICC2002, vol. 1, pp. 160-164, New York, USA, April 2002.
- **F.Alam**, and B.D. Woerner, “Space Time Processing for Third Generation CDMA System,” in the proceedings of ICCIT 2001, pp. 202-206, Dhaka, Bangladesh, Dec. 2001.
- **F.Alam**, D.Shim, and B.D. Woerner, “The Performance of a Beamformer-Rake Receiver for WCDMA Mobile Communication System,” in the proceedings of IEEE Vehicular Technology Conference 2001, vol.1, pp. 521-525, New Jersey, USA, October 2001.
- **F.Alam**, K. A. Zahid, B.D. Woerner and J.H. Reed, “Performance Comparison between Pilot Symbol Assisted and Blind Beamformer-Rake Receivers at the Reverse Link of Third Generation CDMA System,” in the proceedings of IEEE Vehicular Technology Conference 2001, vol. 1, pp. 353-357, New Jersey, USA, October 2001.
- D.Shim, **F.Alam**, J. Kim, and B.D. Woerner, “Performance Analysis of a Smart Antenna System with Blind Algorithm, ” in the proceedings of the 11th Virginia Tech Symposium on Wireless Personal Communications, pp. 187-191, USA, June 2001,
- D. Shim, **F. Alam** and B. D. Woerner, “New Adaptive Downlink Beamforming Method for WCDMA system,” in the proceedings of IEEE Vehicular Technology Conference 2001, vol. 1, pp.157-161, Greece, May 2001.
- R. Mostafa, **F.Alam**, and K. K. Bae, “3G- around the world and back again,” cover story of *RF Design Magazine*, February, 2002.
- R. Mostafa, **F.Alam**, and K. K. Bae, “3G around the world,” cover article of the MPRG Propagator Newsletter, vol. 12, No. 1, November 2001.

9.3 Future Work

We have put forward suggestions for extending the current research work.

9.3.1 Further development of Efficient Algorithms for Eigen-Beamforming

In Chapter 5, the technique of Lagrange multiplier was employed to solve the SE. The Lagrange multiplier can be computed in a different manner and this will result in an alternative adaptive

algorithm. The technique employed in section 6.3.3 to linearize the AMI can be utilized to simplify this alternative Lagrange Multiplier method. We will derive this alternative adaptive algorithm and demonstrate its convergence and tracking. We will also show how a similar technique can be adopted to simplify the Power method for solving the SE. The technique described in section 6.3.3 has also been applied in [147] to develop an alternative algorithm to solve the Generalized Eigenvalue problem. We will provide a brief discussion on this algorithm which employs the Lagrange Multiplier technique. We leave the investigation of the performance of these algorithms in the context of spatial processing for Beamformer-Rake receivers for future researchers.

9.3.1.1 Alternate Linear Lagrange Multiplier Method

The weight vector that maximizes $\underline{w}^H \underline{R}_{ss} \underline{w}$ subject to the constraint $\underline{w}^H \underline{w} = 1$, is attained by maximizing the following functional (see Section 5.2.3 for details)

$$J(\underline{w}) = \underline{w}^H \underline{R}_{ss} \underline{w} + \gamma(1 - \underline{w}^H \underline{w}) \quad (9.1)$$

Therefore as shown in Section 5.2.3 the weight update equation becomes

$$\underline{w}(k+1) = \underline{w}(k) + \mu \left[\underline{R}_{ss}(k) - \gamma(k) \underline{I} \right] \underline{w}(k). \quad (9.2)$$

The local maximas of the functional $J(\underline{w})$ are attained when the Lagrange Multiplier constant γ in Equation 9.1 is equal to any of the eigenvalues of the SE and consequently \underline{w} is the corresponding eigenvector. This is quite straight forward to derive. The weight vector is intended to maximize the functional $J(\underline{w})$ and consequently $\frac{\partial}{\partial \underline{w}^H} [J(\underline{w})] = 0$. This will produce the SE with γ as the eigenvalue. If the initial guess is not an exact eigenvector and the step size μ is a positive real constant that is small enough to guarantee convergence, the iteration given by Equation 4 converges to the normalized principal eigenvector of the SE [145]. Since the Lagrange Multiplier constant $\gamma(k)$ is the largest eigenvalue, we can compute it by following the procedure described in Section 6.3.3 where we simplified the AMI. Therefore,

$$\begin{aligned} \lambda(k) &= \underline{w}^H(k) \underline{R}_{ss}(k) \underline{w}(k) \\ &= \underline{w}^H(k) \left[f \underline{R}_{ss}(k-1) + \underline{s}(k) \underline{s}^H(k) \right] \underline{w}(k) \\ &= f \underline{w}^H(k) \underline{R}_{ss}(k-1) \underline{w}(k) + \underline{w}^H(k) \underline{s}(k) \underline{s}^H(k) \underline{w}(k) \end{aligned}$$

$$\Rightarrow \lambda(k) \approx f \underline{w}^H(k-1) \underline{\underline{R}}_{ss}(k-1) \underline{w}(k-1) + \underline{w}^H(k) \underline{s}(k) \underline{s}^H(k) \underline{w}(k) \quad (9.3)$$

Now if we define $\alpha(k) = \underline{s}^H(k) \underline{w}(k)$, we can write

$$\lambda(k) = f \lambda(k-1) + |\alpha(k)|^2 \quad (9.4)$$

The weight update equation can be written as

$$\underline{w}(k+1) = \underline{w}(k) + \mu \underline{z}(k) \quad (9.5)$$

where,

$$\begin{aligned} \underline{z}(k) &= \left[\underline{\underline{R}}_{ss}(k) - \lambda(k) I \right] \underline{w}(k) \\ &= \left[f \underline{\underline{R}}_{ss}(k-1) + \underline{s}(k) \underline{s}^H(k) \right] \underline{w}(k) - \lambda(k) \underline{w}(k) \\ &= \underline{v}(k) - \lambda(k) \underline{w}(k) \end{aligned} \quad (9.6)$$

Now,

$$\begin{aligned} \underline{v}(k) &= \left[f \underline{\underline{R}}_{ss}(k-1) + \underline{s}(k) \underline{s}^H(k) \right] \underline{w}(k) \\ &\approx f \underline{\underline{R}}_{ss}(k-1) \underline{w}(k-1) + \alpha(k) \underline{s}(k) \\ &= f \underline{v}(k-1) + \alpha(k) \underline{s}(k) \end{aligned} \quad (9.7)$$

with the initial guess being

$$\underline{v}(0) = \alpha(0) \underline{s}(0) \quad (9.8)$$

The flowchart of this algorithm is shown in Figure 9.1. The computational complexity of the alternative simple Lagrange Multiplier algorithm is $O(4.5N)$.

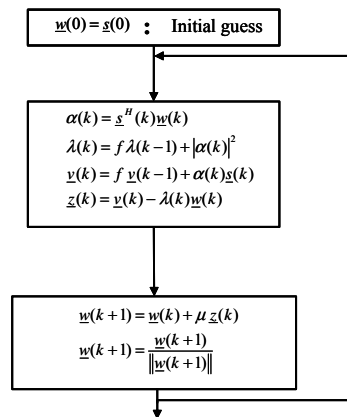


Figure 9.1: Flowchart of the alternate linear Lagrange multiplier algorithm

Let us present some simple simulation results that illustrate two important properties of this low complexity adaptive algorithm namely the convergence and tracking performance. Figure 9.2 compares the MSE of the alternative Lagrange Multiplier algorithm with the simplified Lagrange multiplier method described in Section 5.3.3. Both the algorithms are employed in their reduced complexity linear form. A receiver equipped with a 4 element ULA demodulates Quaternary Phase Shift Keying (QPSK) symbols for a signal to white noise ratio of 10 dB. The white noise accounts for the thermal noise and despread interference. This is a simplified representation of the scenario at the output of a CDMA despreader. We do not consider any multipath fading or Doppler spread. The antenna elements are omni-directional and the spacing between the elements is half the carrier wavelength. Both the algorithms employ the first sample of the received signal vector as the initial condition. We can clearly observe that the MSE of the alternative algorithm converges to its steady state value within the first 50 samples whereas the same for the original Lagrange multiplier algorithm takes more than 1000 samples to converge. This fast convergence property is one of the attractive features of the alternative Lagrange Multiplier method. We can expect this method to exhibit BER performance that is similar to the original Lagrange Multiplier method given the same steady state MSE. It may be worthwhile to compare this algorithm with the other adaptive algorithms investigated in Chapter 5.

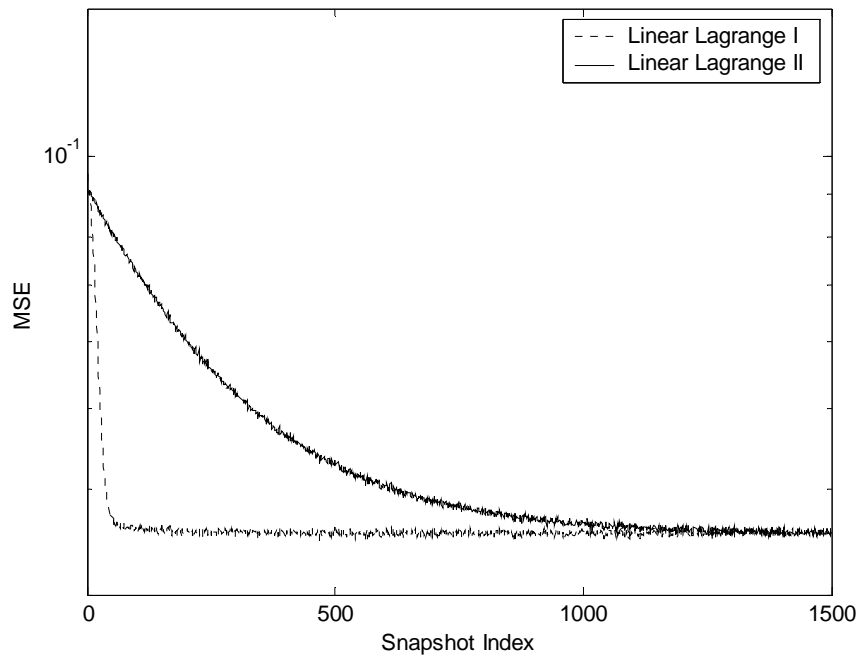


Figure 9.2: MSE for the linear Lagrange multiplier methods. Linear Lagrange I is the simplified alternative algorithm and Linear Lagrange II is simplified original algorithm. The SNR = 10 dB, $\mu = 0.001$

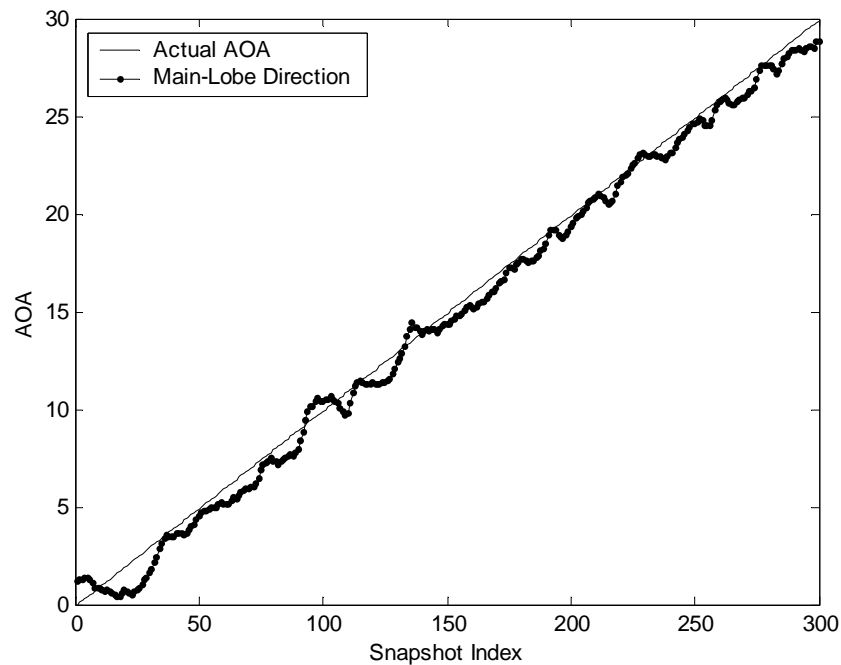


Figure 9.3: Tracking property of the proposed linear adaptive algorithm. The AOA changes by 0.1° at each snapshot. SNR = 0 dB, SIR = 6.99 dB, $f = 0.75$, $\mu = 0.03$

The AOA of the received signal and consequently the eigenvector of the covariance matrix changes with the movement of the mobile station. The adaptive algorithm must be able to track this change and steer the beam accordingly. We investigated the tracking property of the alternative linear Lagrange multiplier based algorithm in a scenario where a receiver equipped with an 8 element ULA is getting QPSK symbols from a mobile source. The spacing between the omni-directional antenna elements is half the carrier wavelength. The signal to white noise ratio is 0 dB. There are 20 interferers randomly distributed within $[-90^\circ, 90^\circ]$. The interfering signals are complex wideband Gaussian noise and the received power of each of them is 20 dB down (accounts for CDMA processing gain) than that of the desired signal. Consequently we have a Signal to Interference Ratio (SIR) of 6.99 dB. Once again we are modeling the output of a CDMA despreader and this is similar to the scenario applied in [142] to investigate the tracking performance of the MCGM. The AOA of the desired signal is incremented by 0.1° at each snapshot. As before we have not considered any multipath fading or Doppler spread. Figure 9.3 compares the main lobe direction of the ULA with the actual AOA for a typical simulation run. We can observe that the adaptive algorithm can track the change in AOA very accurately even for this low SINR of -0.79 dB. The mean difference of the estimated and actual AOA for 10,000 trials is 0.745° which is insignificant compared to the 3 dB

beamwidth [2] of the ULA. Note that in a practical environment the array has to track the composite channel vector (see Appendix B) and this can be a topic of future direction of research.

9.3.1.2 Linear Power Method

The Power method for solving the SE can also be linearized to reduce its computational complexity. Let us rewrite the power iteration again

$$\underline{q}(k+1) = \underline{\underline{R}}_{ss}(k) \underline{w}(k) \quad (9.9)$$

Now, as stated previously, in a time varying environment the covariance matrix can be estimated as

$$\underline{\underline{R}}_{ss}(k) = f \underline{\underline{R}}_{ss}(k-1) + \underline{s}(k) \underline{s}^H(k) \quad (9.10)$$

So Equation 9.9 can be written as,

$$\begin{aligned} \underline{q}(k+1) &= \left[f \underline{\underline{R}}_{ss}(k-1) + \underline{s}(k) \underline{s}^H(k) \right] \underline{w}(k) \\ &= f \underline{\underline{R}}_{ss}(k-1) \underline{w}(k) + \underline{s}(k) \underline{s}^H(k) \underline{w}(k) \\ &\approx f \underline{\underline{R}}_{ss}(k-1) \underline{w}(k-1) + \alpha(k) \underline{s}(k) \end{aligned} \quad (9.11)$$

Here,

$$\alpha(k) = \underline{s}^H(k) \underline{w}(k). \quad (9.12)$$

So the weight update equation for power iteration becomes

$$\begin{aligned} \underline{q}(k+1) &= f \underline{w}(k) + \alpha(k) \underline{s}(k) \\ \underline{w}(k+1) &= \frac{\underline{q}(k+1)}{\|\underline{q}(k+1)\|} \end{aligned} \quad (9.13)$$

The flowchart of this technique is illustrated in Figure 9.4. We can observe that the computational complexity is $O(3.5N)$ which is linear with the number of antenna elements. Also the computational complexity is less than any other method described so far. A similar procedure for linearizing the Power method has been suggested in [146]. A direction of extending our research might be to compare the linear power method with the other adaptive algorithms investigated in this dissertation.

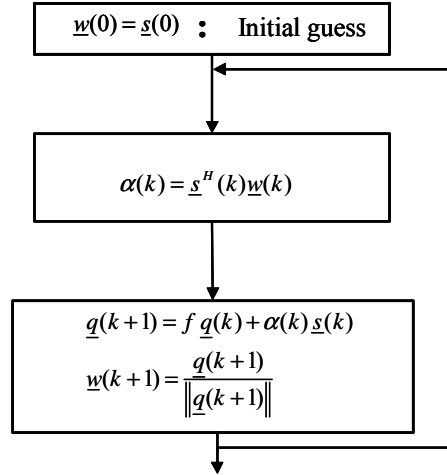


Figure 9.4: Flowchart of linear power method

9.3.1.3 Alternate Linear Generalized Lagrange Multiplier Method

The techniques described in the previous sections and section 6.3.3 have been adopted in [147] to develop a generalized Lagrange multiplier method whose computational complexity is linear with the number of antenna elements. As described in section 6.3.2 the weight vector \underline{w} that maximizes

$\underline{w}^H \underline{R}_{ss} \underline{w}$ subject to the constraint $\underline{w}^H \underline{R}_{uu} \underline{w} = 1$ is given by,

$$\underline{w}(k+1) = \underline{w}(k) + \mu \left[\underline{R}_{ss}(k) \underline{w} - \gamma(k) \underline{R}_{uu}(k) \underline{w}(k) \right] \quad (9.14)$$

Here,

$$\begin{aligned} \underline{R}_{ss}(k) &= f \underline{R}_{ss}(k-1) + \underline{s}(k) \underline{s}^H(k) \\ \underline{R}_{uu}(k) &= f \underline{R}_{uu}(k-1) + \underline{u}(k) \underline{u}^H(k) \end{aligned} \quad (9.15)$$

Following the discussions of Section 9.3.1.1, $\gamma(k)$ is the largest eigenvalue $\lambda(k)$. We have demonstrated in section 6.3.3 that the eigenvalue can be estimated as

$$\begin{aligned} \lambda(k) &= \frac{\lambda_{num}(k)}{\lambda_{den}(k)} \\ \lambda_{num}(k) &= f \lambda_{num}(k-1) + |\alpha(k)|^2 \\ \lambda_{den}(k) &= f \lambda_{den}(k-1) + |\beta(k)|^2 \\ \alpha(k) &= \underline{s}^H(k) \underline{w}(k) \\ \beta(k) &= \underline{u}^H(k) \underline{w}(k) \end{aligned} \quad (9.16)$$

Following similar procedure, the weight update equation can be simplified to the following few steps [147]

$$\underline{w}(k+1) = \underline{w}(k) + \mu \underline{z}(k) \quad (9.17)$$

Here

$$\begin{aligned} \underline{z}(k) &= \underline{v}(k) - \lambda(k)\underline{y}(k) \\ \underline{v}(k) &= f \underline{v}(k-1) + \alpha(k)\underline{g}(k) \\ \underline{y}(k) &= f \underline{y}(k-1) + \beta(k)\underline{u}(k) \end{aligned} \quad (9.18)$$

As we can observe, this algorithm is very similar to the linear AMI. Apart from Equations 9.17 and 9.18, all the equations are exactly the same as the linear AMI. In a very simple simulation scenario, this alternate linear Lagrange multiplier method was shown to have moderate gain over linear AMI method [147].

The flowchart for the alternate linear Generalized Lagrange multiplier method is shown in Figure 9.4. As we can observe, the computational complexity is $O(7N)$, which is a little less than that of the linear AMI. We leave the performance investigation of this alternative linear Lagrange Multiplier algorithm to future researchers. It will be interesting to compare this algorithm with the other adaptive algorithms investigated in this dissertation in the context of a MSINR based Beamformer-Rake receiver.

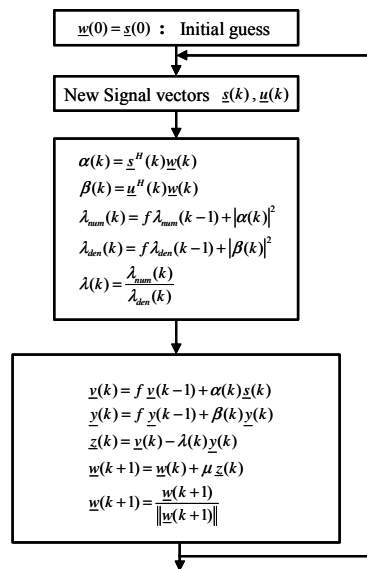


Figure 9.5: Flowchart of the alternate linear generalized Lagrange multiplier method

9.3.2 Study the Effect of Quantization on Adaptive Algorithms

Floating point based arithmetic is applied in the DSPs or FPGAs during practical implementation of a digital communication system. Consequently it may be worthwhile to investigate the effect of quantization on the numerical stability of the algorithms for solving the Eigenvalue problem.

9.3.3 Investigation of the Applicability of Beamformer-Rake Structure at the Handset

An interesting way to extend the current research would be to investigate the possibility of employing the Beamformer-Rake structure at the mobile handset. The interference in the downlink is considerably different in nature than that of the uplink. The major source of interference would be inter-cell interference originating from a few distinct base stations. Therefore the MSINR based beamforming criterion could be a promising candidate. At the same time the lower number of antenna elements and smaller inter element spacing present significant challenge in attaining performance improvements.

9.3.4 Extension of the Beamforming Scheme for OFDM System

The adaptive beamforming scheme developed in this dissertation cancels strong interference and at the same time mitigates channel impairment. A suboptimal alternative would be to compute a single weight vector from the samples of a particular sub-carrier and apply that weight to all the sub-carriers. A channel estimation scheme can be employed at this point to estimate the modified channel at the individual sub-carriers and those estimates can be utilized to mitigate the channel. A future direction of research would be to

- Ascertain the performance penalty associated with the suboptimal scheme.
- Investigate the savings, if any, in terms of computational complexity.

Appendix A

Beamforming in Multipath Environment

In a flat fading channel, the received signal arrives from a number of paths for which the delay is within the symbol duration (or the chip duration for a spread spectrum system). Each of these unresolved components has its own AOA and therefore the composite signal can no longer be associated with a single AOA. Beamforming is still feasible in this environment as long as the number of independent interfering signal is less than the number of array elements.

Let us consider a scenario where the transmitted signals from a source traverse through different paths and arrive at the array with different AOAs. The received signal can be written as

$$\underline{r}(t) = \sum_{k=0}^{K-1} \alpha_k(t) s(t - \tau_k) \underline{a}(\theta_k). \quad (\text{A.1})$$

Here, $\alpha_k(t)$, τ_k and θ_k are the complex gain, relative delay and the AOA of the of the k^{th} path respectively and $\underline{a}(\theta_k)$ is the array response vector for an AOA of θ_k . Now if the maximum relative delay is less than the symbol duration (or chip duration for a spread spectrum signal) so that $s(t - \tau_k) \approx s(t)$, we can write the received signal as

$$\begin{aligned} \underline{r}(t) &= s(t) \sum_{k=0}^{K-1} \alpha_k(t) \underline{a}(\theta_k) \\ &= s(t) \underline{\psi} \end{aligned} \quad (\text{A.2})$$

where $\underline{\psi} = \sum_{k=0}^{K-1} \alpha_k(t) \underline{a}(\theta_k)$ is the channel vector which consists of K unresolved components. It is obvious that the received signal covariance matrix is a *rank 1* matrix which is similar to the case when the signal traverses through a single path. However we can no longer assign a single AOA to the channel vector.

If we have thermal noise and interference present the received signal can be expressed as

$$\underline{r}(t) = \underbrace{s_d(t) \underline{\psi}_d}_{\text{Desired User}} + \underbrace{\sum_{m=1}^M s_m(t) \underline{\psi}_m}_{\text{Interference}} + \underbrace{\underline{n}(t)}_{\text{Thermal Noise}} \quad (\text{A.3})$$

Appendix A Beamforming in Multipath Environment

Each of the interfering signals merits a single degree of freedom. Therefore as long as $M \leq N - 1$, where N is the number of antenna elements, we will be able to perform beamforming and null-steering. Let us revisit the simple null-steering scheme of section 2.3.1. For the sake of simplicity, let us assume that $M = N - 1$. The weight vector for the null-steering scheme is given by the following set of equations:

$$\begin{aligned} \underline{w}^H \underline{\psi}_d &= 1 \\ \underline{w}^H \underline{\psi}_m &= 0; \quad m = 1, 2, \dots, N - 1 \end{aligned} \tag{A.4}$$

We can solve for the weight vector so that

$$\underline{w} = \left(\underline{\Psi}^H \right)^{-1} \begin{bmatrix} 1 \\ 0 \\ \vdots \\ 0 \end{bmatrix} \tag{A.5}$$

where $\underline{\Psi} = [\underline{\psi}_d \quad \underline{\psi}_1 \quad \underline{\psi}_2 \quad \dots \quad \underline{\psi}_{N-1}]$.

Let us consider a simple simulation scenario where the spatial location of the desired user is at 22.5° with respect to the array broadside. There are 3 interferers at 67.5° , -22.5° and -67.5° with respect to the array broadside. The desired user transmits QPSK symbols and the interfering signals are wideband zero mean complex Gaussian random processes. All the interfering signals are being received at a 10 dB higher power than the desired users signal. The transmitted signal from a source (desired user or interferer) travels via 4 equal strength paths of same delay. Let us further assume that the paths are time invariant and their AOAs within $\pm 15^\circ$ of the spatial location of the corresponding transmitter. The receiver is equipped with a 4-element ULA with half wavelength spacing between the elements and employs the simple null-steering scheme described by Equation A.5.

The following Figure show beam patterns for different simulation runs. The E_b/N_0 at each branch is 10 dB for all the runs. We have also marked the AOA of each path. Even though the beamformer produces null for the channel vector of an interferer so that $\underline{w}^H \underline{\psi}_m = 0$ for $m = 1, 2, \dots, N - 1$, the beam pattern does not necessarily show nulls at the individual AOAs of a channel vector of a particular interferer. In fact in some of the beam patterns we can observe gains comparable to the AOAs of the channel vector of the desired signal. This clearly demonstrates that one should not place too much importance on the beam pattern in a multipath scenario.

Appendix A Beamforming in Multipath Environment

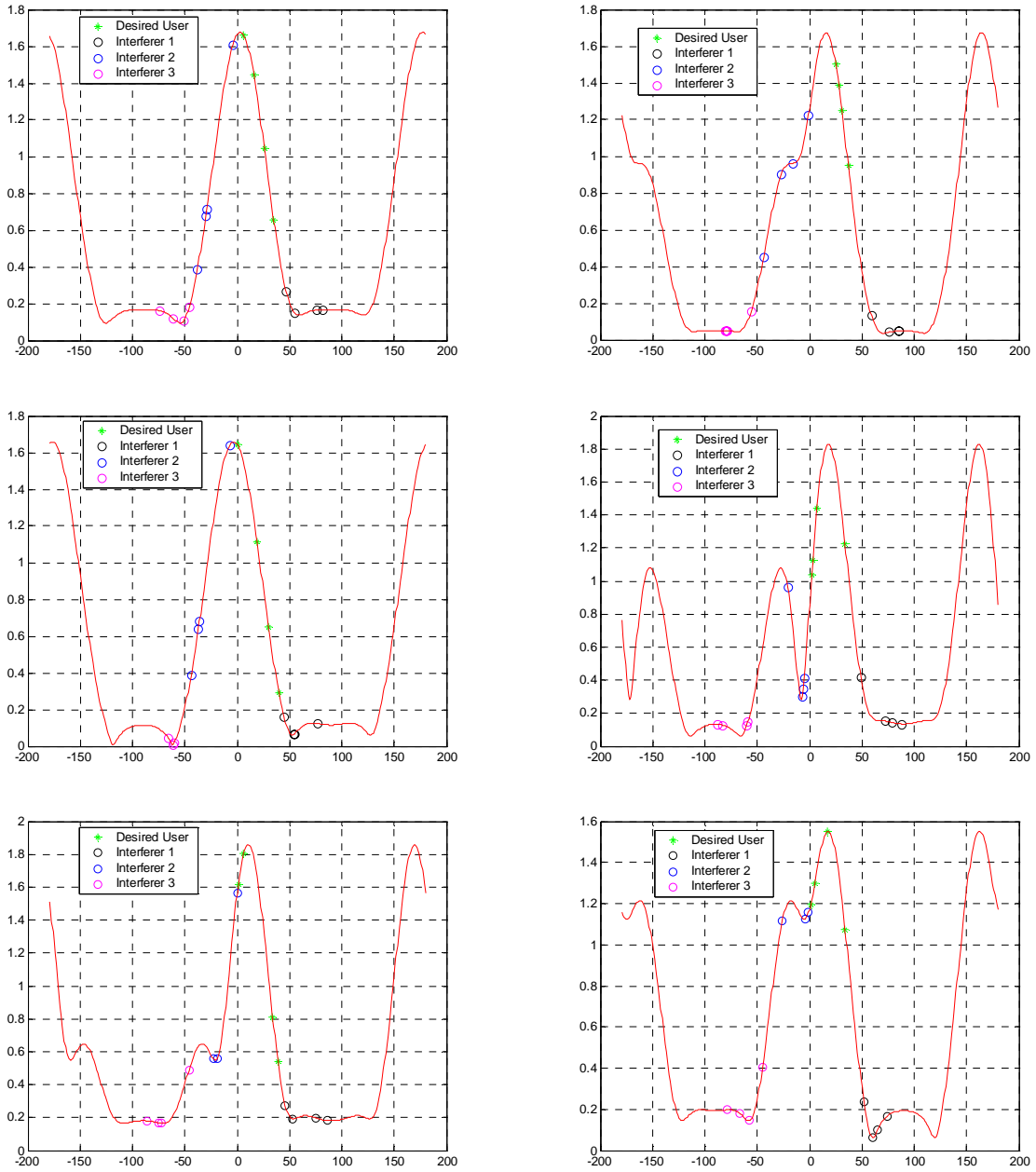


Figure A.1: Sample Beam patterns for the simple null-steering scheme

We can also make similar observations from the beam patterns of the MSINR scheme. Here there are two interferers. The position of the desired user and the interferers are at 0° , 60° and -60° respectively. The rest of the simulation parameters are the same as the null-steering scheme. For all the cases shown the SINR at the output of the beamformer is between 14.5 to 15.5 dB but we can observe that

Appendix A Beamforming in Multipath Environment

the beam patterns are fairly dissimilar. More importantly the gain at the individual AOAs of the desired users channel vector is sometimes much lower than that at the individual AOAs of the interferers.

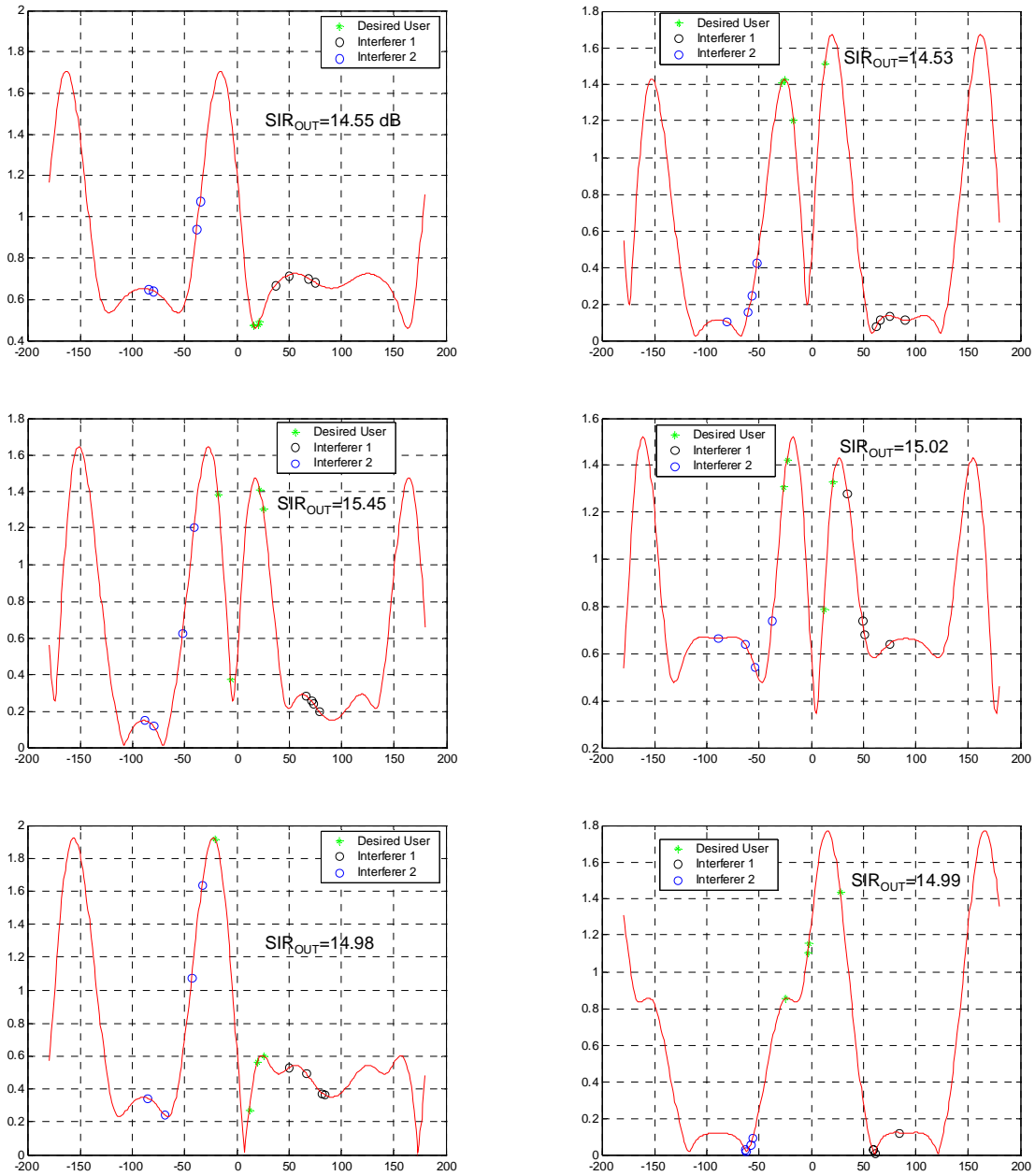


Figure A.2: Sample beam patterns for the MSINR scheme

Appendix B

Alternate Beamformer-Rake for WCDMA Uplink

In Chapters 5 and 6 we developed Beamformer-Rake receivers for the WCDMA uplink. All those receivers compute separate weight vectors for the data and control channels. However for practical implementation it may be more appealing to employ the control channel only to compute a single set of weight vector for both the data and the control channels. In this appendix we provide the block diagram for three Beamformer-Rake receivers that employ Eigen-Beamforming techniques. All these receivers are suitable for the WCDMA uplink. They employ the DPCCH only to compute the weight vectors. The same weight vectors are applied to combine the signals from both DPDCH and DPCCH. Note that the pilot symbols ensure that there is no phase ambiguity resulting from the Eigen-Beamforming (see Section 3.2.3 for details).

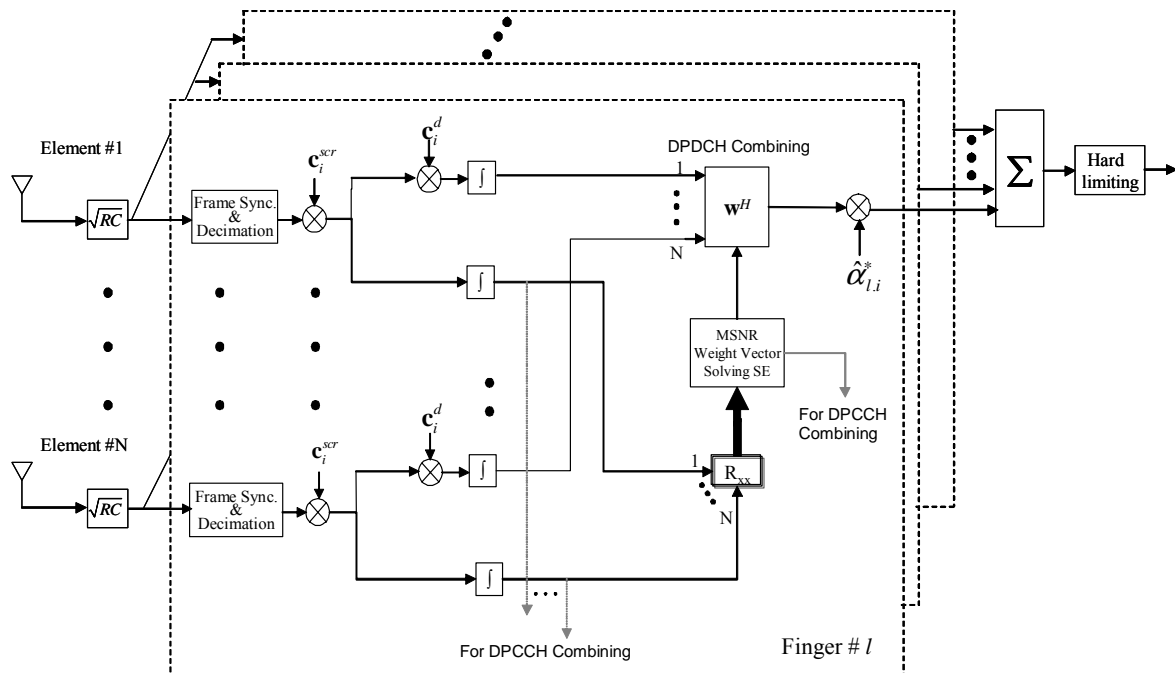


Figure B.1: MSNR based Beamformer-Rake receiver for WCDMA uplink. The weight vector is computed based on DPCCH only.

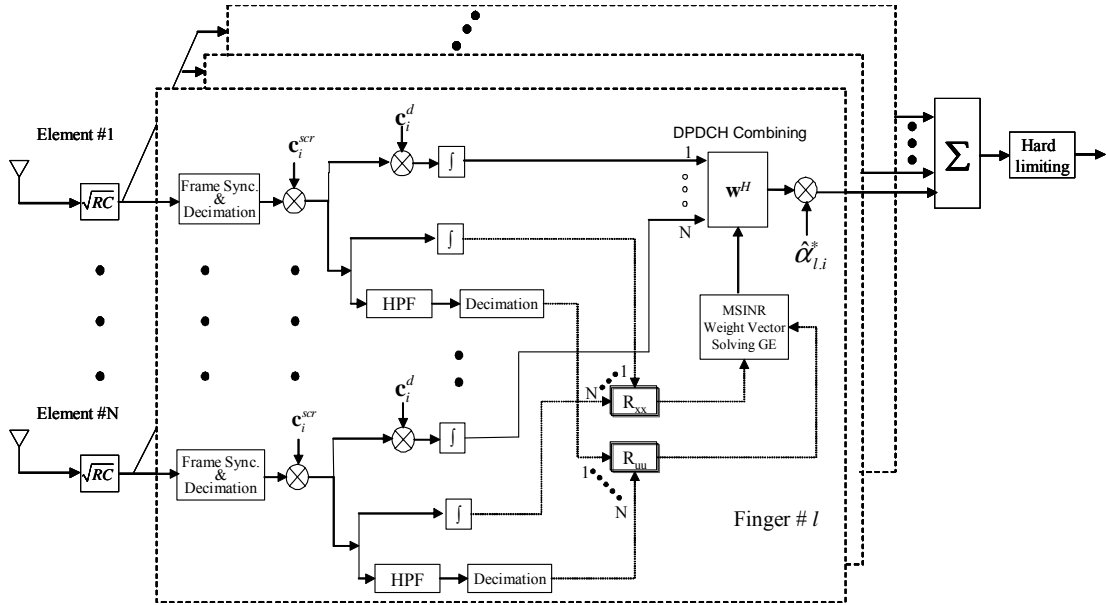


Figure B.2: MSINR based Beamformer-Rake receiver for WCDMA uplink. CGA is utilized for MSINR beamforming. The weight vector is computed based on DPCCH only.

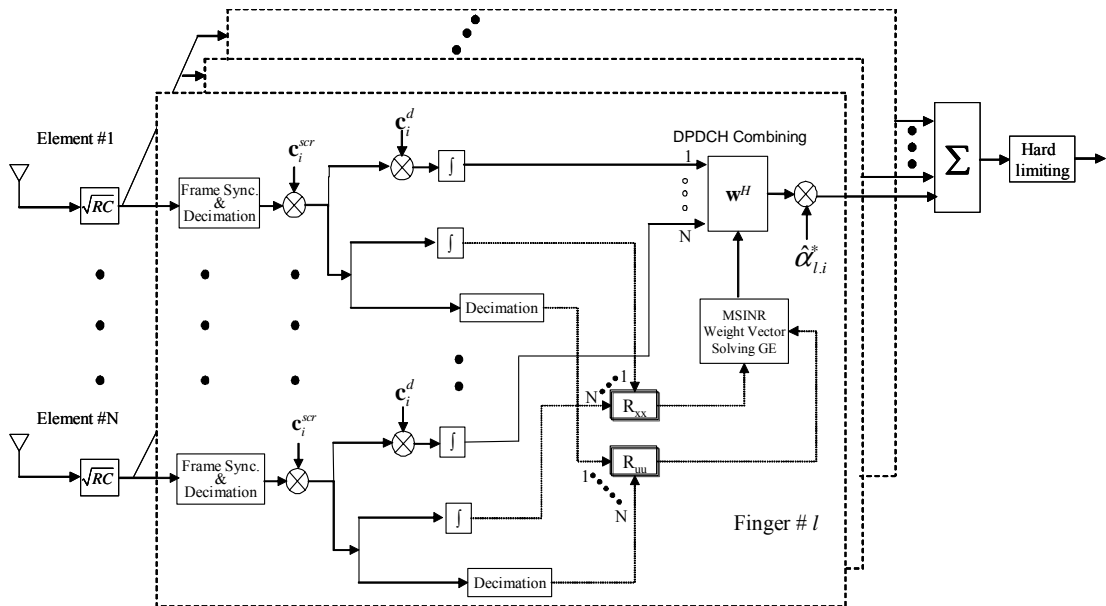


Figure B.3: MSINR based Beamformer-Rake receiver for WCDMA uplink. Modified CFA is utilized for MSINR beamforming. The weight vector is computed based on DPCCH only.

Appendix C

2-D Diversity Combiners

A special type of adaptive antenna array termed as the conventional spatial diversity combiner can mitigate the multipath fading by improving SNR achieved from spatial diversity. It is not targeted towards MAI reduction which is a marked contrast from the beamformer. The antenna array for a diversity combiner is designed so that the signal observed across the elements have very little cross-correlation. As a result, if the signal at one of the elements is going through a deep fade, it is highly unlikely that the signals at the other elements are encountering that at the same time. So there is nearly always good signal reception on one of the antenna elements. Therefore combining the signals from various elements will increase the SNR and the fidelity of the received signal. It is possible to design 2-D diversity combiners that cascade the spatial diversity combiner with a temporal diversity combiner i.e. a conventional Rake receiver. In some ways this is similar to a Beamformer-Rake receiver employing MSNR beamforming technique. However they come from entirely different design philosophy. We are going to discuss these 2-D diversity combiners in this Appendix.

C.1 Combining Techniques for Improved SNR

Different combining techniques can be implemented to improve the SNR with spatial diversity. The most common strategies are Selection Diversity, Maximal Ratio Combining and Equal Gain Combining. These techniques are equally applicable to temporal diversity, in other words they can be applied for combining signals from different fingers of a Rake receiver.

C.1.1 Selection Diversity

At any given instant, the receiver selects only the signal from one antenna element. In the ideal case, the receiver would select the element with the best SNR. However this means additional system complexity as the receiver would need to measure and monitor the instantaneous SNR at all the elements continuously. One practical solution is to monitor the SNR of the current *branch* and then switch to other branch if the SNR gets below some threshold. This is often known as switched diversity [16].

C.1.2 Maximal Ratio Combining

The co-phased desired signal from each antenna element is combined after weighting them by the individual branch SNR. MRC provides the maximum SNR if the interference and noise is ‘white’. However this scheme requires continuous measurement and monitoring of the instantaneous SNR at all the branches. This is the combining scheme that has been employed through out this dissertation for temporal combining.

C.1.3 Equal Gain Combining

The signals from different branches are co-phased and added together. This eliminates the need to estimate the SNR at each branch. However there is approximately 1dB performance penalty compared to MRC [16], [156].

C.2 Conventional 2-D Diversity Combiners for CDMA System

In this section we will introduce two different 2-D diversity combiner structures for a CDMA system. They are termed as Structure-I and Structure-II 2-D diversity combiners and are shown in Figures B.1 and B.2 respectively. Both of these utilize the maximal ratio combining technique for spatial as well as temporal combining. Structure-I combines the temporally resolved signals at the individual antenna elements first. The collective signals from all the elements are combined next. So this can be considered as a collection of parallel simple Rake receivers (for different elements) where the final decision statistic is formed from the soft output of all the Rake structures.

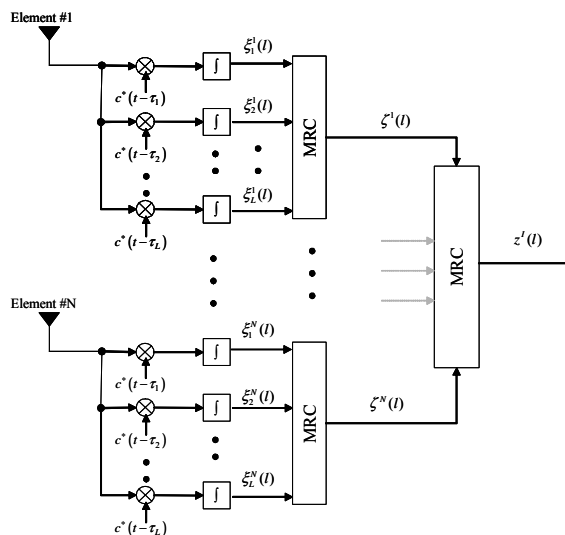


Figure C.1: Structure-I 2-D diversity combiner

Structure-II performs spatial MRC on the signals at different antenna elements that have the same temporal delay. The contribution from different multipath components are then combined to exploit the temporal diversity.

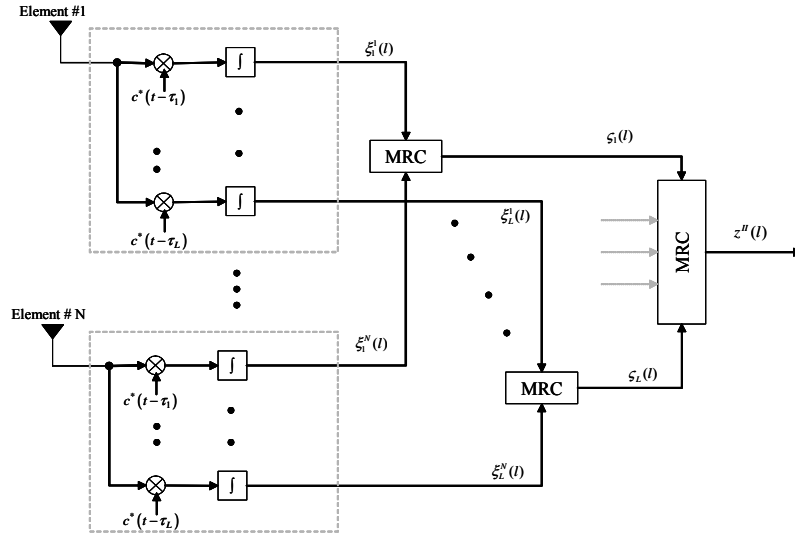


Figure C.2: Structure-II 2-D diversity combiner

If we assume that we have perfect estimation of coefficients to perform the required MRCs at the two structures, they will yield the same final decision statistic. This is not surprising since both the structures essentially perform the same combinings, only the order of temporal and spatial combining is different.

C.2.1 Analysis of Decision Statistics for the 2-D Diversity Combiners

In this Section we will derive the expression for the decision statistics for both the structures of the 2-D diversity combiner. We will show that the decision statistics are in fact identical.

Structure-I:

With reference to Figure B.1

$$\begin{aligned}
 \xi_1^1(l) &= h_1^1(l)s_1(l) + u_1^1 \\
 &\vdots \\
 \xi_L^1(l) &= h_L^1(l)s_1(l) + u_L^1
 \end{aligned} \tag{C.1}$$

and

Appendix C 2-D Diversity Combiners

$$\begin{aligned}
 \xi_1^N(l) &= h_1^N(l)s_1(l) + u_1^N \\
 &\vdots \\
 \xi_L^N(l) &= h_L^N(l)s_1(l) + u_L^N
 \end{aligned} \tag{C.2}$$

Where,

ξ_j^i is the output of correlator of the j^{th} ($j=1,2, \dots, L$) path of the i^{th} ($i = 1,2,\dots,N$) antenna.

h_j^i is the modified channel coefficient of the j^{th} path of the i^{th} antenna. The complex channel coefficient and the antenna response are included in this.

s_1 is the actual symbol sent

u_j^i is the contribution of interference and noise at the j^{th} path of the i^{th} antenna

So the contribution of the signal of the 1st antenna element to the decision statistics is given by

$$\begin{aligned}
 \zeta^1(l) &= \frac{1}{\sqrt{\sum_{i=1}^L |h_i^1(l)|^2}} \sum_{i=1}^L \left[\{h_i^1(l)\}^* \xi_i^1(l) \right] \\
 &= \frac{1}{\sqrt{\sum_{i=1}^L |h_i^1(l)|^2}} \sum_{i=1}^L \left[\{h_i^1(l)\}^* \{h_i^1(l)s_1(l) + u_i^1\} \right] \\
 &= \sqrt{\sum_{i=1}^L |h_i^1(l)|^2} [s_1(l)] + \frac{\sum_{i=1}^L u_i^1}{\sqrt{\sum_{i=1}^L |h_i^1(l)|^2}} \\
 \Rightarrow \zeta^1(l) &= \beta^1 [s_1(l)] + \frac{\sum_{i=1}^L u_i^1}{\beta^1} \quad ; \beta^1 = \sqrt{\sum_{i=1}^L |h_i^1(l)|^2}
 \end{aligned} \tag{C.3}$$

Similarly, the contribution from the N^{th} antenna element is given by

$$\zeta^N(l) = \beta^N [s_1(l)] + \frac{\sum_{i=1}^L u_i^N}{\beta^N} \quad ; \beta^N = \sqrt{\sum_{i=1}^L |h_i^N(l)|^2} \tag{C.4}$$

So the final decision statistics can be expressed as

$$z^l(l) = \frac{1}{\sqrt{\sum_{i=1}^N (\beta^i)^2}} \sum_{i=1}^N \beta^i \zeta^i(l)$$

$$\begin{aligned}
 &= \frac{1}{\sqrt{\sum_{i=1}^N (\beta^i)^2}} \sum_{i=1}^N \left[\beta^i [s_1(l)] + \frac{\sum_{j=1}^L u_j^i}{\beta^i} \right] \beta^i \\
 \Rightarrow z^l(l) &= \sqrt{\sum_{i=1}^N \sum_{j=1}^L |h_j^i(l)|^2} [s_1(l)] + \frac{\sum_{i=1}^N \sum_{j=1}^L u_j^i}{\sqrt{\sum_{i=1}^N \sum_{j=1}^L |h_j^i(l)|^2}}
 \end{aligned} \tag{C.5}$$

Structure-II:

The contribution from the 1st path at all the elements are given by

$$\begin{aligned}
 \varsigma_1(l) &= \frac{1}{\sqrt{\sum_{i=1}^N |h_1^i(l)|^2}} \sum_{i=1}^N \left[\{h_1^i(l)\}^* \xi^i(l) \right] \\
 &= \frac{1}{\sqrt{\sum_{i=1}^N |h_1^i(l)|^2}} \sum_{i=1}^N \left[\{h_1^i(l)\}^* \{h_1^i(l)s_1(l) + u_1^i\} \right] \\
 &= \sqrt{\sum_{i=1}^N |h_1^i(l)|^2} [s_1(l)] + \frac{\sum_{i=1}^N u_1^i}{\sqrt{\sum_{i=1}^N |h_1^i(l)|^2}} \\
 \Rightarrow \varsigma_1(l) &= \kappa_1 [s_1(l)] + \frac{\sum_{i=1}^N u_1^i}{\kappa_1} \quad ; \kappa_1 = \sqrt{\sum_{i=1}^N |h_1^i(l)|^2}
 \end{aligned} \tag{C.6}$$

Similarly the contribution from the L^{th} path at all the elements are given by

$$\varsigma_L(l) = \kappa_L [s_1(l)] + \frac{\sum_{i=1}^N u_L^i}{\kappa_L} \quad ; \kappa_L = \sqrt{\sum_{i=1}^N |h_L^i(l)|^2} \tag{C.7}$$

Therefore the final decision statistic is given by

$$z^H(l) = \frac{1}{\sqrt{\sum_{i=1}^L (\kappa_i)^2}} \sum_{i=1}^L \kappa_i \varsigma_i(l)$$

$$\begin{aligned}
 &= \frac{1}{\sqrt{\sum_{i=1}^L (\kappa_i)^2}} \sum_{i=1}^L \left[\kappa_i [s_1(l)] + \frac{\sum_{j=1}^N u_i^j}{\kappa_i} \right] \kappa_i \\
 \Rightarrow z''(l) &= \sqrt{\sum_{i=1}^L \sum_{j=1}^N |h_i^j(l)|^2} [s_1(l)] + \frac{\sum_{i=1}^L \sum_{j=1}^N u_i^j}{\sqrt{\sum_{i=1}^L \sum_{j=1}^N |h_i^j(l)|^2}} \tag{C.8}
 \end{aligned}$$

We observe that the final decision statistics $z'(l)$ and $z''(l)$ are identical under the assumption of Maximum Ratio Combining and perfect channel estimation.

References:

- [1] A. F. Naguib, *Adaptive Antennas for CDMA Wireless Networks*. Ph.D. dissertation, Stanford University, Aug 1996.
- [2] J. Litva and T. K. Lo, *Digital Beamforming in Wireless Communications*. Boston, MA: Artech House, 1996.
- [3] T.S. Rappaport, *Wireless Communications: Principles and Practice*. Upper Saddle River, NJ: Prentice Hall PTR, 1996.
- [4] J. G. Proakis, *Digital Communications*. New York, NY: McGraw-Hill Inc., third ed., 1995.
- [5] Malcom W. Oliphant, "The Mobile Phone Meets the Internet," *IEEE Spectrum*, pp. 20-28, August 1999.
- [6] UMTS, "Spreading and Modulation," 3G TS 25.213 V3.2.0 (2000-03).
- [7] UMTS, "Physical Channels and Mapping of Transport Channels onto Physical Channels (FDD)," 3G TS 25.211 V3.2.0 (2000-03).
- [8] Tero Ojanpera and Ramjee Prasad, "An Overview of Air Interface Multiple Access for IMT-2000/UMTS," *IEEE Communications Magazine*, vol. 36, pp. 88-95, September 1998.
- [9] Erik Dahlman, Bjorn Gudmundson, Matts Nilsson, and Johan Skold, "UMTS/IMT-2000 Based on Wideband CDMA," *IEEE Communications Magazine*, vol. 36, pp. 70-80, September 1998.
- [10] Erik Dahlman, Per Beming, Jens Knutsson, Fredrik Ovesjo, Magnus Persson, and Christiaan Roobol, "WCDMA- The Radio Interface for Future Mobile Multimedia Communications," *IEEE Transactions on Vehicular Technology*, vol. 47, No. 4, pp. 1105-1118, November 1998.
- [11] G. H. Golub and C.F. Van Loan, *Matrix Computations*, Baltimore, MD, John Hopkins University Press, 1989.
- [12] R. V. Nee, and R. Prasad, *OFDM for Wireless Multimedia Communications*. Boston, Artech House, 1998.
- [13] F.Alam, R. Boyle, R. Gozali, and R. Mostafa, "Space Time Processing Approaches for Third Generation Wireless Systems ", Tutorial conducted in 11th Annual MPRG/Virginia Tech Wireless Personal Symposium, Blacksburg, Virginia, USA, June 6-8, 2001.
- [14] S. Tanaka, M. Sawasashi, and F. Adachi, "Pilot symbol-assisted decision-directed coherent adaptive array diversity for DS-CDMA mobile radio reverse link," *IEICE Trans. Commun.*, vol. E80-A, pp.2445-2454, Dec. 1997.
- [15] K. A. Zahid, *Space Time Processing for the Wideband CDMA System*. M.S. Thesis, Virginia Tech, Jan 2001.
- [16] R. B. Ertel, *Antenna Array Systems: Propagation and Performance*. Ph.D. Dissertation, Virginia Tech, July 1999.
- [17] B. Widrow, P. E. Mantey, L. J. Griffiths and B. B. Goode , "Adaptive Antenna Systems," *IEEE Proceedings*, vol. 55, No. 12, pp. 2143 -2159, Dec. 1967.
- [18] L. C. Van Atta , "Electromagnetic Reflections," U.S. Patent 2908002, Oct. 6, 1959.

References

- [19] "Special Issues on Active and Adaptive Antenna Systems," IEEE Trans. Antennas and Propagation, vol. AP-12, March 1964.
- [20] F. Bryn, "Optimum Signal Processing of Three-Dimensional Arrays Operating on Gaussian Signals and Noise," Journal of Acoust. Soc. Am., vol. 34, pp. 289-297, March 1962.
- [21] H. Mermoz, "Adaptive Filtering and Optimal Utilization of an Antenna," U.S. Navy Bureau of Ships(Translation 903 of Ph.D. thesis, Institut Polytechnique. Grenoble, France), Oct. 4, 1965.
- [22] S. W. W. Shor, "Adaptive Techniques to Discriminate Against Coherent Noise in Narrow-Band System," Journal of Acoust. Soc. Am., vol. 39, pp. 74-78, Jan. 1966.
- [23] V. C. Anderson and P. Rudnick, "Rejection of a coherent arrival at an array," J. Acoust. Soc. Amer., vol. 45, pp. 406-410, 1969.
- [24] V. C. Anderson, "DICANNE, a realizable adaptive process," J. Acoust. Soc. Amer., vol. 45, pp. 398-405, 1969.
- [25] H. A. d'Assumpcao and G. E. Mountford, "An overview of signal processing for arrays of receivers," J. Inst. Eng. Aust. and IREE Aust., vol. 4, pp. 6-19, 1984.
- [26] L. C. Godara and A. Cantoni, "Uniqueness and linear independence of steering vectors in array space," *J. Acoust. Soc. Amer.*, vol. 70, pp. 467-475, 1981.
- [27] Y. Bresler, V. U. Reddy, and T. Kailath, "Optimum beamforming for coherent signal and interferences," IEEE Trans. Acoust., Speech, Signal Processing, vol. 36, pp. 833-843, 1988.
- [28] I. Chiba, T. Takahashi, and Y. Karasawa, "Transmitting null beam forming with beam space adaptive array antennas," in the Proceedings of IEEE 44th Vehicular Technology Conf., Stockholm, Sweden, pp. 1498-1502, 1994.
- [29] L. E. Brennan and I. S. Reed, "Theory of adaptive radar," IEEE Trans. Aerosp. Electron. Syst., vol. AES-9, pp. 237-252, 1973.
- [30] I. S. Reed, J. D. Mallett, and L. E. Brennan, "Rapid convergence rate in adaptive arrays," IEEE Trans. Aerosp. Electron. Syst., vol. AES-10, pp. 853-863, 1974.
- [31] A. M. Vural, "An overview of adaptive array processing for sonar application," EASCON'75 Records, pp. 34A-34M.
- [32] S. P. Applebaum, "Adaptive arrays," IEEE Transaction on Antennas and Propagation, vol. AP-24, pp. 585-598, 1976.
- [33] J. Capon, "High-resolution frequency-wave number spectrum analysis," IEEE Proceedings, vol. 57, pp. 1408-1418, 1969.
- [34] J. H. Winters, "Optimum combining in digital mobile radio with cochannel interference," IEEE Journal on Select Areas of Communications, vol. SAC-2, pp. 528-539, 1984.
- [35] J. H. Winters, "Optimum combining for indoor radio systems with multiple users," IEEE Transactions on Communications, vol. COM-35, pp. 1222-1230, 1987.
- [36] B. Suard, A. F. Naguib, G. Xu, and A. Paulraj, "Performance of CDMA mobile communication systems using antenna arrays," IEEE Int. Conf. Acoustics, Speech, and Signal Processing (ICASSP), Minneapolis, MN, 1993, pp. 153-156.
- [37] A. F. Naguib and A. Paulraj, "Performance of CDMA cellular networks with base-station antenna arrays," in the Proceedings of IEEE Int. Zurich Seminar on Communications, 1994, pp. 87-100.

References

- [38] B. Widrow, J. R. Glover, J. M. McCool, J. Kaunitz, C. S. Williams, R. H. Hearn, J. R. Zeidler, E. Dong, Jr., and R.C. Goodlin, "Adaptive noise canceling: Principles and applications," *IEEE Proceedings*, vol. 63, pp. 1692–1716, 1975.
- [39] S. P. Applebaum and D. J. Chapman, "Adaptive arrays with main beam constraints," *IEEE Transaction on Antennas and Propagation*, vol. AP-24, pp. 650–662, 1976.
- [40] B. Widrow, K. M. Duvall, R. P. Gooch, and W. C. Newman, "Signal cancellation phenomena in adaptive antennas: Causes and cures," *IEEE Trans. Antennas Propagat.*, vol. AP-30, pp.469–478, 1982.
- [41] C. L. Zahm, "Application of adaptive arrays to suppress strong jammers in the presence of weak signals," *IEEE Trans. Aerosp.Electron. Syst.*, vol. AES-9, pp. 260–271, 1973.
- [42] L. J. Griffiths, "A comparison of multidimensional Wiener and maximum-likelihood filters for antenna arrays," in *IEEE Proceedings* ,vol. 55, pp. 2045–2047, 1967.
- [43] A. Flieller, P. Larzabal, and H. Clergeot, "Applications of high resolution array processing techniques for mobile communication system," in the *Proceedings of IEEE Intelligent Vehicles Symposium.*, Paris, France, pp. 606–611,1994.
- [44] J. H. Winters, J. Salz, and R. D Gitlin, "The impact of antenna diversity on the capacity of wireless communication systems,"*IEEE Transaction on Communications*, vol. 42, pp. 1740–1751, 1994.
- [45] S. Anderson, M. Millnert, M. Viberg, and B. Wahlberg, "An adaptive array for mobile communication systems," *IEEE Transaction on Vehicular Technology*, vol. 40, pp. 230–236, 1991.
- [46] T. Gebauer and H. G. Gockler, "Channel-individual adaptive beamforming for mobile satellite communications," *IEEE Journal on Selected Areas of Commun*, vol. 13, pp. 439–448, 1995.
- [47] J. F. Diouris, B. Feuvrie, and J. Saillard, "Adaptive multisensor receiver for mobile communications," *Ann. Telecommun.*, vol.48, pp. 35–46, 1993.
- [48] P. W. Howells, "Explorations in fixed and adaptive resolution at GE and SURC," *IEEE Transaction on Antennas and Propagation*, vol. AP-24, pp. 575–584, 1976.
- [49] L. J. Griffiths and C. W. Jim, "An alternative approach to linearly constrained adaptive beamforming," *IEEE Transaction on Antennas and Propagation*, vol. AP-30, pp. 27–34, 1982.
- [50] C. W. Jim, "A comparison of two LMS constrained optimal array structures," *IEEE Proceedings*, vol. 65, pp. 1730–1731, 1977.
- [51] B. D. Van Veen and R. A. Roberts, "Partially adaptive beamformer design via output power minimization," *IEEE Transaction on Acoust., Speech, Signal Processing*, vol. ASSP-35, pp. 1524–1532, 1987.
- [52] F. Qian and B. D. Van Veen, "Partially adaptive beamformer design subject to worst case performance constraints," *IEEE Transaction on Signal Processing*, vol. 42, pp. 1218–1221, 1994.
- [53] A. Cantoni and L. C. Godara, "Performance of a postbeamformer interference canceller in the presence of broadband directional signals," *J. Acoust. Soc. Amer.*, vol. 76, pp. 128–138,1984.
- [54] E. Brookner and J. M. Howell, "Adaptive-adaptive array processing," *IEEE Proceedings*, 1986, vol. 74, pp. 602–604.
- [55] J. T. Mayhan, "Adaptive nulling with multiple beam antennas," *IEEE Transaction on Antennas and Propagation*, vol. AP-26, pp. 267–273, 1978.

References

- [56] W. E. Rodgers and R. T. Compton Jr., "Adaptive array bandwidth with tapped delay line processing," *IEEE Trans. Aerosp. Electron. Syst.*, vol. AES-15, pp. 21–28, 1979.
- [57] E. W. Vook and R. T. Compton, Jr., "Bandwidth performance of linear arrays with tapped delay line processing," *IEEE Trans. Aerosp. Electron. Syst.*, vol. 28, pp. 901–908, 1992.
- [58] T. S. Durrani, N. L. M. Murukutla, and K. C. Sharman, "Constrained algorithm for multi-input adaptive lattices in array processing," in *The Proceedings of ICASSP, Atlanta, GA, 1981*, pp. 297–301.
- [59] G. R. L. Sohie and L. H. Sibul, "Stochastic convergence properties of the adaptive gradient lattice," *IEEE Trans. Acoust., Speech, Signal Processing*, vol. ASSP-32, pp. 102–107, 1984.
- [60] M. H. Er and A. Cantoni, "Derivative constraints for broadband element space antenna array processors," *IEEE Trans. Acoust., Speech, Signal Processing*, vol. ASSP-31, pp. 1378–1393, 1983.
- [61] I. Thng, A. Cantoni, and Y. H. Leung, "Derivative constrained optimum broadband antenna arrays," *IEEE Trans. Signal Processing*, vol. 41, pp. 2376–2388, 1993.
- [62] K. M. Buckley, "Spatial/spectral filtering with linearly constrained minimum variance beamformers," *IEEE Trans. Acoust., Speech, Signal Processing*, vol. ASSP-35, pp. 249–266, 1987.
- [63] M. H. Er, "On the limiting solution of quadratically constrained broadband beamformers," *IEEE Trans. Signal Processing*, vol. 41, pp. 418–419, 1993.
- [64] N. Ishii and R. Kohno, "Spatial and temporal equalization based on an adaptive tapped-delay-line array antenna," *IEICE Trans. Commun.*, vol. E78-B, pp. 1162–1169, Aug. 1995.
- [65] R. Kohno, H. Wang, and H. Imai, "Adaptive array antenna combined with tapped delay line using processing gain for spread spectrum CDMA systems," presented at the *IEEE Int. Symp. Personal Indoor and Mobile Radio Communications (PIMRC)*, Boston, MA, 1992.
- [66] L. C. Godara, "Application of the fast Fourier transform to broadband beamforming," *J. Acoust. Soc. Amer.*, vol. 98, pp. 230–240, 1995.
- [67] R. Kumaresan, "On a frequency domain analog of Prony's method," *IEEE Trans. Acoust., Speech, Signal Processing*, vol. 38, pp. 168–170, 1990.
- [68] J. X. Zhu and H. Wang, "Adaptive beamforming for correlated signal and interference: A frequency domain smoothing approach," *IEEE Trans. Acoust., Speech, Signal Processing*, vol. 38, pp. 193–195, 1990.
- [69] V. A. N. Barroso, M. J. Rendas, and J. P. Gomes, "Impact of array processing techniques on the design of mobile communication systems," in *The Proceedings of IEEE 7th Mediterranean Electrotechnical, Antalya, Turkey, 1994*, pp. 1291–1294.
- [70] M. I. Miller and D. R. Fuhrmann, "Maximum likelihood narrow-band direction finding and the EM algorithm," *IEEE Trans. Acoust., Speech, Signal Processing*, vol. 38, pp. 1560–1577, 1990.
- [71] J. Makhoul, "Linear prediction: A tutorial review," *IEEE Proceedings*, vol. 63, pp. 561–580, 1975.
- [72] D. P. Skinner, S. M. Hedlicka, and A. D. Mathews, "Maximum entropy array processing," *J. Acoust. Soc. Amer.*, vol. 66, pp. 488–493, 1979.
- [73] V. F. Pisarenko, "The retrieval of harmonics from a covariance function," *Geophys. J. R. Astron. Soc.*, vol. 33, pp. 347–366, 1973.

References

- [74] M. Wax, T. J. Shan, and T. Kailath, "Spatio-temporal spectral analysis by eigenstructure methods," *IEEE Trans. Acoust., Speech, Signal Processing*, vol. ASSP-32, pp. 817–827, 1984.
- [75] V. U. Reddy, B. Egardt, and T. Kailath, "Least-squares type algorithm for adaptive implementation of Pisarenko's harmonic retrieval method," *IEEE Trans. Acoust., Speech, Signal Processing*, vol. ASSP-30, pp. 399–405, 1982.
- [76] J. R. Yang and M. Kaveh, "Adaptive eigensubspace algorithms for direction or frequency estimation and tracking," *IEEE Trans. Acoust., Speech, Signal Processing*, vol. ASSP-36, pp. 241–251, 1988.
- [77] M. G. Larimore, "Adaptive convergence of spectral estimation based on Pisarenko harmonic retrieval," *IEEE Trans. Acoust., Speech, Signal Processing*, vol. ASSP-31, pp. 955–962, 1983.
- [78] H. Ouibrahim, "Prony, Pisarenko and the matrix pencil: A unified presentation," *IEEE Trans. Acoust., Speech, Signal Processing*, vol. ASSP-37, pp. 133–134, 1989.
- [79] B. Friedlander, "A signal subspace method for adaptive interference cancellation," *IEEE Trans. Acoust., Speech, Signal Processing*, vol. 36, pp. 1835–1845, 1988.
- [80] H. Ouibrahim, D. D. Weiner, and T. K. Sarkar, "A generalized approach to direction finding," *IEEE Trans. Acoust., Speech, Signal Processing*, vol. 36, pp. 610–613, 1988.
- [81] A. Paulraj and T. Kailath, "Eigenstructure methods for direction of arrival estimation in the presence of unknown noise field," *IEEE Trans. Acoust., Speech, Signal Processing*, vol. ASSP-34, pp. 13–20, 1986.
- [82] R. O. Schmidt, "Multiple emitter location and signal parameter estimation," *IEEE Trans. Antennas Prop.*, vol. AP-34, pp. 276–280, 1986.
- [83] R. D. DeGroat, E. M. Dowling, and D. A. Linebarger, "The constrained MUSIC problem," *IEEE Trans. Signal Processing*, vol. 41, pp. 1445–1449, 1993.
- [84] R. W. Klukas and M. Fattouche, "Radio signal direction finding in the urban radio environment," in *Proc. Nat. Technical Meeting Institute of Navigation*, San Francisco, CA, 1993, pp. 151–160.
- [85] A. Barabell, "Improving the resolution of eigenstructured based direction finding algorithms," in the *Proceedings of ICASSP*, Boston, MA, 1983, pp. 336–339.
- [86] J. T. Mayhan and L. Niro, "Spatial spectral estimation using multiple beam antennas," *IEEE Trans. Antennas Prop.*, vol. AP-35, pp. 897–906, 1987.
- [87] I. Karasalo, "A high-high-resolution post beamforming method based on semidefinite linear optimization," *IEEE Trans. Acoust., Speech, Signal Processing*, vol. 38, pp. 16–22, 1990.
- [88] S. S. Reddi, "Multiple source location—A digital approach," *IEEE Trans. Aerosp. Electron. Syst.*, vol. AES-15, pp. 95–105, 1979.
- [89] R. Kumaresan and D. W. Tufts, "Estimating the angles of arrival of multiple plane waves," *IEEE Trans. Aerosp. Elect. Systems*, vol. AES-19, pp. 134–139, 1983.
- [90] K. M. Buckley and X. L. Xu, "Spatial spectrum estimation in a location sector," *IEEE Trans. Acoust., Speech, Signal Processing*, vol. ASSP-38, pp. 1842–1852, 1990.
- [91] R. Roy and T. Kailath, "ESPRIT—Estimation of signal parameters via rotational invariance techniques," *IEEE Trans. Acoust., Speech, Signal Processing*, vol. ASSP-37, pp. 984–995, 1989.
- [92] G. Xu, S. D. Silverstein, R. H. Roy, and T. Kailath, "Beamspace ESPRIT," *IEEE Trans. Signal Processing*, vol. 42, pp. 349–356, 1994.

References

- [93] R. Hamza and K. Buckley, "Resolution enhanced ESPRIT," *IEEE Trans. Signal Processing*, vol. 42, pp. 688–691, 1994.
- [94] A. Paulraj, R. Roy, and T. Kailath, "A subspace rotation approach to signal parameter estimation," *IEEE Proceedings*, vol. 74, pp. 1044–1045, 1986.
- [95] A. J. Weiss and M. Gavish, "Direction finding using ESPRIT with interpolated arrays," *IEEE Trans. Signal Processing*, vol. 39, pp. 1473–1478, 1991.
- [96] J. A. Gansman, M. D. Zoltowski, and J. V. Krogmeier, "Multidimensional multirate DOA estimation in beamspace," *IEEE Trans. Signal Processing*, vol. 44, pp. 2780–2792, 1996.
- [97] A. L. Swindlehurst, B. Ottersten, R. Roy, and T. Kailath, "Multiple invariance ESPRIT," *IEEE Trans. Signal Processing*, vol. 40, pp. 867–881, 1992.
- [98] N. Yuen and B. Friedlander, "Asymptotic performance analysis of ESPRIT, higher order ESPRIT, and virtual ESPRIT algorithms," *IEEE Trans. Signal Processing*, vol. 44, pp. 2537–2550, 1996.
- [99] M. D. Zoltowski and D. Stavrinides, "Sensor array signal processing via a procrustes rotations based eigenanalysis of the ESPRIT data pencil," *IEEE Trans. Acoust., Speech, Signal Processing*, vol. 37, pp. 832–861, 1989.
- [100] Y. Wang and J. R. Cruz, "Adaptive antenna arrays for cellular CDMA cellular communication systems," in the *Proceedings of IEEE ICASSP*, Detroit, MI, pp. 1725–1728, 1995.
- [101] M. Viberg, B. Ottersten, and T. Kailath, "Detection and estimation in sensor arrays using weighted subspace fitting," *IEEE Trans. Signal Processing*, vol. 39, pp. 2436–2449, 1991.
- [102] A. Klouche-Djedid and M. Fujita, "Adaptive array sensor processing applications for mobile telephone communications," *IEEE Trans. Veh. Technol.*, vol. 45, pp. 405–416, 1996.
- [103] B. D. Van Veen, "Adaptive convergence of linearly constrained beamformers based on the sample covariance matrix," *IEEE Trans. Signal Processing*, vol. 39, pp. 1470–1473, 1991.
- [104] L. J. Horowitz, H. Blatt, W. G. Brodsky, and K. D. Senne, "Controlling adaptive antenna arrays with the sample matrix inversion algorithm," *IEEE Trans. Aerosp. Electron. Syst.*, vol. AES-15, pp. 840–847, 1979.
- [105] S. Haykin, *Adaptive Filter Theory*. Englewood Cliffs, NJ: Prentice Hall, 1991.
- [106] B. Widrow and J. M. McCool, "A comparison of adaptive algorithms based on the methods of steepest descent and random search," *IEEE Trans. Antennas Prop.*, vol. AP-24, pp. 615–637, 1976.
- [107] W. A. Gardner, "Comments on convergence analysis of LMS filters with uncorrelated data," *IEEE Trans. Acoust., Speech, Signal Processing*, vol. ASSP-34, pp. 378–379, 1986.
- [108] J. B. Foley and F. M. Boland, "A note on the convergence analysis of LMS adaptive filters with Gaussian data," *IEEE Trans. Acoust., Speech, Signal Processing*, vol. 36, pp. 1087–1089, 1988.
- [109] V. Solo, "The limiting behavior of LMS," *IEEE Trans. Acoust., Speech, Signal Processing*, vol. 37, pp. 1909–1922, 1989.
- [110] A. Feuer and E. Weinstein, "Convergence analysis of LMS filters with uncorrelated Gaussian data," *IEEE Trans. Acoust., Speech, Signal Processing*, vol. ASSP-33, pp. 222–229, 1985.
- [111] S. Jaggi and A. B. Martinez, "Upper and lower bounds of the misadjustment in the LMS algorithm," *IEEE Trans. Acoust., Speech, Signal Processing*, vol. 38, pp. 164–166, 1990.

References

- [112] F. B. Boland and J. B. Foley, "Stochastic convergence of the LMS algorithm in adaptive systems," *Signal Process.*, vol. 13, pp. 339–352, 1987.
- [113] R. Y. Chen and C. L. Wang, "On the optimum step size for the adaptive sign and LMS algorithms," *IEEE Trans. Circuits Syst.*, vol. 37, pp. 836–840, 1990.
- [114] V. J. Mathews and S. H. Cho, "Improved convergence analysis of stochastic gradient adaptive filters using the sign algorithm," *IEEE Trans. Acoust., Speech, Signal Processing*, vol. ASSP-35, pp. 450–454, 1987.
- [115] R. Nitzberg, "Application of the normalized LMS algorithm to MSLC," *IEEE Trans. Aerosp. Electron. Syst.*, vol. AES-21, pp. 79–91, 1985.
- [116] N. J. Bershad, "Analysis of the normalized LMS algorithm with Gaussian inputs," *IEEE Trans. Acoust., Speech, Signal Processing*, vol. ASSP-34, pp. 793–806, 1986.
- [117] D. T. M. Slock, "On the convergence behavior of the LMS and the normalized LMS algorithms," *IEEE Trans. Signal Processing*, vol. 41, pp. 2811–2825, 1993.
- [118] M. Rupp, "The behavior of LMS and NLMS algorithms in the presence of spherically invariant processes," *IEEE Trans. Signal Processing*, vol. 41, pp. 1149–1160, 1993.
- [119] O. L. Frost III, "An algorithm for linearly constrained adaptive array processing," *IEEE Proceedings*, vol. 60, pp. 926–935, 1972.
- [120] A. Cantoni, "Application of orthogonal perturbation sequences to adaptive beamforming," *IEEE Trans. Antennas Prop.*, vol. AP-28, pp. 191–202, 1980.
- [121] L. C. Godara, "Improved LMS algorithm for adaptive beamforming," *IEEE Trans. Antennas Prop.*, vol. 38, pp. 1631–1635, 1990.
- [122] G. Raleigh, and A. Paulraj, "Time varying vector channel estimation for adaptive spatial equalization," In the Proceedings of the IEEE Global Telecommunications Conference, pp.218-224, 1995.
- [123] P. Fabre and C. Gueguen, "Improvement of the fast recursive least-squares algorithms via normalization: A comparative study," *IEEE Trans. Acoust., Speech, Signal Processing*, vol. ASSP-34, pp. 296–308, 1986.
- [124] E. Eleftheriou and D. D. Falconer, "Tracking properties and steady state performance of RLS adaptive filter algorithms," *IEEE Trans. Acoust., Speech, Signal Processing*, vol. ASSP-34, pp. 1097–1110, 1986.
- [125] M. S. Mueller, "Least squares algorithms for adaptive equalizers," *Bell Syst. Tech. J.*, pp. 1905–1925, 1981.
- [126] J. M. Cioffi and T. Kailath, "Fast recursive-least-square, transversal filters for adaptive filtering," *IEEE Trans. Acoust., Speech, Signal Processing*, vol. ASSP-32, pp. 998–1005, 1984.
- [127] R. A. Wiggins and E. A. Robinson, "Recursive solution to the multichannel filtering problem," *J. Geophys. Res.*, vol. 70, pp. 1885–1891, 1965.
- [128] G. V. Moustakids and S. Theodoridis, "Fast Newton transversal filters—A new class of adaptive estimation algorithms," *IEEE Trans. Signal Processing*, vol. 39, pp. 2184–2193, 1991.
- [129] S. Qiao, "Fast adaptive RLS algorithms: A generalized inverse approach and analysis," *IEEE Trans. Signal Processing*, vol. 39, pp. 1455–1459, 1991.
- [130] D. T. M. Slock and T. Kailath, "Numerically stable fast transversal filters for recursive least squares adaptive filtering," *IEEE Trans. Signal Processing*, vol. 39, pp. 92–114, 1991.

References

- [131] J. Fernandez, I. R. Corden, and M. Barrett, "Adaptive array algorithms for optimal combining in digital mobile communication systems," in the Proceedings of Inst. Elect. Eng. 8th Int. Conf. Antennas and Propagation, Edinburgh, Scotland, 1993, pp. 983–986.
- [132] Y. Wang and J. R. Cruz, "Adaptive antenna arrays for the reverse link of CDMA cellular communication systems," *Electron. Lett.*, vol. 30, pp. 1017–1018, 1994.
- [133] D. N. Godard, "Self-recovering equalization and carrier tracking in two-dimensional data communication systems," *IEEE Trans. Commun.*, vol. COM-28, pp. 1867–1875, 1980.
- [134] J. R. Treichler and B. G. Agee, "A new approach to multipath correction of constant modulus signals," *IEEE Trans. Acoust., Speech, Signal Processing*, vol. ASSP-31, pp. 459–472, 1983.
- [135] R. Gooch, and J. Lundell, "The CMA array: An adaptive beamformer for constant modulus signal," in the Proceedings of Int. Conf. on Acoust., Speech, Signal Processing,, pp. 2523–2526, April 1986.
- [136] B. G. Agee, "The Least Squares CMA: A new technique for rapid correction of constant modulus signals," in the Proceedings of Int. Conf. on Acoust., Speech, Signal Processing,, pp. 953–956, April 1986.
- [137] B. G. Agee, "Maximum likelihood approaches to blind adaptive signal extraction using narrowband arrays ," in the Proceedings of the Asilomar Conf. on Signals, Systems, and Computers, pp. 716-720, Nov. 1991.
- [138] T. E. Biedka, *A General Framework for the Analysis and Development of Blind Adaptive Algorithms*. Ph.D. dissertation, Virginia Tech, Oct 2001.
- [139] S. Kwon, I. Oh, and S. Choi, "Adaptive Beamforming from the Generalized Eigenvalue Problem with a Linear Complexity for a Wideband CDMA Channel ", In the Proceedings of the IEEE Vehicular Technology Conference 1999/Fall, pp.1890-1894.
- [140] D.Shim, F.Alam, and B.D. Woerner, "Performance Analysis of a Smart Antenna System with Blind Algorithm ", In the Proceedings of the 11th Virginia Tech Symposium on Wireless Personal Communications, June 2001, USA.
- [141] F.Alam, D.Shim, and B.D. Woerner, "A New Low-Complexity Beamformer-Rake Receiver for WCDMA", in the proceedings of IEEE International Conference on Communications, ICC2002, vol. 1, pp. 160-164, New York, USA, April 2002.
- [142] S. Choi and D. Yun , "Design of an adaptive antenna array for tracking the source of maximum power and its application to CDMA mobile communications" *IEEE Transactions on Antenna and Propagations*, vol. 45, No. 9, pp. 1393 -1404, Sept. 1997.
- [143] S. Choi, T. K. Sarkar, and J. Choi, "Adaptive antenna array for direction of arrival estimation utilizing the conjugate gradient method," *Signal Processing*, vol. 45, pp. 313–327, 1995.
- [144] S. Choi and D. Shim, et al, "A New Blind Adaptive Beamforming Procedure Based on Conjugate Gradient Method for CDMA Mobile Communications", *ETRI Journal*, Vol. 22, No.2, pp 133-148, June, 1998
- [145] S. Choi and D. Shim , "A novel adaptive beamforming algorithm for a smart antenna system in a CDMA mobile communication environment" *IEEE Transactions on Vehicular*, vol. 49, No. 5, pp. 1793 -1806, Sept. 2000.
- [146] S. Choi, S. Ahn and T. K. Sarkar, "A Linearized Power Method for Adaptive Beam-forming in a Multipath Fading CDMA Environment", *Microwave and Optical Technology Letter*, Dec.2001.

References

- [147] S. Kim, S. Lee, Y. Yang, and Y. Kim, "A New Efficient Blind Beamforming Algorithm in W-CDMA Systems" to appear in IEEE Signal Processing Magazine.
- [148] F. Alam, D. Shim, and B. D. Woerner, "A New Adaptive Algorithm for MSNR Beamforming in WCDMA System," submitted to the IEEE Vehicular Technology Conference, Spring 2003, Korea, April 2003.
- [149] B. H. Khalaj, A. Paulraj, and T. Kailath, "2D RAKE receivers for CDMA cellular systems," In the Proceedings of IEEE Globecom, pp. 400-404, 1994.
- [150] A. F. Naguib, A. Paulraj, and T. Kailath, "Capacity improvement with base-station antenna arrays in cellular CDMA," IEEE Trans. on Veh. Technol., vol. 43, no. 3, pp. 691-698, August 1994.
- [151] A. F. Naguib and A. Paulraj, "Effects of multipath and base-station antenna arrays on uplink capacity of cellular CDMA," in the Proceedings of IEEE Globecom, pp. 395-399, 1994.
- [152] Y. M. Vasavada, T. E. Biedka, J. H. Reed, "Code Gated Algorithm: A Blind Adaptive Antenna Array Beamforming Scheme for Wideband CDMA", In the Proceedings of the Thirty-fourth Asilomar conference on Signals, Systems and Computers, November 2000, CA, USA.
- [153] M. Dell'Anna, A. H. Aghvami, "Performance of optimum and suboptimum combining at the antenna array of a W-CDMA system," IEEE Journal on Selected Areas in Communications, vol. 17, Issue: 12, pp. 2123-2137, Dec. 1999.
- [154] J. C. Liberti, *Analysis of CDMA Cellular Radio Systems Employing Adaptive Antennas*. Ph.D. Dissertation, Virginia Tech, July 1999.
- [155] J. C. Liberti, and T. S. Rappaport, "A geometrically based model for line-of-sight multipath radio channels", In the Proceedings of the IEEE Vehicular Technology Conference 1996/Spring, pp. 844-848.
- [156] W. C. Jakes, ed., *Microwave Mobile Communications*. New York: IEEE Press. 1974.
- [157] P. Petrus, *Novel adaptive array algorithms and their impact on cellular system capacity*. Ph.D. Dissertation, Virginia Tech, July 1997.
- [158] P. Petrus, J. H. Reed, and T. S. Rappaport, "Geometrically based statistical channel model for macrocellular mobile environments", In the Proceedings of the IEEE GLOBECOM, pp. 1197-1201, 1996.
- [159] P. Petrus, J. H. Reed, and T. S. Rappaport, "Effects of directional antennas at the base station on the Doppler spectrum", IEEE Communications Letters, vol. 1, No:2, pp. 40-42, March 1997.
- [160] P. Zetterberg, "A downlink beam steering technique for GSM/DCS1800/PCS1900: Report version," tech. rep., Royal Institute of Technology, 1996.
- [161] P. Zetterberg, P. Leth-Esperson, and P. Mogensen, "Propagation, beamsteering and uplink combining algorithms for cellular systems," ACTS Mobile Communications Summit, Royal Institute of Technology, Nov. 1996.
- [162] P. Mogensen, P. Zetterberg, H. Dam, P. L. Espensen, S. L. Larsen, and K. Olsen, "Algorithms and antenna array recommendations," Tech Rep. A020/AUC/A12/DR/P/1/xx-D2.1.2, Tsunami(II), September 1996.
- [163] S. P. Stapleton, X. Carbo, and T. Mckeen, "Spatial channel simulator for phased arrays," In the Proceedings of the IEEE Vehicular Technology Conference 1996, pp. 1890-1894.
- [164] O. Norklit, and J. B. Anderson, "Mobile radio environment and adaptive arrays," In the proceedings of PIMRC, pp. 725-728, 1994.

References

- [165] G. G. Raleigh, S. N. Diggavi, A. F. Naguib, and A. Paulraj, "Characterization of fast fading vector channels for multi-antenna communication systems," in the Proceedings of the Asilomar Conf. on Signals, Systems, and Computers, pp. 853-857, 1994..
- [166] Q. Spencer, M. Rice, B. Jeffs, and M. Jensen, "A statistical model for angle of arrival in indoor multipath propagation," In the Proceedings of the IEEE Vehicular Technology Conference 1997.
- [167] Q. Spencer, M. Rice, B. Jeffs, and M. Jensen, "Indoor wideband time/angle of arrival multipath propagation results," In the Proceedings of the IEEE Vehicular Technology Conference 1997.
- [168] R. Michael Buehrer, Achilles G. Kogiantis, Shang-chieh Liu, Jiann-an Tsai, and Dirck Uptegrove, "Intelligent Antennas for Wireless Communications-Uplink," Bell Labs Technical Journal, pp. 73-103, July-September 1999.
- [169] B. R. Salzberg, "Performance of an efficient parallel data transmission system" IEEE Transactions on Communications, vol. COM-15, pp. 805-813, Dec. 1967.
- [170] "Orthogonal Frequency Division Multiplexing" US Patent No. 34884555, filed Nov. 14, 1966, issued Jan. 6, 1970.
- [171] S.B. Weinstein, and P. M. Ebert, "Data transmission by frequency division multiplexing using the discrete Fourier transform" IEEE Transactions on Communications, vol. COM-19, pp. 628-634, Oct. 1971.
- [172] B. Hirosaki, "An orthogonally multiplexed QAM system using the discrete Fourier transform" IEEE Transactions on Communications, vol. COM-29, pp. 982-989, Jul. 1981.
- [173] P. Robertson, and S. Kaiser, "Analysis of the loss of orthogonality through Doppler spread in OFDM systems", Global Telecommunications Conference, 1999, GLOBECOM '99 , Vol. 1b , pp. 701 -706, 1999.
- [174] P. Robertson, and S. Kaiser, "The effects of Doppler spreads in OFDM mobile radio systems," In the Proceedings of VTC Fall, 1999, pp.329-333.
- [175] Y. Sun, "Bandwidth-efficient wireless OFDM," IEEE Journal on Selected Areas of Communication, vol. 19, issue 11, pp. 2267 -2278, Nov. 2001.
- [176] Y. Sun, and L. Tong, "Channel equalization for wireless OFDM systems with ICI and ISI," IEEE International Conference on Communications, ICC'99, vol. 1, pp. 182-186, 1999.
- [177] Y. Sun, and L. Tong, "Channel equalization using one-tap DFE for wireless OFDM systems with ICI and ISI," 2nd IEEE Workshop on Signal Processing Advances in Wireless Communications, SPAWC'99 , vol. 1, pp. 146 -149, 1999.
- [178] M. Russell, G. Stuber, "Interchannel Interference Analysis of OFDM in a Mobile Environment," In the Proceedings of VTC, July 1995, pp.820-824,Chicago, Illinois, USA.
- [179] Y. Li, and L. J. Cimini Jr., "Interchannel interference of OFDM in mobile radio channels", Global Telecommunications Conference, 2000, GLOBECOM '00 , Vol. 2 , pp. 706-710, 1999.
- [180] Y. Li, and L. J. Cimini Jr., "Bounds on the interchannel interference of OFDM in time-varying impairments", IEEE Transactions on Communications, vol. 49, No. 3, pp. 401-404, Mar. 2001.
- [181] H. Boleski, D. Gesbert, and A. J. Paulraj, "On the capacity of OFDM-based multi-antenna systems," in The Proceedings of ICASSP, Atlanta, GA, 1981, pp. 2569-2572.
- [182] H. Boleski, D. Gesbert, and A. J. Paulraj, "On the capacity of OFDM-based spatial multiplexing systems", IEEE Transactions on Communications, vol. 50, No. 2, pp. 225-234, Feb. 2002.

References

- [183] Y. Li, and N. R. Sollenberger, "Adaptive antenna arrays for OFDM systems with cochannel interference", IEEE Transactions on Communications, vol. 47, No. 2, pp. 217-229, Feb. 1999.
- [184] S. Kapoor, D. J. Marchok, and Y. Huang, "Adaptive interference suppression in multiuser wireless OFDM systems using antenna arrays," IEEE Transactions on Signal Processing, vol. 47, No. 12, pp. 3381-3391, Dec. 1999.
- [185] C. K. Kim, K. Lee, and Y. S. Cho, "Adaptive beamforming for OFDM Systems with antenna arrays", IEEE Transactions on Consumer Electronics, vol. 46, No. 4, pp. 1052-1058, Nov. 2000.
- [186] S. Hara, A. Nishikawa, and Y. Hara, "A novel OFDM adaptive antenna array for delayed signal and Doppler-shifted signal suppression," IEEE International Conference on Communications, ICC'2001, vol. 7, pp. 2302-2306, 2001.
- [187] B. L. P. Cheung, F. Alam, J. H. Reed, and B. D. Woerner, "New Adaptive Beamforming Algorithms for OFDM systems", In the Proceedings of the 14th Annual International Conference on Wireless Communications, July 2002 Calgary, Alberta, Canada.
- [188] P. Robertson, and S. Kaiser, "The A novel adaptive antenna architecture - subcarrier clustering for high-speed OFDM systems in presence of rich co-channel interference," In the Proceedings of VTC Spring, 2002, vol.3, pp.1564-1568.
- [189] Z. Rong, *Simulation of Adaptive Array Algorithms for CDMA Systems*. M.S. Thesis, Virginia Tech, Sept 1996.
- [190] S.U. Pauli, *Array Signal Processing*. Springer-Verlag, New York, 1989.
- [191] W. L. Stutzman and G.A. Thiele, *Antenna Theory and Design*. John Wiley & Sons, New York, 1981.
- [192] F.Alam, D.Shim, and B.D. Woerner, "Comparison of Low Complexity Algorithms for MSNR Beamforming," submitted to VTC Spring, May 2002, Birmingham, Alabama, USA.
- [193] D. H. Johnson, and D. E. Dudgeon, *Array Signal Processing: Concepts and Techniques*. Englewood Cliffs, NJ: Prentice Hall PTR, 1993.
- [194] F.Alam, *Simulation of Third Generation CDMA Systems*. M.S. Thesis, Virginia Tech, Dec. 1999.
- [195] Kevin Laird, Nick Whinnet, and Soodesh Buljore, "A Peak-To-Average Power Reduction Method for Third Generation CDMA Reverse Links," in Proc., IEEE Vehicular Technology Conference, 1999.
- [196] UMTS, "Multiplexing and Chanel Coding," 3G TS 25.212 V3.2.0 (2000-03).
- [197] R. Mostafa, F. Alam, and K. K. Bae, "3G around the world," MPRG Propagator Newsletter, vol. 12, No. 1, Nov. 2001.
- [198] R. Mostafa, F. Alam, and K. K. Bae, "3G - around the world and back again," cover story of RF Design Magazine, Feb. 2002.
- [199] R. L. Burden, and J. D. Faires, *Numerical Analysis*. Brooks/Cole, Pacific Grove, California, 7th ed., 2001.
- [200] Y. Li, J. H. Winters, and N. R. Sollenberger, "Spatial-temporal equalization for IS-136 TDMA systems with rapid dispersive fading and cochannel interference", IEEE Transactions on Vehicular Technology, vol. 48, No. 4, pp. 3381-3391, Dec. 1999.

References

- [201] R. L. Cupo, G. D. Golden, C. C. Martin, K. L. Sherman, N. R. Sollenberger, J. H. Winters, and P. W. Wolniansky, "A four-element adaptive antenna array for IS-136 PCS base stations" IEEE Transactions on Vehicular, vol. 47, No. 3, pp. 1182 -1194, July 1999.
- [202] F.Alam, K. A. Zahid, B.D. Woerner and J.H. Reed, "Performance Comparison between Pilot Symbol Assisted and Blind Beamformer-Rake Receivers at the Reverse Link of Third Generation CDMA System", In the Proceedings of IEEE Vehicular Technology Conference, October 2001, New Jersey, USA.
- [203] F.Alam, *Space Time Processing for Third Generation CDMA Systems*. Preliminary Report, Virginia Tech, Nov. 2001.
- [204] K. Pahlavan, and P. Krishnamurthy, *Principles of Wireless Networks*. Upper Saddle River, NJ: Prentice Hall PTR, 2002.
- [205] ETSI, "ETS 300 401: Radio broadcasting systems; Digital Audio Broadcasting (DAB) to mobile, portable and fixed receivers," February, 1995.
- [206] H. Sari, G. Karam, I. Jeanclaude, "Transmission Techniques for Digital Terrestrial TV Broadcasting," IEEE Communications Magazine, pp.100-109, February, 1995.
- [207] IEEE 802.11, *IEEE standard for wireless LAN medium access control and physical layer specifications*, Nov. 1997.
- [208] B. L. P. Cheung, *Simulation of Adaptive Array Algorithms for OFDM and Adaptive Vector OFDM Systems*. M.S. Thesis, Virginia Tech, Sept. 2002.
- [209] COST 207 Management Committee, "COST 207: digital land mobile radio communications," Commission of the European Communities, Luxembourg, 1989.
- [210] T. Biedka, et al., "Smart Antenna for Handsets," *TI DSPFest*, Houston, August 2000.
- [211] W. G. Newhall, *Radio Channel Measurements and Modeling for Wireless Communication Systems Using Smart Antenna Arrays*, Preliminary Report, Virginia Tech, May 2002.

Vita

Fakhrul Alam was born in Dhaka, Bangladesh on April 18, 1972. He received the B.Sc. Degree in Electrical and Electronic Engineering from Bangladesh University of Engineering and Technology (BUET) in 1996. He worked as a lecturer in the EEE Department of his alma mater for a year. He started in the M.S. program at Virginia Tech from the fall of 1997 and joined MPRG in the fall of 1998. He received the Master of Science degree in Electrical Engineering in December 1999 and continued as a Ph.D. student. His research interests include space time processing for third generation CDMA systems and beamforming for OFDM systems.